

R O Z P R A W A D O K T O R S K A

Poszukiwanie nowych mechanizmów
neurodegeneracji w czasie rozwoju
ataksji rdzeniowo-móżdżkowej typu 3
w mysim modelu knock-in SCA3 Ki91

mgr inż. Kalina Katarzyna Wiatr

Praca wykonana pod opieką promotora
dr hab. Macieja Figla, prof. IChB PAN

Zakład Neurobiologii Molekularnej
Instytut Chemiczny Bioorganicznej PAN

Poznań 2021

Dziękuję doktorowi habilitowanemu Maciejowi Figlowi za przekazaną wiedzę, merytoryczne wsparcie i wskazanie możliwości na ścieżce naukowej.

Dziękuję kolegom i koleżankom z Zakładu Neurobiologii Molekularnej za współtworzenie wspaniałego zespołu i atmosfery, dzięki której realizacja pracy doktorskiej była przyjemnością.

Dziękuję wszystkim kolegom i koleżankom z Instytutu Chemii Bioorganicznej za wspaniałą atmosferę w pracy.

Dziękuję Rodzicom, rodzeństwu i Wojtkowi za pomoc, wiarę we mnie, wsparcie w dążeniu do celu oraz za to, że zawsze mogę na Was liczyć.

S P I S T R E Ś C I

1. Streszczenie	5
2. Abstract.....	7
3. Wprowadzenie	9
3.1. Ataksja rdzeniowo-mózdkowa typu 3 (SCA3).....	9
3.2. Mechanizmy molekularne i komórkowe mające udział w rozwoju SCA3	10
3.2.1. Normalna funkcja ataksyny-3	10
3.2.2. Rola agregatów i inkluzji formowanych przez ataksynę-3 w SCA3	12
3.2.3. Zaburzenia metabolizmu energetycznego w SCA3.....	13
3.2.4. Upośledzenie struktury i funkcji cytoszkieletu w SCA3	13
3.3. Modele SCA3.....	14
4. Cel pracy	16
5. Streszczenie prac i ich interpretacja na tle piśmiennictwa przedmiotu	17
5.1. Wstęp.....	17
5.2. Altered Levels of Proteins and Phosphoproteins, in the Absence of Early Causative Transcriptional Changes, Shape the Molecular Pathogenesis in the Brain of Young Presymptomatic Ki91 SCA3/MJD Mouse	19
5.3. Broad influence of mutant ataxin-3 on the proteome of the adult brain, young neurons, and axons reveals central molecular processes and biomarkers in SCA3/MJD using knock-in mouse model	22
6. Podsumowanie i perspektywy	26
7. Bibliografia	29
8. Załączniki	37

Wykaz artykułów zawartych w rozprawie doktorskiej:

1. **Wiatr K**, Piasecki P, Marczak Ł, Wojciechowski P, Kurkowiak M, Płoski R, Rydzanicz M, Handschuh L, Jungverdorben J, Brüste O, Figlerowicz M, Figiel M. Altered level of proteins and their decreased phosphorylation in the absence of transcriptomic changes shape the molecular pathogenesis in the pre-symptomatic SCA3/MJD brain. *Mol. Neurobiol.* 56, 8168–8202.
2. **Wiatr K**, Marczak L, Perot JB, Brouillet E, Flament J, Figiel M. Broad influence of mutant ataxin-3 on the proteome of the adult brain, young neurons, and axons reveals central molecular processes and biomarkers in SCA3/MJD using knock-in mouse model. *Front. Mol. Neurosci.* 14. doi:10.3389/fnmol.2021.658339.

Artykuły nie wchodzące w skład rozprawy doktorskiej:

1. Szlachcic WJ, Switonski PM, Kurkowiak M, **Wiatr K**, Figiel M. Mouse polyQ database: a new online resource for research using mouse models of neurodegenerative diseases. *Mol Brain.* 2015;8:6
2. Szlachcic WJ, **Wiatr K**, Trzeciak M, Figlerowicz M, Figiel M. The Generation of Mouse and Human Huntington Disease iPS Cells Suitable for In vitro Studies on Huntingtin Function. *Front Mol Neurosci.* 2017;10:253.
3. **Wiatr K**, Szlachcic WJ, Trzeciak M, Figlerowicz M, Figiel M. Huntington Disease as a Neurodevelopmental Disorder and Early Signs of the Disease in Stem Cells. *Mol Neurobiol.* 2018 Apr;55(4):3351-3371.

1

STRESZCZENIE

Choroby neurodegeneracyjne, takie jak choroba Alzheimera, Parkinsona czy choroby poliglutaminowe są poważnym i rosnącym obciążeniem dla współczesnych społeczeństw. Charakteryzują się ciężkimi zaburzeniami motorycznymi i/lub poznawczymi wynikającymi z postępujących uszkodzeń specyficznych populacji neuronów oraz połączeń nerwowych w mózgu, co ostatecznie skutkuje kalectwem i utratą samodzielności pacjentów. Co więcej, choroby neurodegeneracyjne występują coraz częściej w związku z wydłużającą się średnią długością życia. Pomimo, że mają pewne elementy wspólne, ich dokładny patomechanizm wciąż nie jest poznany i dlatego nie istnieje żadna skuteczna terapia. W odróżnieniu od choroby Alzheimera i innych chorób neurodegeneracyjnych o niedostatecznie zdefiniowanej etiologii, choroby poliglutaminowe (polyQ) są skutkiem dominującej mutacji - ekspansji powtórzeń CAG w pojedynczych genach. Do chorób tych należy również ataksja rdzeniowo-mózdkowa typu 3 (SCA3), wywołana przez ekspansję CAG w egzonie 10 genu *ATXN3* kodującego białko ataksynę-3.

Głównym celem badań prowadzonych przeze mnie w ramach pracy doktorskiej było poznanie patomechanizmu, który prowadzi do rozwoju ataksji rdzeniowo-mózdkowej typu 3. Aby zrealizować cel główny pracy, sformuowałam także cele szczegółowe. Pierwszym z nich była charakterystyka fenotypu homozygotycznego modelu knock-in SCA3 Ki91 oraz wyróżnienie fazy pre-symptomatycznej i symptomatycznej SCA3 poprzez szereg testów behawioralnych i komórkowych. Drugi istotny cel moich badań stanowiła identyfikacja procesów molekularnych, które powodują powstanie choroby neurodegeneracyjnej (faza pre-symptomatyczna), a następnie procesów kluczowych dla patogenezy SCA3 w czasie progresji choroby w modelu Ki91. Cel ten realizowałam poprzez wielkoskalową analizę zmian w poziomie białek w 2 regionach mózgu: korze mózgowej i mózdku w poszczególnych fazach SCA3 w modelu Ki91. Kolejne cele obejmowały wytypowanie białek, mogących posłużyć jako biomarkery SCA3 oraz szczegółowe zbadanie procesów molekularnych, które mogą być zmienione w modelu SCA3 Ki91 przy pomocy testów funkcjonalnych i mikroskopii. W badaniach w ramach mojej pracy doktorskiej wykorzystałam mysi model Ki91 typu knock-in ze wstawioną ludzką sekwencją egzonów 7-11, zawierającą 91 powtórzenie CAG w mysim genie *Atxn3*. Model ten zaprojektowany został w Instytucie Chemii Bioorganicznej PAN (Switonski et al., 2015). Testy behawioralne objęły zwierzęta 2-miesięczne aż do ukończenia 18 miesiąca życia w wygenerowanej przeze mnie kohortie myszy ($n=18$ na genotyp). Różnice w poziomie białek analizowałam wysokoprzepustową metodą spektrometrii mas LC-MS/MS w wiekach myszy, które uznałam za ważne punkty czasowe w przebiegu SCA3 na podstawie testów behawioralnych. Następnie, przeprowadziłam analizę procesów komórkowych i ścieżek molekularnych z wykorzystaniem narzędzi bioinformatycznych na podstawie białek o zmienionym poziomie w poszczególnych wiekach.

Po analizie otrzymanych wyników wyróżniłam 4 fazy choroby, a wśród nich fazę pre-symptomatyczną, w której nie obserwowałam żadnych objawów motorycznych i innych, co zostało opisane w publikacji (Wiatr et al., 2019). Wyodrębnienie stadium pre-symptomatycznego w modelu choroby jest ważne, ponieważ umożliwia precyjne odróżnienie procesów, które są przyczyną neurodegeneracji od tych, które są skutkiem progresji choroby lub naturalnego starzenia. Ustaliłam, że białka o zmienionym poziomie w fazie pre-symptomatycznej SCA3 zaangażowane były w translację, naprawę uszkodzeń DNA, neurogenezę i tworzenie struktur neuronalnych, oraz metabolizm energetyczny i transport komórkowy. Dodatkowo analizowałam również poziom fosforylacji białek i odkryłam globalne obniżenie fosforylacji w korze mózgowej i mózdzku Ki91 oraz zmieniony poziom i fosforylację kilku kinaz, jak Pak1. Dużą grupę białek o obniżonej fosforylacji stanowiły ważne regulatory funkcji cytoskieletu i transportu w aksonach. Druga publikacja zebrała wyniki stanowiące kontynuację moich badań w kolejnych stadiach choroby, począwszy od utraty przyrostu masy ciała u młodych zwierząt do poważnych zaburzeń motorycznych u myszy 18-miesięcznych (Wiatr et al., 2021). Białka o zmienionym poziomie w kolejnych wiekach zaangażowane są w takie procesy jak metabolizm energetyczny, formowanie cytoskieletu, transport wzduż aksonu, przekaźnictwo synaptyczne, a także degradacja w proteasomie i apoptoza. W późniejszych fazach zwiększa się ilość białek, które lokalizują w lisosomach, a także w pęcherzykach synaptycznych i synapsach i które związane są z metabolizmem. Na podstawie wyników otrzymanych w analizie zmienionych białek i procesów molekularnych opracowałam model patogenezy SCA3 składający się z zaburzeń w transporcie pęcherzyków synaptycznych, mitochondriów i autofagosomów wzduż aksonu SCA3. Dlatego w następnym etapie przeprowadziłam eksperymenty mających na celu wykazanie, że wczesne patogenne procesy SCA3 zachodzą w aksonach. Wykazałam deficyt w metabolizmie energetycznym neuronów mózdkowych Ki91 w teście funkcjonalnym, w którym mierzona była szybkość zakwaszania komórki (tempo glikolizy) i pomiar zużycia tlenu. Zademonstrowałam akumulację neurofilamentów i pęcherzyków (znakowanych Rab7) w ciałach i aksonach neuronów mózdkowych Ki91. Następnie, wyprowadziłam kulturę hodowli neuronów kortikalnych i mózdkowych *in vitro*, z których izolowałam osobno aksony i część somatodendryczną. W tym celu wykorzystałam zmodyfikowane komory Boydena, które separam aksony od ciał komórek nerwowych poprzez porowy filtr. Następnie analizowałam, które białka lokalizują w zmienionej ilości w aksonach w stosunku do części somatodendrycznej neuronów pochodzących z modelu SCA3 Ki91 w porównaniu do kontroli (C57). Analiza białek, które znajdują się w aksonach w zmienionej ilości pozwoliła na wstępную ocenę czy w modelu SCA3 Ki91 występuje zaburzenie transportu aksonalnego i których organelli lub białek dotyczy. Białka wzbogacone w aksonach SCA3 to przede wszystkim białka maszyneryi translacyjnej, podczas gdy białka zubożone w aksonach SCA3 to m.in. białka cytoskieletarne, regulujące transport i budujące pęcherzyki.

Podsumowując, zidentyfikowałam wiele zmian na poziomie białek w modelu SCA3, które wskazują na zaburzenie procesów i ścieżek molekularnych takich jak metabolizm energetyczny i transport w aksonach. Wytacza to nowe kierunki badań, które przybliżą zrozumienie patomechanizmu SCA3 będącego podstawą neurodegeneracji.

2

ABSTRACT

Neurodegenerative diseases such as Alzheimer, Parkinson, and polyglutamine diseases are a serious and growing burden for modern societies. The diseases are characterized by severe motor and/or cognitive impairment resulting from progressive damage to specific populations of neurons and nerve connections in the brain, ultimately resulting in disability and loss of patients' independence. Moreover, neurodegenerative diseases are becoming more common since life expectancy is increasing. Although neurodegenerative diseases share some common features, their exact pathomechanism is still unknown, and therefore no effective therapy exists. Unlike Alzheimer disease and other neurodegenerative diseases with an insufficiently defined etiology, polyglutamine diseases (polyQ) result from a dominant mutation - the expansion of CAG repeats in single genes. The group of polyQ diseases also include spinocerebellar ataxia type 3 (SCA3), caused by the expansion of CAG repeats in exon 10 of the *ATXN3* gene encoding the ataxin-3 protein.

The main goal of the research conducted as a part of my Ph.D. thesis was discovering the pathomechanism, that leads to the development of spinocerebellar ataxia type 3. Next to the primary goal of my project, I also defined specific aims. The first specific aim was to characterize the phenotype of the SCA3 Ki91 homozygous knock-in model and distinguish the pre-symptomatic and symptomatic stages of SCA3 using behavioral and cellular tests. The second important aim of my research was to identify the molecular processes that give rise to neurodegenerative disease (pre-symptomatic phase), and then the key processes for SCA3 pathogenesis during disease progression in the Ki91 model. I have achieved this goal by performing large-scale analysis of changes in the protein levels in 2 brain regions: the cerebral cortex and the cerebellum of the Ki91 model in distinct SCA3 stages. A further aim was selecting proteins that could serve as SCA3 biomarkers and a detailed analysis of molecular processes that could be altered in the SCA3 Ki91 model using functional tests and microscopy. In my Ph.D. research, I have used the Ki91 mouse knock-in model with a human sequence of exons 7-11, containing 91 CAG repeats in the mouse *Atxn3* gene. This model was designed at the Institute of Bioorganic Chemistry of the Polish Academy of Sciences (Switonski et al., 2015). Behavioral tests were performed on mice from 2-month-old till 18- months of age in the cohort generated by me ($n = 18$ per genotype). I have analyzed the differences in the protein levels with the high-throughput LC-MS / MS mass spectrometry in the age of mice, which I have selected as the most crucial time points for SCA3 development based on behavioral results. Next, in order to reveal the cellular processes and molecular pathways, which might contribute to the SCA3 pathogenesis, I have performed an analysis of dysregulated proteins using bioinformatic tools.

After analyzing the results, I have distinguished 4 phases of the disease, including the pre-symptomatic phase, in which I did not observe any motor or other symptoms that were described in the publication (Wiatr et al., 2019). Definition of the pre-symptomatic stage in the disease model is essential because it enables the precise distinction between processes

that cause neurodegeneration from those that are a result of disease progression or natural aging. I have found that altered proteins in the pre-symptomatic phase of SCA3 were involved in translation, DNA damage repair, neurogenesis, and neural structure formation, as well as energy metabolism and cellular transport. In addition, I have also analyzed the level of protein phosphorylation and discovered a global reduction in phosphorylation in the cerebral cortex and cerebellum of Ki91, and altered levels and phosphorylation of several kinases, such as Pak1. A large group of proteins with reduced phosphorylation were important regulators of cytoskeleton function and axonal transport. The second publication gathered the results that were a continuation of my research in the subsequent stages of the disease, ranging from weight loss in young animals to severe motor impairment in 18-month-old mice (Wiatr et al., 2021). Proteins with altered levels in the older animals are involved in processes such as energy metabolism, cytoskeleton formation, transport along the axon, synaptic transmission, degradation in the proteasome, and apoptosis. In the later phases, the number of proteins that localized in lysosomes, synaptic vesicles, and synapses, and which are involved in metabolism, increases. Based on the results obtained in the analysis of altered proteins and molecular processes, I have developed a model of SCA3 pathogenesis consisting of disturbances in the transport of synaptic vesicles, mitochondria, and autophagosomes along the SCA3 axon. Therefore, in the next stage, I have performed experiments to demonstrate that early pathogenic SCA3 processes occur in axons. I have shown a deficit in the energy metabolism of Ki91 cerebellar neurons in a functional test in which the rate of cell acidification (glycolysis rate) and oxygen consumption were measured. I have demonstrated the accumulation of neurofilaments and vesicles (labeled with Rab7) in the bodies and axons of the Ki91 cerebellar neurons. Then, I obtained an *in vitro* culture of cortical and cerebellar neurons, from which I have isolated the axons and the somatodendritic parts separately. For this purpose, I have used modified Boyden chambers, which separate axons from the bodies of neurons through a porous filter. Next, I have analyzed which proteins localize in altered amounts in axons in comparison to the somatodendritic part of neurons derived from the SCA3 Ki91 model and compared to the control (C57). The analysis of axonal proteins that demonstrated altered levels allowed for initial assessment of whether the disturbance of axonal transport occurs in the SCA3 Ki91 model and which organelles or proteins it concerns. Proteins enriched in SCA3 axons are primarily proteins of the translational machinery, while proteins depleted in SCA3 axons include cytoskeletal proteins that regulate the transport and build vesicles.

Overall, I have identified many changes at the protein level in the SCA3 model that indicate disruption of molecular processes and pathways such as energy metabolism and axonal transport. The results of my Ph.D. thesis set new directions of research that will bring us closer to understanding the pathomechanism of SCA3 underlying neurodegeneration.

3

WPROWADZENIE

3.1. ATAKSJA RDZENIOWO-MÓŽDŽKOWA TYPU 3 (SCA3)

Ataksja rdzeniowo-mózdkowa typu 3 (ang. spinocerebellar ataxia type 3; SCA3), znana także jako choroba Machado-Josepha (ang. Machado-Joseph Disease; MJD) należy do grupy neurodegeneracyjnych chorób polyQ (Riess et al., 2008). Do tej grupy chorób należy również choroba Huntingtona, rdzeniowo-opuszkowy zanik mięśni (SBMA), zanik jądra zębatego, czerwiennego, galki bladej i jądra Luysa (DRPLA) oraz pięć innych ataksji rdzeniowo-mózdkowych (SCA1, 2, 6, 7 i 17). Choroby polyQ łączy wspólny typ mutacji, który polega na ekspansji powtórzeń CAG w odcinkach kodujących w genach, co sprawia, że etiologia tych chorób jest dość dobrze zdefiniowana.

SCA3 została po raz pierwszy opisana w USA w 1972 roku jako nowa forma ataksji mózdkowej dziedziczonej autosomalnie dominująco, zaobserwowanej u emigrantów pochodzących z Azorów, gdzie częstość występowania jest bardzo wysoka (wyspa Flores wchodząca w skład Azorów – 1/239) (Nakano et al., 1972; Bettencourt et al., 2008). Średnia częstość występowania SCA3 na świecie wynosi 1–5 / 100 000 (Li et al., 2019), a wyższą względna częstotliwość (procent przypadków SCA3 w ogólnej liczbie innych SCA) obserwuje się w Portugalii (57.8%), Brazylii (59.6%), Japonii (43%), Chinach (62.6%) i Niemczech (42%) (Schöls et al., 1997; Takano et al., 1998; Vale et al., 2010; de Castilhos et al., 2014; Chen et al., 2018).

SCA3 jest najczęstszym typem ataksji dziedziczoną w sposób autosomalny dominujący na całym świecie i wywołana jest przez ekspansję powtórzeń CAG w egzonie 10 genu *ATXN3*. U osób zdrowych liczba powtórzeń CAG wynosi zazwyczaj między 14 a 42, natomiast u pacjentów SCA3 liczba powtórzeń CAG wzrasta do 52-91 w jednym allele *ATXN3* (Lima and Raposo, 2018). Mutacja powoduje powstanie białka ATXN3 z wydłużonym traktem poliglutaminowym. Liczba powtórzeń CAG w genie *ATXN3* jest niestabilna, co oznacza, że ciąg CAG może ulec skróceniu lub wydłużeniu (Riess et al., 2008). Istnieje silna korelacja między długością powtórzeń CAG, a wiekiem wystąpienia pierwszych objawów i stopniem ciężkości przebiegu choroby (Maciel et al., 1995; Leotti et al., 2021). Jednakże, długość powtórzeń CAG nie jest jedynym czynnikiem wpływającym na rozwój choroby. Istnieją dodatkowe czynniki genetyczne i epigenetyczne, które wpływają na początek i przebieg (Weishäupl et al., 2019; Akçimen et al., 2020; Zhao et al., 2020).

Pierwsze objawy SCA3 obserwuje się zazwyczaj między trzecią a piątą dekadą życia (Rüb et al., 2013). Objawy kliniczne to przede wszystkim zaburzenia motoryczne, które są skutkiem procesu neurodegeneracyjnego obejmującego różne struktury układu nerwowego. Degenerację neuronów obserwuje się w obrębie mózdku (szczególnie w jądrach głębokich mózdku), kolumnach grzbietowych i drogach rdzeniowo-mózdkowych w rdzeniu

kręgowym, a także w pniu mózgu (w tym w istocie czarnej), jądrach podkorowych i samej korze mózgowej. Zmiany w jądrze zębatego mózdku i jądrach grzbietowych w kolumnach Clarke'a odpowiadają za rozwój ataksji mózdkowej, zaburzenia chodu, równowagi i koordynacji ruchowej, podczas gdy parkinsonizm związany jest z degeneracją istoty czarnej. Natomiast zanik jąder motorycznych i degeneracja jądra nerwu podjęzykowego zlokalizowanych w pniu mózgu powoduje złożone zaburzenia motoryczne oczu i języka, zaburzenia mowy (dyzartię) i polkowania (dysfagię) (Koeppen, 2018). Do objawów występujących u pacjentów SCA3 należy również utrata masy ciała bez utraty apetytu, zaburzenia snu oraz neuropatie (Riess et al., 2008). Degeneracja istoty szarej w SCA3 obejmuje także inne regiony, włączając w to również korę mózgową (Schmidt et al., 2019; Guo et al., 2020a). U pacjentów SCA3 nie zaobserwowano demencji, funkcje poznawcze mogą jednak być upośledzone (Mendonça et al., 2018; Maas et al., 2021). SCA3 obecnie jest chorobą nieuleczalną, pomimo podjętych licznych prób terapeutycznych.

3.2. MECHANIZMY MOLEKULARNE I KOMÓRKOWE MAJĄCE UDZIAŁ W ROZWOJU SCA3

3.2.1. NORMALNA FUNKCJA ATAksyny-3

Ataksyna-3 (ATXN3) jest proteazą cysteinową wykazującą aktywność deubikwitynazy, należącą do rodziny MJD (Grasty et al., 2019). Bialko ATXN3 ma masę 42 kDa i składa się z globularnego końca N, w którym znajduje się domena katalityczna Josephin, 2-3 motywów oddziałujących z ubikwityną (UIM), traktu poliglutaminowego (polyQ), sygnału lokalizacji jądrowej i eksportu z jądra oraz elastycznego końca C (Antony et al., 2009). ATXN3 wiąże się do reszty tetraubikwityny połączonej lizynami w pozycji 48 i/lub 63, którą oznakowane jest docelowe bialko, po czym hydrolizuje połączenie między łańcuchem ubikwityny a białkiem, usuwając w ten sposób molekularny znaczniak (Costa and Paulson, 2012).

Ataksyna-3 odgrywa istotną rolę w dwóch głównych szlakach kontroli jakości i degradacji białek w komórce, tj. autofagii oraz systemie ubikwityna-proteasom (UPS), które przede wszystkim różnią się wielkością degradowanych struktur. W procesie autofagii degradowane są duże białka, kompleksy białkowe, agregaty komórkowe, a nawet organella, szczególnie w sytuacji stresu komórkowego. Podczas gdy do rozkładu w proteasomie kierowane są białka o mniejszej masie, lub nieprawidłowo sfaldowane (Pohl and Dikic, 2019). Ataksyna-3 bierze udział w transporcie ubikwitynowanych białek do proteasomu, gdzie oddziałuje z różnymi białkami zaangażowanymi w UPS i uwalnia źle sfaldowane białka do degradacji (Doss-Pepe et al., 2003; Riess et al., 2008). Ponadto, ATXN3 jako deubikwitynaza pełni ważną rolę w kontroli, które białka mają ulec degradacji w proteasomie (Zhong and Pittman, 2006; Matos et al., 2019; Singh et al., 2019).

Wagę tego mechanizmu dla komórki demonstruje deubikwitynacja przez ataksynę-3 takich białek jak RNF8, CHK1 czy beklina-1. Odlączenie znacznika poliubikwitynowego od CHK1 i RNF8 chroni je przed przedwczesną degradacją, umożliwiając kontrolę cyklu komórkowego i naprawę DNA (Tu et al., 2017; Singh et al., 2019). Deubikwitynacja beclin-1 natomiast zapobiega degradacji tego białka w proteasomie, a ponieważ jest ono kluczowym regulatorem formowania autofagosomów, umożliwia to zajście autofagii (Hill et al., 2021). Co więcej, ATXN3 poprzez modyfikację łańcuchów ubikwityny, kieruje źle sfaldowane

białka do struktur określanych jako agresom, a następnie degradacji poprzez autofagię (Yao, 2010). Ostatnio zademonstrowano także, że ataksyna-3 reguluje degradację na drodze autofagi, bezpośrednio oddziałując ze znanyymi autofagicznymi regulatorami, takimi jak LC3 i GABARAP (Herzog et al., 2020).

Funkcja normalnej ataksyny-3 wykracza jednak poza kontrolę jakości białek. Jako, że ATXN3 ma powinowactwo do łańcuchów ubikwityny łączonych przez resztę lizyny w pozycji 63 (K63), ma wpływ na wiele innych procesów komórkowych, takich jak endocytoza, translacja oraz aktywacja kinaz (Winborn et al., 2008; Chen and Sun, 2009). Łańcuchy ubikwityny służą jako sygnał do rekrutacji białek, które zawierają domeny wiążące ubikwitynę, w celu wykonania określonej funkcji biologicznej. Ponadto, ATXN3 może również wpływać na ekspresję genów poprzez zmianę metylacji DNA, sekwestrację CBP (ang. CREB-binding protein) oraz interakcję z deacetylaszą histonową HDAC3 (Chai et al., 2001; Evert et al., 2006; Ding et al., 2020). Bierze także udział w kluczowych procesach komórkowych takich jak zachowanie integralności genomu, obrona przed stresem oksydacyjnym i apoptoza (Chakraborty et al., 2020; Tu et al., 2020).

Podsumowując, ataksyna-3 reguluje wiele istotnych procesów komórkowych, m.in. poprzez zapobieganie degradacji białek, które uległy przedwczesnej lub błędnej ubikwitynacji. Z drugiej strony, zmiana normalnej funkcji ATXN3 w wyniku mutacji może powodować niewydolność degradacji białek w systemie ubikwityna-proteasom. W konsekwencji, nagromadzenie nieprawidłowo sfalduwanych białek może spowodować przeciążenie proteasomu i hamować jego aktywność (Bence et al., 2001). Biologiczna rola ataksyny-3 związana jest więc bezpośrednio z modulowaniem poziomu białek w komórce, co odróżnia SCA3 od innych chorób polyQ. Pomimo to, do tej pory badania w obszarze mechanizmów molekularnych w SCA3 skupiały się raczej na zmianach transkryptomicznych (Toonen et al., 2018; Zeng et al., 2018). Zmiany w poziomie białek wynikają jednak nie tylko z regulacji na poziomie transkrypcyjnym (m.in. kontrola translacji białek, modyfikacje potranslacyjne). Tym samym, ważna część proteomu, która może być zmieniona w czasie procesu chorobowego ulega pominięciu w badaniach skupiających się wyłącznie na zmianach transkryptomicznych. Co więcej, to właśnie białka są głównymi efektorami funkcji komórkowych. Do tej pory prace, które odnosili się do zmian białkowych w SCA3, korzystały z metod niskoprzepustowych, identyfikując jedynie pojedyncze zmienione białka w SCA3 (Hsieh et al., 2013; Duarte Lobo et al., 2020). Inne prace poruszające nieco szerszy aspekt zmian proteomicznych zawężały obszar badań do interaktorów ataksyny-3, białek fosforylowanych oraz zmian proteomicznych związanych z obniżeniem poziomu normalnej ataksyny-3 (Kristensen et al., 2018; Toulis et al., 2020; Sowa et al., 2021). Uzupełnienie istniejącej luki w wiedzy poprzez dokładne poznanie globalnych zmian proteomu w SCA3 może przynieść wiele cennych poszlak dotyczących patomechanizmu tej choroby.

3.2.2. ROLA AGREGATÓW I INKLUZJI FORMOWANYCH PRZEZ ATAKSYNĘ-3 W SCA3

Wspólnym elementem chorób neurodegeneracyjnych (m.in. Choroby Alzheimera, Parkinsona, chorób poliglutaminowych) jest gromadzenie się nieprawidłowo sfaldowanych białek, które formując agregaty wewnętrz- lub zewnętrzkomórkowe stają się toksyczne dla neuronów (Soto and Pritzkow, 2018). W przypadku SCA3 obserwuje się toksyczne agregaty i inkluzje formowane przez zmutowaną ataksynę-3. ATXN3 w formie agregatów, nierożpuszczalnych inkluzji i rozpuszczalnych oligomerów białkowych może zaburzać wiele procesów komórkowych.

Inkluzje ataksyny-3 mogą sekwestrować inne białka, takie jak chaperony, białka wiążące ubikwitynę, elementy proteasomu czy czynniki transkrypcyjne, powodując ich niedobór w regionach komórki, w których są potrzebne (Chai et al., 1999a, 2001; Schmidt et al., 2002; Donaldson et al., 2003). Normalna ataksyna-3 lokalizuje zarówno w jądrze komórkowym jak i cytoplazmie, jednak w warunkach stresu ma tendencję do gromadzenia się w jądrze, gdzie również lokalizują inkluzje zmutowanej formy białka. W celu usunięcia inkluzji ataksyny-3 proteasom 26S jest rekrutowany do jądra, co jednak powoduje jego niedostateczną ilość w cytoplazmie (Chai et al., 1999b; Donaldson et al., 2003; Berke et al., 2005). W konsekwencji, nagromadzenie nieprawidłowo sfaldowanych białek w komórce może spowodować przeciążenie proteasomu i hamować jego aktywność (Bence et al., 2001).

Ataksyna-3 występuje w 3 różnych izoformach, które różnią się lokalizacją subkomórkową (np. ataksyna-3aS występuje w jądrze), aktywnością enzymatyczną i kinetyką agregacji (Macedo-Ribeiro et al., 2009; Harris et al., 2010). Istnieją różne hipotezy na temat agregatów formowanych przez ataksynę-3. Wg jednej z nich, agregaty są toksyczne dla komórki. Według innej, zyskującej ostatnio na popularności, mogą spełniać funkcję neuroprotekcyjną, sekwestrując zmutowane białko (Invernizzi et al., 2012; Todd and Lim, 2013; Vinatec et al., 2015). Istnieje także hipoteza według, której agregaty zmutowanej ATXN3 spełniają protekcyjną rolę w pierwszych etapach choroby, później jednak stają się szkodliwe, sekwestrując inne białka, które nie mogą dłużej spełniać swojej funkcji (Sánchez et al., 2003). Sklonność do agregacji ataksyny-3 wynika z obecności wydłużonego ciągu glutamin w sekwencji białka, które kodowane są przez powtórzenia CAG w zmutowanym genie. Zaproponowano także inny mechanizm, w którym proteolityczne produkty rozpadu ataksyny-3 inicjują proces agregacji służąc jako swoiste centra kondensacji (ang. seeds) (Haacke et al., 2007). Dodatkowo, modyfikacje potranslacyjne ataksyny-3 również wpływają na jej skłonność do agregacji i lokalizację jądrową oraz modyfikują jej aktywność deubikwitynizową (Fei et al., 2007; Mueller et al., 2009; Todi et al., 2009).

Sama agregacja ataksyny-3 nie jest jednak wystarczająca, aby spowodować degenerację neuronów (Evers et al., 2014). Utrata lub zyskanie nowych funkcji przez zmutowane białko jak i udział toksycznego transkryptu *ATXN3* jest również istotnym komponentem patogenezy SCA3 (Dantuma and Herzog, 2020). Pomimo, że do tej pory zademonstrowano wpływ zmutowanej ataksyny-3 na różnorodne procesy w komórce, wciąż jednak nadzędny mechanizm wiodący do neurodegeneracji i rozwoju choroby nie jest znany.

3.2.3. ZABURZENIA METABOLIZMU ENERGETYCZNEGO W SCA3

Podobnie do innych chorób neurodegeneracyjnych w SCA3 obserwuje się dysfunkcje mitochondriów. Delecje mitochondrialnego DNA (mtDNA) występują w modelach zwierzęcych SCA3, a także u pacjentów (Kazachkova et al., 2013; Raposo et al., 2019). Ponadto, wykazano, że zarówno normalna, zmutowana i skrócona forma ataksyny-3 lokalizuje w mitochondriach, a także oddziałuje z kilkoma białkami zaangażowanymi w metabolizm energetyczny (Pozzi et al., 2008; Kristensen et al., 2018). Skrócona forma białka (fragment n-końcowy) zmutowanej ataksyny-3 upośledza morfologię mitochondriów, promuje ich rozszczepienie (ang. mitochondrial fission) oraz powoduje obniżony potencjał błony mitochondrialnej i zmniejszoną pojemność oddechową mitochondriów w modelach komórkowych, a także wzrost ilości reaktywnych form tlenu (Hsu et al., 2017; Harmuth et al., 2018). Skrócone formy ATXN3 powstają poprzez enzymatyczne cięcie dokonane przez kaspazy i kalpainy, przy czym zarówno fragmenty n- i c- końcowe (zawierające ciąg polyQ) wykazują cytotoxisyczność (Berke et al., 2004; Breuer et al., 2010; Hübener et al., 2013; Simões et al., 2014). Fragmentacja i upośledzenie funkcji mitochondriów zarówno przez formę skróconą i pełną ATXN3 prowadzi do mitofagii (degradacja mitochondriów na drodze autofagii) i aktywacji kaskady apoptotycznej za pośrednictwem mitochondriów (Tsai et al., 2004; Chou et al., 2011; Harmuth et al., 2018). Zmutowana ataksyna-3 zaburza również sygnalizację wapniową w neuronach, a nadmiar jonów wapnia w komórce prowadzi m.in. do permeabilizacji mitochondriów oraz neurotoxisyczności (Chen et al., 2008; Zhivotovsky and Orrenius, 2011; Pellistri et al., 2013).

Z uwagi na to, że neurony mają wyjątkowo duże zapotrzebowanie energetyczne, uszkodzenie mitochondriów jest dla nich prawdopodobnie bardziej dotkliwe niż dla większości innego typu komórek. Jest to więc jeden z procesów komórkowych, który mimo licznych badań już dokonanych, powinien być w dalszym ciągu eksplorowany podczas próby zrozumienia neurodegeneracji.

3.2.4. UPOŚLEDZENIE STRUKTURY I FUNKCJI CYTOSZKIELETU W SCA3

Wspólnym komponentem wielu chorób neurodegeneracyjnych są zaburzenia transportu aksonalnego, takie jak transport neurofilamentów, endosomów czy czynników troficznych jak BDNF (Millecamps and Julien, 2013). Neurony zmuszone są transportować różnego typu molekuły i organella na bardzo duże odległości między ciałem komórki a zakończeniem nerwowym. Akson może mieć u człowieka nawet ponad 1 m długości (nerw kulsowy biegnie od podstawy rdzenia kręgowego do dużego palca u stopy), jest też strukturą stosunkowo delikatną i dlatego potencjalnie wrażliwą na skutki odkładania się nieprawidłowych białek. Upośledzenie transportu aksonalnego może wynikać z wielu mechanizmów, w tym defektów w organizacji cytoszkieletu, nieprawidłowego zakotwiczenia białek motorycznych do mikrotubul, zmienionej aktywności kinaz, deficytów energetycznych związanych z uszkodzeniem mitochondriów jak również prostej blokady mechanicznej przez agregaty białkowe (Millecamps and Julien, 2013).

Do tej pory nie wykazano w bezpośredni sposób za pomocą mikroskopii *in vivo*, aby w SCA3 dochodziło do zaburzeń transportu aksonalnego. Jednak istnieją pewne poszlaki, wskazujące na zakłócenie organizacji aksonów w tej chorobie (de Rezende et al., 2015; Farrar et al., 2016; Lu et al., 2017). W badaniu MRI obserwuje się ubytek istoty białej w mózgu, a także neuropatię obwodową u pacjentów SCA3 (D'Abreu et al., 2009; Graves and Guiloff, 2011; Rezende et al., 2018). Ponadto, wykazano, że ATXN3 oddziaływa z mikrotubulami, a w przypadku zmutowanej formy białka, interakcja ta jest utrudniająca co zaburza funkcje cytoszkieletu (Mazzucchelli et al., 2009; Chen et al., 2012). ATXN3 wiąże się również z dyneiną, która odgrywa kluczową rolę w retrogradowym transporcie w aksonach (Burnett and Pittman, 2005). Utrata aktywności deubikwitynazy przez ataksynę-3 negatywnie wpływa na organizację cytoszkieletu aktynowego oraz obniża poziom podjednostki integryny $\alpha 5$ (ITGA5), prowadząc do zmniejszonej adhezji komórek oraz skrócenia neurytów i zmniejszenia ich ilości (Neves-Carvalho et al., 2015). Co więcej, ostatnio zademonstrowano także, że zmniejszenie poziomu normalnej ataksyny-3 w komórkach siatkówki, która jest częścią układu nerwowego, powoduje zmianę poziomu białek motorycznych (m.in. podjednostek dyneiny i dynaminy) oraz zaburzenie transportu endosomów (Toulis et al., 2020). Szereg eksperymentów sugeruje więc, że funkcja normalnej ataksyny-3 jest związana z regulacją transportu wzduż mikrotubul.

Co istotne, ataksyna-3 tworzy inkluzje nie tylko w jądrach komórkowych, ale również w aksonach u pacjentów SCA3 (Seidel et al., 2010). Inkluzje ataksyny-3 mogą stanowić przeszkodę mechaniczną w transporcie aksonalnym, a także mogą sekwestrować inne białka niezbędne do prawidłowego funkcjonowania aksonu. Ponadto, agregaty zmutowanej ATXN3 zakłócają endocytozę, uwalnianie neuroprzekaźników, a także mogą powodować pęcznienie i nieprawidłowe rozgałęzianie się neurytów (Khan et al., 2006; Rosselli-Murai et al., 2020). Podsumowując, dotychczasowe badania sugerują, że ataksyna-3 w formie rozpuszczalnego białka i w formie agregatów może wpływać na organizację cytoszkieletu i transport w aksonach. Procesy molekularne, które zachodzą w aksonach w SCA3 powinny więc zostać szerzej zbadane.

3.3. MODELE SCA3

Badanie fizjologicznej funkcji ataksyny-3 w kontrolowanych warunkach i mechanizmów komórkowych w czasie rozwoju choroby na materiale ludzkim związane jest z wieloma ograniczeniami. Tkanki od pacjentów *post-mortem*, choć umożliwiły wiele cennych badań, mają ograniczoną dostępność, szczególnie w przypadku chorób rzadkich. Ponadto, ostatnio wykazano, że w momencie śmierci w mózgu człowieka aktywuje się ekspresja grupy genów, m.in. związanych z odpowiedzią na stan zapalny (Dachet et al., 2021). Z kolei wiele transkryptów związanych z aktywnością neuronów jest degradowana w bardzo krótkim czasie po śmierci. W ten sposób tracących być może wiele cennych informacji, istotnych dla zrozumienia chorób neurologicznych. Z kolei, technologia iPSC umożliwia otrzymanie neuronów z komórek skóry pobranych od pacjentów, które następnie mogą być kultywowane *in vitro* w hodowli 2D lub jako organoidy i służyć w badaniach naukowych (Takahashi and Yamanaka, 2006; Chen et al., 2020). Dzięki temu powstało wiele nowych możliwości, należy jednak pamiętać, że takie kultury również wiążą się z pewnymi ograniczeniami. Odpowiadają one stadium rozwojowemu komórek embrionalnych, tak więc służą jako świetny model wczesnych procesów chorobowych, ale już niekoniecznie tego co zachodzi w komórkach w późnej fazie symptomatycznej chorób neurodegeneracyjnych (Cornacchia and Studer, 2017).

Technologia iPSC nieustannie rozwija się, na ten jednak moment wykorzystanie modeli zwierzęcych w nauce jest wciąż nieocenione. Szczególnie jeżeli chodzi o badania na poziomie całego organizmu. Istnieje wiele zwierzęcych modeli SCA3. Bezkręgowce *C. elegans* oraz *D. melanogaster* z ekspresją genu *Atx3* były użyteczne m.in. w badaniu toksyczności zmutowanej ATXN3 oraz przesiewowym poszukiwaniu związków terapeutycznych (Chan et al., 2002; Bilen and Bonini, 2007; Teixeira-Castro et al., 2011). Najpopularniejszym modelem wykorzystywanym w nauce jest jednak *Mus musculus* (Hickman et al., 2017). Genom myszy szczeputu C57BL został zsekwencjonowany w drugiej kolejności po ludzkim, a analiza porównawcza genomów wykazała, że dla 80% ludzkich genów istnieją mysie ortologi (Chinwalla et al., 2002; Church et al., 2009). Większość mysich modeli SCA3 to modele transgeniczne, z ekspresją cDNA ludzkiej zmutowanej ataksyny-3 lub jej fragmentu, pod kontrolą egzogennego promotora (Cemal et al., 2002; Griffin et al., 2004; Bichelmeier et al., 2007; Colomer Gould et al., 2007; Chou et al., 2008; Silva-Fernandes et al., 2010; Hübener et al., 2011). Modele te posłużyły m.in. do badania roli skróconych form ATXN3, mechanizmu lokalizacji jądrowej, zmian transkrypcyjnych i metabolicznych oraz ścieżki przekazywania sygnału w SCA3.

Stosunkowo niedawno powstały też dwa modele typu knock-in (Raman et al., 2015, 2017; Switonski et al., 2015). Modele tego typu, charakteryzują się ekspresją zmutowanego białka zbliżoną do naturalnej, jako że są wprowadzone w endogenne locus, w jednej kopii, i są pod kontrolą promotora naturalnego dla tego genu. Modele uzyskane przy pomocy technologii knock-in są dokładniejsze, w porównaniu z mniej finezyjnymi modelami transgenicznymi, u których nadekspresja transgenu wbudowanego w kilka miejsc w genomie pod kontrolą obcych promotorów prowadzi do niefizjologicznego poziomu białka w komórkach. To natomiast może zaburzać obraz choroby.

Pierwszy model SCA3 typu knock-in został wygenerowany w Instytucie Chemii Bioorganicznej PAN i nazwany został Ki91 (Switonski et al., 2015). Model ten został uzyskany poprzez wprowadzenie ludzkiego cDNA zawierającego egzon 8-11 genu *ATXN3* z 91 powtórzeniami CAG w egzonie 10, w miejsce mysich egzonów i intronów 7-11 (egzon 7 jest hybrydowy) mysiego genu *Atxn3*. Z uwagi na fakt, że egzony 1-7 w mysim genie *Atxn3* myszy i ludzkim *ATXN3* są bardzo podobne, nie było potrzeby aby je zastępować. Fenotyp charakterystyczny dla SCA3 w heterozygotycznym modelu Ki91 obejmuje zaburzenia motoryczne, formowanie agregatów białkowych w neuronach, zwyrodnienie i obumieranie neuronów w mózdku, powstawanie stanów zapalnych w mózgu, oraz niestabilność genetyczną powtórzeń CAG (Switonski et al., 2015). Na tej podstawie model Ki91 został uznany za użyteczny w badaniu patogenezy SCA3.

Pomimo postępu jaki dokonał się w dziedzinie badań chorób neurodegeneracyjnych, dokładna sekwenca zdarzeń składających się na skomplikowany patomechanizm tej grupy chorób wciąż nie jest znana. Prześledzenie krok po kroku zmian zachodzących w czasie choroby na poziomie organizmu i komórki, w dobrze skonstruowanym genetycznym modelu, może uzupełnić luki w brakującej wiedzy o procesie neurodegeneracji. A w konsekwencji może przyczynić się do opracowania skutecznej terapii tej nieuleczalnej grupy chorób.

4 CEL PRACY

Główym celem mojej pracy doktorskiej było zdefiniowanie mechanizmów patogennych, które prowadzą do rozwoju ataksji rdzeniowo-móżdżkowej typu 3. Analiza fenotypu behawioralnego oraz masowa identyfikacja zmian proteomicznych miała również na celu poznanie szczegółowej osi czasu w rozwoju ataksji rdzeniowo-móżdżkowej typu 3 w mysim modelu knock-in SCA3 Ki91. W ten sposób uzyskany miał zostać pełen obraz choroby na poziomie molekularnym, komórki oraz całego organizmu, a wzajemne powiązanie tych poziomów miało przynieść lepsze zrozumienie mechanizmu SCA3. W dalszej perspektywie badania wykonane w ramach niniejszej pracy mogą przybliżyć poznanie uniwersalnych mechanizmów neurodegeneracji, które mogą być wspólne także dla innych chorób neurodegeneracyjnych.

Cele szczegółowe pracy doktorskiej:

- Cel 1. Charakterystyka fenotypu i wyróżnienie stadiów choroby w mysim homozygotycznym modelu knock-in SCA3 Ki91 poprzez testy behawioralne i komórkowe.
- Cel 2. Identyfikacja procesów molekularnych, które inicjują proces neurodegeneracji, poprzez analizę białek o zmienionym poziomie w korze mózgowej i mózdku Ki91 w fazie pre-symptomatycznej SCA3 wysokoprzepustową metodą spektrometrii mas LC-MS/MS.
- Cel 3. Identyfikacja procesów molekularnych i określenie kolejności ich występowania w czasie progresji SCA3, w korze mózgowej i mózdku modelu Ki91 poprzez analizę zmian proteomicznych (LC-MS/MS).
- Cel 4. Wytypowanie białek mogących posłużyć jako biomarkery SCA3, na podstawie analizy proteomicznej LC-MS/MS kory mózgowej i mózdku Ki91.
- Cel 5. Szczegółowe zbadanie procesów molekularnych wytypowanych poprzez realizację celu 2 i 3, które mogą być zmienione w modelu SCA3 Ki91 przy pomocy testów funkcjonalnych i mikroskopii konfokalnej.

5

STRESZCZENIE PRAC I ICH INTERPRETACJA NA TLE PIŚMIENNICTWA PRZEDMIOTU

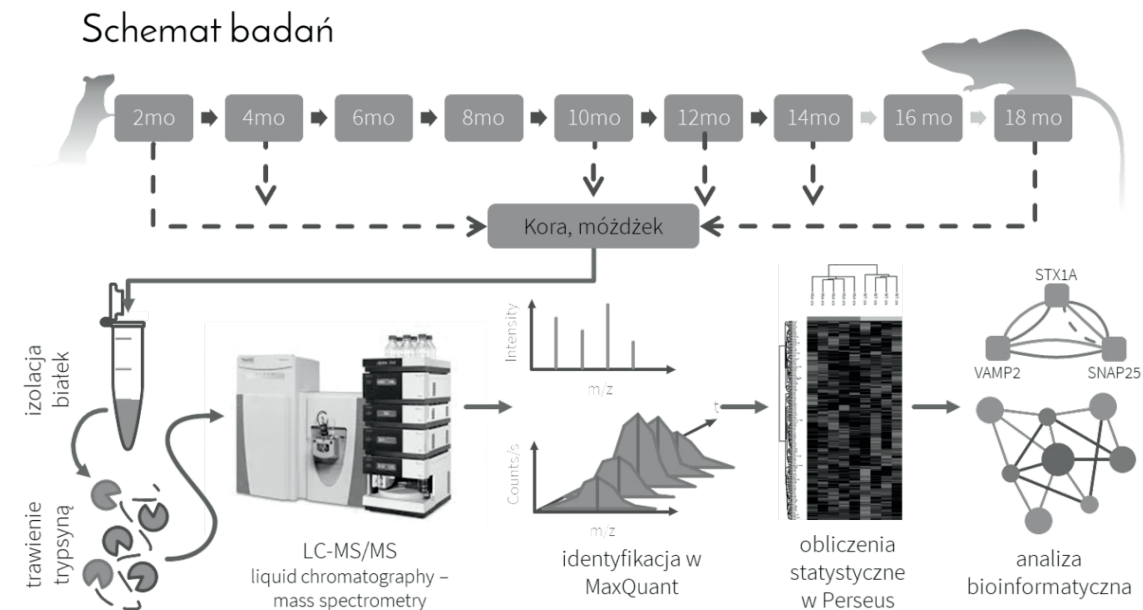
5.1. WSTĘP

Choroby neurodegeneracyjne są coraz bardziej powszechnie we współczesnych społeczeństwach. Charakteryzują się obumieraniem populacji neuronów specyficznej dla danej jednostki chorobowej, a konsekwencją są zaburzenia poznawcze, w tym pamięci tak jak w Chorobie Alzheimera i innych typach demencji lub poważne zaburzenia motoryczne jak w przypadku chorób poliglutaminowych czy choroby Parkinsona. W obu przypadkach końcowym efektem jest utrata samodzielności i kalectwo, wiążące się z koniecznością otoczenia opieką tej grupy osób, stanowiących coraz większy odsetek w społeczeństwie krajów, w których średnia długość życia ulega wydłużeniu. W tej różnorodnej grupie chorób obserwuje się wiele wspólnych lub podobnych zaburzeń na poziomie molekularnym i komórkowym w ośrodkowym układzie nerwowym, m.in. agregacja nieprawidłowo sfaldowanych białek, nieprawidłowe działanie systemu degradacji białek, czy zaburzony metabolizm energetyczny (Gan et al., 2018). Jednak całokształt patologicznych procesów wiodących do rozwoju chorób neurodegeneracyjnych, jak i kolejność w jakiej po sobie następują, nie jest znana. Odkrycie nadzędnych molekularnych mechanizmów tej grupy chorób jest podstawą do opracowania takich terapii, które będą precyzyjnie celować w źródło problemu, zamiast łagodzić skutki w zaawansowanych stadiach symptomatycznych.

Dobrym modelem do badania procesu neurodegeneracji są choroby poliglutaminowe (ang. polyQ), u których podłożem stoi ekspansja trójnukleotydowych powtórzeń CAG w sekwencjach kodujących kilku niepowiązanych ze sobą genów. Z powodu znanych monogenowych, dominujących mutacji wiodących do rozwoju chorób polyQ możliwe było wytworzenie różnych modeli zwierzęcych, w tym wielu modeli mysich, stanowiących bardzo użyteczne narzędzia obrazujące przebieg patogenezy bardzo podobny do choroby u pacjentów. Modele uzyskane przy pomocy technologii knock-in są dokładniejsze, w porównaniu z modelami transgenicznymi, ze względu na ekspresję genu na fizjologicznym poziomie. Modele knock-in mają również łagodniejszy fenotyp, w porównaniu z prostymi modelami z wprowadzonym egzogenem, co lepiej odzwierciedla przebieg choroby u pacjentów. Model na którym prowadziłam badania w ramach pracy doktorskiej jest właśnie modelem typu knock-in. Wygenerowany został w jednostce badawczej, w której prowadziłam badania, w Instytucie Chemii Bioorganicznej PAN, w rezultacie wcześniejszych prac zespołu (Switonski et al., 2015).

W niniejszej pracy doktorskiej podjęłam próbę odkrycia procesów komórkowych i ścieżek molekularnych, których rola nie została wcześniej zademonstrowana w patomechanizmie SCA3. Atutem projektu było wykorzystanie modelu Ki91, który jest precyzyjnym modelem ataksji rdzeniowo-móżdżkowej typu 3, należącej do grupy chorób neurodegeneracyjnych. Zdecydowaliśmy, że badania będą prowadzone na myszach homozygotycznych. W wyniku dwukrotnego zwiększenia ilości zmutowanego białka w mysim modelu oraz braku wpływu ze strony normalnej ataksyny-3, która może łagodzić przebieg choroby, spodziewanym efektem miało być nasilenie fenotypu w stosunku do myszy heterozygotycznych. Spowodowanie zaostrzenia fenotypu miało na celu bardziej precyzyjną obserwację zmian, które u myszy heterozygotycznych mogą być zbyt delikatne, aby zmierzyć je dostępymi testami. Kohortę myszy do badań w ramach pracy doktorskiej uzyskałam poprzez krzyżowanie par myszy o odpowiednim genotypie. Długość powtórzeń CAG u testowanych zwierząt wynosiła między 91 a 122, w wyniku ekspansji międzypokoleniowej. Szczegółowa analiza objawów choroby na poziomie behawioralnym jak i zmian molekularnych w poszczególnych stadiach choroby miała na celu ustalenie kolejności w jakiej dochodzi do zaburzeń procesów biologicznych. Kolejne testy behawioralne zdecydowano się prowadzić w odstępach 2-miesięcznych w celu wyodrębnienia fazy pre- i symptomatycznej. Wieki myszy, które okazały się być kluczowe w rozwoju choroby w testach behawioralnych, zostały wyselekcjonowane do analiz proteomicznych. Schemat badań pokazany jest na Rycinie 1.

W kolejnych rozdziałach przedstawię rezultaty badań wchodzących w skład niniejszej pracy doktorskiej, które zostały opisane w dwóch obszernych artykułach. W pierwszej kolejności omówię pracę, w której opisano zmiany w poziomie i fosforylacji białek w korze mózgowej i mózdku myszy Ki91 przy jednoczesnym braku zmian transkrypcyjnych na etapie presymptomatycznym (Wiatr et al., 2019). Następnie przedstawię artykuł, który stanowi kontynuację eksperymentów opublikowanych w pracy Wiatr et al. 2019 i który objął analizy wykonane w dalszych etapach choroby z obszerną analizą fenotypu behawioralnego oraz zmian w poziomie białek i testy funkcjonalne (Wiatr et al., 2021).



Ryc. 1 Schemat badań. Testy behawioralne obejmują zwierzęta w wieku 2 – 18 miesięcy. Analiza białek izolowanych z kory mózgowej i mózdku zwierząt 2, 4, 10, 12, 14 i 18-miesięcznych wykonywana była z wykorzystaniem wysokoprzepustowej metody spektrometrii mas i różnych programów i narzędzi informatycznych.

5.2. ALTERED LEVELS OF PROTEINS AND PHOSPHOPROTEINS, IN THE ABSENCE OF EARLY CAUSATIVE TRANSCRIPTIONAL CHANGES, SHAPE THE MOLECULAR PATHOGENESIS IN THE BRAIN OF YOUNG PRESYMPOMATIC KI91 SCA3/MJD MOUSE

Wiatr K, Piasecki P, Marczak Ł, Wojciechowski P, Kurkowiak M, Płoski R, Rydzanicz M, Handschuh L, Jungverdorben J, Brüstle O, Figlerowicz M, Figiel M.
Molecular Neurobiology 2019; 56(12): 8168–8202.
doi: 10.1007/s12035-019-01643-4

Niniejszy artykuł opisuje obraz zmian molekularnych na etapie pre-symptomatycznym w modelu SCA3 Ki91. Odkrycie wczesnych zmian molekularnych przed wystąpieniem pełnoobjawowej choroby neurodegeneracyjnej pozwala zdefiniować najbardziej fundamentalne mechanizmy choroby.

Pierwszym zadaniem w mojej pracy doktorskiej było utworzenie kohorty myszy ($n = 36$), składającej się z 18 homozygotycznych myszy Ki91 i 18 myszy kontrolnych bez zmodyfikowanego genu *Atxn3* (tło genetyczne C57BL), pochodzących ze wspólnych rozrodów myszy heterozygotycznych. Wykonałam szereg testów behawioralnych, w których przede wszystkim oceniałam różne parametry motoryczne i koordynację ruchową zwierząt, z wykorzystaniem testu Rotarod, testu prętów statycznych (ang. elevated beam walk), testu śladów, zautomatyzowanego testu prętów równoległych i testów punktowych. Przy pomocy testów behawioralnych ustaliłam, że 2-miesięczne myszy Ki91 nie wykazują żadnych różnic w zadaniach oceniających ich kondycję ruchową (Fig. 1 w artykule). Nie różniły się także wagą ciała. W ten sposób mogłam uznać wiek 2 miesięcy w modelu Ki91 za stadium pre-symptomatyczne. Wyodrębnienie wczesnej fazy pre-symptomatycznej jest kluczowe, aby móc precyźniej zidentyfikować procesy, które wiodą do neurodegeneracji i odróżnić je od tych, które są skutkiem choroby w zaawansowanym stadium. W mózdzku i korze mózgowej 2-miesięcznych myszy Ki91 wczesne procesy patologiczne zostały zainicjowane na poziomie komórkowym, m.in. agregaty ataksyny-3 zostały wykryte w niewielkiej ilości jąder komórkowych (Fig. 2 w artykule).

Do analiz molekularnych zdecydowano wybrać mózdzek i korę mózgową. Mózdzek stanowi jeden z głównych, znanych od wielu lat regionów neurodegeneracji w SCA3 (Koeppen, 2018). Natomiast kora mózgowa jest niezwykle złożoną strukturą, połączoną z niemal każdym regionem mózgu, zaangażowaną w wiele ważnych funkcji, w tym funkcji poznawczych i motorycznych i ostatnio również została powiązana z procesami chorobowymi w SCA3 (Schmidt et al., 2019; Guo et al., 2020a). Co ciekawe, w mózdzku i korze mózgowej Ki91 na etapie pre-symptomatycznym nie wykryto zmian transkryptomicznych z wykorzystaniem sekwenowania RNA. Jedyne różnice jakie wykryto w poziomie mRNA w stadium 2-miesięcznym, związane były z tłem genetycznym (Tabela 1- 3, Fig. 3, 4 i S6 w artykule). 5 spośród zidentyfikowanych genów o zmienionej ekspresji leży bardzo blisko locus *Atxn3*, a kolejne 3 geny były również skupione blisko siebie. Na podstawie tej obserwacji oraz analizy SNP, wywnioskowano, że loci te mają inne pochodzenie genetyczne niż reszta genomu myszy Ki91 (C57BL / 6) i że ich źródłem są komórki macierzyste 129sv, do których wprowadzono konstrukt genetyczny w czasie tworzenia modelu Ki91. Zmiany w ekspresji różnych genów wykazano dopiero w późniejszych etapach choroby, u 10- i 14- miesięcznych myszy Ki91, a część z nich pokazano również w ludzkich neuronach zróżnicowanych z komórek pobranych od pacjentów SCA3 (Tabela 4, S1 i S2, Fig. 5, 6 i S1 w artykule).

Po analizie wyników otrzymanych w sekwencjonowaniu RNA, potwierdzonych przez qPCR, zadaliśmy sobie pytanie czy w pre-symptomatycznym stadium SCA3 w modelu Ki91 zaobserwujemy zmiany w poziomie białek. Ataksyna-3 jest proteazą o aktywności deubikwitynazy, tak więc bezpośrednio moduluje poziom białek, kierując lub chroniąc je przed degradacją (Doss-Pepe et al., 2003; Riess et al., 2008; Singh et al., 2019; Herzog et al., 2020; Hill et al., 2021). Na jeszcze inne białka wpływa poprzez powinowactwo do ubikwityny łączonej przez lisynę w pozycji 63, a jej zmutowana forma sekwestruje szereg innych białek (Donaldson et al., 2003; Winborn et al., 2008; Chen and Sun, 2009). Pomimo to, do tej pory jedynie nieliczne prace podjęły tematykę zmian w poziomie białek, a żadna z nich nie pokazała globalnych zmian proteomicznych zachodzących w czasie rozwoju SCA3 (Hsieh et al., 2013; Kristensen et al., 2018; Duarte Lobo et al., 2020; Sowa et al., 2021). Dlatego w kolejnym etapie, wykonałam analizę proteomiczną z wykorzystaniem wysokoprzepustowej metody spektrometrii mas w podejściu label-free (LC-MS/MS) w regionach mózgu, które analizowane były poprzez sekwencjonowanie RNA. Analizowałam zarówno poziom białek jak i ich fosforylację za pomocą dwóch zestawów dedykowanych odczynników do wzbogacania w peptydy fosforylowane. Fosforylacja jest jedną z najczęstszych modyfikacji potranslacyjnych, wpływających na wiele procesów komórkowych (Ardito et al., 2017). Dzięki wyróżnieniu fazy pre-symptomatycznej możliwe było ustalenie, które z procesów biologicznych są najwcześniejsze i nie są jedynie skutkiem obumierania neuronów. Morfologię neuronów ocenialiłam za pomocą markerów na skrawkach mózgów pobranych od 2-miesięcznych myszy, w których nie zidentyfikowałam żadnych oznak degeneracji.

W analizie proteomicznej łącznie zidentyfikowałam 93 białka o zmienionym poziomie w mózdku i 133 białka w korze mózgowej (Fig. S2 i Tabela S6 w artykule). Natomiast różnice w poziomie fosforylacji zidentyfikowałam dla 83 białek w mózdku i aż 335 białek w korze mózgowej, przy czym część z tych białek miała zmieniony poziom fosforylacji w więcej niż jednej reszcie aminokwasowej. Co ciekawe, prawie wszystkie z tych białek miały obniżony poziom fosforylacji, co może wskazywać na jeszcze niepoznany mechanizm regulacji poziomu fosforylacji białek w SCA3. Ponadto, 68 % białek o zmienionej fosforylacji pokrywało się między mózdkiem i korą mózgową. Jednym ze zidentyfikowanych przez mnie białek o znacząco obniżonej fosforylacji w mózdku (w pozycji Ser-223) i korze mózgowej (w pozycji Ser-174) modelu Ki91 jest PAK1.

Kinaza PAK1 stanowiła centrum interakcji w sieci powiązań w mózdku, zarówno z białkami o zmienionym totalnym poziomie jak i białkami o zmienionej fosforylacji (Fig. 7 w artykule). Fosforylacja Ser-223 wydaje się być szczególnie istotna, jako że jest wymagana do aktywacji PAK1 i jest katalizowana przez kinazę CSNK2A1, która jest znanym interaktorem ataksyny-3 (Tao et al., 2008; Kim et al., 2015). Ponadto, wykazałam podwyższony poziom fosfatazy PP2B-A (PPP3CA), modulującej aktywność PAK1 oraz obniżenie fosforylacji ARPP19 / ENSA, które reguluje PPP3CA (Wlodarchak and Xing, 2016). PAK1 odgrywa rolę w szlakach komórkowych związanych głównie z organizacją i transportem cytoszkieletu, proliferacją i apoptozą, jest także powiązana z chorobami neurodegeneracyjnymi (Ma et al., 2012; Kim et al., 2016; UniProt: the universal protein knowledgebase, 2017). Wykazano m.in., że PAK1 promuje agregację polyQ w HD (Luo et al., 2008). Potencjalnie więc kinaza PAK1 i ścieżki sygnalowe, które reguluje mogą być ważnym komponentem patogenezy SCA3, wymagającym dalszych badań. W korze mózgowej, sieć interakcji białek o zmienionej fosforylacji była znacznie większa ze względu na większą ilość zidentyfikowanych białek o zmienionym poziomie fosforylacji (Fig. 7 w artykule). Obok PAK1 znalazły się takie kinazy jak BRSK1, BRSK2 zaangażowane w rozwojową ścieżkę wzrostania aksonów (ang. axon guidance), SRC, BRAF, wielofunkcyjne MAPK i GSK3B, CAMK2 istotna dla neurotransmisji oraz PRKC (Rankin et al., 2008; Winograd-Katz et al., 2011; Poplawski et al., 2012; Sample et al., 2015).

Analiza bioinformatyczna wykazała że za 77% zmian w poziomie fosforylacji w obu badanych tkankach odpowiedzialne są kinazy CK1 i 2, PKA, CDK2 oraz CAMK2, wg bazy danych PHOSIDA (Fig. 7 w artykule). Interakcja ataksyny-3 z kinazami GSK3B, CK2B i RPS6KA1 czy MAP3K1 zostały już wcześniej zademonstrowane (Fei et al., 2007; Tao et al., 2008; Kristensen et al., 2018).

Przy pomocy metody Western blot potwierdziłem zmieniony poziom kilku ważnych białek dla których dostępne były komercyjne przeciwciała (Fig. 8 w artykule). W mózdku wykazałem zmieniony poziom białka zaangażowanego w naprawę DNA (DDB1), oraz białek cytoskieleturnych NEFH i fosforylowanej formy białka Tau. W korze mózgowej zademonstrowałem zmieniony poziom białka PABP1, związanego z granulkami stresu sekwestrującymi mRNA, oligocytarnego MBP, tubuliny 3 i fosforylowanych form Tau i DARPP32.

Następnie, wyodrębniłem 3 grupy procesów komórkowych zidentyfikowanych przy użyciu bioinformatycznych baz danych ConsensusPathDB i ClueGO (Cytoscape), w które zaangażowane były białka o zmienionym poziomie w mózgu Ki91 (Fig. 9 i S3, Tabele 5-12 i S3-S5 w artykule). W pierwszej grupie znalazły się białka, które biorą udział w naprawie DNA oraz modulują poziom białek w komórce. Znalazły się tutaj m.in. czynniki inicjacji translacji i podjednostki rybosomów, które, co ciekawe, w przeważającej większości miały podwyższony poziom w korze mózgowej Ki91. Do drugiej grupy zostały zaliczone białka odpowiedzialne za organizację organelli i innych struktur w neuronie, takich jak pęcherzyki, cytoskiele, aksony i dendryty, których zmieniony poziom może wynikać ze zmian w grupie 1. Zarówno w korze mózgowej jak i w mózdku zidentyfikowałem zmieniony poziom różnych podjednostek tubulin i dynein lub białek mających rolę w rekrutacji pęcherzyków transportowych do kompleksu dyneina-dynaktyna. Może mieć to związek z udowodnioną interakcją ataksyny-3 z tymi białkami, która może być zmieniona w zmutowanej formie (Burnett and Pittman, 2005; Mazzucchelli et al., 2009). Ponadto, w korze mózgowej była ogromna grupa białek o obniżonym poziomie fosforylacji odgrywających kluczową rolę w transporcie aksonalnym wzduż mikrotubul. W trzeciej grupie zostały uwzględnione białka związane z zaburzonymi funkcjami neuronu, wynikającymi ze zmianami w grupie 2, takimi jak metabolizm energetyczny i transport pęcherzyków. Liczne białka o zmienionym poziomie i fosforylacji w obu testowanych tkankach Ki91 to białka budujące pęcherzyki synaptyczne, regulujące ich transport i uwalnianie lub w inny sposób związane z neurotransmisją. Grupa białek odpowiedzialnych za metabolizm energetyczny miała podwyższony poziom zarówno w mózdku jak i korze mózgowej. Pośród nich były SDHB i NDUFA4, dla których wykazano interakcję z ataksyną-3 (Kristensen et al., 2018). Co ciekawe, nie było wśród nich żadnych białek fosforylowanych. I wreszcie kilka białek o zmienionym poziomie w mózgu Ki91 sugeruje, że apoptoza i mitofagia (np. VDAC1) mogą odgrywać rolę już na tym wczesnym etapie. Należy jednak podkreślić, że nie zidentyfikowano żadnych klasycznych markerów apoptotycznych. W ostatniej części pracy przy użyciu baz danych Dropviz, Brainmap (Allen Brain Atlas) i ConsensusPathDB ustaliłem, że białka o zmienionym poziomie i fosforylacji ulegają ekspresji przede wszystkim w neuronach (szczególnie w neuronach hamujących) i lokalizują w największej ilości w egzosomach, cytoskielecie i mitochondriach (Fig. S4 i S5, Tabela S7).

Podsumowując, etap pre-symptomatyczny w modelu SCA3 Ki91 charakteryzuje się brakiem zmian na poziomie transkryptomicznym przy jednoczesnej zmianie w poziomie dużej liczby białek i ich fosforylacji (Fig. 10 w artykule). Wśród białek i ich fosforylowanych form o zmienionym poziomie była duża liczba białek mitochondrialnych i związanych z inicjacją translacji. Najliczniejszą grupę zmienionych białek i białek fosforylowanych stanowiły jednak białka cytoskieletu, pęcherzyków transportowych oraz regulujące transport aksonalny.

5.3. BROAD INFLUENCE OF MUTANT ATAXIN-3 ON THE PROTEOME OF THE ADULT BRAIN, YOUNG NEURONS, AND AXONS REVEALS CENTRAL MOLECULAR PROCESSES AND BIOMARKERS IN SCA3/MJD USING KNOCK-IN MOUSE MODEL

Wiatr K, Marczak L, Perot JB, Brouillet E, Flament J, Figiel M

W DRUKU

doi: 10.3389/fnmol.2021.658339

Niniejsza publikacja stanowi kontynuację badań opisanych opublikowanych w (Wiatr et al., 2019) i podsumowanych w poprzednim podrozdziale. Po wyróżnieniu fazy pre-symptomatycznej w 2-miesięcznych myszach Ki91 kontynuowałam testy behawioralne na tej samej kohortie myszy. Testy te miały na celu ustalenie wieku myszy Ki91, w którym pojawią się pierwsze objawy motoryczne lub inne oznaki choroby, a następnie śledzenie rozwoju zidentyfikowanych zmian behawioralnych w czasie.

Po analizie otrzymanych wyników z testów behawioralnych wyróżniłam 3 fazy choroby następujące po fazie pre-symptomatycznej: 1. faza ze spowolnieniem przyrostu masy ciała (myszy 4-10-miesięczne), 2. wcześnie faza symptomatyczna (myszy 12-14-miesięczne), w której obserwowała jest zaburzona koordynacja ruchowa, 4. Późna faza symptomatyczna (myszy 16-18 miesięcy), w której pogorszeniu ulega koordynacja ruchowa, występują zaburzenia chodu, postawy ciała, przykurcze kończyn, stany lękowe, a także osłabiona jest siła mięśniowa. Gradacja symptomów w modelu Ki91 dobrze oddaje rozwój objawów choroby obserwowany u pacjentów SCA3 (Fig. 1 w artykule) (Coutinho and Andrade, 1978; Jacobi et al., 2015; Pulido-Valdeolivas et al., 2016; Coarelli et al., 2018). Ponadto, wykazano że myszy 18-miesięczne cechuje atrofia wielu regionów mózgu Ki91, w tym obszarów bogatych w aksony takie jak ciało modzelowe (Fig. 2 w artykule). Na tym etapie choroby, zidentyfikowałam również liczne, dużych rozmiarów inkluzje ataksyny-3 w jądrach komórkowych w różnych regionach mózgu, w tym mózdku i korze mózgowej (Fig. 3 w artykule). Inkluzje te były zdecydowanie liczniejsze niż u zwierząt pre-symptomatycznych, u których tylko w nielicznych jądrach można było zaobserwować agregaty zmutowanego białka (Wiatr et al., 2019). Duża liczba inkluzji pozytywnych na ATXN3 rezydowała w jądrach głębokich mózdku, co wiąże się prawdopodobnie z dużą podatnością tego rejonu na degenerację (Koeppen, 2018). Co istotne, zademonstrowałam też obecność inkluzji ataksyny-3 w aksonach mózdkowych Ki91 w wieku 18 miesięcy, czego nie obserwowałam u myszy pre-symptomatycznych. Obecność inkluzji w aksonach zademonstrowano także u pacjentów SCA3 (Seidel et al., 2010). Duża część inkluzji w Ki91 była ubikwitynowana (Fig. S1 i S2 w artykule).

Następnie, wybrałam kluczowe wieki w rozwoju SCA3 w modelu Ki91 w celu wykonania analiz proteomicznych. Badane punkty czasowe to 4 miesiące (pierwszy symptom w postaci obniżonej masy ciała), 10 miesięcy (tuż przed wystąpieniem pierwszych objawów motorycznych), 12 i 14 miesięcy (pojawienie się i rozwój pierwszych symptomów motorycznych) oraz 18 miesięcy jako stadium końcowe. Podobnie jak w poprzedniej pracy, analizowałam dwa regiony mózgu – mózdek i korę mózgową metodą LC-MS/MS (Tabele S1-3, Fig. S3 i S5, w artykule). Badanie zmian w poziomie białek w wiekach odpowiadających przelomowym punktom czasowym w testach behawioralnych miało w zamyśle pozwolić na ustalenie kolejności zdarzeń molekularnych, które wiodą do neurodegeneracji. Poziom wybranych białek sprawdziłam także metodą vacuum dot blot (Fig. S4 w artykule). Białka o zmienionym poziomie w wiekach 4 – 14 miesięcy Ki91 poddałam analizie z użyciem

ConsensusPathDB, mającej na celu identyfikację obszarów subkomórkowych, procesów komórkowych i ścieżek molekularnych, które mogą być zaburzone w określonym stadium choroby (Fig. 4 w artykule). Na podstawie analizy w ConsensusPathDB wyodrębniłam 5 kategorii procesów i rejonów subkomórkowych, z którymi związane są białka o zmienionym poziomie. Były to kolejno: transport pęcherzyków i endocytoza; transmisja synaptyczna; cytoszkielet i transport wzduż mikrotubul; metabolizm energetyczny i modulacja poziomu białek.

Ustaliłam, że białka o zmienionym poziomie lokalizują w różnych obszarach komórki, w tym w pęcherzykach, cytoszkielecie i mitochondriach. W późniejszych wiekach (10 miesięcy i więcej) zwiększa się ilość białek o zmienionym poziomie, które lokalizują w lizosomach, fagosomach i proteasomie, a także w pęcherzykach synaptycznych i synapsach i związanych z metabolizmem. Ponieważ jest to okres, w którym pojawiają się pierwsze symptomy motoryczne w Ki91, wymienione procesy mogą mieć istotne znaczenie w patogenezie SCA3. Konsekwentnie, białka o zmienionym poziomie w kolejnych wiekach zaangażowane są w takie procesy jak metabolizm energetyczny, formowanie cytoszkieletu, transport wzduż aksonu, przekaźnictwo synaptyczne, a także degradacja w proteasomie i apoptoza. Procesy komórkowe, w które zaangażowane były białka o zmienionym poziomie w mózdku i korze mózgowej były zasadniczo zbliżone. Jedną z różnic stanowił większy udział białek o zmienionym poziomie, związanych z przekaźnictwem synaptycznym, w korze mózgowej. Wśród zidentyfikowanych białek, które mogą być istotne dla patogenezy SCA3 należy wymienić QDPR i GLUL zaangażowane w metabolizm neurotransmiterów, CRYAB stabilizujący cytoszkielet oraz CA2, związane z kontrolą transportu mleczanu, który jest ważnym surowcem energetycznym dla neuronów (Ghosh et al., 2007; Houck and Clark, 2010; Stridh et al., 2012; Karus et al., 2015; Cox and Ecroyd, 2017; Zhu and Reiser, 2018; Breuer et al., 2019; Kurosaki et al., 2019; Zhou et al., 2019).

Analizę proteomiczną późnego symptomatycznego stadium w wieku 18-miesięcy przeprowadziłam osobno, na myszach pochodzących z kohorty behawioralnej. Umożliwiło mi to powiązanie zmian w poziomie białek z grupami fenotypowymi. Na podstawie skali punktowej, którą poddałam testowi statystycznemu, wyodrębniłam fenotyp łagodny, umiarkowany i ciężki w finalnym stadium testów (Fig. S6 w artykule). Fenotyp ciężki charakteryzował się obniżeniem poziomu białek związanych z transportem wewnętrzkomórkowym i aksonalnym (m.in. KLC1, KIF5C, ATCAY). Jedno z białek o podwyższonym poziomie w mózdku myszy Ki91 z ciężkim fenotypem, KPNA4, należy do tej samej rodziny co KPNA3, której rola w transporcie ataksyny-3 do jądra komórkowego została wcześniej zademonstrowana (Sowa et al., 2018). Białka o zmniejszonym poziomie w łagodnym fenotypie były związane z mitochondriami w mózdku i synapsą w korze mózgowej. Natomiast białka o zwiększym poziomie w mózdku w grupie łagodnej to przede wszystkim białka cytoszkieletarne.

Na podstawie wyników uzyskanych we wszystkich badanych wiekach opracowałam hipotezę zaburzeń w transporcie pęcherzyków synaptycznych, mitochondriów i lizosomów wzduż aksonu, na skutek czego następuje degeneracja aksonów, a później także ciał komórek nerwowych. Podobne zaburzenie obserwuje się w innych chorobach neurodegeneracyjnych, a interakcja ataksyny-3 z tubuliną i dyneiną i obecność agregatów ATXN3 w aksonach sugerują, że dysfunkcja aksonów może być komponentem patogenezy SCA3 (Burnett and Pittman, 2005; Mazzucchelli et al., 2009; Seidel et al., 2010). Dlatego, w kolejnym etapie przeprowadziłam eksperymenty mające na celu wykazanie, że wcześnie patogenne procesy SCA3 zachodzą w aksonach.

Wyprowadziłam kulturę hodowli neuronów kortikalnych i mózdkowych *in vitro* z myszy Ki91 i kontrolnych (C57BL6), z których izolowałam osobno aksony i część somatodendryczną. W tym celu wykorzystałam zmodyfikowane komory Boydena, które separamają aksony od ciał komórek nerwowych poprzez porowy filtr. Wielkość porów (1 µm)

pozwala przerastać jedynie cienkim wypustkom – w pierwszej kolejności aksonom. Następnie analizowałam, które białka lokalizują w zmienionej ilości w aksonach w stosunku do części somatodendrytycznej neuronów pochodzących z modelu SCA3 Ki91 w porównaniu do kontroli (Fig. 5, 6 i S7, Tabele S4-8 w artykule). Analiza białek, które znajdują się w aksonach w zmienionej ilości miała na celu pozwolić na wstępna ocenę czy w modelu SCA3 Ki91 występuje zaburzenie transportu aksonalnego i których organelli lub białek dotyczy. Wyniki tej analizy wykazały grupę białek związanych z maszynerią translacyjną, które były wzbogacone w aksonach Ki91 zarówno w neuronach kortikalnych jak i mózdkowych. Wzbogacenie aksonów Ki91 w stosunku do somy i w porównaniu do kontroli w białka związane z translacją w aksonach Ki91 może być odpowiedzią komórki na stres, na co wskazuje też podwyższony poziom kilku innych białek, jak TPP1 czy TMEM33 (Baleriola and Hengst, 2015; Sakabe et al., 2015; Mukherjee et al., 2019). Białka rybosomowe i wiążące RNA są także składnikiem granulek stresowych, które sekwestrują mRNA w celu ochrony w czasie stresu komórkowego i wstrzymania translacji transkryptów, które w tej sytuacji nie są kluczowe dla funkcjonowania komórki (Sossin and DesGroseillers, 2006; El Fatimy et al., 2016). Jeden ze znanych komponentów takich granulek, FXR2, był również wzbogacony w mózdkowych aksonach Ki91. Natomiast, grupa białek związanych z cytoskielem, transportem i mitochondriami wykazała obniżony poziom w aksonach SCA3 w stosunku do somy i porównaniu z kontrolą. W tej grupie znalazły się m.in. komponenty SNARE, odpowiedzialne za transport pęcherzyków, takie jak NAPA (a.k.a. α -SNAP), VTI1B i NSF. Co ważne, NSF jest niezbędnym białkiem dla funkcjonowania neuronów, a jego obniżony poziom powoduje zatrzymanie transportu przez błonę komórkową i śmierć komórek nerwowych (Stenbeck, 1998; Emperador-Melero et al., 2018; Yuan et al., 2018). Białka zubożone w aksonach Ki91, wskazujące na zmieniony transport aksonalny obejmowały także ważne regulatory transportu mitochondriów i pęcherzyków, takie jak ACTR1A i ANK2 (Holleran et al., 1996; Moughamian et al., 2013; Lorenzo et al., 2014). Co istotne, zmieniony poziom ACTR1A, NAPA i NSF zidentyfikowałam w poprzednim eksperymencie również w mózdku Ki91. Z uwagi na to, że wśród białek zubożonych w aksonach Ki91 znalazło się kilka białek mitochondrialnych, zaburzony transport aksonalny w SCA3 może dotyczyć właśnie tych organelli.

Ta obserwacja współgra również z następnym eksperymentem, w którym wykazałam deficit w metabolizmie energetycznym neuronów mózdkowych Ki91 w kulturze *in vitro* w teście funkcjonalnym Seahorse (Agilent, CA, USA). Test obejmował pomiar szybkości zakwaszania komórki (wskazujący na tempo glikolizy) i pomiar zużycia tlenu (Fig. 7 i S8 w artykule). Co ważne, deficit energii występuje wcześnie w neuronach SCA3 izolowanych z młodych myszy 5 dni po urodzeniu, a zatem nie jest zdarzeniem wtórnym wynikającym z wcześniejszego uszkodzenia neuronów. Interesującym aspektem tego eksperymentu były różnice w fenotypie oksydatywnej fosforylacji w zależności od stadium rozwojowego neuronów *in vitro*. W DIV (ang. day *in vitro*) 3 i 11, w których w kulturze obecne są jeszcze progenitory neuronalne obserwowałam wyższe zużycie tlenu przez komórki Ki91 w porównaniu z kontrolą. Może być to odpowiedź komórek SCA3 na inicjację patologicznych procesów, wiążących się z wyższym zapotrzebowaniem energetycznym. W późniejszych dniach hodowli (DIV 18 i 21) zużycie tlenu w hodowlach Ki91 drastycznie spadło w porównaniu z kontrolą. Na tym etapie w kulturze *in vitro* nie ma już progenitorów i neurony, które w tym stadium powinny czerpać swoje główne źródło energii z oksydatywnej fosforylacji nie wytwarzają jej dostatecznej ilości. Można spekulować, że taka sytuacja wynika z defektu w wymianie mitochondriów między somą a zakończeniem nerwowym w transporcie aksonalnym.

W kolejnym eksperymencie, zademonstrowałam podwyższony poziom fosforylacji neurofilamentów i akumulację neurofilamentów niefosforylowanych w mózdku symptomatycznych myszy SCA3 Ki91 (Fig. 8 w artykule). Akumulacja neurofilamentów

niefosforylowanych związana jest najczęściej z uszkodzeniem aksonów, natomiast zwiększona fosforylacja neurofilamentów jest często oznaką wadliwego transportu, również związanego z mitochondriami. Jest to więc kolejny proces sugerujący dysfunkcję aksonów, tym razem nie w neuronach pobranych z mysich embrionów/noworodków, a u dorosłych 12-miesięcznych myszy wykazujących objawy motoryczne.

W ostatnim eksperymencie, pokazałam akumulację pęcherzyków z ekspresją markerowego białka RAB7 w somie i aksonach neuronów mózdkowych Ki91 *in vitro* (Fig.9 w artykule). Pęcherzyki pozytywne na RAB7 były powiększone i było ich więcej w Ki91, co może wskazywać na ich zaburzony transport. Co więcej, RAB7 jest markerem populacji pęcherzyków komórkowych, nazywanych późnymi endosomami. Ostatnio została zademonstrowana nieznana wcześniej rola późnych endosomów w transporcie mRNA i maszynery translacyjnej w aksonach (Cioni et al., 2019). Ponadto, inkluzje komórkowe zaburzają aksonalny transport endosomów i autofagosomów (Volpicelli-Daley et al., 2014; Guo et al., 2020b). W połączeniu z eksperymentem, w którym pokazałam wzmacnianie aksonów Ki91 w białka związane z translacją, sugeruje to istnienie wcześniego patomechanizmu w SCA3 opierającego się na zaburzonym transporcie i homeostazie białek w aksonach.

Podsumowując, w niniejszym artykule opisałam po raz pierwszy globalne zmiany z poziomie białek, które zachodzą w określonych fenotypach i stadiach choroby. Po raz pierwszy wykazałam, że neurony SCA3 nie dokonują prawidłowo przejścia z glikolizy do oksydatywnej fosforylacji, typowego dla zdrowych neuronów. Nowym odkryciem była także identyfikacja białek o zmienionej lokalizacji między somą a aksonem w SCA3, a także nie pokazana do tej pory akumulacja pęcherzyków RAB7, oraz neurofilamentów w neuronach mózdkowych Ki91. Zaproponowałam patomechanizm choroby oparty na niedostatecznej produkcji energii w mitochondriach, zaburzonej homeostazie białek i zaburzonym transporcie aksonalnym organelli takich jak mitochondria i pęcherzyki (Fig. 10 w artykule). Hipoteza ta wskazuje dalszy kierunek badań, w których powinny zostać przeprowadzone bezpośrednie eksperymenty wykazujące upośledzenie transportu aksonalnego w SCA3.

6

PODSUMOWANIE I PERSPEKTYWY

Choroby neurodegeneracyjne stanowią poważny problem dla społeczeństw, w którym średnia życia ulega wydłużeniu. Mechanizm wiodący do neurodegeneracji wciąż jest nie w pełni poznany, co skutkuje brakiem skutecznych terapii. Choroby polyQ, takie jak SCA3, ze względu na znaną etiologię mogą stanowić model innych chorób neurodegeneracyjnych, z którymi dzielą wiele wspólnym cech. Aby móc odróżnić procesy, które są przyczyną neurodegeneracji od tych, które są jedynie skutkiem obumierania neuronów kluczowe jest użycie pre-symptomatycznego modelu choroby. Dlatego wyróżnienie fazy pre-symptomatycznej w modelu SCA3 Ki91 przy użyciu wielu testów, oceniających różnorodne parametry było ważnym etapem. Model ten w określonych stadiach, zarówno pre- jak i symptomatycznym, może posłużyć do wielu dalszych badań.

Wielkoskalowa identyfikacja zmian w poziomie białek umożliwiła predykcję procesów i ścieżek molekularnych, które mogą być zaangażowane w patogenezę SCA3. Najważniejsze procesy zostały potwierdzone w testach funkcjonalnych, m.in. zaburzony metabolizm energetyczny w neuronach SCA3 oraz upośledzenie organizacji i funkcji cytoszkieletu. Choć dysfunkcja mitochondrialna została już wcześniej zademonstrowana w SCA3, w niniejszej pracy nowo prezentowanym aspektem jest niepowodzenie w przejściu neuronów z glikolizy do oksydatywnej fosforylacji, która jest głównym procesem pozyskiwania energii przez dojrzałe neurony. Zmieniona lokalizacja białek między aksonem a somą w neuronach SCA3 jest kolejną poszlaką, że proces transportu aksonalnego w SCA3 może być zaburzony. W celu potwierdzenia tego zjawiska wykonałam wstępne badania mające na celu bezpośrednie wykazanie upośledzenia transportu mitochondriów w aksonach SCA3, wykorzystując metodę obrazowania *in vivo*. Proces ten jest jednak złożony i wymaga głębszych analiz. Niemniej, wyznacza nowy fascynujący kierunek dla przyszłych badań, którego rezultatem potencjalnie może być powiązanie deficytu w oddychaniu komórkowym w neuronach SCA3 z zaburzeniem transportu aksonalnego mitochondriów.

Na zaburzenie transportu w aksonach SCA3 wskazuje także akumulacja pęcherzyków i neurofilamentów w neuronach mózdkowych modelu Ki91. Bardzo ciekawym odkryciem jest też wzbogacenie aksonów SCA3 w elementy maszynerii translacyjnej, a także globalne obniżenie fosforylacji białek w mózgu SCA3. Interesującym byłoby też zbadać zmiany w innej modyfikacji potranslacyjnej, bezpośrednio wiążącej się z funkcją ataksyny-3, tj. ubikwitynacji. Podsumowując, w mojej pracy doktorskiej zidentyfikowałam wiele nowych zmian na poziomie białek i procesów komórkowych SCA3, które wytyczają nowe kierunki badań mogące przybliżyć poznanie patomechanizmu tej choroby, wiodącego do neurodegeneracji. Podsumowanie odkryć w niniejszej pracy doktorskiej zaprezentowane jest w formie graficznej na Rycinie 2.

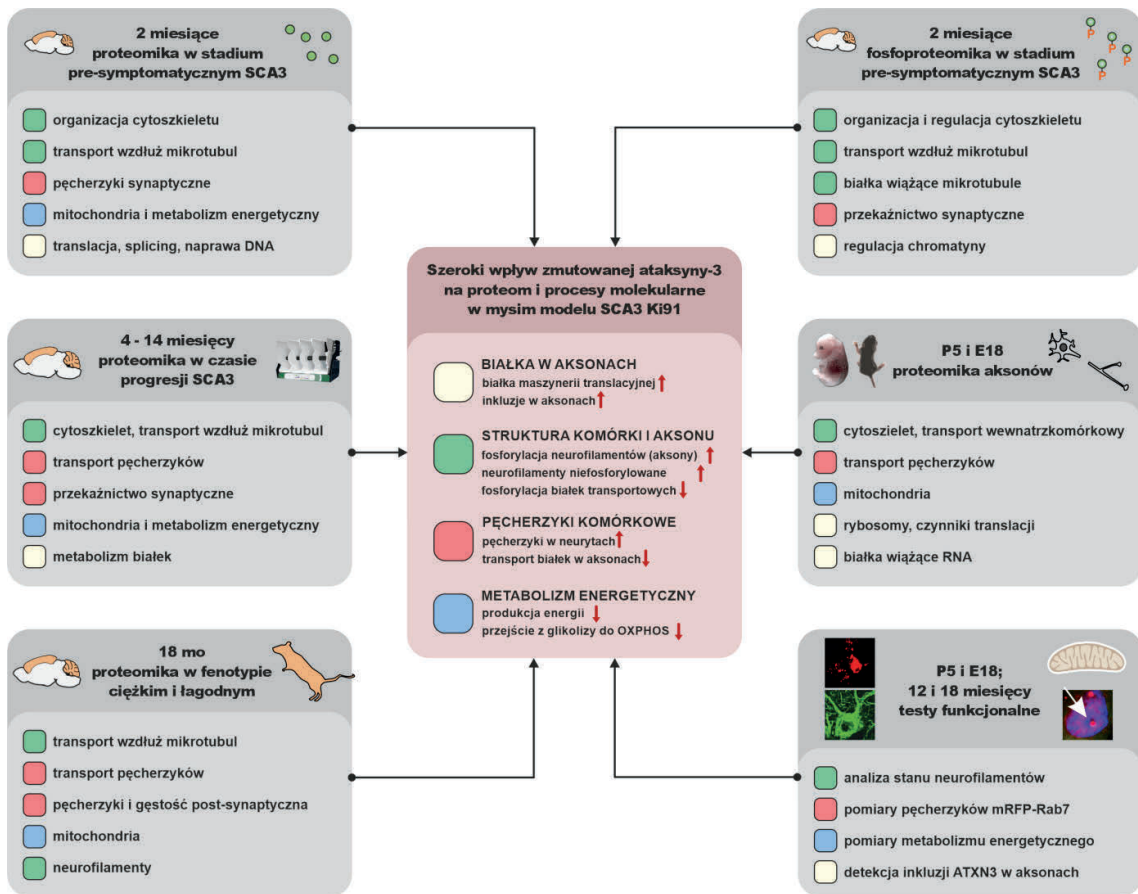
NAJWAŻNIEJSZYMI OSIĄgniĘCIAMI OPISANYMI W NINIEJSZEJ ROZPRAWIE SA:

1. Charakterystyka modelu SCA3 Ki91 pod względem molekularnym i behawioralnym.

- ~ Wyróżnienie fazy pre- i symptomatycznej w mysim modelu SCA3 Ki91.
- ~ Globalna identyfikacja zmian w poziomie fosforylacji białek w korze mózgowej i mózdziku Ki91 na etapie pre-symptomatycznym za pomocą wysokoprzepustowej metody spektrometrii mas.
- ~ Odkrycie zmian w poziomie i fosforylacji kinaz białkowych, m.in. PAK1, CAMK2, MAPK i GSK3B.
- ~ Zidentyfikowanie po raz pierwszy za pomocą wysokoprzepustowej metody spektrometrii mas globalnych zmian w poziomie białek w korze mózgowej i mózdziku SCA3 w modelu Ki91 na etapie pre-symptomatycznym i w czasie progresji choroby. Do ważnych białek mogących posłużyć jako biomarkery SCA3 w fazie pre-symptomatycznej należą m.in. DDB1, NEDD8, TRIM28, PAPC1, GJA1, NDRG1, TUBA1A, DYNC1I1, ITPR3, GAD1 i MT-CO3.

2. Zaproponowanie modelu patomechanizmu SCA3 opartego o defekt transportu w aksonach i wytyczenie nowych kierunków badań nad różnymi procesami i ścieżkami molekularnymi w SCA3.

- ~ Odkrycie po raz pierwszy zmienionej lokalizacji białek między somą a aksonem SCA3 i w porównaniu z kontrolą w hodowli neuronów mózdkowych i kortikalnych wyprowadzonych z mysich embrionów (E18)/noworodków (P5).
- ~ Identyfikacja zwiększonej ilości elementów maszyneryi translacyjnej w aksonach SCA3 Ki91, takich jak podjednostki rybosomów, białka wiążące RNA i czynniki translacyjne oraz zmniejszonej ilości białek związanych z transportem, pęcherzykami i mitochondriami.
- ~ Odkrycie zaburzonej struktury cytoszkieletu i wielu białek regulujących jego funkcję, takich jak neurofilamenty, tubuliny oraz białka wiążące się z mikrotubulami i aktyną.
- ~ Wykazanie akumulacji pęcherzyków Rab7 w aksonach i ciałach neuronów mózdkowych SCA3 Ki91.
- ~ Po raz pierwszy wykazanie defektu przejścia z glikolizy do oksydatywnej fosforylacji w neuronach mózdkowych SCA3 reprezentujących wcześnie stadium rozwojowe.



Ryc. 2. Graficzne podsumowanie szerokiego wpływu zmutowanej ataksyny 3 na proteom i procesy komórkowe w mysim modelu knock-in SCA3 / MJD.

BIBLIOGRAFIA

- Akçimen, F., Martins, S., Liao, C., Bourassa, C. V., Catoire, H., Nicholson, G. A., et al. (2020). Genome-wide association study identifies genetic factors that modify age at onset in Machado-Joseph disease. *Aging* 12, 4742–4756. doi:10.18632/aging.102825.
- Antony, P. M. A., Mäntele, S., Mollenkopf, P., Boy, J., Kehlenbach, R. H., Riess, O., et al. (2009). Identification and functional dissection of localization signals within ataxin-3. *Neurobiol. Dis.* 36, 280–292. doi:10.1016/j.nbd.2009.07.020.
- Ardito, F., Giuliani, M., Perrone, D., Troiano, G., and Lo Muzio, L. (2017). The crucial role of protein phosphorylation in cell signaling and its use as targeted therapy (Review). *Int. J. Mol. Med.* 40, 271–280. doi:10.3892/ijmm.2017.3036.
- Baleriola, J., and Hengst, U. (2015). Targeting axonal protein synthesis in neuroregeneration and degeneration. *Neurother. J. Am. Soc. Exp. Neurother.* 12, 57–65. doi:10.1007/s13311-014-0308-8.
- Bence, N. F., Sampat, R. M., and Kopito, R. R. (2001). Impairment of the ubiquitin-proteasome system by protein aggregation. *Science* 292, 1552–1555. doi:10.1126/science.292.5521.1552.
- Berke, S. J. S., Chai, Y., Marrs, G. L., Wen, H., and Paulson, H. L. (2005). Defining the role of ubiquitin-interacting motifs in the polyglutamine disease protein, ataxin-3. *J. Biol. Chem.* 280, 32026–32034. doi:10.1074/jbc.M506084200.
- Berke, S. J. S., Schmied, F. A. F., Brunt, E. R., Ellerby, L. M., and Paulson, H. L. (2004). Caspase-mediated proteolysis of the polyglutamine disease protein ataxin-3. *J. Neurochem.* 89, 908–918. doi:10.1111/j.1471-4159.2004.02369.x.
- Bettencourt, C., Santos, C., Kay, T., Vasconcelos, J., and Lima, M. (2008). Analysis of segregation patterns in Machado-Joseph disease pedigrees. *J. Hum. Genet.* 53, 920–923. doi:10.1007/s10038-008-0330-y.
- Bichelmeier, U., Schmidt, T., Hübener, J., Boy, J., Rüttiger, L., Häbig, K., et al. (2007). Nuclear Localization of Ataxin-3 Is Required for the Manifestation of Symptoms in SCA3: In Vivo Evidence. *J. Neurosci.* 27, 7418–7428. doi:10.1523/JNEUROSCI.4540-06.2007.
- Bilen, J., and Bonini, N. M. (2007). Genome-wide screen for modifiers of ataxin-3 neurodegeneration in Drosophila. *PLoS Genet.* 3, 1950–1964. doi:10.1371/journal.pgen.0030177.
- Breuer, M., Guglielmi, L., Zielonka, M., Hemberger, V., Kölker, S., Okun, J. G., et al. (2019). QDPR homologues in *Danio rerio* regulate melanin synthesis, early gliogenesis, and glutamine homeostasis. *PloS One* 14, e0215162. doi:10.1371/journal.pone.0215162.
- Breuer, P., Haacke, A., Evert, B. O., and Wüllner, U. (2010). Nuclear aggregation of polyglutamine-expanded ataxin-3: fragments escape the cytoplasmic quality control. *J. Biol. Chem.* 285, 6532–6537. doi:10.1074/jbc.M109.036335.
- Burnett, B. G., and Pittman, R. N. (2005). The polyglutamine neurodegenerative protein ataxin 3 regulates aggresome formation. *Proc. Natl. Acad. Sci. U. S. A.* 102, 4330–4335. doi:10.1073/pnas.0407252102.
- Cemal, C. K., Carroll, C. J., Lawrence, L., Lowrie, M. B., Ruddle, P., Al-Mahdawi, S., et al. (2002). YAC transgenic mice carrying pathological alleles of the MJD1 locus exhibit a mild and slowly progressive cerebellar deficit. *Hum. Mol. Genet.* 11, 1075–1094. doi:10.1093/hmg/11.9.1075.
- Chai, Y., Koppenhafer, S. L., Bonini, N. M., and Paulson, H. L. (1999a). Analysis of the role of heat shock protein (Hsp) molecular chaperones in polyglutamine disease. *J. Neurosci. Off. J. Soc. Neurosci.* 19, 10338–10347.

- Chai, Y., Koppenhafer, S. L., Shoesmith, S. J., Perez, M. K., and Paulson, H. L. (1999b). Evidence for proteasome involvement in polyglutamine disease: localization to nuclear inclusions in SCA3/MJD and suppression of polyglutamine aggregation in vitro. *Hum. Mol. Genet.* 8, 673–682. doi:10.1093/hmg/8.4.673.
- Chai, Y., Wu, L., Griffin, J. D., and Paulson, H. L. (2001). The role of protein composition in specifying nuclear inclusion formation in polyglutamine disease. *J. Biol. Chem.* 276, 44889–44897. doi:10.1074/jbc.M106575200.
- Chakraborty, A., Tapryal, N., Venkova, T., Mitra, J., Vasquez, V., Sarker, A. H., et al. (2020). Deficiency in classical nonhomologous end-joining-mediated repair of transcribed genes is linked to SCA3 pathogenesis. *Proc. Natl. Acad. Sci. U. S. A.* 117, 8154–8165. doi:10.1073/pnas.1917280117.
- Chan, H. Y. E., Warrick, J. M., Andriola, I., Merry, D., and Bonini, N. M. (2002). Genetic modulation of polyglutamine toxicity by protein conjugation pathways in Drosophila. *Hum. Mol. Genet.* 11, 2895–2904. doi:10.1093/hmg/11.23.2895.
- Chen, L., Stone, M. C., Tao, J., and Rolls, M. M. (2012). Axon injury and stress trigger a microtubule-based neuroprotective pathway. *Proc. Natl. Acad. Sci. U. S. A.* 109, 11842–11847. doi:10.1073/pnas.1121180109.
- Chen, S.-D., Li, H.-Q., Cui, M., Dong, Q., and Yu, J.-T. (2020). Pluripotent stem cells for neurodegenerative disease modeling: an expert view on their value to drug discovery. *Expert Opin. Drug Discov.* 15, 1081–1094. doi:10.1080/17460441.2020.1767579.
- Chen, X., Tang, T.-S., Tu, H., Nelson, O., Pook, M., Hammer, R., et al. (2008). Deranged calcium signaling and neurodegeneration in spinocerebellar ataxia type 3. *J. Neurosci. Off. J. Soc. Neurosci.* 28, 12713–12724. doi:10.1523/JNEUROSCI.3909-08.2008.
- Chen, Z., and Sun, L. J. (2009). Nonproteolytic functions of ubiquitin in cell signaling. *Mol. Cell* 33, 275–286. doi:10.1016/j.molcel.2009.01.014.
- Chen, Z., Wang, P., Wang, C., Peng, Y., Hou, X., Zhou, X., et al. (2018). Updated frequency analysis of spinocerebellar ataxia in China. *Brain J. Neurol.* 141, e22. doi:10.1093/brain/awy016.
- Chinwalla, A. T., Cook, L. L., Delehaunty, K. D., Fewell, G. A., Fulton, L. A., Fulton, R. S., et al. (2002). Initial sequencing and comparative analysis of the mouse genome. *Nature* 420, 520–562. doi:10.1038/nature01262.
- Chou, A.-H., Lin, A.-C., Hong, K.-Y., Hu, S.-H., Chen, Y.-L., Chen, J.-Y., et al. (2011). p53 activation mediates polyglutamine-expanded ataxin-3 upregulation of Bax expression in cerebellar and pontine nuclei neurons. *Neurochem. Int.* 58, 145–152. doi:10.1016/j.neuint.2010.11.005.
- Chou, A.-H., Yeh, T.-H., Ouyang, P., Chen, Y.-L., Chen, S.-Y., and Wang, H.-L. (2008). Polyglutamine-expanded ataxin-3 causes cerebellar dysfunction of SCA3 transgenic mice by inducing transcriptional dysregulation. *Neurobiol. Dis.* 31, 89–101. doi:10.1016/j.nbd.2008.03.011.
- Church, D. M., Goodstadt, L., Hillier, L. W., Zody, M. C., Goldstein, S., She, X., et al. (2009). Lineage-Specific Biology Revealed by a Finished Genome Assembly of the Mouse. *PLoS Biol.* 7. doi:10.1371/journal.pbio.1000112.
- Cioni, J.-M., Lin, J. Q., Holtermann, A. V., Koppers, M., Jakobs, M. A. H., Azizi, A., et al. (2019). Late Endosomes Act as mRNA Translation Platforms and Sustain Mitochondria in Axons. *Cell* 176, 56–72.e15. doi:10.1016/j.cell.2018.11.030.
- Coarelli, G., Brice, A., and Durr, A. (2018). Recent advances in understanding dominant spinocerebellar ataxias from clinical and genetic points of view. *F1000Research* 7. doi:10.12688/f1000research.15788.1.
- Colomer Gould, V. F., Goti, D., Pearce, D., Gonzalez, G. A., Gao, H., Bermudez de Leon, M., et al. (2007). A mutant ataxin-3 fragment results from processing at a site N-terminal to amino acid 190 in brain of Machado-Joseph disease-like transgenic mice. *Neurobiol. Dis.* 27, 362–369. doi:10.1016/j.nbd.2007.06.005.
- Cornacchia, D., and Studer, L. (2017). Back and Forth in Time: Directing Age in iPSC-Derived Lineages. *Brain Res.* 1656, 14–26. doi:10.1016/j.brainres.2015.11.013.
- Costa, M. do C., and Paulson, H. L. (2012). Toward understanding Machado-Joseph Disease. *Prog. Neurobiol.* 97, 239–257. doi:10.1016/j.pneurobio.2011.11.006.
- Coutinho, P., and Andrade, C. (1978). Autosomal dominant system degeneration in Portuguese families of the Azores Islands. A new genetic disorder involving cerebellar, pyramidal, extrapyramidal and spinal cord motor functions. *Neurology* 28, 703–709.
- Cox, D., and Ecroyd, H. (2017). The small heat shock proteins α B-crystallin (HSPB5) and Hsp27 (HSPB1) inhibit the intracellular aggregation of α -synuclein. *Cell Stress Chaperones* 22, 589–600. doi:10.1007/s12192-017-0785-x.
- D'Abreu, A., França, M., Appenzeller, S., Lopes-Cendes, I., and Cendes, F. (2009). Axonal dysfunction in the deep white matter in Machado-Joseph disease. *J. Neuroimaging Off. J. Am. Soc. Neuroimaging* 19, 9–12. doi:10.1111/j.1552-6569.2008.00260.x.

Dachet, F., Brown, J. B., Valyi-Nagy, T., Narayan, K. D., Serafini, A., Boley, N., et al. (2021). Selective time-dependent changes in activity and cell-specific gene expression in human postmortem brain. *Sci. Rep.* 11, 6078. doi:10.1038/s41598-021-85801-6.

Dantuma, N. P., and Herzog, L. K. (2020). Machado-Joseph Disease: A Stress Combating Deubiquitylating Enzyme Changing Sides. *Adv. Exp. Med. Biol.* 1233, 237–260. doi:10.1007/978-3-030-38266-7_10.

de Castilhos, R. M., Furtado, G. V., Gheno, T. C., Schaeffer, P., Russo, A., Barsottini, O., et al. (2014). Spinocerebellar ataxias in Brazil—frequencies and modulating effects of related genes. *Cerebellum Lond. Engl.* 13, 17–28. doi:10.1007/s12311-013-0510-y.

de Rezende, T. J. R., D'Abreu, A., Guimarães, R. P., Lopes, T. M., Lopes-Cendes, I., Cendes, F., et al. (2015). Cerebral cortex involvement in Machado-Joseph disease. *Eur. J. Neurol.* 22, 277–283, e23–24. doi:10.1111/ene.12559.

Ding, D., Wang, C., Chen, Z., Xia, K., Tang, B., Qiu, R., et al. (2020). Polyglutamine-expanded ataxin3 alter specific gene expressions through changing DNA methylation status in SCA3/MJD. *Aging* 13, 3680–3698. doi:10.18632/aging.202331.

Donaldson, K. M., Li, W., Ching, K. A., Batalov, S., Tsai, C.-C., and Joazeiro, C. A. P. (2003). Ubiquitin-mediated sequestration of normal cellular proteins into polyglutamine aggregates. *Proc. Natl. Acad. Sci. U. S. A.* 100, 8892–8897. doi:10.1073/pnas.1530212100.

Doss-Pepe, E. W., Stenroos, E. S., Johnson, W. G., and Madura, K. (2003). Ataxin-3 interactions with rad23 and valosin-containing protein and its associations with ubiquitin chains and the proteasome are consistent with a role in ubiquitin-mediated proteolysis. *Mol. Cell. Biol.* 23, 6469–6483. doi:10.1128/mcb.23.18.6469-6483.2003.

Duarte Lobo, D., Nobre, R. J., Oliveira Miranda, C., Pereira, D., Castelhano, J., Sereno, J., et al. (2020). The blood-brain barrier is disrupted in Machado-Joseph disease/spinocerebellar ataxia type 3: evidence from transgenic mice and human post-mortem samples. *Acta Neuropathol. Commun.* 8, 152. doi:10.1186/s40478-020-00955-0.

El Fatimy, R., Davidovic, L., Tremblay, S., Jaglin, X., Dury, A., Robert, C., et al. (2016). Tracking the Fragile X Mental Retardation Protein in a Highly Ordered Neuronal RiboNucleoParticles Population: A Link between Stalled Polyribosomes and RNA Granules. *PLoS Genet.* 12, e1006192. doi:10.1371/journal.pgen.1006192.

Emperador-Melero, J., Huson, V., van Weering, J., Bollmann, C., Fischer von Mollard, G., Toonen, R. F., et al. (2018). Vti1a/b regulate synaptic vesicle and dense core vesicle secretion via protein sorting at the Golgi. *Nat. Commun.* 9, 3421. doi:10.1038/s41467-018-05699-z.

Evers, M. M., Toonen, L. J. A., and van Roon-Mom, W. M. C. (2014). Ataxin-3 Protein and RNA Toxicity in Spinocerebellar Ataxia Type 3: Current Insights and Emerging Therapeutic Strategies. *Mol. Neurobiol.* 49, 1513–1531. doi:10.1007/s12035-013-8596-2.

Evert, B. O., Araujo, J., Vieira-Saecker, A. M., de Vos, R. A. I., Harendza, S., Klockgether, T., et al. (2006). Ataxin-3 represses transcription via chromatin binding, interaction with histone deacetylase 3, and histone deacetylation. *J. Neurosci. Off. J. Soc. Neurosci.* 26, 11474–11486. doi:10.1523/JNEUROSCI.2053-06.2006.

Farrar, M. A., Vucic, S., Nicholson, G., and Kiernan, M. C. (2016). Motor cortical dysfunction develops in spinocerebellar ataxia type 3. *Clin. Neurophysiol. Off. J. Int. Fed. Clin. Neurophysiol.* 127, 3418–3424. doi:10.1016/j.clinph.2016.09.005.

Fei, E., Jia, N., Zhang, T., Ma, X., Wang, H., Liu, C., et al. (2007). Phosphorylation of ataxin-3 by glycogen synthase kinase 3beta at serine 256 regulates the aggregation of ataxin-3. *Biochem. Biophys. Res. Commun.* 357, 487–492. doi:10.1016/j.bbrc.2007.03.160.

Gan, L., Cookson, M. R., Petruccielli, L., and La Spada, A. R. (2018). Converging pathways in neurodegeneration, from genetics to mechanisms. *Nat. Neurosci.* 21, 1300–1309. doi:10.1038/s41593-018-0237-7.

Ghosh, J. G., Houck, S. A., and Clark, J. I. (2007). Interactive sequences in the stress protein and molecular chaperone human alphaB crystallin recognize and modulate the assembly of filaments. *Int. J. Biochem. Cell Biol.* 39, 1804–1815. doi:10.1016/j.biocel.2007.04.027.

Grasty, K. C., Weeks, S. D., and Loll, P. J. (2019). Structural insights into the activity and regulation of human Josephin-2. *J. Struct. Biol. X* 3, 100011. doi:10.1016/j.jysbx.2019.100011.

Graves, T. D., and Guiloff, R. J. (2011). SCA3 presenting as an isolated axonal polyneuropathy. *Arch. Neurol.* 68, 653–655. doi:10.1001/archneurol.2011.86.

Griffin, J. L., Cemal, C. K., and Pook, M. A. (2004). Defining a metabolic phenotype in the brain of a transgenic mouse model of spinocerebellar ataxia 3. *Physiol. Genomics* 16, 334–340. doi:10.1152/physiolgenomics.00149.2003.

Guo, J., Chen, H., Biswal, B. B., Guo, X., Zhang, H., Dai, L., et al. (2020a). Gray matter atrophy patterns within the cerebellum-neostriatum-cortical network in SCA3. *Neurology* 95, e3036–e3044. doi:10.1212/WNL.0000000000010986.

- Guo, W., Stoklund Dittlau, K., and Van Den Bosch, L. (2020b). Axonal transport defects and neurodegeneration: Molecular mechanisms and therapeutic implications. *Semin. Cell Dev. Biol.* 99, 133–150. doi:10.1016/j.semcd.2019.07.010.
- Haacke, A., Hartl, F. U., and Breuer, P. (2007). Calpain inhibition is sufficient to suppress aggregation of polyglutamine-expanded ataxin-3. *J. Biol. Chem.* 282, 18851–18856. doi:10.1074/jbc.M611914200.
- Harmuth, T., Prell-Schicker, C., Weber, J. J., Gellerich, F., Funke, C., Driessén, S., et al. (2018). Mitochondrial Morphology, Function and Homeostasis Are Impaired by Expression of an N-terminal Calpain Cleavage Fragment of Ataxin-3. *Front. Mol. Neurosci.* 11, 368. doi:10.3389/fnmol.2018.00368.
- Harris, G. M., Dodelzon, K., Gong, L., Gonzalez-Alegre, P., and Paulson, H. L. (2010). Splice isoforms of the polyglutamine disease protein ataxin-3 exhibit similar enzymatic yet different aggregation properties. *PLoS One* 5, e13695. doi:10.1371/journal.pone.0013695.
- Herzog, L. K., Kevei, É., Marchante, R., Böttcher, C., Bindesbøll, C., Lystad, A. H., et al. (2020). The Machado-Joseph disease deubiquitylase ataxin-3 interacts with LC3C/GABARAP and promotes autophagy. *Aging Cell* 19, e13051. doi:10.1111/acel.13051.
- Hickman, D. L., Johnson, J., Vemulapalli, T. H., Crisler, J. R., and Shepherd, R. (2017). Commonly Used Animal Models. *Princ. Anim. Res. Grad. Undergrad. Stud.*, 117–175. doi:10.1016/B978-0-12-802151-4.00007-4.
- Hill, S. M., Wrobel, L., Ashkenazi, A., Fernandez-Estevez, M., Tan, K., Bürl, R. W., et al. (2021). VCP/p97 regulates Beclin-1-dependent autophagy initiation. *Nat. Chem. Biol.* 17, 448–455. doi:10.1038/s41589-020-00726-x.
- Holleran, E. A., Tokito, M. K., Karki, S., and Holzbaur, E. L. (1996). Centractin (ARP1) associates with spectrin revealing a potential mechanism to link dynactin to intracellular organelles. *J. Cell Biol.* 135, 1815–1829. doi:10.1083/jcb.135.6.1815.
- Houck, S. A., and Clark, J. I. (2010). Dynamic subunit exchange and the regulation of microtubule assembly by the stress response protein human alphaB crystallin. *PLoS One* 5, e11795. doi:10.1371/journal.pone.0011795.
- Hsieh, M., Chang, W.-H., Hsu, C.-F., Nishimori, I., Kuo, C.-L., and Minakuchi, T. (2013). Altered expression of carbonic anhydrase-related protein XI in neuronal cells expressing mutant ataxin-3. *Cerebellum Lond. Engl.* 12, 338–349. doi:10.1007/s12311-012-0430-2.
- Hsu, J.-Y., Jhang, Y.-L., Cheng, P.-H., Chang, Y.-F., Mao, S.-H., Yang, H.-I., et al. (2017). The Truncated C-terminal Fragment of Mutant ATXN3 Disrupts Mitochondria Dynamics in Spinocerebellar Ataxia Type 3 Models. *Front. Mol. Neurosci.* 10, 196. doi:10.3389/fnmol.2017.00196.
- Hübener, J., Vauti, F., Funke, C., Wolburg, H., Ye, Y., Schmidt, T., et al. (2011). N-terminal ataxin-3 causes neurological symptoms with inclusions, endoplasmic reticulum stress and ribosomal dislocation. *Brain J. Neurol.* 134, 1925–1942. doi:10.1093/brain/awr118.
- Hübener, J., Weber, J. J., Richter, C., Honold, L., Weiss, A., Murad, F., et al. (2013). Calpain-mediated ataxin-3 cleavage in the molecular pathogenesis of spinocerebellar ataxia type 3 (SCA3). *Hum. Mol. Genet.* 22, 508–518. doi:10.1093/hmg/dds449.
- Invernizzi, G., Aprile, F. A., Natalello, A., Ghisleni, A., Penco, A., Relini, A., et al. (2012). The relationship between aggregation and toxicity of polyglutamine-containing ataxin-3 in the intracellular environment of Escherichia coli. *PLoS One* 7, e51890. doi:10.1371/journal.pone.0051890.
- Jacobi, H., du Montcel, S. T., Bauer, P., Giunti, P., Cook, A., Labrum, R., et al. (2015). Long-term disease progression in spinocerebellar ataxia types 1, 2, 3, and 6: a longitudinal cohort study. *Lancet Neurol.* 14, 1101–1108. doi:10.1016/S1474-4422(15)00202-1.
- Karus, C., Ziemens, D., and Rose, C. R. (2015). Lactate rescues neuronal sodium homeostasis during impaired energy metabolism. *Channels Austin Tex* 9, 200–208. doi:10.1080/19336950.2015.1050163.
- Kazachkova, N., Raposo, M., Montiel, R., Cymbron, T., Bettencourt, C., Silva-Fernandes, A., et al. (2013). Patterns of mitochondrial DNA damage in blood and brain tissues of a transgenic mouse model of Machado-Joseph disease. *Neurodegener. Dis.* 11, 206–214. doi:10.1159/000339207.
- Khan, L. A., Bauer, P. O., Miyazaki, H., Lindenberg, K. S., Landwehrmeyer, B. G., and Nukina, N. (2006). Expanded polyglutamines impair synaptic transmission and ubiquitin-proteasome system in *Caenorhabditis elegans*. *J. Neurochem.* 98, 576–587. doi:10.1111/j.1471-4159.2006.03895.x.
- Kim, H., Oh, J.-Y., Choi, S.-L., Nam, Y.-J., Jo, A., Kwon, A., et al. (2016). Down-regulation of p21-activated serine/threonine kinase 1 is involved in loss of mesencephalic dopamine neurons. *Mol. Brain* 9, 45. doi:10.1186/s13041-016-0230-6.
- Kim, Y.-B., Shin, Y. J., Roy, A., and Kim, J.-H. (2015). The Role of the Pleckstrin Homology Domain-containing Protein CKIP-1 in Activation of p21-activated Kinase 1 (PAK1). *J. Biol. Chem.* 290, 21076–21085. doi:10.1074/jbc.M115.675124.

- Koeppen, A. H. (2018). The Neuropathology of Spinocerebellar Ataxia Type 3/Machado-Joseph Disease. *Adv. Exp. Med. Biol.* 1049, 233–241. doi:10.1007/978-3-319-71779-1_11.
- Kristensen, L. V., Oppermann, F. S., Rauen, M. J., Fog, K., Schmidt, T., Schmidt, J., et al. (2018). Mass spectrometry analyses of normal and polyglutamine expanded ataxin-3 reveal novel interaction partners involved in mitochondrial function. *Neurochem. Int.* 112, 5–17. doi:10.1016/j.neuint.2017.10.013.
- Kurosaki, H., Yamaguchi, K., Man-Yoshi, K., Muramatsu, S.-I., Hara, S., and Ichinose, H. (2019). Administration of tetrahydrobiopterin restored the decline of dopamine in the striatum induced by an acute action of MPTP. *Neurochem. Int.* 125, 16–24. doi:10.1016/j.neuint.2019.02.005.
- Leotti, V. B., de Vries, J. J., Oliveira, C. M., de Mattos, E. P., Te Meerman, G. J., Brunt, E. R., et al. (2021). CAG Repeat Size Influences the Progression Rate of Spinocerebellar Ataxia Type 3. *Ann. Neurol.* 89, 66–73. doi:10.1002/ana.25919.
- Li, T., Martins, S., Peng, Y., Wang, P., Hou, X., Chen, Z., et al. (2019). Is the High Frequency of Machado-Joseph Disease in China Due to New Mutational Origins? *Front. Genet.* 9. doi:10.3389/fgene.2018.00740.
- Lima, M., and Raposo, M. (2018). Towards the Identification of Molecular Biomarkers of Spinocerebellar Ataxia Type 3 (SCA3)/Machado-Joseph Disease (MJD). *Adv. Exp. Med. Biol.* 1049, 309–319. doi:10.1007/978-3-319-71779-1_16.
- Lorenzo, D. N., Badea, A., Davis, J., Hostettler, J., He, J., Zhong, G., et al. (2014). A PIK3C3-ankyrin-B-dynactin pathway promotes axonal growth and multiorganelle transport. *J. Cell Biol.* 207, 735–752. doi:10.1083/jcb.201407063.
- Lu, M.-K., Chen, J.-C., Chen, C.-M., Duann, J.-R., Ziemann, U., and Tsai, C.-H. (2017). Impaired Cerebellum to Primary Motor Cortex Associative Plasticity in Parkinson's Disease and Spinocerebellar Ataxia Type 3. *Front. Neurosci.* 8, 445. doi:10.3389/fnneur.2017.00445.
- Luo, S., Mizuta, H., and Rubinsztein, D. C. (2008). p21-activated kinase 1 promotes soluble mutant huntingtin self-interaction and enhances toxicity. *Hum. Mol. Genet.* 17, 895–905. doi:10.1093/hmg/ddm362.
- Ma, Q.-L., Yang, F., Frautschy, S. A., and Cole, G. M. (2012). PAK in Alzheimer disease, Huntington disease and X-linked mental retardation. *Cell. Logist.* 2, 117–125. doi:10.4161/cl.21602.
- Maas, R. P. P. W. M., Killaars, S., van de Warrenburg, B. P. C., and Schutter, D. J. L. G. (2021). The cerebellar cognitive affective syndrome scale reveals early neuropsychological deficits in SCA3 patients. *J. Neurol.* doi:10.1007/s00415-021-10516-7.
- Macedo-Ribeiro, S., Cortes, L., Maciel, P., and Carvalho, A. L. (2009). Nucleocytoplasmic shuttling activity of ataxin-3. *PLoS One* 4, e5834. doi:10.1371/journal.pone.0005834.
- Maciel, P., Gaspar, C., DeStefano, A. L., Silveira, I., Coutinho, P., Radvany, J., et al. (1995). Correlation between CAG repeat length and clinical features in Machado-Joseph disease. *Am. J. Hum. Genet.* 57, 54–61.
- Matos, C. A., de Almeida, L. P., and Nóbrega, C. (2019). Machado-Joseph disease/spinocerebellar ataxia type 3: lessons from disease pathogenesis and clues into therapy. *J. Neurochem.* 148, 8–28. doi:10.1111/jnc.14541.
- Mazzucchelli, S., De Palma, A., Riva, M., D'Urzo, A., Pozzi, C., Pastori, V., et al. (2009). Proteomic and biochemical analyses unveil tight interaction of ataxin-3 with tubulin. *Int. J. Biochem. Cell Biol.* 41, 2485–2492. doi:10.1016/j.biocel.2009.08.003.
- Mendonça, N., França, M. C., Gonçalves, A. F., and Januário, C. (2018). Clinical Features of Machado-Joseph Disease. *Adv. Exp. Med. Biol.* 1049, 255–273. doi:10.1007/978-3-319-71779-1_13.
- Millicamps, S., and Julien, J.-P. (2013). Axonal transport deficits and neurodegenerative diseases. *Nat. Rev. Neurosci.* 14, 161–176. doi:10.1038/nrn3380.
- Moughamian, A. J., Osborn, G. E., Lazarus, J. E., Maday, S., and Holzbaur, E. L. F. (2013). Ordered recruitment of dynein to the microtubule plus-end is required for efficient initiation of retrograde axonal transport. *J. Neurosci. Off. J. Soc. Neurosci.* 33, 13190–13203. doi:10.1523/JNEUROSCI.0935-13.2013.
- Mueller, T., Breuer, P., Schmitt, I., Walter, J., Evert, B. O., and Wüllner, U. (2009). CK2-dependent phosphorylation determines cellular localization and stability of ataxin-3. *Hum. Mol. Genet.* 18, 3334–3343. doi:10.1093/hmg/ddp274.
- Mukherjee, A. B., Appu, A. P., Sadhukhan, T., Casey, S., Mondal, A., Zhang, Z., et al. (2019). Emerging new roles of the lysosome and neuronal ceroid lipofuscinoses. *Mol. Neurodegener.* 14. doi:10.1186/s13024-018-0300-6.
- Nakano, K. K., Dawson, D. M., and Spence, A. (1972). Machado disease. A hereditary ataxia in Portuguese emigrants to Massachusetts. *Neurology* 22, 49–55. doi:10.1212/wnl.22.1.49.
- Neves-Carvalho, A., Logarinho, E., Freitas, A., Duarte-Silva, S., Costa, M. do C., Silva-Fernandes, A., et al. (2015). Dominant negative effect of polyglutamine expansion perturbs normal function of ataxin-3 in neuronal cells. *Hum. Mol. Genet.* 24, 100–117. doi:10.1093/hmg/ddu422.

- Pellistri, F., Bucciantini, M., Invernizzi, G., Gatta, E., Penco, A., Frana, A. M., et al. (2013). Different ataxin-3 amyloid aggregates induce intracellular Ca(2+) deregulation by different mechanisms in cerebellar granule cells. *Biochim. Biophys. Acta* 1833, 3155–3165. doi:10.1016/j.bbamcr.2013.08.019.
- Pohl, C., and Dikic, I. (2019). Cellular quality control by the ubiquitin-proteasome system and autophagy. *Science* 366, 818–822. doi:10.1126/science.aax3769.
- Poplawski, G. H. D., Tranziska, A.-K., Leshchyns'ka, I., Meier, I. D., Streichert, T., Sytnyk, V., et al. (2012). L1CAM increases MAP2 expression via the MAPK pathway to promote neurite outgrowth. *Mol. Cell. Neurosci.* 50, 169–178. doi:10.1016/j.mcn.2012.03.010.
- Pozzi, C., Valtorta, M., Tedeschi, G., Galbusera, E., Pastori, V., Bigi, A., et al. (2008). Study of subcellular localization and proteolysis of ataxin-3. *Neurobiol. Dis.* 30, 190–200. doi:10.1016/j.nbd.2008.01.011.
- Pulido-Valdeolivas, I., Gómez-Andrés, D., Sanz-Gallego, I., Rausell, E., and Arpa, J. (2016). Patterns of motor signs in spinocerebellar ataxia type 3 at the start of follow-up in a reference unit. *Cerebellum Ataxias* 3, 4. doi:10.1186/s40673-016-0042-6.
- Ramani, B., Harris, G. M., Huang, R., Seki, T., Murphy, G. G., Carmo Costa, M. do, et al. (2017). A knockin mouse model of spinocerebellar ataxia type 3 exhibits prominent aggregate pathology and aberrant splicing of the disease gene transcript. *Hum. Mol. Genet.* 26, 3232–3233. doi:10.1093/hmg/ddx176.
- Ramani, B., Harris, G. M., Huang, R., Seki, T., Murphy, G. G., Costa, M. do C., et al. (2015). A knockin mouse model of spinocerebellar ataxia type 3 exhibits prominent aggregate pathology and aberrant splicing of the disease gene transcript. *Hum. Mol. Genet.* 24, 1211–1224. doi:10.1093/hmg/ddu532.
- Rankin, C. A., Sun, Q., and Gamblin, T. C. (2008). Pre-assembled tau filaments phosphorylated by GSK-3b form large tangle-like structures. *Neurobiol. Dis.* 31, 368–377. doi:10.1016/j.nbd.2008.05.011.
- Raposo, M., Ramos, A., Santos, C., Kazachkova, N., Teixeira, B., Bettencourt, C., et al. (2019). Accumulation of Mitochondrial DNA Common Deletion Since The Preataxic Stage of Machado-Joseph Disease. *Mol. Neurobiol.* 56, 119–124. doi:10.1007/s12035-018-1069-x.
- Rezende, T. J. R., Paiva, J. L. R. de, Martinez, A. R. M., Lopes-Cendes, I., Pedroso, J. L., Barsottini, O. G. P., et al. (2018). Structural signature of SCA3: From presymptomatic to late disease stages. *Ann. Neurol.* 84, 401–408. doi:10.1002/ana.25297.
- Riess, O., Rüb, U., Pastore, A., Bauer, P., and Schöls, L. (2008). SCA3: neurological features, pathogenesis and animal models. *Cerebellum Lond. Engl.* 7, 125–137. doi:10.1007/s12311-008-0013-4.
- Rosselli-Murai, L. K., Joseph, J. G., Lopes-Cendes, I., Liu, A. P., and Murai, M. J. (2020). The Machado-Joseph disease-associated form of ataxin-3 impacts dynamics of clathrin-coated pits. *Cell Biol. Int.* 44, 1252–1259. doi:10.1002/cbin.11312.
- Rüb, U., Schöls, L., Paulson, H., Auburger, G., Kermer, P., Jen, J. C., et al. (2013). Clinical features, neurogenetics and neuropathology of the polyglutamine spinocerebellar ataxias type 1, 2, 3, 6 and 7. *Prog. Neurobiol.* 104, 38–66. doi:10.1016/j.pneurobio.2013.01.001.
- Sakabe, I., Hu, R., Jin, L., Clarke, R., and Kasid, U. N. (2015). TMEM33: a new stress-inducible endoplasmic reticulum transmembrane protein and modulator of the unfolded protein response signaling. *Breast Cancer Res. Treat.* 153, 285–297. doi:10.1007/s10549-015-3536-7.
- Sample, V., Ramamurthy, S., Gorshkov, K., Ronnett, G. V., and Zhang, J. (2015). Polarized activities of AMPK and BRSK in primary hippocampal neurons. *Mol. Biol. Cell* 26, 1935–1946. doi:10.1091/mbc.E14-02-0764.
- Sánchez, I., Mahlke, C., and Yuan, J. (2003). Pivotal role of oligomerization in expanded polyglutamine neurodegenerative disorders. *Nature* 421, 373–379. doi:10.1038/nature01301.
- Schmidt, J., Mayer, A. K., Bakula, D., Freude, J., Weber, J. J., Weiss, A., et al. (2019). Vulnerability of frontal brain neurons for the toxicity of expanded ataxin-3. *Hum. Mol. Genet.* 28, 1463–1473. doi:10.1093/hmg/ddy437.
- Schmidt, T., Lindenberg, K. S., Krebs, A., Schöls, L., Laccone, F., Herms, J., et al. (2002). Protein surveillance machinery in brains with spinocerebellar ataxia type 3: redistribution and differential recruitment of 26S proteasome subunits and chaperones to neuronal intranuclear inclusions. *Ann. Neurol.* 51, 302–310. doi:10.1002/ana.10101.
- Schöls, L., Amoiridis, G., Büttner, T., Przuntek, H., Epplen, J. T., and Riess, O. (1997). Autosomal dominant cerebellar ataxia: phenotypic differences in genetically defined subtypes? *Ann. Neurol.* 42, 924–932. doi:10.1002/ana.410420615.
- Seidel, K., den Dunnen, W. F. A., Schultz, C., Paulson, H., Frank, S., de Vos, R. A., et al. (2010). Axonal inclusions in spinocerebellar ataxia type 3. *Acta Neuropathol. (Berl.)* 120, 449–460. doi:10.1007/s00401-010-0717-7.
- Silva-Fernandes, A., Costa, M. do C., Duarte-Silva, S., Oliveira, P., Botelho, C. M., Martins, L., et al. (2010). Motor uncoordination and neuropathology in a transgenic mouse model of Machado-Joseph disease lacking intranuclear inclusions and ataxin-3 cleavage products. *Neurobiol. Dis.* 40, 163–176. doi:10.1016/j.nbd.2010.05.021.

- Simões, A. T., Gonçalves, N., Nobre, R. J., Duarte, C. B., and Pereira de Almeida, L. (2014). Calpain inhibition reduces ataxin-3 cleavage alleviating neuropathology and motor impairments in mouse models of Machado-Joseph disease. *Hum. Mol. Genet.* 23, 4932–4944. doi:10.1093/hmg/ddu209.
- Singh, A. N., Oehler, J., Torrecilla, I., Kilgas, S., Li, S., Vaz, B., et al. (2019). The p97-Ataxin 3 complex regulates homeostasis of the DNA damage response E3 ubiquitin ligase RNF8. *EMBO J.* 38, e102361. doi:10.15252/embj.2019102361.
- Sossin, W. S., and DesGroseillers, L. (2006). Intracellular trafficking of RNA in neurons. *Traffic Cph. Den.* 7, 1581–1589. doi:10.1111/j.1600-0854.2006.00500.x.
- Soto, C., and Pritzkow, S. (2018). Protein misfolding, aggregation, and conformational strains in neurodegenerative diseases. *Nat. Neurosci.* 21, 1332–1340. doi:10.1038/s41593-018-0235-9.
- Sowa, A. S., Martin, E., Martins, I. M., Schmidt, J., Depping, R., Weber, J. J., et al. (2018). Karyopherin α -3 is a key protein in the pathogenesis of spinocerebellar ataxia type 3 controlling the nuclear localization of ataxin-3. *Proc. Natl. Acad. Sci. U. S. A.* 115, E2624–E2633. doi:10.1073/pnas.1716071115.
- Sowa, A. S., Popova, T. G., Harmuth, T., Weber, J. J., Pereira Sena, P., Schmidt, J., et al. (2021). Neurodegenerative phosphoprotein signaling landscape in models of SCA3. *Mol. Brain* 14, 57. doi:10.1186/s13041-020-00723-0.
- Stenbeck, G. (1998). Soluble NSF-attachment proteins. *Int. J. Biochem. Cell Biol.* 30, 573–577. doi:10.1016/s1357-2725(97)00064-2.
- Stridh, M. H., Alt, M. D., Wittmann, S., Heidtmann, H., Aggarwal, M., Riederer, B., et al. (2012). Lactate flux in astrocytes is enhanced by a non-catalytic action of carbonic anhydrase II. *J. Physiol.* 590, 2333–2351. doi:10.1113/jphysiol.2011.220152.
- Switonski, P. M., Szlachcic, W. J., Krzyzosiak, W. J., and Figiel, M. (2015). A new humanized ataxin-3 knock-in mouse model combines the genetic features, pathogenesis of neurons and glia and late disease onset of SCA3/MJD. *Neurobiol. Dis.* 73, 174–188. doi:10.1016/j.nbd.2014.09.020.
- Takahashi, K., and Yamanaka, S. (2006). Induction of pluripotent stem cells from mouse embryonic and adult fibroblast cultures by defined factors. *Cell* 126, 663–676. doi:10.1016/j.cell.2006.07.024.
- Takano, H., Cancel, G., Ikeuchi, T., Lorenzetti, D., Mawad, R., Stevanin, G., et al. (1998). Close associations between prevalences of dominantly inherited spinocerebellar ataxias with CAG-repeat expansions and frequencies of large normal CAG alleles in Japanese and Caucasian populations. *Am. J. Hum. Genet.* 63, 1060–1066. doi:10.1086/302067.
- Tao, R.-S., Fei, E.-K., Ying, Z., Wang, H.-F., and Wang, G.-H. (2008). Casein kinase 2 interacts with and phosphorylates ataxin-3. *Neurosci. Bull.* 24, 271–277. doi:10.1007/s12264-008-0605-5.
- Teixeira-Castro, A., Ailion, M., Jalles, A., Brignull, H. R., Vilaça, J. L., Dias, N., et al. (2011). Neuron-specific proteotoxicity of mutant ataxin-3 in *C. elegans*: rescue by the DAF-16 and HSF-1 pathways. *Hum. Mol. Genet.* 20, 2996–3009. doi:10.1093/hmg/ddr203.
- Todd, T. W., and Lim, J. (2013). Aggregation Formation in the Polyglutamine Diseases: Protection at a Cost? *Mol. Cells* 36, 185–194. doi:10.1007/s10059-013-0167-x.
- Todi, S. V., Winborn, B. J., Scaglione, K. M., Blount, J. R., Travis, S. M., and Paulson, H. L. (2009). Ubiquitination directly enhances activity of the deubiquitinating enzyme ataxin-3. *EMBO J.* 28, 372–382. doi:10.1038/emboj.2008.289.
- Toonen, L. J. A., Overzier, M., Evers, M. M., Leon, L. G., van der Zeeuw, S. A. J., Mei, H., et al. (2018). Transcriptional profiling and biomarker identification reveal tissue specific effects of expanded ataxin-3 in a spinocerebellar ataxia type 3 mouse model. *Mol. Neurodegener.* 13, 31. doi:10.1186/s13024-018-0261-9.
- Toulis, V., García-Monclús, S., de la Peña-Ramírez, C., Arenas-Galnares, R., Abril, J. F., Todi, S. V., et al. (2020). The Deubiquitinating Enzyme Ataxin-3 Regulates Ciliogenesis and Phagocytosis in the Retina. *Cell Rep.* 33, 108360. doi:10.1016/j.celrep.2020.108360.
- Tsai, H.-F., Tsai, H.-J., and Hsieh, M. (2004). Full-length expanded ataxin-3 enhances mitochondrial-mediated cell death and decreases Bcl-2 expression in human neuroblastoma cells. *Biochem. Biophys. Res. Commun.* 324, 1274–1282. doi:10.1016/j.bbrc.2004.09.192.
- Tu, Y., Li, X., Zhu, X., Liu, X., Guo, C., Jia, D., et al. (2020). Determining the Fate of Neurons in SCA3: ATX3, a Rising Decision Maker in Response to DNA Stresses and Beyond. *Front. Cell Dev. Biol.* 8, 619911. doi:10.3389/fcell.2020.619911.
- Tu, Y., Liu, H., Zhu, X., Shen, H., Ma, X., Wang, F., et al. (2017). Ataxin-3 promotes genome integrity by stabilizing Chk1. *Nucleic Acids Res.* 45, 4532–4549. doi:10.1093/nar/gkx095.
- UniProt: the universal protein knowledgebase (2017). *Nucleic Acids Res.* 45, D158–D169. doi:10.1093/nar/gkw1099.

- Vale, J., Bugalho, P., Silveira, I., Sequeiros, J., Guimarães, J., and Coutinho, P. (2010). Autosomal dominant cerebellar ataxia: frequency analysis and clinical characterization of 45 families from Portugal. *Eur. J. Neurol.* 17, 124–128. doi:10.1111/j.1468-1331.2009.02757.x.
- Vinatier, G., Corsi, J.-M., Mignotte, B., and Gaumer, S. (2015). Quantification of Ataxin-3 and Ataxin-7 aggregates formed in vivo in *Drosophila* reveals a threshold of aggregated polyglutamine proteins associated with cellular toxicity. *Biochem. Biophys. Res. Commun.* 464, 1060–1065. doi:10.1016/j.bbrc.2015.07.071.
- Volpicelli-Daley, L. A., Gamble, K. L., Schultheiss, C. E., Riddle, D. M., West, A. B., and Lee, V. M.-Y. (2014). Formation of α -synuclein Lewy neurite-like aggregates in axons impedes the transport of distinct endosomes. *Mol. Biol. Cell* 25, 4010–4023. doi:10.1091/mbc.E14-02-0741.
- Weishäupl, D., Schneider, J., Peixoto Pinheiro, B., Ruess, C., Dold, S. M., von Zweydorf, F., et al. (2019). Physiological and pathophysiological characteristics of ataxin-3 isoforms. *J. Biol. Chem.* 294, 644–661. doi:10.1074/jbc.RA118.005801.
- Wiatr, K., Marczak, L., Perot, J.-B., Brouillet, E., Flament, J., and Figiel, M. (2021). Broad influence of mutant ataxin-3 on the proteome of the adult brain, young neurons, and axons reveals central molecular processes and biomarkers in SCA3/MJD using knock-in mouse model. *Front. Mol. Neurosci.* 14. doi:10.3389/fnmol.2021.658339.
- Wiatr, K., Piasecki, P., Marczak, L., Wojciechowski, P., Kurkowiak, M., Ploski, R., et al. (2019). Altered Levels of Proteins and Phosphoproteins, in the Absence of Early Causative Transcriptional Changes, Shape the Molecular Pathogenesis in the Brain of Young Presymptomatic Ki91 SCA3/MJD Mouse. *Mol. Neurobiol.* 56, 8168–8202. doi:10.1007/s12035-019-01643-4.
- Winborn, B. J., Travis, S. M., Todi, S. V., Scaglione, K. M., Xu, P., Williams, A. J., et al. (2008). The deubiquitinating enzyme ataxin-3, a polyglutamine disease protein, edits Lys63 linkages in mixed linkage ubiquitin chains. *J. Biol. Chem.* 283, 26436–26443. doi:10.1074/jbc.M803692200.
- Winograd-Katz, S. E., Brunner, M. C., Mirlas, N., and Geiger, B. (2011). Analysis of the signaling pathways regulating Src-dependent remodeling of the actin cytoskeleton. *Eur. J. Cell Biol.* 90, 143–156. doi:10.1016/j.ejcb.2010.07.006.
- Wlodarchak, N., and Xing, Y. (2016). PP2A as a master regulator of the cell cycle. *Crit. Rev. Biochem. Mol. Biol.* 51, 162–184. doi:10.3109/10409238.2016.1143913.
- Yao, T.-P. (2010). The Role of Ubiquitin in Autophagy-Dependent Protein Aggregate Processing. *Genes Cancer* 1, 779–786. doi:10.1177/1947601910383277.
- Yuan, D., Liu, C., and Hu, B. (2018). Dysfunction of Membrane Trafficking Leads to Ischemia-Reperfusion Injury After Transient Cerebral Ischemia. *Transl. Stroke Res.* 9, 215–222. doi:10.1007/s12975-017-0572-0.
- Zeng, L., Zhang, D., McLoughlin, H. S., Zalon, A. J., Aravind, L., and Paulson, H. L. (2018). Loss of the Spinocerebellar Ataxia type 3 disease protein ATXN3 alters transcription of multiple signal transduction pathways. *PLoS One* 13, e0204438. doi:10.1371/journal.pone.0204438.
- Zhao, H., Yang, L., Dong, Y., and Wu, Z.-Y. (2020). Phenotypic variance in monozygotic twins with SCA3. *Mol. Genet. Genomic Med.* 8, e1438. doi:10.1002/mgg3.1438.
- Zhivotovsky, B., and Orrenius, S. (2011). Calcium and cell death mechanisms: a perspective from the cell death community. *Cell Calcium* 50, 211–221. doi:10.1016/j.ceca.2011.03.003.
- Zhong, X., and Pittman, R. N. (2006). Ataxin-3 binds VCP/p97 and regulates retrotranslocation of ERAD substrates. *Hum. Mol. Genet.* 15, 2409–2420. doi:10.1093/hmg/ddl164.
- Zhou, Y., Dhaher, R., Parent, M., Hu, Q.-X., Hassel, B., Yee, S.-P., et al. (2019). Selective deletion of glutamine synthetase in the mouse cerebral cortex induces glial dysfunction and vascular impairment that precede epilepsy and neurodegeneration. *Neurochem. Int.* 123, 22–33. doi:10.1016/j.neuint.2018.07.009.
- Zhu, Z., and Reiser, G. (2018). The small heat shock proteins, especially HspB4 and HspB5 are promising protectants in neurodegenerative diseases. *Neurochem. Int.* 115, 69–79. doi:10.1016/j.neuint.2018.02.006.

8

ZAŁĄCZNIKI

1. OŚWIADCZENIA O WKŁADZIE PRACY KANDYDATA
W PUBLIKACJE ZAWARTE W ROZPRAWIE DOKTORSKIEJ.

2. PUBLIKACJA NR 1.

ALTERED LEVELS OF PROTEINS AND PHOSPHOPROTEINS, IN THE ABSENCE OF
EARLY CAUSATIVE TRANSCRIPTIONAL CHANGES, SHAPE THE MOLECULAR
PATHOGENESIS IN THE BRAIN OF YOUNG PRESYMPTOMATIC KI91 SCA3/MJD MOUSE

3. PUBLIKACJA NR 2.

BROAD INFLUENCE OF MUTANT ATAXIN-3 ON THE PROTEOME OF THE ADULT
BRAIN, YOUNG NEURONS, AND AXONS REVEALS CENTRAL MOLECULAR PROCESSES
AND BIOMARKERS IN SCA3/MJD USING KNOCK-IN MOUSE MODEL

Poznań, 29.04. 2021r.

Mgr inż. Kalina Katarzyna Wiatr
Zakład Neurobiologii Molekularnej
Instytut Chemiczny Bioorganicznej PAN
Ul. Z. Noskowskiego 12/14
61-704 Poznań

OŚWIADCZENIE KANDYDATA DO NADANIA STOPNIA DOKTORSKIEGO

Tytuł artykułu naukowego: „Altered level of proteins and their decreased phosphorylation in the absence of transcriptomic changes shape the molecular pathogenesis in the pre-symptomatic SCA3/MJD brain.”

Autorzy: Wiatr K, Piasecki P, Marczak Ł, Wojciechowski P, Kurkowiak M, Płoski R, Rydzanicz M, Handschuh L, Jungverdorben J, Brüstle O, Figlerowicz M, Figiel M.

Czasopismo: Molecular Neurobiology

Data opublikowania: grudzień 2019

Oświadczam, że mój wkład autorski w artykuł naukowy zatytułowany „Altered level of proteins and their decreased phosphorylation in the absence of transcriptomic changes shape the molecular pathogenesis in the pre-symptomatic SCA3/MJD brain ” obejmuje:

- Znaczący udział w pisaniu publikacji;
- Analizę wyników otrzymanych w testach behawioralnych i eksperymentach proteomicznych;
- Utworzenie rycin (Fig. 1, 7-9 oraz Suppl. Fig. 2-5) i tabel (5 – 12 i Suppl. 3-7) zawartych w artykule;
- Utworzenie kohorty 36 myszy i wykonanie testów behawioralnych;
- Przeprowadzenie eksperymentów proteomicznych (LC-MS/MS), które obejmowały analizę ilościową białek totalnych i poziom fosforylacji białek w korze mózgowej i mózdku mysiego modelu ataksji rdzeniowo-mózdkowej typu 3 SCA3/Ki91 na etapie presymptomatycznym;
- Przeprowadzenie eksperymentów western-blot w celu potwierdzenia zmienionego poziomu wybranych białek.

Podpis kandydata



Tytuł artykułu naukowego: „ Broad influence of mutant ataxin-3 on the proteome of the adult brain, young neurons, and axons reveals central molecular processes and biomarkers in SCA3/MJD using knock-in mouse model.”

Autorzy: Wiatr K, Marczak L, Perot JB, Brouillet E, Flament J, Figiel M

Czasopismo: Frontiers in molecular neuroscience

W DRUKU

Oświadczam, że mój wkład autorski w artykuł naukowy zatytułowany „Broad influence of mutant ataxin-3 on the proteome of the adult brain, young neurons, and axons reveals central molecular processes and biomarkers in SCA3/MJD using knock-in mouse model” obejmuje:

- Znaczny udział w pisaniu publikacji;
- Analiza danych otrzymanych we wszystkich przeprowadzonych eksperymentach (za wyjątkiem eksperymentu MRI) zawartych w artykule;
- Utworzenie wszystkich rycin i tabel zawartych w artykule, z wyjątkiem Fig. 2 (MRI);
- Wykonanie testów behawioralnych na kohortie 36 myszy w wieku od 4 do 18 miesięcy, w 2-miesięcznych odstępach czasu;
- przeprowadzenie eksperymentów proteomicznych (LC-MS/MS), które obejmowały analizę ilościową białek totalnych w korze mózgowej i mózdku mysiego modelu ataksji rdzeniowo-mózdkowej typu 3 SCA3/Ki91 w poszczególnych fazach choroby;
- Wyróżnienie fenotypu ciężkiego, pośredniego i łagodnego w końcowym stadium testów behawioralnych i przeprowadzenie analizy proteomicznej w korelacji z fenotypami;
- Zaprojektowanie eksperymentu mającego na celu ocenę, które białka znajdują się w zmienionej ilości w aksonach i ciałach neuronów SCA3 w porównaniu do kontroli. Wyprowadzenie hodowli neuronów kortikalnych i mózdkowych z mysiego modelu SCA3 Ki91 oraz przeprowadzenie analizy proteomicznej frakcji aksonalnej i ciał komórek z dendrytami;
- Zaprojektowanie i przeprowadzenie testu funkcjonalnego, w którym mierzone było tempo glikolizy i zużycia tlenu (oksydatywnej fosforylacji);
- Wykonanie immunobarwienia skrawków mózgu modelu Ki91 i myszy kontrolnych w celu wykrycia inkluzji, ubikvitynacji, neurofilamentów fosforylowanych i niefosforylowanych;
- Namnożenie plazmidu mRFP-Rab7, przeprowadzenie transfekcji neuronów mózdkowych mRFP-Rab7, oraz analiza stanu pęcherzyków.

Podpis kandydata



Poznań, 29.04. 2021r.

Dr hab. Maciej Figiel, prof. ICHB
Zakład Neurobiologii Molekularnej
Instytut Chemii Bioorganicznej PAN
Ul. Z. Noskowskiego 12/14
61-704 Poznań

OŚWIADCZENIE AUTORA KORESPONDENCYJNEGO ARTYKUŁÓW ZAWARTYCH W ROZPRAWIE

Tytuł artykułu naukowego: „Altered level of proteins and their decreased phosphorylation in the absence of transcriptomic changes shape the molecular pathogenesis in the pre-symptomatic SCA3/MJD brain.”

Autorzy: Wiatr K, Piasecki P, Marczak Ł, Wojciechowski P, Kurkowiak M, Płoski R, Rydzanicz M, Handschuh L, Jungverdorben J, Brüstle O, Figlerowicz M, Figiel M.

Czasopismo: Molecular Neurobiology

Data opublikowania: grudzień 2019

Oświadczam, że wkład autorski mgr inż. Kaliny Katarzyny Wiatr w artykuł naukowy zatytułowany „Altered level of proteins and their decreased phosphorylation in the absence of transcriptomic changes shape the molecular pathogenesis in the pre-symptomatic SCA3/MJD brain” obejmuje:

- Znaczący udział w pisaniu publikacji;
- Analizę wyników otrzymanych w testach behawioralnych i eksperymentach proteomicznych;
- Utworzenie rycin (Fig. 1, 7-9 oraz Suppl. Fig. 2-5) i tabel (5 – 12 i Suppl. 3-7) zawartych w artykule;
- Utworzenie kohorty 36 myszy i wykonanie testów behawioralnych;
- Przeprowadzenie eksperymentów proteomicznych (LC-MS/MS), które obejmowały analizę ilościową białek totalnych i poziom fosforylacji białek w korze mózgowej i mózdku mysiego modelu ataksji rdzeniowo-mózdkowej typu 3 SCA3/Ki91 na etapie presymptomatycznym;
- Przeprowadzenie eksperymentów western-blot w celu potwierdzenia zmienionego poziomu wybranych białek.



Maciej Figiel

Podpis autora korespondencyjnego

Tytuł artykułu naukowego: „ Broad influence of mutant ataxin-3 on the proteome of the adult brain, young neurons, and axons reveals central molecular processes and biomarkers in SCA3/MJD using knock-in mouse model.”

Autorzy: Wiatr K, Marczak L, Perot JB, Brouillet E, Flament J, Figiel M

Czasopismo: Frontiers in molecular neuroscience

W DRUKU

Oświadczam, że wkład autorski mgr inż. Kaliny Katarzyny Wiatr w artykuł naukowy zatytułowany „Broad influence of mutant ataxin-3 on the proteome of the adult brain, young neurons, and axons reveals central molecular processes and biomarkers in SCA3/MJD using knock-in mouse model” obejmuje:

- znaczny udział w pisaniu publikacji;
- Analiza danych otrzymanych we wszystkich przeprowadzonych eksperymentach (za wyjątkiem eksperymentu MRI) zawartych w artykule;
- Utworzenie wszystkich rycin i tabel zawartych w artykule, z wyjątkiem Fig. 2 (MRI);
- Wykonanie testów behawioralnych na kohortie 36 myszy w wieku od 4 do 18 miesięcy, w 2-miesięcznych odstępach czasu;
- przeprowadzenie eksperymentów proteomicznych (LC-MS/MS), które obejmowały analizę ilościową białek totalnych w korze mózgowej i mózdku mysiego modelu ataksji rdzeniowo-mózdkowej typu 3 SCA3/Ki91 w poszczególnych fazach choroby;
- Wyróżnienie fenotypu ciężkiego, pośredniego i łagodnego w końcowym stadium testów behawioralnych i przeprowadzenie analizy proteomicznej w korelacji z fenotypami;
- Zaprojektowanie eksperymentu mającego na celu ocenę, które białka znajdują się w zmienionej ilości w aksonach i ciałach neuronów SCA3 w porównaniu do kontroli. Wyprawdzenie hodowli neuronów kortikalnych i mózdkowych z mysiego modelu SCA3 Ki91 oraz przeprowadzenie analizy proteomicznej frakcji aksonalnej i ciał komórek z dendrytami;
- Zaprojektowanie i przeprowadzenie testu funkcjonalnego, w którym mierzone było tempo glikolizy i zużycia tlenu (oksydatywnej fosforylacji);
- Wykonanie immunobarwienia skrawków mózgu modelu Ki91 i myszy kontrolnych w celu wykrycia inkluzji, ubikwitynacji, neurofilamentów fosforylowanych i niefosforylowanych;
- Namnożenie plazmidu mRFP-Rab7, przeprowadzenie transfekcji neuronów mózdkowych mRFP-Rab7, oraz analiza stanu pęcherzyków.



Podpis autora korespondencyjnego



Altered Levels of Proteins and Phosphoproteins, in the Absence of Early Causative Transcriptional Changes, Shape the Molecular Pathogenesis in the Brain of Young Presymptomatic Ki91 SCA3/MJD Mouse

Kalina Wiatr¹ · Piotr Piasecki¹ · Łukasz Marczak¹ · Paweł Wojciechowski^{1,2} · Małgorzata Kurkowiak¹ · Rafał Płoski³ · Małgorzata Rydzanicz³ · Luiza Handschuh¹ · Johannes Jungverdorben⁴ · Oliver Brüstle⁴ · Marek Figlerowicz¹ · Maciej Figiel¹

Received: 7 February 2019 / Accepted: 10 May 2019 / Published online: 14 June 2019
© The Author(s) 2019

Abstract

Spinocerebellar ataxia type 3 (SCA3/MJD) is a polyQ neurodegenerative disease where the presymptomatic phase of pathogenesis is unknown. Therefore, we investigated the molecular network of transcriptomic and proteomic triggers in young presymptomatic SCA3/MJD brain from Ki91 knock-in mouse. We found that transcriptional dysregulations resulting from mutant ataxin-3 are not occurring in young Ki91 mice, while old Ki91 mice and also postmitotic patient SCA3 neurons demonstrate the late transcriptomic changes. Unlike the lack of early mRNA changes, we have identified numerous early changes of total proteins and phosphoproteins in 2-month-old Ki91 mouse cortex and cerebellum. We discovered the network of processes in presymptomatic SCA3 with three main groups of disturbed processes comprising altered proteins: (I) modulation of protein levels and DNA damage (Pabpc1, Ddb1, Nedd8), (II) formation of neuronal cellular structures (Tubb3, Nefh, p-Tau), and (III) neuronal function affected by processes following perturbed cytoskeletal formation (Mt-Co3, Stx1b, p-Syn1). Phosphoproteins downregulate in the young Ki91 mouse brain and their phosphosites are associated with kinases that interact with ATXN3 such as casein kinase, Camk2, and kinases controlled by another Atxn3 interactor p21 such as Gsk3, Pka, and Cdk kinases. We conclude that the onset of SCA3 pathology occurs without altered transcript level and is characterized by changed levels of proteins responsible for termination of translation, DNA damage, spliceosome, and protein phosphorylation. This disturbs global cellular processes such as cytoskeleton and transport of vesicles and mitochondria along axons causing energy deficit and neurodegeneration also manifesting in an altered level of transcripts at later ages.

Keywords Ataxin-3 · Mouse · Knock-in · SCA3 · MJD · Ataxia · Spinocerebellar · CAG · PolyQ · Presymptomatic · Proteome · Phosphoproteome

Kalina Wiatr and Piotr Piasecki contributed equally to this work.

Kalina Wiatr and Piotr Piasecki are co-first authors.

Electronic supplementary material The online version of this article (<https://doi.org/10.1007/s12035-019-01643-4>) contains supplementary material, which is available to authorized users.

✉ Maciej Figiel
mfigiel@ibch.poznan.pl

¹ Institute of Bioorganic Chemistry, Polish Academy of Sciences, Z. Noskowskiego 12/14, 61-704 Poznań, Poland

² Institute of Computing Science, Poznań University of Technology, Poznań, Poland

³ Department of Medical Genetics, Medical University of Warsaw, Warsaw, Poland

⁴ Institute of Reconstructive Neurobiology, LIFE & BRAIN Center, University of Bonn School of Medicine & University Hospital Bonn, 53127 Bonn, Germany

Introduction

Spinocerebellar ataxia type 3 (SCA3), also called Machado–Joseph disease (MJD), is a dominantly inherited genetic disease resulting from the special type of mutation–expansion of CAG repeats in the *ATXN3* gene [1] (MJD and *ATXN3*: OMIM 109150 and 607047). The presence of mutant allele evokes motor abnormalities, such as gait ataxia, ocular symptoms, and later cognitive disturbances, all characteristics for a symptomatic phase of the disease and usually occurring in the third or fourth decade of life [2]. The causative protein to these symptoms is ataxin-3, a protease/deubiquitinase [3, 4], and its mutant version which contains a prolonged stretch of glutamines inside the protein structure [1]. Its natural protease function does not directly imply transcriptional regulation as a mechanism in SCA3 but rather suggests the influence of the mutant ataxin-3 on the level of various kinds of proteins [5]. A number of already identified SCA3 mechanisms also propose affected regulation of processes related to changes in protein level or pathway activation largely independent of transcription. SCA3 pathogenic processes are based on the toxicity of the polyQ tract, proteolytic cleavage of mutant ataxin-3 protein, and accumulation of intranuclear inclusions [6]. Such accumulation is related to dysfunction of proteasome and transport of the protein into the nucleus [7, 8]. In addition, the SCA3 mechanism involves autophagy defects, metabolism and mitochondrial impairment, defective transport along the axons, and dysregulation of intracellular calcium turnover [9–11]. The mechanisms of pathogenesis in SCA3 have been previously thoroughly discussed [12, 13]. Moreover, expanded polyQ stretches alone reside in the nucleus and may bind transcription factors and influence transcriptional activity. Several works also have reported the interaction of ataxin-3 with TBP, CREB-binding protein, p300, MMP-2, and HDAC3 (for review, see [12]).

The already described disease mechanisms and the late occurrence of symptoms in SCA3 patients [6] and models [14, 15] and other neurodegenerative disorders underline the existence of presymptomatic disease phase which consists of molecular and cellular events important to the onset and mechanism of disease. In general, the types of molecular events which probably contribute to the presymptomatic phase and lead to disease pathogenesis are transcriptional changes and alterations in the levels of proteins and their phosphorylation state which all can influence cellular processes [6]. Unfortunately, the disease early presymptomatic phase is presently unknown, and it is also unclear what is the contribution of transcriptional and proteome changes in young SCA3 carriers. To detect potential transcriptional and protein initiators of SCA3 pathology resulting from a direct influence of ataxin-3,

we used adult but presymptomatic, young, 2-month-old Ki91 knock-in mouse model homozygous for mutant *Atxn3* gene. The heterozygous version of the Ki91 SCA3/MJD mouse model was already published by us [14]. The present Ki91 mouse is homozygous and contains a higher number of CAG triplet repeats in the mutant *Atxn3* gene. Now, we have tested the cohort of the 2-month-old homozygous Ki91 animals using several behavioral tests and found no significant motor symptoms at this early stage. Using the animals, we profiled the transcriptome by RNAseq and proteome by mass spectrometry (MS) and phosphoproteome enriched in the cerebellum and cerebral cortex where we search for protein and mRNA changes defining the onset of SCA3. In addition, we performed qPCR profiling of proteomic-based markers and cellular markers in search for late, symptomatic or cell type-dependent transcriptomic dysregulations characteristic for neurodegenerative disease. For targeted late transcriptomic profile, we used 10–14-month-old homozygous Ki91 animals. Subsequently, in the bioinformatics part, we used our dysregulated proteomic hits and performed a systematic identification of processes, pathways, subcellular localization, and discovery cell origin of the dysregulated molecules by Cytoscape/ClueGO/Consensus Path DB and other tools. Our work prioritizes the proteomic changes in response to mutant ataxin-3 as the first molecular events occurring in the brain which lacks changes in the levels of mRNA resulting from the presence of mutant ataxin-3. We demonstrated that the transcriptome changes are secondary in SCA3 and appear later in the disease progression in 10–14-month-old Ki91 animals. Moreover, based on early proteomic changes, we discovered several groups of processes that define the onset of SCA3/MJD in Ki91 animals. Among the processes, we identified disturbed termination of translation, spliceosome phosphorylation, chromatin remodeling, protein phosphorylation, mitochondria organization, DNA damage, axon development, and transport of organelles along the axon.

Results

Two-Month-Old Ki91 SCA3/MJD Mice Show Normal Motor Performance, While 14-Month-Old Animals Show Incoordination, Decreased Body Weight, and Symptoms in Scoring Test

In order to determine if there are any signs of motor incoordination in young 2-month-old Ki91 mice, we performed several tests measuring motor skills. We observed no motor deficits in 2-month-old Ki91 mice on the rotarod and parallel rod floor test (Fig. 1e, h). The scoring test of 2-month-old Ki91

mice demonstrated no signs of incoordination, gait disturbances, kyphosis, muscle weakness, or uncontrolled muscle contraction (Fig. 1g). In elevated beam walk, we evaluated two parameters: time to turn of 180° at the end of the rod and time to traverse the rod, each performed on six rods with decreasing diameter: 35, 28, 21, 17, 10 and 9 mm. We did not detect any statistically significant differences between 2-month-old Ki91 and control mice, except the time to turn on the last rod diameter 9 mm ($p < 0.01$; Bonferroni post hoc test) (Fig. 1a, c). We attributed this result to a novelty effect, not related to the first sign of pathology since the observation was not reproduced on this rod for 14-month-old animals. Furthermore, there were no differences in body weight in young 2-month-old animals (Fig. 1f). In contrast to young animals, 14-month-old Ki91 mice demonstrated significant motor deficits in elevated beam walk test on rod diameter 28 mm in time to turn ($p < 0.05$; Bonferroni post hoc test; Fig. 1b) and on rod diameters 35 mm and 28 mm ($p < 0.05$; Bonferroni post hoc test) and rod diameters 21 and 17 mm in time to traverse ($p < 0.01$; Bonferroni post hoc test) (Fig. 1d). In the scoring test, old animals also demonstrated disturbed gait and coordination, kyphosis, and mild muscle contraction ($p < 0.001$; two-sample t test; Fig. 1k). From motor tests, only the rotarod demonstrated no alterations in 14-month-old animals (Fig. 1i). Body weight was significantly lower in 14-month-old animals compared to age-matched controls ($p < 0.001$; two-sample t test) (Fig. 1j).

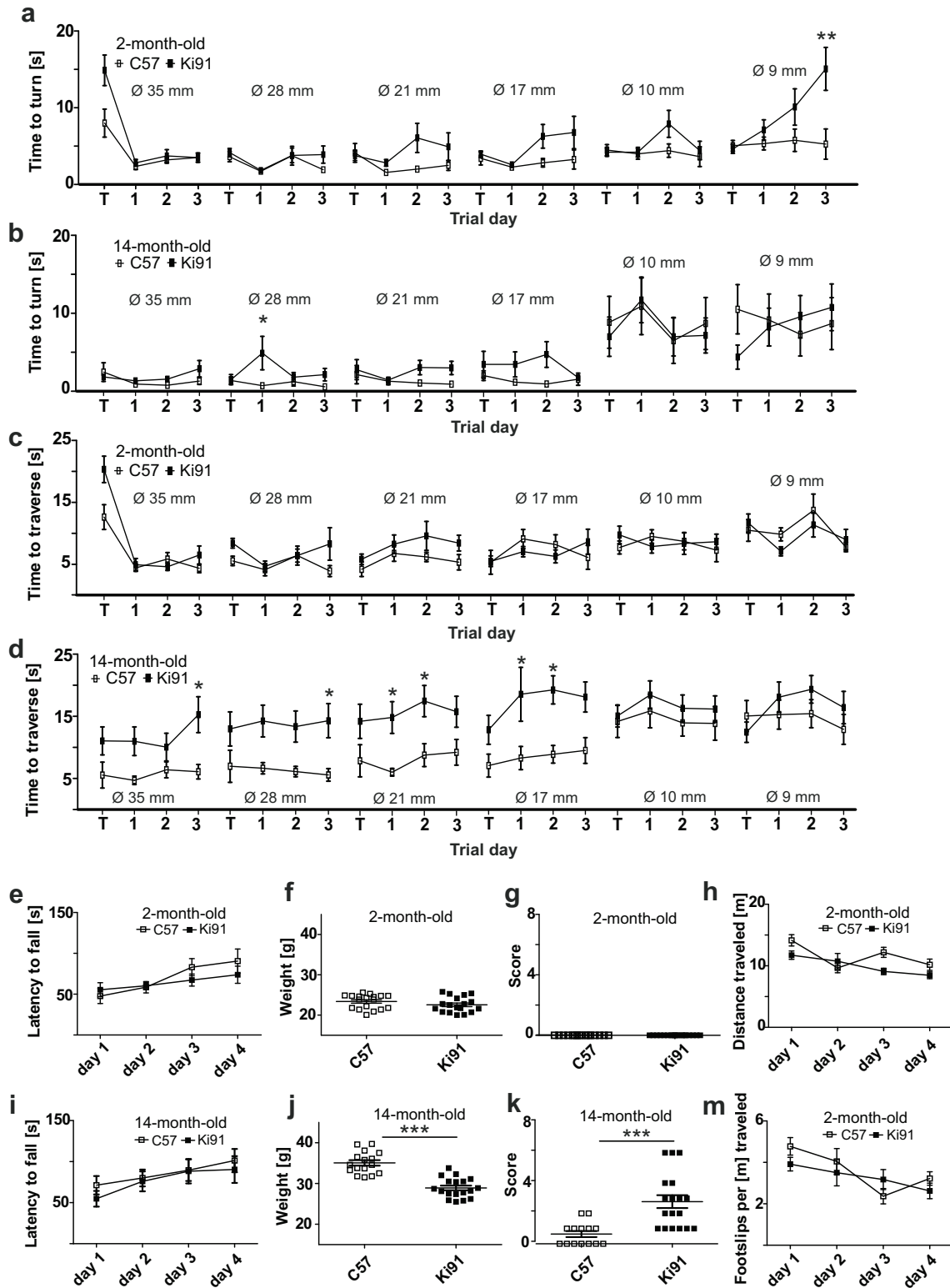
The Cerebellum and Cerebral Cortex of Young Ki91 SCA3/MJD Mouse Demonstrate the Occurrence of Cells with Accumulation of Atxn3-Positive Signal in the Nuclei

One of the cellular hallmarks of SCA3 pathogenesis is the nuclear localization of ataxin-3. Therefore, we investigated ataxin-3 staining of Ki91 2-month-old mouse brain and found cells with nuclei positive for ataxin-3 stained with monoclonal 1H9 anti-ataxin-3 antibody in the white matter of the cerebellum (Fig. 2d–f) and cerebral cortex (Fig. 2j–l). Of note, ataxin-3 accumulation co-localizes with the staining of the nucleus and was restricted to a subset of cells in both regions. Occasionally, the nuclei of young Ki91 mouse cells reveal ataxin-3-positive intranuclear aggregates (Fig. 2e, k). In turn, the localization of ataxin-3 in the cerebellum and cortex of WT animals is uniformly distributed throughout the cytoplasm and cell nucleus (Fig. 2a–c, g–i).

Transcriptional Changes Related to Mutant Ataxin-3 Do Not Occur in the Cerebellum and Cortex of Young Homozygous Ki91 SCA3/MJD Mouse

RNA sequencing was performed using the cerebellum and cortex of four Ki91 mice and four control mice at the age of

2 months. Tables 1 and 2 summarize differentially expressed genes in the cerebellum and cortex, fold changes, p values, and adjusted p values. The genes significantly dysregulated versus control C57BL/6 mice were all located within two relatively small “hot spots” on two mouse chromosomes. In the first hot spot located on chromosome 12, we identified dysregulated expression of *Serpina3n*, *Slc38a6*, *Ccdc88c*, *Fbln5*, and *Ttc8*, where all the dysregulated genes are located very close to the targeted *Atxn3* locus. In the second hot spot on chromosome 19, we found dysregulated expression of *Btaf1*, *Ide*, and *Ablim1* which are all located in close proximity in the genome. Such clustering of dysregulated genes in the hot spot loci also closely surrounding the targeted locus may indicate that the loci have different genetic origin than the rest of the Ki91 mouse genome (congenic; C57BL/6) and may stem from a 129sv background which was the source of stem cells where the Ki91 construct was introduced. We have performed a comparison of SNP signatures of *Serpina3n* gene using the RNAseq data on Ki91 mouse and using the MGI database on 129sv, FVB, and C57BL/6 strains. It turned out that the SNP signatures of the *Serpina3n* gene were the same on 129sv, FVB, and Ki91 mice and different from C57BL/6 mouse. This suggested that the region on chromosome 12 near the transgenic *Atxn3* locus was segregating together with the transgene and was selected by genotyping of transgenic *Atxn3* Ki91 animals. As an additional conclusion to our analysis, we would like to state that we no longer consider *Serpina3n* as a SCA3 transcriptional marker as stated previously in [14]. The next step was the investigation of identified transcriptomic changes using real-time qPCR. Therefore, to assess the validity of transcriptional dysregulation in Ki91 mouse and the influence of foreign 129sv mouse background on the expression of dysregulated genes, we examined the cerebellum and cortex from homozygous Ki91 mouse versus a double set of controls including the cerebellum and cortex from FVB mouse strain (same SNP signatures as 129sv) and from C57BL/6 mouse strain (Figs. 3 and 4). The transcriptional dysregulations in Ki91 mouse tissues investigated versus mRNA isolated from C57BL/6 mouse tissues again demonstrated the dysregulation of these genes. A similar analysis did not reveal any change in the level of transcripts when tissues of Ki91 mouse were investigated versus mRNA isolated from tissues of FVB mouse strain. Particularly, a pronounced difference between C57BL/6 and FVB mouse strains was detected for *Serpina3n* where the cerebellum and cortex from C57BL/6 mice demonstrate almost no expression of *Serpina3n* and the cerebellum and cortex from FVB mice demonstrated high levels of *Serpina3n* similar to the one found in Ki91 mice. Other dysregulations of genes in Ki91 mouse revealed by RNAseq also demonstrated dependency on FVB levels in the qPCR cross-control experiment. Detailed fold changes and p values are summarized in Table 3. The analysis confirmed that the transcriptomic



dysregulation of genes in presymptomatic cerebellum and cortex of Ki91 mouse is the result of genetic background occurring in proximity of transgenic locus and in the locus spot on chromosome 19. In addition, the slightly dysregulated levels of *Fgfbp3*, *Btaf1*, and *Ide* may be the result of known CNV

characteristic for C57BL/6 (but not FVB) and covering this region of chromosome 19 [16]. Moreover, the *Btaf1* and *Ablim1* expression was not altered in symptomatic 14-month-old Ki91 animals (Supplementary Fig. 1). To summarize, we have systematically demonstrated that transcriptional

Fig. 1 Motor performance of 2-month-old and 14-month-old Ki91 SCA3/MJD mice. Each behavioral test consisted of one training day and three consecutive days of measurement, except of scoring test. In the elevated beam walk (**a–d**), two parameters “time to turn” and “traverse time” were tested on each rod (diameter of rods is indicated by Ø in mm). Two-month-old Ki91 mice demonstrated significant differences compared to C57BL/6 (C57) in “time to turn” only on the 9-mm rod on the 3rd day of testing (**a**) and no differences in “traverse time” (**c**). Fourteen-month-old Ki91 mice needed significantly more “time to turn” on the 28-mm rod on the first day of testing (**b**) and significantly more “time to traverse” on four rods: 35, 28, 21 and 17 mm (**d**). There were no significant differences for both 2- and 14-month-old mice in rotarod setup which accelerated from 4 to 40 rpm in 9.5 min (**e, i**). No significant difference in body weight was observed in 2-month-old Ki91 mice, while 14-month-old Ki91 mice demonstrated significant difference (**f, j**). In the scoring test, 2-month-old Ki91 mice scored no parameters associated with SCA3 (**g**), while 14-month-old Ki91 mice scored for characteristic SCA3 phenotypic hallmarks such as: incoordination, gait disturbances, kyphosis, and hind limb clasping (**k**). In the parallel rod floor test, the number of footslips (**m**) and locomotor activity (**h**) was evaluated during 10 min in 2-month-old animals, which demonstrated no differences (**d**). ANOVA with Bonferroni post hoc test ($p \leq 0.05$; total number of biological replicates: $n = 36$, $n = 18$ per genotype), error bars: SEM

changes related to the direct influence of mutant ataxin-3 protein do not occur in our young presymptomatic Ki91 animals in the cortex and cerebellum. This also may indicate that there are no transcriptomic changes in SCA3 cortex and cerebellum that occur very early in life as a direct result of expansion mutation in *Atxn3*. Our results may also indicate that transcriptomic changes, in general, are not direct triggers for the onset of SCA3.

Transcriptional Changes in Homozygous, Old Ki91 SCA3/MJD Animals at 10 and 14 Months Old Characterize Affected Cell Types in SCA3

Since the early transcriptional changes dependent on mutant ataxin-3 do not occur in young Ki91 mice, we sought to determine the transcriptional phenotype in later stages of SCA3. We also asked if the transcriptional changes in the symptomatic phase of SCA3/MJD are markers of any specific cell types in the affected cerebellum and cortex. Identification of such markers could indicate changes in the number of cells in population relevant for brain pathogenesis. Therefore, we made use of old homozygous Ki91 animals at the age of 10 and 14 months. According to our behavioral experiments, 14-month-old Ki91 animals are symptomatic and demonstrate altered motor performance, altered scoring test, and decreased body weight (Fig. 1). Decreased body weight observed in Ki91 animals is one of the hallmarks of SCA3 phenotype in patients [17–20]. Based on preliminary pilot proteomic experiments in old Ki91 mice, we have selected 16 most promising dysregulated protein hits (*Atp2b1*, *Psat1*, *Ppp2r1a*, *Idh1*,

Akr1b1, *Srsf2*, *Plp1*, *Glul*, *Ca2*, *Ndufa9*, *Pea15a*, *Tuba1a*, *Psmd4*, *Omg*, *Cox7a2*, and *Qdpr*) to examine potential transcriptional events in old Ki91 animals at 10 and 14 months old. In addition to these 16 genes, we also included gene candidates selected based on the scRNASeq database (<http://celltypes.brain-map.org/rnaseq/human>) as markers of differentiating oligodendrocytes (*Olig1*, *Olig2*), mature oligodendrocytes (*Mag*, *Omg*, *Cldn11*, *Plp1*), microglia (*Cd68*), neurons (*Reln*, *Npy*, *Sst*), and markers of energy metabolism [21, 22]. Table 4 summarizes gene names (total number of 25 genes), fold changes, and p values of the qPCR investigation in 10- and 14-month-old Ki91 animals. We found that the mRNA of markers of differentiating oligodendrocytes such as *Olig1* and *Olig2* is elevated in both the cerebellum and cortex of Ki91 mouse indicating an increase of demand for new oligodendrocytes in the SCA3/MJD brain (Fig. 5). Moreover, we have detected decreased markers of myelination such as *Plp1* and *Cldn11* in both the cerebellum and cortex also related to tight junctions and all being markers of mature oligodendrocytes. In addition, we detected dysregulated markers of metabolism such as *Psat1*, *Ndufa9*, *Qdpr*, and *Pea15a* (Fig. 5). There was no change in the expression of neuronal markers such as *Npy*, *Sst*, and *Reln* (Fig. 5). In general, we observed a higher number of dysregulated genes in animals at the age of 14 months as compared to animals at 10 months old. Together, our observation of transcriptional changes in young and old animals indicates that observed transcriptional changes are related to cell damage and not directly to ataxin-3 effects. The fold changes of all transcriptional changes in old animals did not exceed 1.5 value with the exception of *Olig1* in the cerebellum. Since the transcriptional changes first appear in older mice and after changes in the proteome (see next sections), we can conclude that changes in mRNA appear in the brain probably when the compensation of cell degeneration and loss is no longer possible and as a result of previous pathogenic processes.

Transcriptional Changes Occurring in Old Ki91 SCA3/MJD Mouse Also Occur in Neurons from SCA3/MJD Patients

Since the transcriptome changes in our Ki91 mouse model occurred in the older brain, we asked if such changes would also occur in terminally differentiated SCA3 neural culture from SCA3 iPSC. Therefore, we used SCA3 iPSC-derived neural cultures from two SCA3 patients and two genetically related healthy individuals [23]. Neural differentiation comprising 6 weeks therefore represented adult neural cells [24]. The mRNA isolation and qPCR revealed the changes in the genes related to neuronal precursors and oligodendrocytes (*Olig1*, *Olig2*, and *Plp1*) and energy metabolism (*Psat1*) (Fig. 6).

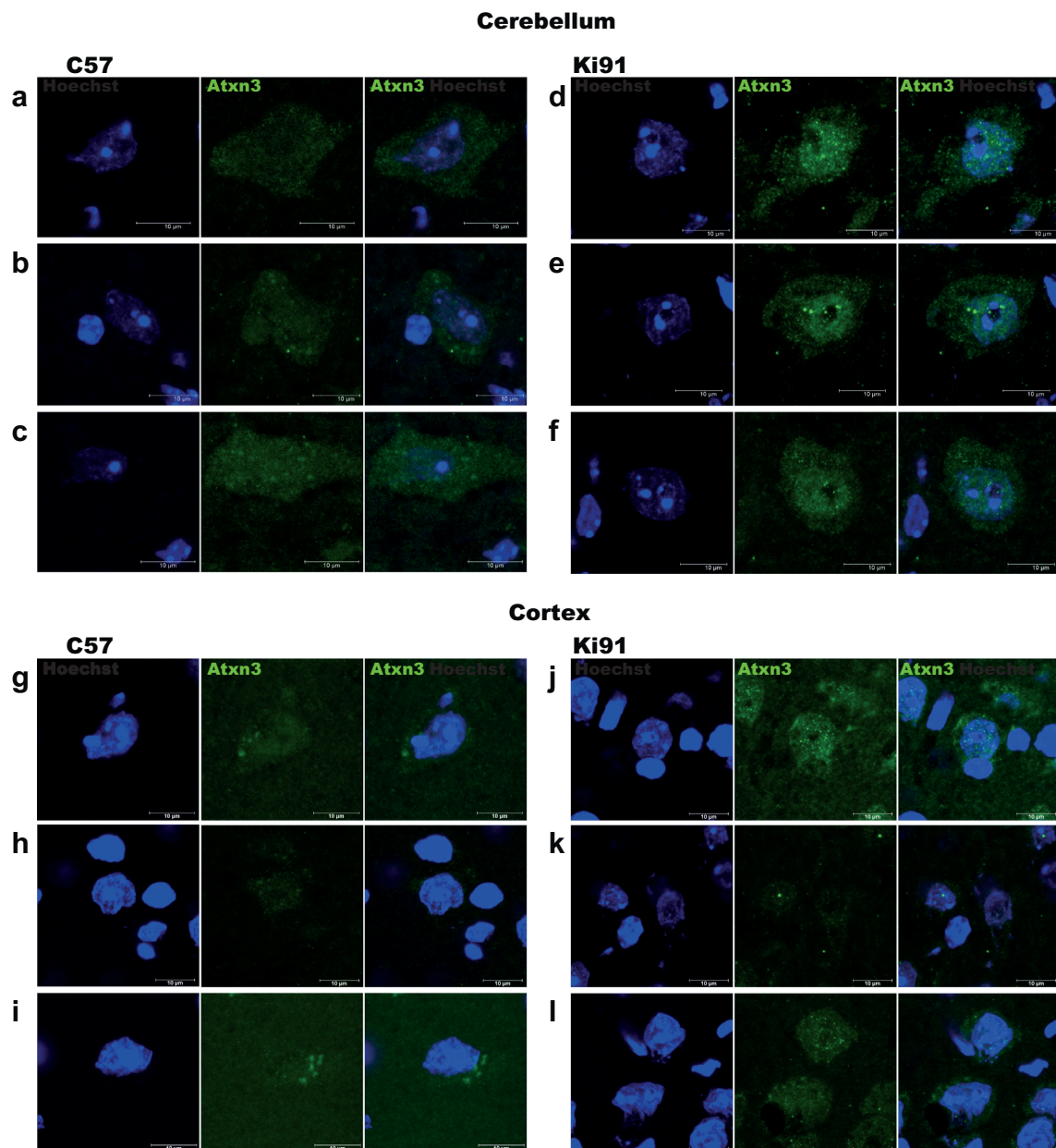


Fig. 2 Nuclear localization of ataxin-3 in 2-month-old presymptomatic Ki91 SCA3/MJD mice. The brain sections revealed small number of cells with ataxin-3-positive staining (green; 1H9 antibody) in the white matter of the cerebellum and cerebral cortex where the ataxin-3 localizes mainly in the cell nucleus (blue; Hoechst 33342) of Ki91 mice, whereas in control samples, ataxin-3 localizes uniformly throughout the whole cell.

Moreover, the micrograph demonstrates localization of microaggregates in the nucleus of cells in Ki91 mice. The figure demonstrates micrographs of three cells per genotype and brain region; cerebellum of C57BL/6 (C57) (a–c), cerebellum of Ki91 mice (d–f) cortex of C57BL/6 (g–i), and cortex of Ki91 mice (j–l). Each cell is presented as green and blue fluorescent channel in addition to micrograph with merged channels

Early Dysregulations of the Total Proteome in Young Ki91 SCA3/MJD Mouse Cerebellum and Cortex

In the next set of experiments, we asked if any molecular presymptomatic changes exist in the proteome of young Ki91 animals. The processing of mass spectra detected 2753 unique proteins in eight samples of both the cortex and cerebellum (FDR < 0.01, at least two different peptides per protein). After filtering and selection for proteins presenting valid

values (see “Methods” section), the number of proteins was reduced to 1098 and 917 proteins in the cerebral cortex and cerebellum, respectively, and these proteins were considered for further analysis in order to detect dysregulated proteins (Supplementary Table 6).

Comparing Ki91 mouse samples to control mouse samples, significant differences ($p < 0.05$; two-sample t test) in protein levels were observed for 133 proteins in the cerebral cortex and 93 in the cerebellum (Supplementary Table 6). In the

Table 1 List of dysregulated transcripts identified by RNAseq in the cerebellum of 2-month-old Ki91 SCA3/MJD mice

Ensemble ID	Gene ID	Chromosome	Log2 fold change	p value	p adjusted
ENSMUSG00000021091	Serpina3n	12	4.17	8.4E-202	2E-197
ENSMUSG00000047632	Fgfbp3	19	1.12	1.53E-15	7.33E-12
ENSMUSG00000021182	Ccdc88c	12	1	5.23E-23	4.17E-19
ENSMUSG00000056999	Ide	19	0.95	4.81E-34	5.75E-30
ENSMUSG00000021186	Fbln5	12	0.94	3.82E-13	1.3E-09
ENSMUSG00000092083	Kcnb2	1	0.71	1.83E-08	4.37E-05
ENSMUSG00000040565	Btaf1	19	0.49	1.57E-09	4.69E-06
ENSMUSG00000021062	Rab15	12	-0.44	2.85E-06	0.004863
ENSMUSG00000044712	Slc38a6	12	-0.61	1.37E-08	3.64E-05
Additional genes identified by JunctionSeq					
ENSMUST00000079360.11	Ablm1				
ENSMUSG00000021013	Ttc8				

cerebellum, the vast majority of proteins were upregulated (77) and 16 proteins were downregulated in Ki91 mice compared to controls, whereas in the cortex, there were slightly more proteins which were upregulated (76) as compared to downregulated (57) (Supplementary Table 6). The heatmap constructed after filtering of dysregulated proteins demonstrates distinct clustering of the datasets (Supplementary Fig. 2). Interestingly, 14 dysregulated proteins were identified both in the cerebellum and cerebral cortex (Hist1h1d, Trim28, Tubb3, Tubb4a, Tubb5, Rac1, Ran, Arpc3, Uba1, Syngr3, Gna12, Rap1gds1, Kpnb1, Gcsh).

The lists of all upregulated and downregulated proteins were subjected to separate analysis of GO terms (*p* value cutoff < 0.001) and pathways (at least 10% of dysregulated hits) in CPDB (Tables 5 and 6). In the cerebellum, downregulated proteins are associated mainly with apoptosis, whereas upregulated proteins are involved in metabolism, in particular the citric acid cycle and electron transport chain and carboxylic acids (Table 5). In addition, upregulated proteins in the cerebellum are also implicated in Parkinson disease and microtubules (Table 5). On the contrary, in the cerebral cortex, energy metabolism (oxidative phosphorylation, NADH dehydrogenase activity), Alzheimer

disease, and retrograde endocannabinoid signaling involve downregulated proteins (Table 6). Meanwhile, upregulated proteins of the cerebral cortex are associated with microtubules, neuronal projections, membrane trafficking, and transport of synaptic vesicles (Table 6).

Early Dysregulations of Phosphoproteome in Young Ki91 SCA3/MJD Mouse Cerebellum and Cortex

Following an analysis of total proteome, we asked whether there are any alterations regarding phosphorylation of proteins. Since there are no transcriptional changes in young 2-month-old pre-symptomatic Ki91 mice, we speculated that dysregulation of protein levels could be related to other cellular mechanisms of protein amount control, such as phosphorylation, which is the most abundant posttranslational modification of proteins. Analysis of mass spectra of enriched samples enabled total identification of 4034 unique proteins. Similar to processing data of total proteins, filtration of valid values and statistical tests were performed on the results obtained in the analysis of the phosphoproteome. The analysis revealed significant differences in the phosphorylation level of 82 individual proteins in the

Table 2 List of dysregulated transcripts identified by RNAseq in cerebral cortex of 2-month-old Ki91 SCA3/MJD mice

Ensemble ID	Gene ID	Chromosome	Log2 fold change	p value	p adjusted
ENSMUSG00000079012	Serpina3m	12	6.22	4.19E-30	3.34E-26
ENSMUSG00000021091	Serpina3n	12	3.27	3.39E-184	8.11E-180
ENSMUSG00000056999	Ide	19	1.07	1.00E-30	1.20E-26
ENSMUSG00000047632	Fgfbp3	12	0.75	7.53E-06	1.80E-02
ENSMUSG00000040565	Btaf1	19	0.62	6.30E-12	3.77E-08
ENSMUSG00000021182	Ccdc88c	12	-0.49	4.09E-06	1.22E-02
ENSMUSG00000047415	Gpr68	12	-0.79	4.03E-06	1.22E-02
Additional genes identified by JunctionSeq					
ENSMUSG00000021013	Ttc8				
ENSMUST00000025961.6	Prdx3				

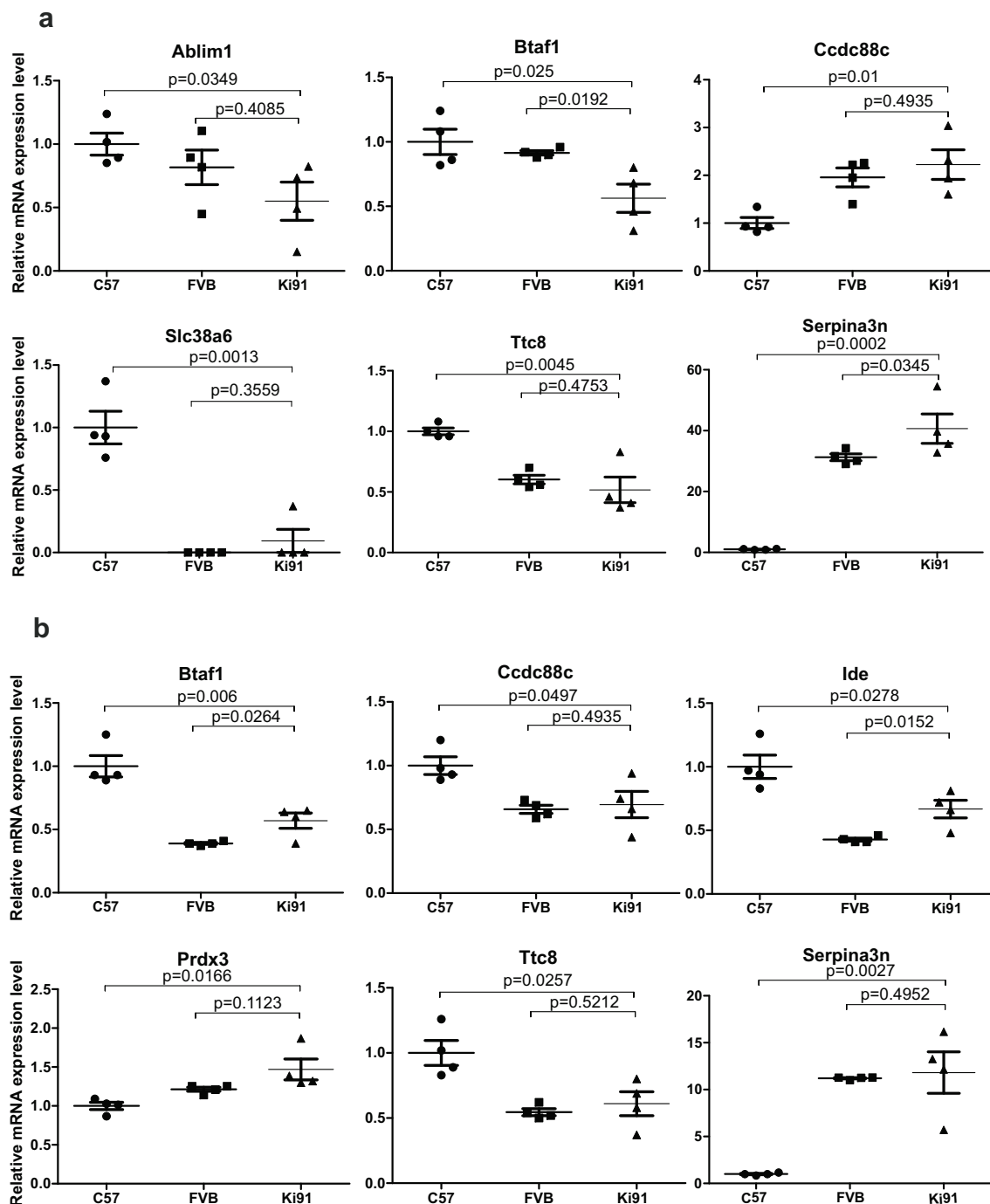


Fig. 3 qPCR analysis of RNAseq results reveals lack of transcriptional changes related to mutant ataxin-3 in 2-month-old presymptomatic mice. Genes identified by RNAseq were analyzed by qPCR using control brain tissue collected from C57BL/6 (C57) and FVB mouse strains to exclude the influence of the genetic background (BG) on the level of gene expression. The differences in expression levels of genes would be considered statistically significant if the tested gene demonstrated $p \leq 0.01$ for each of the brain tissue controls (unpaired Student's t test; error

bars: SEM; total number of samples $n = 12$, $n = 4$ per experimental group). However, none of the tested genes from the **a** cerebellum and **b** cerebral cortex consistently reached such significance value across controls and brain tissues. The qPCR results indicate that the differences in expression level measured by RNAseq are the result of genetic background and are not the result of the influence of the mutant ataxin-3. Hence, the presymptomatic cerebellum and cortex from Ki91 mouse do not demonstrate SCA3 causative changes in mRNA levels

cerebellum and 335 individual proteins in the cerebral cortex (Supplementary Table 6). Part of those proteins had altered modification level in more than one site which increased the number

of hits (total number of altered phosphorylation sites: cerebellum = 95, cortex = 481). In both the cerebral cortex and cerebellum, we observed that the phosphorylation levels of dysregulated

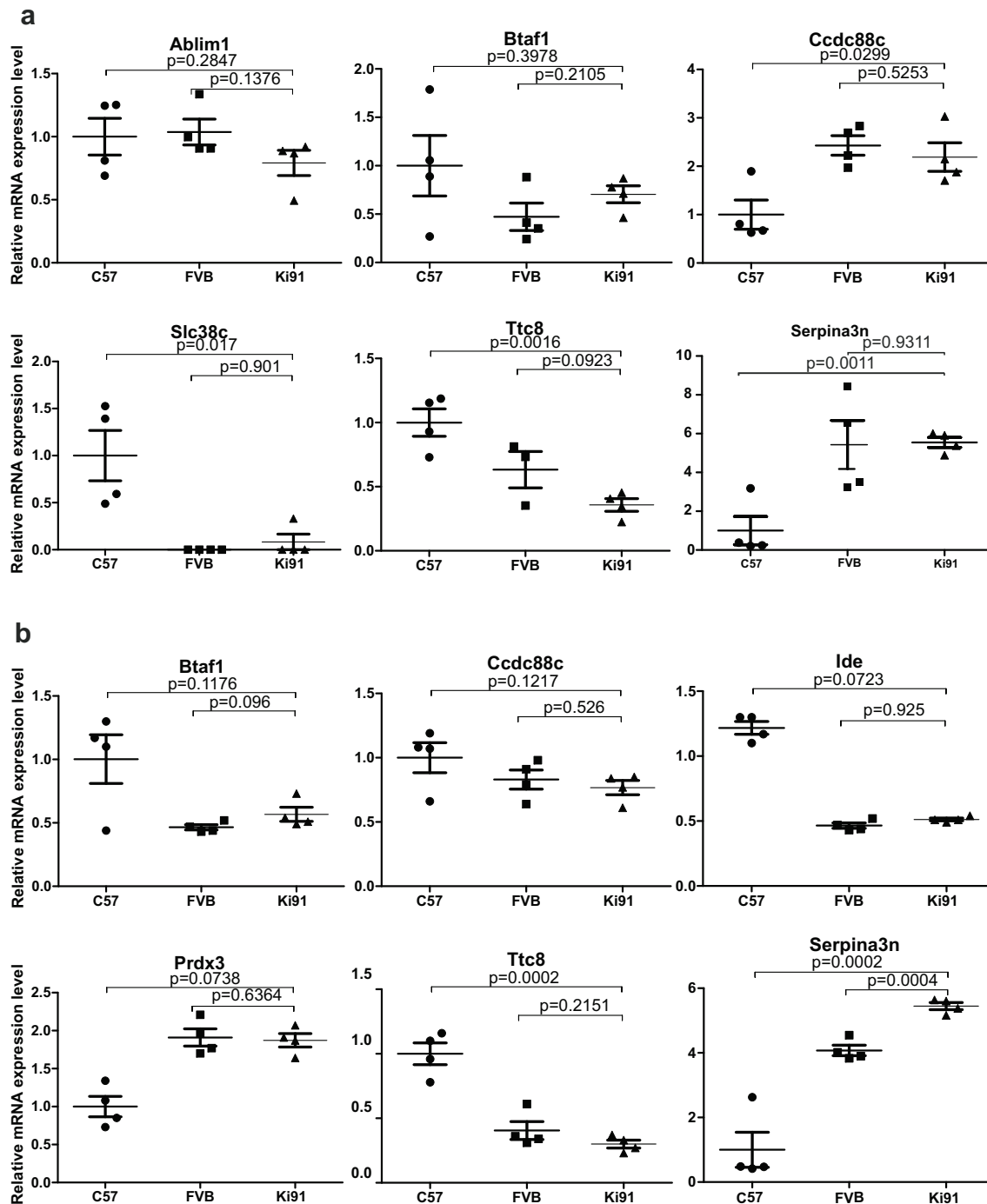


Fig. 4 qPCR analysis of RNAseq results reveals lack of transcriptional changes related to mutant ataxin-3 in 4-month-old Ki91 mouse. The presymptomatic changes in mRNA levels of genes identified by RNAseq were examined by qPCR, however using brain tissue from 4-month-old Ki91 mice. The differences in expression levels of genes for

the **a** cerebellum and **b** cerebral cortex did not reach consistent statistical significance across controls and tissues ($p \leq 0.01$ for each of the brain tissue controls in unpaired Student's *t* test; total number of samples $n = 12$, $n = 4$ per tissue; C57BL6 (C57) or FVB mouse tissue was the control for Ki91 mouse tissues; error bars: SEM)

proteins were decreased and phosphorylation of only three residues in three proteins was increased (cerebellum: Hist1h1d; cerebral cortex: Prkcg and Pclo). Notably, the majority of dysregulated phosphoproteins in the cerebellum overlap with the list of dysregulated phosphoproteins in the cerebral cortex (68% of

individual cerebellar phosphoproteins overlap with the cortex; $N = 56$ and 73% cerebellar phosphosites overlap with the cortex; $N = 70$) (Supplementary Table 6).

We have constructed a network of dysregulated kinases with the highest number of substrates among dysregulated

Table 3 Table summarizing qPCR validation of RNAseq results using brain tissue from 2- and 4-month-old Ki91 SCA3/MJD versus two control mouse strains (C57BL/6 and FVB)

Gene	Tissue	<i>p</i> value C57 vs SCA3	Fold change C57 vs SCA3	<i>p</i> value FVB vs SCA3	Fold change FVB vs SCA3
2-month-old					
Ablim1	CERE	0.0349	0.4795	0.4085	0.756189875
Btafl	CERE	0.025	0.5638	0.0192	0.614754098
Ccdc88c	CERE	0.01	2.225	0.4935	1.136363636
Slc38a6	CERE	0.0013	0.0925	0.3559	1.0925
Ttc8	CERE	0.0045	0.5175	0.4753	0.858921162
Serpina3n	CERE	0.0002	40.66	0.1071	1.30112
Btafl	CTX	0.006	0.57	0.0264	1.461538
Ccdc88c	CTX	0.0497	0.695	0.7408	1.057034221
Ide	CTX	0.0278	0.6675	0.0146	1.561404
Prdx3	CTX	0.2785	1.228	0.3696	1.16952381
Ttc8	CTX	0.0257	0.61	0.5212	1.119266055
Serpina3n	CTX	0.0027	11.82	0.7911	1.055357143
4-month-old					
Ablim1	CERE	0.2847	0.7922	0.1376	0.763934426
Btafl	CERE	0.3978	0.7049	1.492167655	1.492167655
Ccdc88c	CERE	0.0299	2.19	0.5253	0.901234568
Slc38a6	CERE	0.017	0.08285	0.901234568	1.08285
Ttc8	CERE	0.0016	0.3577	0.0923	0.565354829
Serpina3n	CERE	0.0011	554.5	0.9311	10.08775731
Btafl	CTX	0.1176	0.5425	0.096	1.437086093
Ccdc88c	CTX	0.1217	0.7675	0.526	0.924698795
Ide	CTX	0.0723	0.5675	0.924698795	1.220430108
Prdx3	CTX	0.0738	1.416	0.6364	0.947157191
Ttc8	CTX	0.0002	0.3	0.2151	0.740740741
Serpina3n	CTX	0.0002	5.445	0.0004	1.3365243

proteins (altered total levels or phosphorylation pattern) using the CPDB tool, protein–protein interaction networks (induced network) visualized in Fig. 7. The network of proteins of the cerebral cortex separates the most important kinases, which are arranged in the outer space, circularly around their substrates (Fig. 7a). This arrangement demonstrates that most of the identified dysregulated kinases are interactors (CPDB) and have an influence on common protein substrates which were identified by us as dysregulated in total proteome or phosphoproteome analysis. The smaller network organizing proteins of the cerebellum places the kinase Pak1 in the center of protein–protein interactions (Fig. 7b). Pak1 has a role in cellular pathways related mainly to cytoskeleton organization and transport, proliferation, and apoptosis [25]. In the cerebral cortex, Pak1 is also one of the most compelling kinases, together with Brsk1 and Brsk2 also playing role in axon guidance, Src, Braf, and multifunctional Mapk and Gsk3b (Fig. 7a). Other important kinases of the network are involved in trans-synaptic signaling: calcium/calmodulin-dependent kinases Camk2a and Camk2b and isoforms of protein kinase c: Prkca, Prkcd, and Prkcg (Fig. 7a). On the other hand,

substrates which may be modified by the highest number of kinases in the network are MAPT and MAP2—both regulating functions of the microtubule of axons and dendrites.

Furthermore, we have performed another analysis with the use of PHOSIDA in order to find those kinases, which are not necessarily dysregulated, but which phosphorylate dysregulated proteins at identified residues within motifs. The analysis identified five kinases, namely Ck1 and 2, Pka, Cdk2, and Camk2 for both the cerebellum and cerebral cortex (Fig. 7c, d), which are mainly responsible for the altered level of phosphorylation on most residues and motifs (77% in the cerebellum, 78% in the cerebral cortex).

In addition, comparison of total proteome and phosphoproteome identified 7 proteins in the cerebellum which were altered commonly (Hist1h1d, Uba1, Nefh, Tmpo, Trim28, Dyncl1l1, Add3) and 19 such proteins in the cerebral cortex (Basp1, Slc9a3r1, Dyncl1l2, Gap43, Mbp, Slc6a17, Marcks, Stx1b, Ndrg2, Kif5c, Map1b, Uba1, Pcdh1, Plcb1, Tomm70a, Eef1d, Trim28, Sept4, Gja1) (Supplementary Table 6). However, in both the cerebral cortex and cerebellum, there were groups of biological processes containing dysregulated phosphoproteins,

Table 4 Transcriptomic changes in 10- and 14-month-old symptomatic homozygous Ki91 SCA3/MJD mice

10-month-old				14-month-old			
Gene	Tissue	p value	Fold change	Gene	Tissue	p value	Fold change
Olig1	CERE	0.0054	1.653	Olig1	CERE	0.1147	1.388
Atp2b1	CERE	0.0337	1.29	Cd68	CERE	0.0114	1.278
Psat1	CERE	0.005	1.26	Mesh1	CERE	0.4267	1.268
Mag	CERE	0.0968	1.169	Olig2	CERE	0.0654	1.248
Cldn11	CERE	0.4082	1.153	Sst	CERE	0.5174	1.19
Ppp2r1a	CERE	0.3191	1.085	Mag	CERE	0.1139	1.185
Olig2	CERE	0.0955	1.074	Reln	CERE	0.2437	1.07
Idh1	CERE	0.6792	1.065	Plekhb1	CERE	0.4829	1.065
Akr1b1	CERE	0.3954	1.043	Pdgfra	CERE	0.6852	1.05
Srsf2	CERE	0.7069	1.033	Ppp2r1a	CERE	0.6153	1.027
Plp1	CERE	0.8646	0.955	Npy	CERE	0.8756	1.018
Cd68	CERE	0.7641	0.9541	Cldn11	CERE	0.9458	1.01
Glul	CERE	0.5006	0.9425	Idh1	CERE	0.5816	0.95
Reln	CERE	0.4208	0.9406	Syp1	CERE	0.1438	0.9375
Pdgfra	CERE	0.2705	0.8538	Glul	CERE	0.1805	0.9167
Npy	CERE	0.1851	0.8473	Atp2b1	CERE	0.0366	0.88
Sst	CERE	0.2524	0.7936	Ca2	CERE	0.0024	0.6867
Ca2	CERE	0.0844	0.7675	Plp1	CERE	0.0003	0.5967
Psat1	CTX	0.0006	1.385	Omg	CTX	0.0825	1.46
Srsf2	CTX	0.0041	1.32	Olig1	CTX	0.0356	1.447
Mag	CTX	0.0027	1.294	Ndufa9	CTX	0.0307	1.298
Olig1	CTX	0.0134	1.293	Srsf2	CTX	0.1636	1.278
Olig2	CTX	0.0604	1.164	Psat1	CTX	0.0042	1.263
Sst	CTX	0.0763	1.151	Pea15a	CTX	0.0536	1.26
Ndufa9	CTX	0.1586	1.143	Sst	CTX	0.3694	1.23
Pea15a	CTX	0.0385	1.12	Mag	CTX	0.0126	1.201
Tuba1a	CTX	0.0985	1.098	Olig2	CTX	0.05	1.198
Npy	CTX	0.2445	1.056	Npy	CTX	0.0751	1.174
Psmd4	CTX	0.6667	1.033	Psmd4	CTX	0.0455	1.14
Pdgfra	CTX	0.5033	1.033	Cd68	CTX	0.019	1.126
Reln	CTX	0.6198	1.026	Tuba1a	CTX	0.1073	1.123
Omg	CTX	0.5851	1.023	Cox7a2	CTX	0.4625	1.068
Cox7a2	CTX	1	1	Reln	CTX	0.5893	1.033
Cd68	CTX	0.8199	0.9814	Cldn11	CTX	0.0356	0.7996
Qdpr	CTX	0.2533	0.9	Mash1	CTX	0.0945	0.7891
Cldn11	CTX	0.005	0.8894	Qdpr	CTX	0.0347	0.7225
Plp1	CTX	0.0009	0.7031	Plp1	CTX	0.0024	0.5745

which correspond well with groups of processes containing dysregulated total proteins (Supplementary Tables 3–5).

Western Blot Analysis of Dysregulated Proteins and Phosphoproteins in Presymptomatic Ki91 SCA3/MJD Mice

The selected proteins and phosphoproteins identified in label-free mass spectrometry analysis were subjected to

western blot analysis using commercial antibodies. The criteria for validation of proteins were the fold change of dysregulation, the affected processes, and in the case of phosphoproteins, also the commercial availability of the phospho-specific antibodies. p-Darpp32, p-Tau, Pabpc1, Mbp, Tubb3, Ddb1, and Nefh were assayed versus α -actin as loading control (Fig. 8). We confirmed the down-regulation of p-Darpp32 (phosphosite Ser97; fold change (FC) = 0.62; $p = 0.045$; two-sample t test) in the cerebral

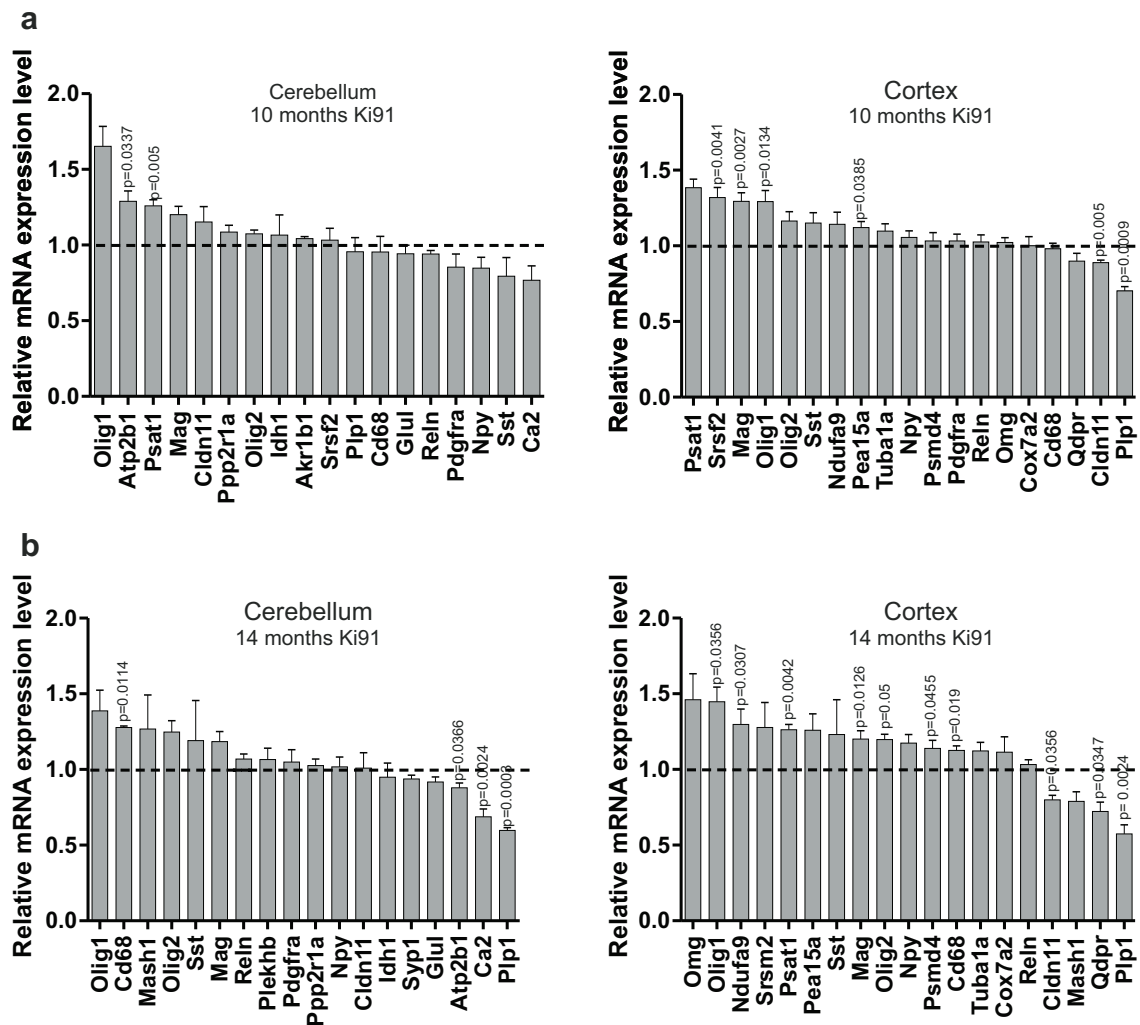


Fig. 5 Transcriptomic changes occur in 10- and 14-month-old symptomatic homozygous Ki91 SCA3/MJD mice and are also related to changes associated with particular cell types. In 10-month-old Ki91 mice, the analysis revealed the elevated level of Psat1 and Olig1 in the cerebellum and cortex (**a**). Mag gene related to oligodendrocytes revealed upregulated level in the cortex. Plp1 demonstrated decreased level in the cortex of 10-month-old Ki91 mice suggesting loss of adult oligodendrocytes during disease progression. Fourteen-month-old Ki91 mice demonstrate more pronounced alterations in tested mRNA levels (**b**). In the cerebellum, the Cd68, a microglial marker, demonstrated upregulated expression level. The metabolism-associated genes, Apt2b1 and Ca2, are downregulated. The gene highly expressed in adult oligodendrocytes Plp1 is also downregulated in the cerebellum. In the cortex, the level of transcripts, characteristic for oligodendrocyte precursors, is upregulated (Olig1, Olig2) and, on the other hand, decreased the level of transcripts characteristic for adult oligodendrocytes (Plp1 and Cldn11) and also increased the level of

Mag. We did not detect transcriptional changes characteristic for neuronal markers both in 10- and 14-month-old Ki91 mouse brains. We also observe the changed level of genes characteristic for metabolism (Psat1, Qdpr, and Psmd4). $p \leq 0.05$, using unpaired Student's t test; total number of samples $n = 8$ per age per cerebellum or cortex; $n = 4$ for the control group per individual tissue of 10 or 14 months, $n = 4$ for the SCA3 group per tissue of 10-month-old. In the case of 14-month-old Ki91 mouse, $n = 3$ or $n = 4$ depending on the gene tested: $n = 3$ in the Ki91 mouse group for the following genes in the cerebellum: Srsf2, Ppp2r1a, Idh1, Glul, Atp2b1, Ca2, Plp1; $n = 3$ in Ki91 mouse for the following genes in the cortex: Olig1, Olig2, Cd68, Cox7a2, Rein, Cldn11, Mash, Plp1; $n = 4$ in the Ki91 mouse group in the cerebellum: Olig1, Cd68, Mash1, Olig2, Sst, Mag, Rein, Plekhb1, Pdgfra, Npy, Cldn11; $n = 4$ in the Ki91 mouse group for the following genes in the cortex: Omg, Ndufa9, Srsf2, Psat1, Pea15a, Sst, Mag, Npy, Psmd4, Tuba1a, Qdpr (\pm SEM).

cortex and p-Tau in the cerebral cortex ($FC = 0.5$; $p = 0.0012$; two-sample t test) (Fig. 8a, c) and cerebellum ($FC = 0.58$; $p = 0.0035$; two-sample t test) (Fig. 8b, d). Furthermore, we selected several relevant proteins related to such biological processes as translation [26] (Pabpc1), DNA damage and repair [27] (Ddb1), myelin formation

[28] (Mbp), and neuronal microtubule function [29, 30] (Tubb3, Nefh). We confirmed increased levels of Pabpc1 ($FC = 1.5$; $p = 0.013$; two-sample t test) and decreased levels of Mbp ($FC = 0.78$; $p = 0.0012$; two-sample t test) and Tubb3 ($FC = 0.78$; $p = 0.011$; two-sample t test) in the cerebral cortex (Fig. 8a, c) as well as increased levels

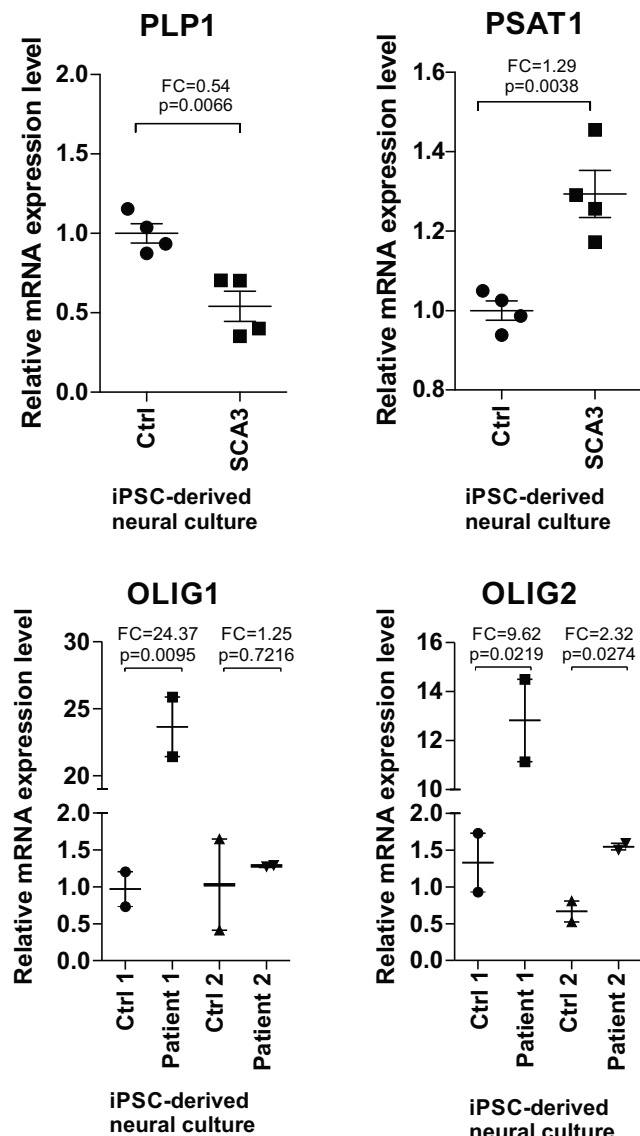


Fig. 6 Human SCA3 neural cultures demonstrated mRNA changes similar to late changes in Ki91 SCA3/MJD mouse. iPSC-derived neural cultures from SCA3 patients were tested for dysregulated expression of PLP1, OLIG1, and OLIG2 (classically associated with oligodendrocytes and in neuronal precursors) and for dysregulation of PSAT1 which is associated with serine and glycine metabolism. The marker of precursors of oligodendrocytes and neurons, Olig1, was upregulated in one patient and Olig2 was upregulated in neural cultures from both patients. PLP1, which is highly expressed in mature oligodendrocyte, was decreased in SCA3 patients. The PSAT1 marker was slightly upregulated in both patients. Provisional *p* values (unpaired Student's *t* test; two cell culture technical replicates per patient) were calculated for the evaluation of differences between patient and control; however, the statistical criteria for using *t* test were not met due to a small number of available patients (patients *n* = 2; unaffected patient controls *n* = 2). PLP1 FC for both patients—0.54, PSAT1 FC for both patients—1.29, OLIG1 patient 1 FC—24.37, patient 2 FC—1.25; OLIG2 patient 1 FC—9.62, patient 2 FC—2.32 (error bars: SEM)

of Ddb1 ($FC = 1.34; P = 0.011$; two-sample *t* test) and Nefh ($FC = 1.7; p = 0.007$; two-sample *t* test) in the cerebellum (Fig. 8b, d) ($p < 0.05$; two-sample *t* test).

Dysregulations of Total Proteome and Phosphoproteome Reveal Three Major Arbitrary Groups of Disturbed Biological Processes in the Brain of Young Ki91 SCA3/MJD Mouse

Based on the CPDB and ClueGO analysis (GO term analysis (B, MF, level 5) and pathway enrichment), we have selected three groups of biological processes, which are enriched among dysregulated proteins in both the cerebral cortex and cerebellum. The complete lists of GO terms and pathways related to dysregulated proteins and phosphoproteins are included in Supplementary Tables 3–5. Of note, results obtained with both bioinformatic tools (CPDB and ClueGO) showed overlap in the majority of biological processes and pathways (see Supplementary Tables 3–5). The analysis is visualized in Fig. 9 where the processes were grouped arbitrarily and in Supplementary Figs. 3 and 4 with no arbitrary grouping. Selection of the groups was performed according to mutual relations and similarity of biological function of pathways and GO terms. We termed the first group “Disturbed mechanisms of modulation of protein levels and DNA damage” associated with either protein ubiquitination, translation initiation, splicing, or chromatin organization (Tables 7 and 8; Fig. 9, group I). The second group consists of biological processes that likely result from the initial dysregulations in the first group. The second group was termed “Disturbed formation of neuronal cellular structures: organelles and macromolecules” and is related to aberrant protein folding and affected organelle biogenesis and maintenance, which includes microtubule and actin cytoskeleton organization, the formation of axons and dendrites, axon guidance, the formation of gap junctions, and cellular vesicles (Tables 9 and 10; Fig. 9, group II). The third group was termed “Neuronal cell functionality affected by processes following perturbed cytoskeletal complex formation and apoptosis” (Tables 11 and 12; Fig. 9, group III). The processes affected in this group consist of axonal transport along microtubules, including synaptic vesicles and mitochondria, and consequently, mitochondrial respiratory chain complex formation and integration of energy metabolism (related to trans-synaptic signaling). Of note, several proteins participating in the processes belonging to this group were previously associated with other neurodegenerative disorders like HD, PD, and AD (Supplementary Tables 3–4). In this group, we also included programmed cell death as the final effect of all affected processes.

Disturbed Mechanism of Modulation of Protein Levels and DNA Damage (Group 1)

In the cerebellum (Table 7; Fig. 9, I; Supplementary Tables 3–5), several dysregulated proteins are involved in joining and releasing of ribosomal subunits and hydrolysis of mRNA with premature codon termination (Ppp2r1a ↑, Rplp2 ↑, Rps27a

Table 5 Summary of six top pathways and GO terms separately analyzed for up- and downregulated proteins in the cerebellum (CPDB)

Up/ downregulation	GO term/pathway	Source	Number of dysregulated proteins	p value	q value
Analysis for downregulated proteins					
	Apoptosis	Reactome	5	4.47E-08	1.72E-06
	Programmed cell death	Reactome	5	5.07E-08	1.72E-06
	Activation of BH3-only proteins	Reactome	3	2.47E-06	5.61E-05
	Intrinsic pathway for apoptosis	Reactome	3	7.48E-06	0.00012
	Alpha6Beta4Integrin	NetPath	3	3.41E-05	0.00046
	Apoptotic mitochondrial changes	GO:0008637	3	8.43E-05	0.00455
Analysis for upregulated proteins					
	The citric acid (TCA) cycle and respiratory electron transport	Reactome	9	1.10E-07	1.21E-06
	Parkinson's disease— <i>Homo sapiens</i> (human)	KEGG	8	3.23E-07	1.78E-06
	Metabolism	Reactome	25	9.80E-07	3.59E-06
	Carboxylic acid metabolic process	GO:0019752	14	5.87E-06	0.00113
	Microtubule	GO:0005874	9	6.90E-06	0.00015
	ATP synthesis–coupled electron transport	GO:0042773	5	1.56E-05	0.00117

(↓); (↑) upregulated in Ki91 mouse; (↓) downregulated in Ki91 mouse; (p) phosphoproteins). Several proteins with altered levels of phosphorylation are related to such GO terms as nucleosome assembly (*Hist1h1a* (↓), *HIst1h1d* (t↓; p↓), *Hist1h4a* (↓)) or chromatin organization (*Tom1l2* (↓), *Trim28* (↓), *Numa1* (↓)). Coherently, the total level of chromatin remodeling factor *Rbbp4* (↑) is markedly increased. Signs of dysregulated mRNA splicing are suggested by dysregulation of several proteins at the level of phosphoprotein isoforms (*Acin1* (p↓), *Npm1* (p↓), *Srsf9* (p↓), and *Thrap3* (p↓)) and dysregulated proteins (*Hnrnpk* (↑), *Ddx5* (↑), *Snrnp200* (↑)), highly upregulated *Hnrnph2* (↑), and

downregulated *Srsf1* (↓)). Aberrations regarding mRNA processing may be linked to GO terms implicating DNA damage: DNA repair and global genome nucleotide excision repair (*GG-NER*), which involve *Ppp5c* (↑), and highly upregulated *Ddb1* (↑). In turn, *Uba1* (↑), *Uba52* (↓), and *Usp9x* (↓) are taking part in ubiquitin activation, whereas highly elevated *Rab5a* (↑) and *Vps35* (↑) have a role in the maturation of macroautophagosomes.

Compared to the cerebellum, in the cerebral cortex (Table 8; Fig. 9, I; Supplementary Tables 3–5), we have also identified similar processes involved in modulation of the protein level. These processes were predominantly represented by

Table 6 Summary of six top pathways and GO terms separately analyzed for up- and downregulated proteins in the cerebral cortex (CPDB)

Up/ downregulation	GO term/pathway	Source	Number of dysregulated proteins	p value	q value
Analysis for downregulated proteins					
	Membrane trafficking	Reactome	7	0.00378733	0.02140158
	Vesicle-mediated transport	Reactome	7	0.00535039	0.02140158
	Microtubule	GO:0005874	9	1.31E-06	1.52E-05
	Microtubule cytoskeleton	GO:0015630	14	1.52E-06	1.52E-05
	Neuron projection development	GO:0031175	12	5.71E-06	0.00080027
Analysis for upregulated proteins					
	Oxidative phosphorylation— <i>Homo sapiens</i> (human)	KEGG	7	2.34E-06	2.80E-05
	Retrograde endocannabinoid signaling— <i>Homo sapiens</i> (human)	KEGG	7	4.76E-06	2.86E-05
	Alzheimer's disease— <i>Homo sapiens</i> (human)	KEGG	7	1.23E-05	4.92E-05
	NADH dehydrogenase (quinone) activity	GO:0050136	4	2.09E-05	0.0005652
	Peptide transport	GO:0015833	19	3.15E-05	0.0022926
	Mitochondrial electron transport, NADH to ubiquinone	GO:0006120	4	3.41E-05	0.0022926

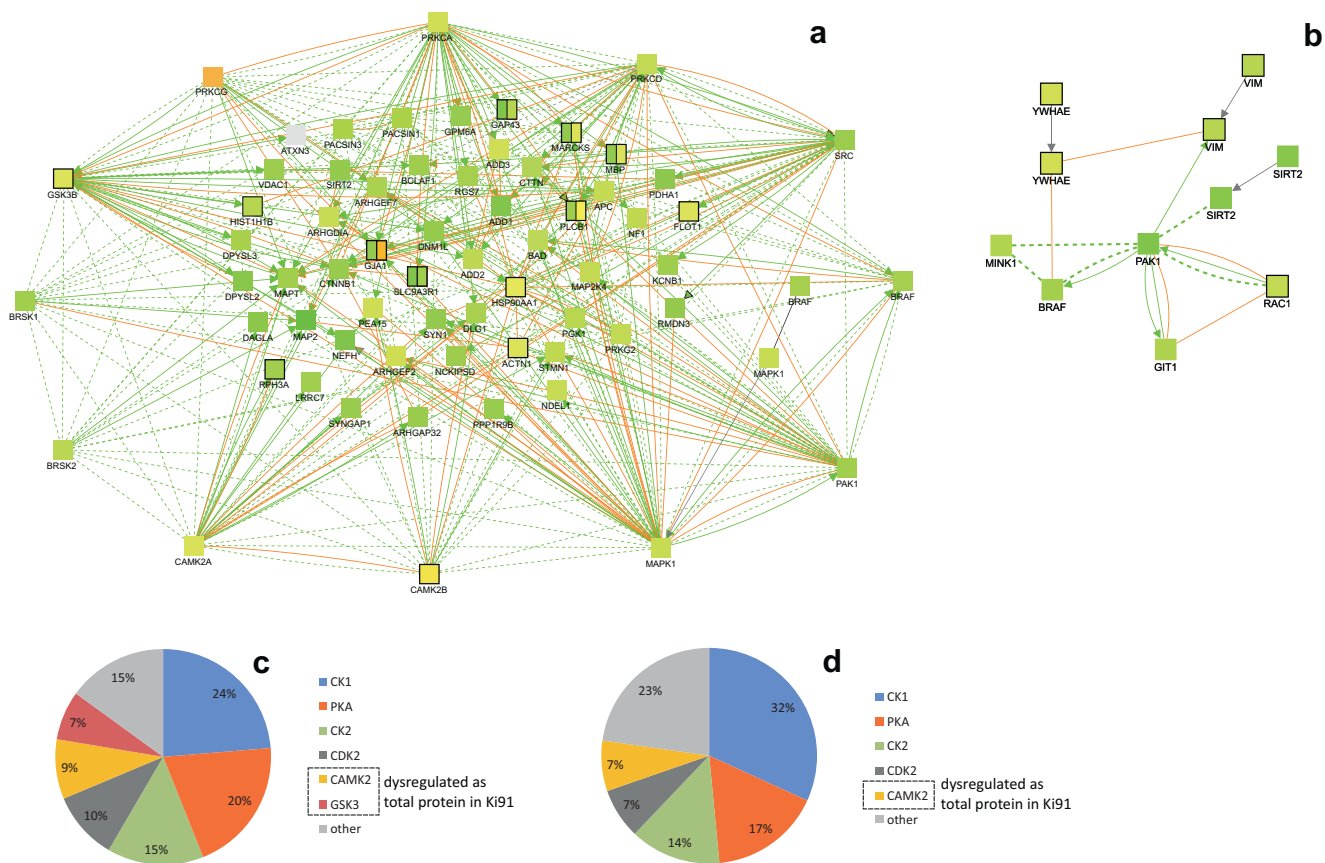


Fig. 7 Dysregulation of protein phosphorylation in Ki91 SCA3/MJD mouse brains: kinases and their substrates. Network of dysregulated kinases and their substrates was generated with the CPDB tool: induced network modules using gene names coding for dysregulated proteins and phosphoproteins (high and medium confidence), number of dysregulated proteins and phosphoproteins in the cerebellum $n = 175$; in the cerebral cortex $n = 486$, four biological replicates (Z -score calculated with the binomial proportions test). The gradient of red color is for upregulated proteins, green color for downregulated proteins. Nonframed squares denote proteins with altered phosphorylation; one-color, framed squares denote total dysregulated proteins; and two-color, framed squares denote proteins, which are dysregulated both at phosphorylation and total levels (left part of the square—phosphorylation, right part of the square—total

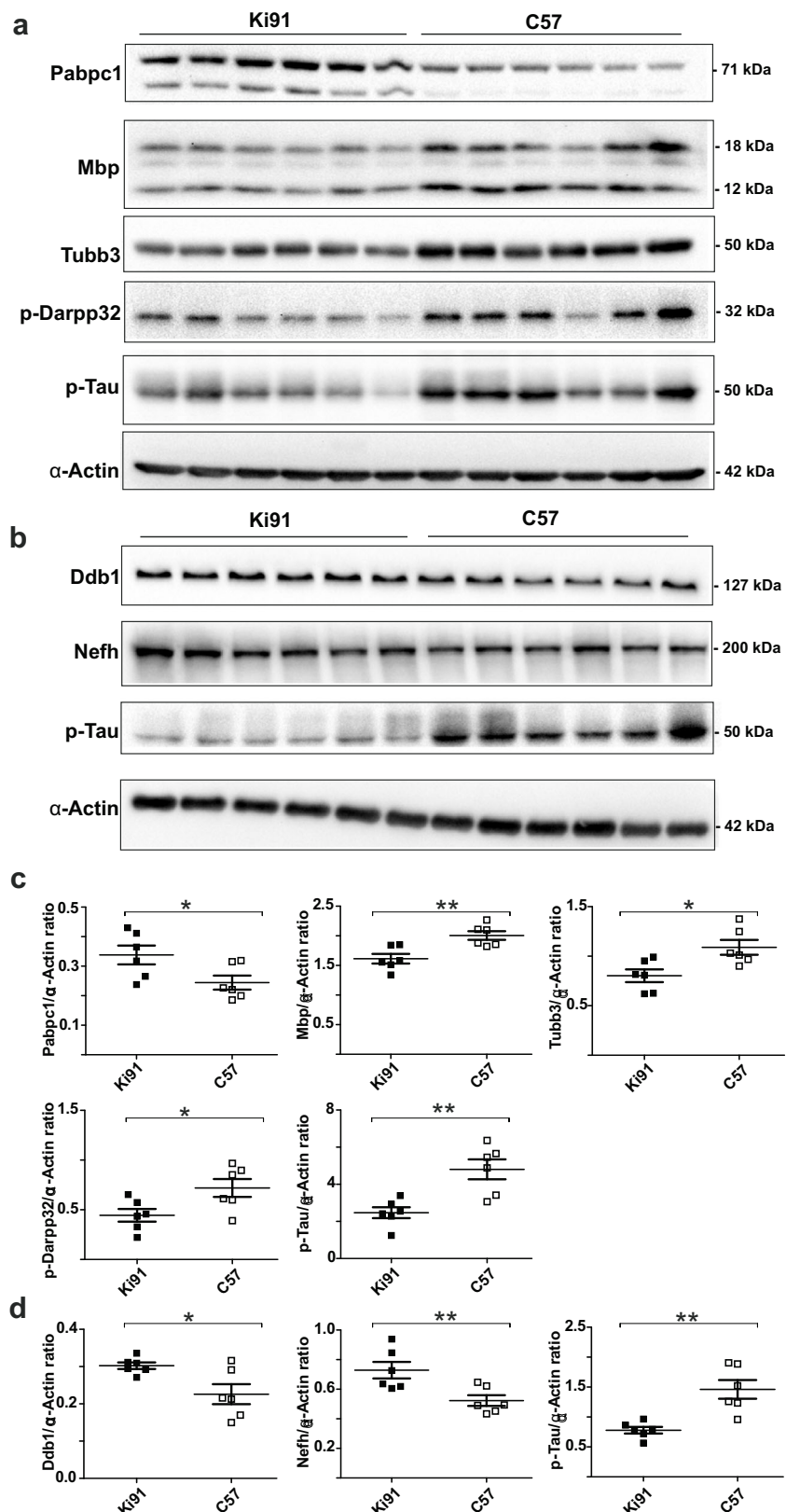
level). Orange arrows are for biochemical reactions and green arrows for physical interactions. Kinases with the highest number of dysregulated substrates are arranged in the outer space of the network. There are several such kinases identified in the cerebral cortex (a) and one kinase: Pak1 in the cerebellum (b). In the cerebral cortex, the substrate, which is modified by several different dysregulated kinases, is Mapt and Map2, both regulating microtubule functions. Further analysis of peptides with modified phosphosites using PHOSIDA revealed additional kinases (CKs, Pka, Cdks, Camk2a) common for the cerebellum and cerebral cortex, which phosphorylate the highest number of dysregulated phosphoproteins in the cerebral cortex, $n = 335$ (c), and cerebellum, $n = 82$ (d); total number of biological replicates: $n = 8$, $n = 4$ per genotype

proteins related to translation initiation, including translational factors (Eef1b2, Eef1d, Eif3f, Eif5a, Pabpc1) belonging to the list of top dysregulated proteins (all \uparrow); log₂ fold change ≤ -1.0) and ribosomal proteins responsible for joining and releasing ribosomal subunits and premature termination of translation (Rpl13, Rplp0, Rps13, Rps27, Rps5; all \uparrow), which interestingly also are all being upregulated. Similar to the cerebellum, there were several histone proteins with altered levels (Hist1h1b, Hist1h1d, H2af2 (all \downarrow)). Among proteins with altered level of phosphorylation were those which are implicated in forming nucleosomes or remodeling chromatin (Hdac2, Nap1l4, all $(p\downarrow)$), transcription (Sltm, Trim28, all $(p\downarrow)$) or translation (Eif4g3, Eif3c, all $(p\downarrow)$), and ubiquitination (Uba1, Usp10, all $p\downarrow$). Several proteins with more than one site of altered phosphorylation were related to splicing (Srsf9,

Prpf4b, Zranb2, Rbm39, Srrm1, Srrm2, all $(p\downarrow)$), and among the top dysregulated proteins, there was highly downregulated Sfl protein ($\log_2 FC = -2.08$).

Disturbed Formation of Neuronal Cellular Structures: Organelles and Macromolecules (Group 2)

The second group of molecules with altered levels indicates aberrant turnover of cellular microtubule cytoskeleton which in turn may disturb various cell structures in neuronal cells. In the cerebellum (Table 9; Fig. 9, II; Supplementary Tables 3–5), proteins required for interphase microtubule organization from centrosome are upregulated (Ppp2r1a, Tuba1a, Tubb4a, Tubb5, Ywhae (all \uparrow)) together with several other microtubule proteins



(DynII2, Dynlrb1, Tuba3a, Tubb3 (all ↑)). Remarkably, Tuba1/Tuba3a is a top upregulated protein in the cerebellum with log₂ FC 3.51 (Supplementary Table 6). Along

this line, neuron projection organization might be affected, which manifests through elevated levels of Cfl1, Dpysl2, Gna12, and Kras (all ↑) and decreased levels of Rac1–3,

Fig. 8 Western blotting analysis of proteins and phosphoproteins dysregulated in presymptomatic 2-month-old Ki91 mice. Western blot analysis confirmed increased levels of Pabpc1 ($p = 0.013$; two-sample t test) and decreased levels of Mbp ($p = 0.0012$; two-sample t test), Tubb3 ($p = 0.011$; two-sample t test), p-Darpp32 ($p = 0.045$; two-sample t test), and p-Tau ($p = 0.0012$; two-sample t test) in the cerebral cortex of 2-month-old Ki91 mice (a, c). In the cerebellum of Ki91 animals, increased levels of Ddb1 ($p = 0.011$; two-sample t test) and Nefh ($p = 0.007$; two-sample t test) and decreased levels of p-Tau ($p = 0.0035$; two-sample t test) were demonstrated (b, d). α -Actin was used as a loading control. $N=6$ per genotype, error bars: SEM. All experiments were performed in three technical replicates

Atp1a3, and Vps35 (all ↓), and Baiap2 (↑)) (Table 9; Fig. 9, II; Supplementary Tables 3–5). A similar subset of proteins (Gnai2, Itpr3, Kras, Tuba3a, Tubb3, Tubb4a, Tubb5 all ↑) is also responsible for the exchange of small molecules through gap junctions. Among dysregulated proteins are also Rho GTPase effectors, which are important modifiers of microtubule and actin dynamics (Baiap2, Rac1, Dyncl1l (all ↑)). Proteins of NGF and EGFR1 signaling pathways are mostly elevated. *NGF signaling* included Baiap2 (↑), Cltc (↑), Dnm1 (↑), Dpysl2 (↑), Kras (↑), Nedd8 (↑), Ppp2r1a (↑), Rab5a (↑), Rac1 (↑), Arpc3 (↓), Rps27a (↓), and Ywhae (↓), while *EGFR1 signaling* included Actn4 (↑), Atp6v1c1 (↑), Cltc (↑), Dnm1 (↑), Dpysl2 (↑), Dyncl1l (↑), Kras (↑), Ndufa13 (↑), Plec (↑), Rab5a (↑), Rac1 (↑), Stxbp1 (↑), and Syp (↓) (Table 9; Fig. 9, II; Supplementary Table 4). Likewise, proteins which have biological function in processes related to microtubule formation demonstrate decreased phosphorylated isoforms such as phosphoproteins involved in axonogenesis (Braf, Ctnn, Map1b, Map2, Mapt, Pak1, Rtn4 (all p↓)) and dendrite development (Ctnnd2, Farp1, Git1, Map1b, Map2, Mapk8, Mink1, Pak1, Palm, Slc12a5 (all p↓)) (Table 9; Fig. 9, II; Supplementary Tables 3–5). Axon guidance is one of the two pathways containing the highest number of top decreased phosphoproteins (Ablim1, Dpysl4, Pak1, Braf, Ncam1, Dpysl3, Git1 (all ↓)) along with the EGFR pathway (Tjp2, Pak1, Braf, Plec, To112, Mink1, Git (all p↓)). Decreased levels of phosphorylation also encompass proteins associated with response to NGF (Braf, Ehd1, Kcnc1, Stmn2 (all p↓)).

In the cerebral cortex (Table 10; Fig. 9, II; Supplementary Tables 3–5), we also identified proteins comprising terms related to microtubule organization, which pertained to recruiting various proteins to the centrosome during its maturation (Actrla (↓), Hsp90aa1 (↑), Tubb4a (↓), Tubb5 (↑), and Ywhag) and axon guidance (Camk2b (↑), Gnai2 (↑), Gsk3b (↓), Ppp3r1 (↑), Rac1–3 (↓), Pfn2 (↑), Arp3 (↓), Arpc4 (↑)). Furthermore, altered levels of proteins responsible for the binding vesicle to dynein and dynactin were detected (Uso1 (↑), Actrla (↓), Copz1 (↑), Pafah1b2 (↑), Rab1b (↓)). There are much more prominent changes associated with microtubules in the

phosphoproteome of the cortex. Those include tubulin binding (Brsk1, Kif3a, Kif5b, Lzts1, Map1a, Map1b, Map2, Map4, Map6d1, Mapt, Ndel1, Sgip1 (all p↓)), transport along microtubules (Kif3a, Kif5b, Klcl1, Map1b, Mapt, Ndel1 (all p↓)), and axonogenesis (Bmpr2, Braf, Brsk1, Brks2, Cdh11, Crmp1, Dclk1, Gsk3b, Kif5b, Map1b, Map2, Mapt, Myh10, Ndel1, Pak1, Rufy3, Syngap1 (all p↓)) (Table 10; Fig. 9, II; Supplementary Tables 3–5). In total, 48 downregulated phosphoproteins play a role in neuron projection organization (among them, there are 22 proteins with $\log_2 \text{FC} \leq -3.0$), 20 in microtubule binding (9 proteins with $\log_2 \text{FC} \leq -3.0$) and 45 in the regulation of organelle organization (17 proteins with $\log_2 \text{FC} \leq -3.0$). Moreover, several phosphoproteins are related to negative regulation of protein complex assembly (Add1, Add2, Dmtn, Gsk3b, Sptbn1, Tfip11 (all p↓)).

Neuronal Cell Functionality Affected by Processes Following Perturbed Cytoskeletal (Microtubule) Complex Formation (Group 3)

Transport along microtubules in the axon is essential for proper localization of organelle and particles in neurons. Since proteins of cytoskeleton-dependent transport are dysregulated in the cerebellum (Table 11; Fig. 9, III; Supplementary Tables 3–5), synaptic vesicle localization is likely to be affected. This is consistent with observed dysregulation of proteins involved in synaptic vesicle transport and transmission (Baiap2 (↑), Itpr3 (↑), Kras (↑), Rac1 (↑), Stxbp1 (↑), Tnr (↑), Syp (↓)) belonging to the list of top dysregulated proteins (Supplementary Table 6). Likewise, proteins with decreased levels of phosphorylation are implicated in neurotransmitter transport (Braf, Pak1, Pclo, Rims1, Slc32a1, Stx1b, Syn1, Syn2 (all p↓)). Notably, a group of proteins with highly dysregulated levels of phosphorylation has a main biological function related to trans-synaptic signaling (Braf, Ncam1, Slc3a1, Syn1, Bsn, Mink1, Slc32a1, Shank1, Shank2, Slc12a5 (all p↓)) (Table 11; Fig. 9, III; Supplementary Tables 3–6).

Disturbed transport along axons may also have an impact on the imbalance in the exchange between newly synthesized and used or damaged mitochondria in nerve cell ending. Several proteins with increased levels in the cerebellum (Table 11; Fig. 9, III; Supplementary Tables 3–5) are involved in glycolysis, gluconeogenesis, and citric acid cycle (Akr1a1, Aldoa, Gpi1, Cs, Cycs (all ↑)) as well as a large subset of proteins with higher fold increase involved in the respiratory electron transport chain (Atp5b, Atp5f1, Etfdh, Ndula10, Ndula13, Ndula8, Sdhb, Uqcrh, Uqcrq (all ↑)). Interestingly, there is no GO term related to energy metabolism involving dysregulated phosphoproteins, neither for the cerebellum nor the cerebral cortex.

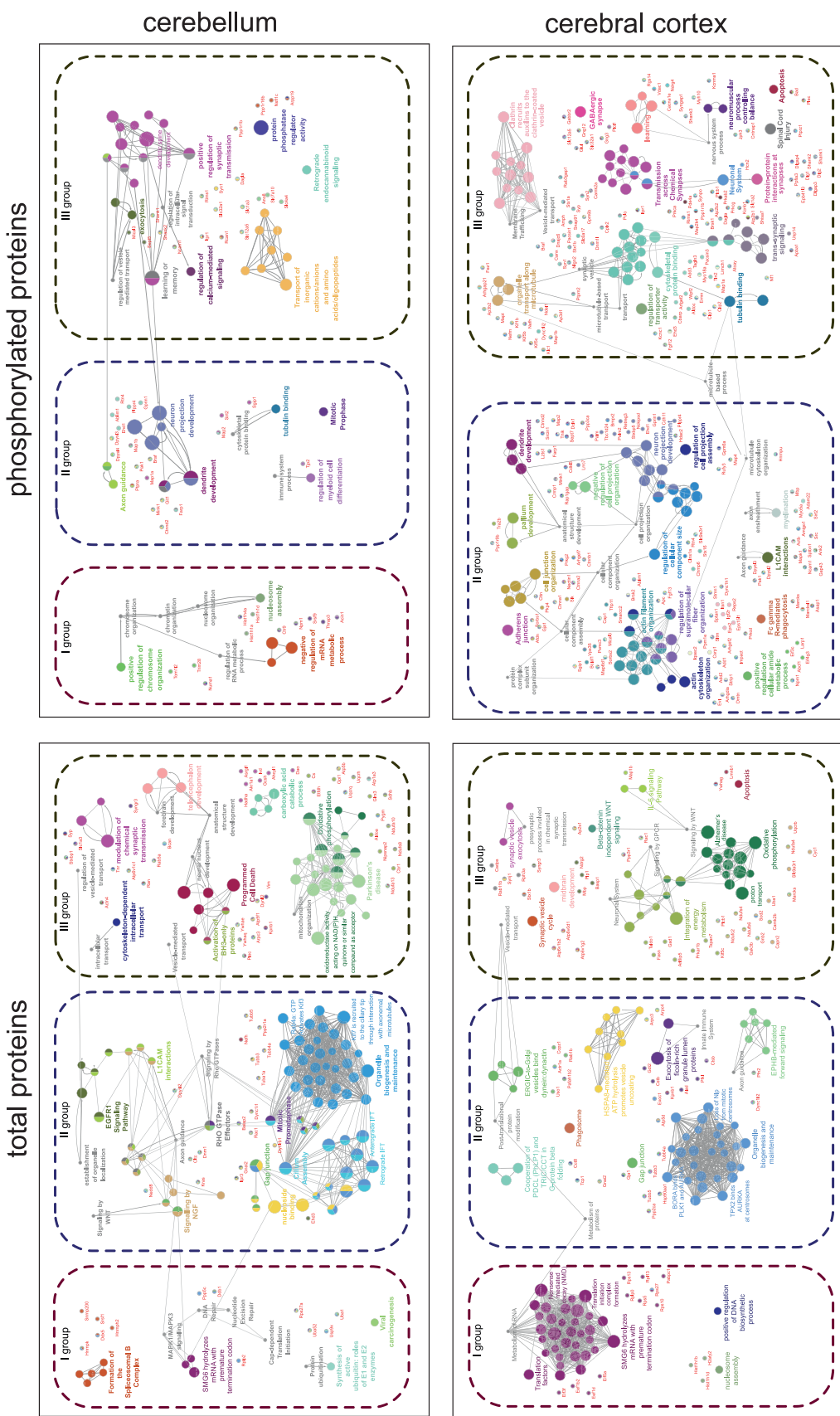


Fig. 9 Major groups of affected biological processes based on the proteomic and phosphoproteomic analysis in K91 SCA3/MJD mouse brains. A network of GO terms and pathways (two-sided hypergeometric test with Bonferroni step-down correction, p value cutoff = 0.05, tree interval 3–5, kappa score = 0.5) was generated for dysregulated proteins and phosphoproteins in the cerebellum and cerebral cortex with ClueGO (Cytoscape) using organic layout. GO terms and pathways were arranged into three major groups described in chapters: “Disturbed mechanism of modulation of protein levels and DNA damage,” “Disturbed formation

of neuronal cellular structures: organelles and macromolecules,” and “Neuronal cell functionality affected by processes following perturbed cytoskeletal (microtubule) complex formation.” Proteins were assigned to GO terms and pathways based on ClueGO analysis (genes with corresponding functions). The same analysis, however, with no arrangement is included as Supplementary Fig. 3 in order to enable free interpretation of data. The lists of GO terms and pathways with p values included in Tables 7, 8, 9, 10, 11, and 12 and Supplementary Tables 3–5

Table 7 Summary of GO terms and pathways containing three top dysregulated proteins and phosphoproteins (italics) from the cerebellum from group 1 (fold changes, *p* values, and GO terms)

Category	GO term/pathway	Source	Pathway or term <i>p</i> value/ <i>q</i> value * or Bonferroni <i>p</i> value#	3 top dysregulated proteins	Log2 FC <i>p</i> value
DNA damage	Recognition of DNA damage by PCNA-containing replication complex	Reactome R-MM-U:110314	0/0.02#	(Protiens) <i>Ddb1</i> <i>Ppp5c</i>	1.7/0.0349 0.5/0.0202
	Recruitment and ATM-mediated phosphorylation of repair and signaling proteins at DNA double strand breaks	Reactome R-MMU:5693565	0.0024/0.0472#	<i>Rps27a</i>	-0.4/0.031
	Global genome nucleotide excision repair (GG-NER)	Reactome R-MM-U:5696399	0.0046/0.0421#		
	Based on [31]			(Protiens) <i>Nedd</i> <i>Plec</i>	1.6/0.0144 0.3/0.0349
	DNA damage/telomere stress-induced senescence	Reactome R-HSA-2559586	0.0082/0.0433*	(Phosphoproteins) <i>Hist1h1a</i> <i>Hist1h1d</i>	-1.4/0.0241 -1.0/0.0382
	Based on [31, 32]			<i>Sirt2</i> <i>Acin1</i> <i>Plec</i>	-2.3/0.0262 -2.0/0.018 -1.4/0.0343
Regulation of chromatin remodeling and transcription	Euchromatin	GO:0000791	0.0072/0.0315*	(Protiens) <i>Trim28</i> <i>Hist1h1d</i>	1.0/0.0027 -1.0/0.0418
	RNA polymerase II transcription cofactor activity	GO:0001104	0.0076/0.0296*	(Phosphoproteins) <i>Sirt2</i>	-2.3/0.0262
	Euchromatin	GO:0000791	0.0002/0.0031*	<i>Hist1h1d Npm1</i>	-1.4/0.0382
	Heterochromatin	GO:0000792	0.0027/0.0140*		-1.3/0.0209
Ubiquitination	Protein ubiquitination	Reactome R-MMU:8852135	0.0001/0.0135	(Proteins) <i>Ddb1</i>	1.7/0.0349
	Synthesis of active ubiquitin: roles of E1 and E2 enzymes	Reactome R-MMU:8866652	1.92E-05/0.0022	<i>Nedd8</i>	1.6/0.0144
	Parkin–ubiquitin proteasomal system pathway	WikiPathways WP2359	0.0081/0.0264	<i>Kras</i>	1.4/0.0007

In the cerebral cortex (Table 12; Fig. 9, III; Supplementary Tables 3–5), probably also as a consequence of microtubule dysfunction, several biological processes may be perturbed such as synaptic vesicle cycle and exocytosis (*Cadps* (↓), *Pfn2* (↑), *Rph3a* (↓), *Stx1b* (↓), *Synj1* (↓), *Atp6v1b2* (↑), *Atp6v0d1* (↑), *Atp6v1g2* (↑)). Moreover, proteins with decreased levels of phosphorylation are also involved in exocytosis of synaptic vesicles (*Amph*, *Braf*, *Pclo*, *Rab3gap1*, *Rims1*, *Syn1* (all p↓)) and modulation of chemical synaptic transmission (*Atp2b2*, *Braf*, *Ctnnd2*, *Kif5b*, *Lzts1*, *Pak1*, *Plcl1*, *Ppfia3*, *Rab3gap1*, *Rims1*, *Shank1*, *Shank2*, *Shisa7*, *Syn1*, *Syngap1*, *Synpo* (all p↓)). In total, 55 phosphoproteins are involved in trans-synaptic signaling and 18 in synaptic vesicle localization. From these, 21 belong to the list of top dysregulated phosphoproteins with log2 FC < -3.0 (*Stx16*, *Src*, *Ank2*, *Tbc1d24*, *Gja1*, *Sgip1*, *Pacsin1*, *Klc1*, *Reps2*, *Sptbn1*, *Epn2*, *Eps15l1* (all p↓)) (Supplementary Table 6). Similar to the cerebellum, we observed dysregulation of many proteins involved in oxidative phosphorylation (*Atp5d* (↓),

Cyc1 (↓), *Ndufa4* (↑), *Ndufb6* (↑), *Ndufc2* (↑), *Ndufs4* (↑), *Uqrbc* (↓)), and *Cyb5a*, *Ndufb6*, and *Ndufc2* are highly upregulated, and at the top of it, *Mtc01* has the highest level of log2 FC 2.95 in all dysregulated proteins in the cortex (Table 12; Fig. 9, III; Supplementary Tables 3–6).

Finally, altered levels of proteins in the cerebellum (Table 11, Fig. 9, III) suggest that pathway related to apoptosis is activated (*Kpnb1* (↑), *Plec* (↑), *Vim* (↓)). Another GO term, activation of BH3-only proteins (*DynII2* (↓), *Ywhae* (↓)), implies canonical mitochondrial apoptosis [34]. There are also cerebellar phosphoproteins related to apoptosis (*Mapk10*, *Mapk8*, *Sept4*, *Tjp2*, *Hist1h1d1*, *Hist1h1a*, *Plec*, *Acin1* (all p↓)) and mitophagy (*Atg4b*, *Cttn*, *Htt*, *Tom1l2*, *Vdac1* (all p↓)). In the cortex (Table 12; Fig. 9, III; Supplementary Tables 3–5), we found only a few proteins related to apoptosis (*Kpnb1* (↑), *Lmnb1* (↑), *Ppp3r1* (↑), *Ywhag* (↑)). However, proteins from the list of top dysregulated proteins (*Exoc1* (↑), *Rab1b* (↓), *Vps26b* (↑)) (Supplementary Table 6) are implicated in the regulation of macroautophagy.

Table 8 Summary of GO terms and pathways containing three top dysregulated proteins and phosphoproteins (italics) from cerebral cortex from group 1 (fold changes, *p* values, and GO terms)

Category	GO term/pathway	Source	Pathway or term <i>p</i> value/ <i>q</i> value* or Bonferroni <i>p</i> value#	3 top dysregulated proteins	Log2 FC/ <i>p</i> value
DNA damage	DNA damage response, signal transduction by p53 class mediator	GO:0030330	0.0014/0.0205#	(Proteins) <i>Gja1</i>	2.3/0.0286
	DNA damage/telomere stress-induced senescence	Reactome R-HSA-2559586	0.0017/0.0120*	<i>Ndrg1</i>	1.8/0.0167
	Activation of DNA fragmentation factor	Reactome R-HSA-211227	0.0001/0.0027*	<i>Hist1h1d</i>	-1.0/0.0006
	Based on [31, 32, 33]		-	(Phosphoproteins) <i>Sirt2</i> <i>Bclaf1</i> <i>Plec</i>	-3.9/0.0091 -3.2/0.0226 -2.5/0.0126
Translation	Formation of translation initiation complexes containing mRNA that does not circularize	Reactome R-MMU:157849	0.0013/0.0222#	(Proteins) <i>Pabpc1</i>	2.0/0.0274
	Ribosome assembly	GO:0042255	0.0085/0.0501*	<i>Eif3f</i>	1.2/0.0091
	Cap-dependent translation initiation	Reactome R-HSA-72737	1.82E-05/0.0009*	<i>Eif5a</i>	1.2/0.0488
Protein folding	Chaperonin-mediated protein folding	Reactome R-MMU:390466	5.5E-05/0.0039#	(Proteins) <i>Tubb3</i>	-0.9/0.0057
	Protein folding	Reactome R-MMU:391251	5.5E-05/0.0039#	<i>Tcp1</i>	-0.5/0.0155
	Cooperation of Prefoldin and TrIC/CCT in actin and tubulin folding	Reactome R-HSA-389958	0.0001/0.0027*	<i>Gnai2</i>	-0.4/0.0411
	Cooperation of PDCL (PhLP1) and TrIC/CCT in G protein beta folding	Reactome R-HSA-6814122	0.0078/0.0356*	(Phosphoproteins) <i>Arfgef2</i>	-4.5/0.0004
	Chaperonin-mediated protein folding	Reactome R-HSA-390466	0.0089/0.0386*	<i>Gng3</i>	-3.6/0.0162
				<i>Rgs7</i>	-2.8/0.0093

Subcellular Localization of Dysregulated Proteins

We performed analysis of “cellular component” GO terms (*p* value cutoff < 0.01) in CPDB to examine putative cellular localization of dysregulated proteins and phosphoproteins (Supplementary Fig. 4; Supplementary Table 7). The majority of the differentially expressed total proteins (Supplementary Fig. 4A, C) were assigned to localize in “extracellular exosome” (42% cerebellum and 46% cerebral cortex) or assigned as *cytoplasmic* (39% cerebellum and 44% cortex). A large number of dysregulated proteins were also identified as *mitochondrial* (28% cerebellum and 20% cortex) and *cytoskeletal* (26% cerebellum and 24% cortex). There were also proteins which were assigned to cellular structures which are typical for neurons, such as *dendrites* (14% cerebellum and 6% cortex) and *axons* (13% cerebellum and 8% cortex). In addition, in the cerebellar cortex, 9% of proteins are associated with *lytic vacuoles*.

Coherently with total proteome, proteins with altered level of phosphorylation (Supplementary Fig. 4B, D) were assigned as *cytoplasmic* (30% cerebellum and 35% cortex), *cytoskeletal* (27% cerebellum and 29% cortex), and *secretory vesicles*

(7% cerebellum and 21% cortex). Respectively, 19% (cerebellum) and 17% (cortex) of proteins localized in *dendrites* and 9% (cerebellum) and 15% (cortex) were assigned for *axons*.

In apparent contrast to the total proteome, a prominent number of 26% of all phosphorylated proteins in the cerebellum (Supplementary Fig. 4B) were associated with the nucleus. In the cortex (Supplementary Fig. 4D), there were 22% of phosphoproteins localized in the nucleus and 4% associated with the cell membrane. Decreased phosphorylated proteins predicted to be localized in the nucleus included *Sirt2*, *Srrm2*, *Thrap3*, *Acin1*, *Bclaf1*, *Ctr9*, *Rbm39*, *Numa1*, *Npm1*, *Trim28*, *Srsf9*, *Matr3*, *Sept4*, *Ndrg2*, and *Ppp6r3* (Supplementary Table 7). These nuclear proteins are implicated in cell cycle, DNA damage, and splicing; however, no GO terms containing dysregulated nuclear phosphoproteins were identified which relate to transcription factors or direct gene expression control. In coherence with the analysis of biological processes, we found no proteins with altered level of phosphorylation, which localized in the mitochondria, neither in the cerebellum nor in the cerebral cortex.

Table 9 The summary of GO terms and pathways containing 3 top dysregulated proteins and phosphoproteins (italics) from cerebellum from Group2 (fold changes, *p* values, and GO terms)

Category	GO term/pathway	Source	Pathway or term <i>p</i> value/ <i>q</i> value* or Bonferroni <i>p</i> value#	3 top dysregulated proteins	Log2 FC/ <i>p</i> value
Microtubule cytoskeleton	KIF7 is recruited to the ciliary tip through interaction with axonemal microtubules	Reactome R-MMU:5610733	6.54E-07/8.89E-05#	(Proteins) <i>Tuba1a</i> <i>Baiap2</i> <i>Dync1il</i>	3.5/0.0276 1.0/0.0126 1.0/0.038
	Microtubule	GO:0005874	5.16E-06/0.0001*		
	Association of NuMA with microtubules	Reactome R-MMU:380316	4.97E-05/0.0047#		
	Regulation of microtubule cytoskeleton organization	GO:0070507	4.73E-05/0.001*	(Phosphoproteins) <i>Pak1</i>	- 2.5/0.0273
	Microtubule binding	GO:0008017	0.0036/0.0217*	<i>Sirt2</i>	- 2.3/0.0262
Actin cytoskeleton	Regulation of microtubule cytoskeleton	WikiPathways WP2038	0.0014/0.0214*	<i>Klc1</i>	- 1.8/0.0398
	Regulation of actin dynamics for phagocytic cup formation	Reactome R-MMU:2029482	0.0027/0.0470#	(Proteins) <i>Kras</i>	1.4/0.0007
	SNX9 recruits components of the actin polymerizing machinery	Reactome R-MMU:8868230	0.0011/0.0438#	<i>Actn4</i>	1.3/0.0332
	Regulation of actin cytoskeleton— <i>Homo sapiens</i> (human)	KEGG:04810	0.0064/0.0245*	<i>Baiap2</i>	1.0/0.0126
	Actin filament bundle organization	GO:0061572	0.0024/0.0144*	(Phosphoproteins) <i>Numa1</i> <i>Sept4</i> <i>Rims1</i>	- 1.6/0.0052 - 1.5/0.0071 - 1/0.0269
Axon	Axon guidance	KEGG:04360	3.52E-05/0.0037#	(Proteins)	
	Neuron projection organization	GO:0106027	0.0002/0.0039*	<i>Tuba1a rab5a</i>	3.5/0.0276
	Neuron projection development	GO:0031175	0.0012/0.0112*	<i>Vps35</i>	1.7/0.0149
	Neuron projection development	GO:0031175	1.30E-09/2.76E-07*	(Phosphoproteins)	
	Regulation of cell projection organization	GO:0031344	2.42E-05/0.0007*	<i>Map2</i> <i>Pak1</i>	- 2.8/0.0134 - 2.5/0.0273
Dendrites	Axon guidance	Reactome R-HSA-422475	0.0017/0.0214*	<i>Gprin1</i>	- 2.2/0.0029
	Dendrite development	GO:0016358	9.36E-07/3.37E-05#	(Phosphoproteins)	
	Dendrite morphogenesis	GO:0048813	0.0004/0.0068#	<i>Map2</i>	- 2.8/0.0134
Gap junction	Regulation of dendrite extension	GO:1903859	0.0031/0.0162*	<i>Pak1</i>	- 2.5/0.0273
	Gap junction	KEGG:04540	1.48E-08/2.24E-06#	<i>Rtn4</i>	- 2.0/0.0003
	Gap junction— <i>Homo sapiens</i> (human)	KEGG:04540	0.0001/0.0033*	(Proteins)	
Apoptosis	Apoptosis	Reactome R-MMU:109581	5.74E-07/7.87E-05#	(Proteins) <i>Fam162a</i>	1.6/0.0268
	Cell death signaling via NRAGE, NRIF and NADE	Reactome R-MMU:204998	0.0003/0.0231#	<i>Vps35</i>	1.4/0.0333
	Apoptotic execution phase	Reactome R-MMU:75153	0.0014/0.0445#	<i>Hist1h1d</i>	- 1.0/0.0418
	Apoptotic execution phase	Reactome R-HSA-75153	5.20E-06/0.0008*	(Phosphoproteins)	
	Apoptosis-induced DNA fragmentation	Reactome R-HSA-140342	0.0017/0.0214*	<i>Acin1</i> <i>Tjp2</i>	- 2.0/0.018 - 1.9/0.0001
	Apoptosis	Reactome R-HSA-109581	0.0002/0.0086*	<i>Hist1h1a</i>	- 1.4/0.0241

Table 10 Summary of GO terms and pathways containing three top dysregulated proteins and phosphoproteins (italics) from the cerebral cortex from group 2 (fold changes, *p* values, and GO terms)

Category	GO term/pathway	Source	Pathway or term <i>p</i> value/ <i>q</i> value* or Bonferroni <i>p</i> value #	3 top dysregulated proteins	Log2 FC/ <i>p</i> value
Microtubule cytoskeleton	Kinetochores capture of astral microtubules	Reactome R-MMU:5666169	0.0062/0.0187#	(Proteins)	2.1/0.0011
	Microtubule cytoskeleton	GO:0015630	2.46E-05/0.0002*	Sept4	1.8/0.0167
	Association of NuMA with microtubules	Reactome R-MMU:380316	0.0002/0.0115#	Ndrg1	-1.0/0.0023
	Organelle transport along microtubule	GO:0072384	1.92E-08/2.66E-06#	Dync1i1	
	Microtubule binding	GO:0008017	1.16E-11/8.48E-10*	(Phosphoproteins)	-7.0/4.22E-05
	Regulation of microtubule cytoskeleton	WikiPathways WP2038	1.67E-06/8.08E-05*	<i>Map2</i>	-5.1/0.0002
				<i>Nefh</i>	-4.9/0.0005
Actin cytoskeleton	Regulation of actin dynamics for phagocytic cup formation	Reactome R-MMU:2029482	0.0007/0.0168*	(Proteins)	1.6/0.0028
	Actin cytoskeleton	GO:0015629	0.0016/0.0043*	Capn2	-1.0/3.67E-05
	Y branching of actin filaments	BioCarta actinYPathway	0.0003/0.0042*	Slc9a3r1	0.6/0.0124
				actn1	
	Actin-based cell projection	GO:0098858	8.95E-09/1.34E-06#	(Phosphoproteins)	-7.0/4.22E-05
	Actin cytoskeleton	GO:0015629	1.70E-11/5.32E-10*	<i>Map2</i>	-5.6/0.0006
	Regulation of actin cytoskeleton	WikiPathways WP51	0.0004/0.0056*	<i>Bsn</i>	-5.1/0.0002
Axon	Axon guidance	KEGG:04360	0.0003/0.0125#	(Proteins)	2.3/0.0286
	Neuron projection development	GO:0031175	0.00049/0.0078*	<i>Gja1</i>	-2.1/0.0011
	Sema3A PAK-dependent axon repulsion	Reactome R-HSA-399954	0.0083/0.0292*	Sept4	-1.0/3.67E-05
	Axon guidance	KEGG:04360	0.0014/0.0070#	Slc9a3r1	
	Neuron projection development	GO:0031175	8.26E-34/4.81E-31*	(Phosphoproteins)	-7.0/4.22E-05
	Axonal growth inhibition (RHOA activation)	Reactome R-HSA-193634	0.0087/0.0381*	<i>Map2</i>	-5.6/0.0006
				<i>Bsn</i>	-5.1/0.0002
Dendrites	Dendrite development	GO:0016358	6.66E-13/1.33E-10#	(Phosphoproteins)	-7.0/4.22E-05
	Dendrite morphogenesis	GO:0048813	5.07E-10/8.32E-08#	<i>Map2</i>	-5.6/0.0006
	Regulation of dendrite development	GO:0050773	0.0001/0.0053#	<i>Bsn</i>	-4.7/0.0287
Gap junction	Gap junction	KEGG:04540	4.72E-05/0.0036#	(Proteins)	2.3/0.0286
	Gap junction— <i>Homo sapiens</i> (human)	KEGG:04540	0.001/0.0082*	<i>Gja1</i>	-0.9/0.0057
				<i>Tubb3</i>	0.5/0.0383
	Gap junction— <i>Homo sapiens</i> (human)	KEGG:04540	0.0002/0.0033*	(Phosphoproteins)	-3.4/0.0001
Apoptosis	Apoptosis	Reactome R-MMU:109581	0.0055/0.0335#	<i>Src</i>	-2.8/0.0001
	Apoptosis induced DNA fragmentation	Reactome R-HSA-140342	0.0001/0.0027*	<i>Itp1</i>	2.5/0.0225
	Programmed cell death	Reactome R-HSA-5357801	0.0006/0.0063*	<i>Prkcg</i>	
	Regulation of neuron apoptotic process	GO:0043523	0.0005/0.0016#	(Proteins)	2.3/0.0286
	Programmed cell death	Reactome R-HSA-5357801	7.85E-05/0.0016*	<i>Gja1</i>	-1.0/0.0006
	Regulation of neuron death	GO:1901214	3.34E-05/0.0017*	Hist1h1d	-0.9/0.0057
				<i>Tubb3</i>	

Cellular Identity of Dysregulated Proteins

The analysis of cellular markers among dysregulated proteins and phosphoproteins was performed using the BrainMap tool

of the *Allen Brain Atlas* for cerebral cortex (Supplementary Fig. 5A) and DropViz for cerebellum (Supplementary Fig. 5B). The analysis revealed a characteristic pattern of cellular markers of inhibitory neurons, which consisted of *Gad1*

Table 11 Summary of GO terms and pathways containing three top dysregulated proteins and phosphoproteins (italics) from the cerebellum from group 3 (fold changes, *p* values, and GO terms)

Category	GO term/pathway	Source	Pathway or term <i>p</i> value/ <i>q</i> value* or Bonferroni <i>p</i> value#	3 top dysregulated proteins	Log2 FC/ <i>p</i> value
Synaptic vesicle	Synaptic vesicle cycle	KEGG:04721	0.0003/0.0201#	(Proteins)	
	Regulation of synaptic vesicle cycle	GO:0098693	0.0006/0.0095*	Rab5a	1.7/0.0149
	Synaptic vesicle pathway	WikiPathways WP2267	9.79E-06/0.0003*	Syp	-0.9/0.025
	Regulation of synaptic vesicle exocytosis	GO:2000300	2.28E-06/0.0001*	Arpc3	-0.8/0.0435
	Regulation of synaptic vesicle cycle	GO:0098693	2.12E-05/0.0007*	(Phosphoproteins)	
	Synaptic vesicle pathway	WikiPathways WP2267	0.0001/0.0061*	<i>Syn1</i>	-2.4/0.0245
Trans-synaptic signaling and neurotransmitters	Anterograde trans-synaptic signaling	GO:0098916	7.04E-05/0.0025*	(Proteins)	
	Dopamine receptor binding	GO:0050780	2.18E-05/0.0002*	Rab5a	1.7/0.0149
	Glutamate neurotransmitter release cycle	Reactome R-HSA-210500	0.008/0.0264*	Vps35	1.4/0.0333
	Gamma-aminobutyric acid receptor life cycle pathway	BioCarta gabaPathway	0.0031/0.0141*	Kras	1.4/0.0007
	Anterograde trans-synaptic signaling	GO:0098916	4.25E-05/0.001*	(Phosphoproteins)	
	Glutamatergic synapse	KEGG:04724	0.0018/0.0181#	<i>Map2</i>	-2.8/0.0134
Glycolysis	GABA synthesis, release, reuptake, and degradation	Reactome R-HSA-888590	0.0038/0.028*	<i>Pak1</i>	-2.5/0.0273
	Serotonin neurotransmitter release cycle	Reactome R-HSA-181429	0.0034/0.028*	<i>Syn1</i>	-2.4/0.0245
	Glycolysis/gluconeogenesis	KEGG:00010	0.0004/0.0247#	(Proteins)	
	Glycolysis	Reactome R-MMU:70171	0.0039/0.043#	Mpc1	1.4/0.0433
	Glycolysis and gluconeogenesis	WikiPathways WP:157	0.0023/0.047#	Aldoa	0.5/0.0064
				Akr1a1	0.5/0.0422
TCA and oxidative phosphorylation	The citric acid (TCA) cycle and respiratory electron transport	Reactome R-MMU:1428517	2.33E-10/3.66E-08#	(Proteins)	
	Oxidative phosphorylation	KEGG:00190	3.18E-08/4.74E-06#	Uqrch	3.4/0.0134
	Mitochondrial electron transport, NADH to ubiquinone	GO:0006120	0.0011/0.0112*	Mpc1	1.4/0.0433
Signaling pathways	EGF–EGFR signaling pathway	WikiPathways WP437	3.56E-05/0.0011*	Etfdh	1.4/0.0144
	ErbB1 downstream signaling	PID	1.40E-07/5.61E-05*	(Proteins)	
	PDGFR-beta signaling pathway	PID	5.32E-07/7.21E-05*	Rab5a	1.7/0.0149
	EGFR1	NetPath	0.0015/0.0214*	Nedd8	1.6/0.0144
	Ephrin signaling	Reactome R-HSA-3928664	0.0038/0.028*	Kras	1.4/0.0007
	MAPK cascade	WikiPathways WP422	0.0087/0.0450*	(Phosphoproteins)	
				<i>Map2</i>	-2.8/0.0134
				<i>Pak1</i>	-2.5/0.0273
				<i>Tjp2</i>	-1.9/0.0001

(log2 FC change = 2.06, total), Pvalb (log2 FC = -2.92, total), Aldoc (log2 FC = -3.24, phospho), Chgb (log2 FC = -4.2, phospho), and Fgf13 (log2 FC = -0.86, phospho) in the cortex (Supplementary Fig. 5A). Another pair of markers, namely Pak1 (log2 FC = -3.03, phospho) and Arhgap32 (log2 FC = -3.48, phospho), was characteristic for excitatory neurons. The third group of markers consisted of dysregulated proteins which were characteristic for oligodendrocytes and their precursor cells. Phosphorylated Ermn (log2 FC = -4.4, phospho) and

Opalin (log2 FC = -4.33, phospho) were highly expressed in mature oligodendrocytes, while Mbp (log2 FC = -0.69, total; -1.77, phospho), Bcas1 (log2 FC = -3.68, phospho), and Plp1 (log2 FC = -0.5, total) are markers of oligodendrocyte precursors and mature oligodendrocytes. Moreover, there was also one highly upregulated astrocytic protein—Gja1 (log2 FC = -2.27, total; -3.78, phospho) (Supplementary Table 6). In the cerebellum (Supplementary Fig. 5B), the analysis demonstrated several cellular markers with the ratio of relative

Table 12 Summary of GO terms and pathways containing three top dysregulated proteins and phosphoproteins (italics) from the cerebral cortex from group3 (fold changes, *p* values, and GO terms)

Category	GO term/pathway	Source	Pathway or term <i>p</i> value/ <i>q</i> value* or Bonferroni <i>p</i> value#	3 top dysregulated proteins	Log2 FC/ <i>p</i> value
Synaptic vesicle	Synaptic vesicle cycle	KEGG:04721	0.0001/0.0063#	(Proteins)	
	Establishment of synaptic vesicle localization	GO:0097480	0.0001/0.0032*	Rab1b	-1.5/0.0006
	Synaptic vesicle exocytosis	GO:0016079	0.0002/0.0103#	Rph3a	-1.1/0.0004
	Synaptic vesicle cycle	GO:0099504	5.25E-12/1.01E-09#	(Phosphoproteins)	-5.0/0.0003
	Synaptic vesicle pathway	WikiPathways WP2267	3.24E-07/2.48E-05*	<i>Rims</i>	-4.9/0.0027
	Synaptic vesicle localization	GO:0097479	3.79E-13/7.65E-11#	<i>Pacsin1</i>	-4.9/0.0349
Trans-synaptic signaling and neurotransmitters	Anterograde trans-synaptic signaling	GO:0098916	9.92E-06/0.0003*	(Proteins)	
	Dopaminergic synapse	KEGG:04728	8.01E-06/0.0007#	Gad1	2.1/0.015
	Opioid signaling	Reactome R-MMU:111885	5.33E-05/0.0038#	Cspg5	-1.6/0.0367
	Glutamate binding, activation of AMPA receptors, and synaptic plasticity	Reactome R-HSA-399721	0.0024/0.0139*	Tspan7	1.5/0.0044
	Anterograde trans-synaptic signaling	GO:0098916	6.42E-24/1.25E-21*	(Phosphoproteins)	
	Glutamatergic synapse	KEGG:04724	1.56E-07/1.86E-05#	<i>Map2</i>	-7.0/4.22E-05
Glycolysis	GABAergic synapse	KEGG:04727	4.44E-06/0.0003#	<i>Bsn</i>	-5.6/0.0006
	Dopaminergic synapse	KEGG:04728	3.42E-05/0.0017#	<i>Rims</i>	-5.0/0.0003
	Glucose-6-phosphate dehydrogenase deficiency	SMPDB SMP00518	0.0063/0.024*	(Proteins)	
	Glycolysis	HumanCyc PWY66-400	0.0093/0.0398*	Pfk1	1.0/0.033
				Taldo1	-0.4/0.009
				(Phosphoproteins)	
TCA and oxidative phosphorylation	The citric acid (TCA) cycle and respiratory electron transport	Reactome R-MMU:1428517	0.0008/0.0179#	<i>Aldoc</i>	-3.2/5.81E-05
	Oxidative phosphorylation	KEGG:00190	7.08E-08/8.85E-06#	<i>Enol</i>	-2.5/0.013
	Mitochondrial respiratory chain	GO:0005746	1.58E-05/0.00139#	<i>Pgk1</i>	-1.9/0.0454
				(Proteins)	
				Mt-Co3	-1.8/0.0494
				Ndufc2	1.6/0.0333
Signaling pathways	EGFR1	NetPath	0.0019/0.0126*	Chchd6	-1.3/0.0258
	ErbB1 downstream signaling	PID	0.0003/0.0038*	(Proteins)	
	PDGFR-beta signaling pathway	PID	0.0008/0.0072*	Gja1	2.3/0.0286
				Cstb	2.0/0.0471
				Capn2	1.6/0.0028
	EGFR1	NetPath	3.28E-06/0.00012*	(Phosphoproteins)	
	VEGF	INOH	1.88E-06/8.66E-05*	<i>Spibnl</i>	-4.7/0.0159
	MAPK signaling pathway	KEGG:04010	0.0003/0.0074#	<i>Epn2</i>	-4.3/0.0032
				<i>Rras2</i>	-3.8/0.0019

expression between 3.14 and 63 (particular cell type vs other cell types). We found three proteins, which could be considered as markers of inhibitory neurons, namely Purkinje cells and pvalb-positive interneurons: *Slc32a1* (log2 FC = -1.66, phospho), *Nefh* (log2 FC = 0.4, total), and *Baiap2* (log2 FC = 1.01, total). In addition, *Itpr1* (log2 FC = -1.21, phospho) is expressed strongly in Purkinje neurons, but not in other cell types. Furthermore, three proteins are markers for Bergmann glia and astrocytes: *Slc1a3* (log2 FC = 0.35, total; -1.36, phospho), *Slc7a10* (log2 FC = -1.15, phospho), and *Dao*

(log2 FC = 0.74, total), and one protein specific for oligodendrocytes: *Enpp6* (log2 FC = 0.65, total). Among proteins with altered level and assigned log fold change, we did not identify conclusive markers for microglia and endothelial cells. However, *Hist1h1d* (cerebellum log2 FC = -0.96, total; 1.77, phospho; cortex = -1.04, total), a microglia marker (with a low percentage of presence in microglia and no expression (0%) in any other cell types), is dysregulated in three analysis (total proteome and phosphoproteome of the cerebellum and total proteome of the cerebral cortex) (Supplementary Table 6).

Altogether, proteomic changes occur mainly in neurons and oligodendrocytes in the cerebral cortex (Supplementary Fig. 5A), and inhibitory neurons, Bergmann glia, and astrocytes in the cerebellum (Supplementary Fig. 5B).

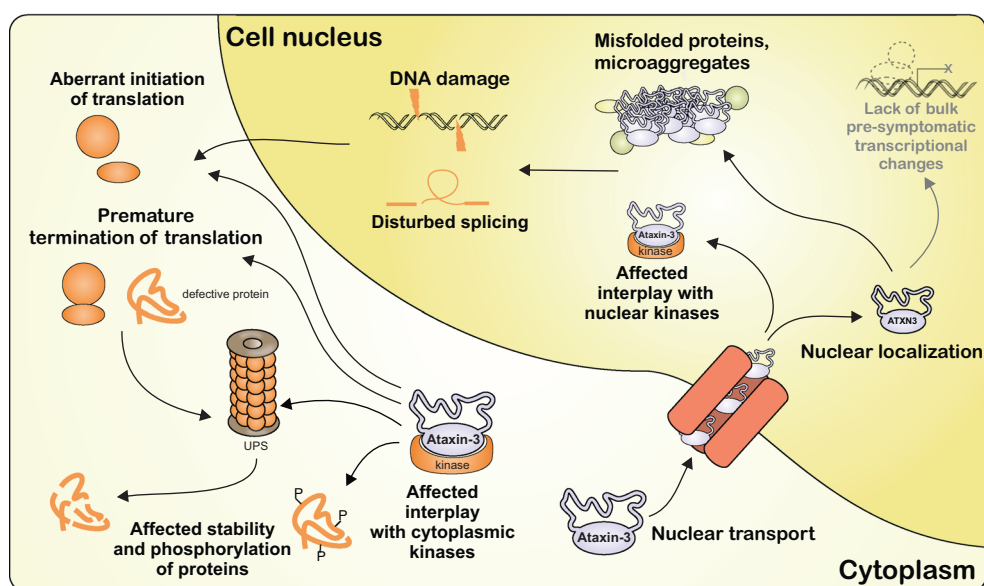
Discussion

In the present work, we have defined the early molecular signs of SCA3/MJD polyQ neurodegenerative disease. We used a homozygous Ki91 mouse knock-in model, which mimics the genetics and pathological SCA3 situation in patients including presymptomatic phase and later disease onset [14]. Taking advantage of the model, we challenged the question of which molecular events take place before the disease outbreak in the brain by selecting a set of high-throughput methods to define the brain transcriptome first in 2-month-old and later at 10–14-month-old animals by qPCR. Subsequently, we identified the brain proteome and phosphoproteome in 2-month-old Ki91 animals. Our goal was to identify the molecular triggers of the disease which may be evident early in life and early in disease pathology and therefore are not “contaminated” by secondary molecular signs originating from neuronal dysfunction and death. In our work, we included the cerebellar cortex as an important source of early signs in SCA3 brain [35]. Recent findings also emphasize the role of communication between the cortex and cerebellum as one of the pathology hallmarks of SCA3 [36–39].

The first essential finding is the sequence of general molecular events, which governs the disease onset process in SCA3/MJD. We found that Ki91 homozygous animals do not contain mutant ataxin-3-related transcriptional changes in cerebellum and cortex tissue at 2 months of age and do not show any behavioral changes at that stage; however, in

the cerebellum and cortex, there are sparsely occurring cells with nuclear localization of mutant ataxin-3. At the same time, 2-month-old Ki91 animals already demonstrate prominent changes both at the level of total proteome and at the level of phosphoproteins. Importantly, the general level of phosphorylation of proteins is greatly decreased in our Ki91 SCA3/MJD mouse model. Of note, many of the changes exceed the decrease of $\log_2 \text{FC} - 3$ and lower. Furthermore, we demonstrate that later ages of 10–14-month-old Ki91 animals do contain transcriptional changes in both the cerebellum and cerebral cortex, and the mature postmitotic neural cultures from patient neurons from iPSC also contain some transcriptional changes identified in our 10–14-month-old Ki91 animals. The type of neural cultures that we used was reported to be positive for GABA and GAD67 and originate from cells that display differentiation profile toward hindbrain identity [24], whereas the mouse data are generated from the cortex and cerebellum. For example, Olig1 is elevated both in mouse tissue and MJD iPSC-derived neural cells, but there are a number of different cells (including different types of neurons) that evolve from OLIG-positive progenitors depending on the brain region. Thus, concordant expression changes might not necessarily argue for the same changes at the cellular level. Comparison of data from WT and Ki91 mouse hindbrain (pons, medulla) versus MJD iPSC-derived neural cells and isogenic controls requires further studies. Together, the findings demonstrate that the possible sequence of events that leads to full-featured brain disease is composed of the changes at the level of many important proteins and phosphoproteins in the initial absence of mRNA changes dependent on mutant ataxin-3 (depicted in Fig. 10). These early events may further lead to transcriptional changes at later ages. Therefore, transcriptional changes in SCA3 can be classified as secondary and more severe disease signs. Previous reports demonstrated

Fig. 10 The diagram of processes affected by molecules identified in young Ki91 mouse brain during the early SCA3/MJD pathogenesis



that the SCA3 disease pathogenic process includes relatively direct transcriptomic changes by binding of mutant ataxin-3 to chromatin and transcription factors [40–42]. Considering widespread expression of ataxin-3 across cells and tissues of Ki91 mouse [14], such direct interaction could occur early and readily and evoke transcriptional changes. However, the scenario that one cannot exclude is the direct influence of ataxin-3 on transcriptional changes which may start only at certain cellular lineages in the brain and that the present tissue-based NGS resolution does not allow for identification of transcriptional changes restricted to the initially small number of cells. We performed the analysis of the dysregulated protein markers to identify types of cells relevant to pathogenesis in the brain. Based on the analysis, we conclude that one of the affected cell types is the parvalbumin-positive neurons. Such neurons are usually GABAergic interneurons in the cortex, Purkinje cells, and other GABAergic neurons of the cerebellum [43, 44]. Another prominently affected cell type was astrocytes in the cerebellum and, to a lesser extent, in the cerebral cortex. In addition, according to our analysis of cell types using BrainMap, oligodendrocytes and excitatory neurons are also affected in the cerebral cortex. Another important possibility for the lack of transcriptional changes at the presymptomatic stage is the direct or indirect ataxin-3 effect on transcriptional changes, which start during later adult life as a response to another factor such as aging, stress, DNA damage, or protein interactions. The transcriptomic changes in SCA3 were so far investigated in the symptomatic phase of the disease such as in patient blood or in older brain tissue collected from mouse models [45–48]. One of the interesting outcomes from our analysis of transcriptome in older Ki91 animals suggests that precursors of oligodendrocytes are upregulated. This may suggest that demyelination and myelin repair responses occur later in the disease course. Since neuronal activity promotes myelination [49], the start of demyelination in SCA3 may be the result of the collapse of neuronal and axonal function which occurs later in the disease course.

On the other hand, elevated Olig1 level suggests some developmental abnormalities in SCA3. One possibility could be an increase in the prolonged existence of the Olig1-positive progenitor pool, which could disrupt the lineage segregation process. Another part of the results which indicate a developmental component in SCA3 pathogenesis is a group of dysregulated proteins involved in such processes as axon guidance and dendrite development.

In view of the fact that we did not find transcriptional changes in the brain of young Ki91 SCA3/MJD mouse model, we reasoned that proteomic changes were the other type of general molecular events that may be disturbed during the disease onset and presymptomatic SCA3 phase. We found a number of proteins with an altered level indicating that the dysregulations in protein level occur earlier and with greater intensity as compared to transcriptional changes during the disease progression.

The changes in protein level in the cell can be evoked by post-translational modifications such as protein phosphorylation. We tested the global phosphorylation of proteins and we found numerous decreased phosphoproteins in the cerebellum and cortex of young Ki91 animals (most of them exceeded log FC -2) even reaching -7 in Ki91 animals versus WT animals in the cerebral cortex. In addition, several common proteins were identified for both total proteome and phosphoproteome.

Interestingly, there were only 1 upregulated versus 94 downregulated and 2 upregulated versus 479 downregulated among dysregulated phosphoproteins in the cerebellum and cortex, respectively. This suggests that a general downregulation process of phosphorylated proteins in the cortex and cerebellum may exist in SCA3/MJD at young presymptomatic stage. Of note, ataxin-3 was demonstrated to interact with several kinases such as casein kinase 2 beta (Ck2b), glycogen synthase kinase 3 beta (Gsk3b), checkpoint kinase 1 (Chk1), cyclin-dependent kinase 4 (Cdk4), ribosomal protein S6 kinase (RPS6KA1), MAP kinase interacting serine/threonine kinase 1 (MKNK1), and mitogen-activated protein kinase kinase kinase 1 (MAP3K1) [50–54]. Importantly, ataxin-3 is the interactor of the powerful inhibitor of kinases, cyclin-dependent kinase inhibitor 1A (p21) [54]. p21 is controlling a multitude of kinases including the Cdk5, Camk2d, Cdc28, Ywhaq, Mapk8 (Jnk), Mapk14, Prkaca, Csnk2b, Map3k5, and another powerful inhibitor Cdkn1b (p27) (source: BIOGRID and references therein). In fact, after analyzing the phosphorylation motifs of downregulated phosphoproteins, we discovered that the majority of motifs are targets for Ck1 and 2, Pka, Cdk5 kinases, Camk2, Gsk3, and other kinases such as the genome stabilizer Chk1.

Commonly dysregulated kinase for both analyzed cerebral regions is p21-activated kinase 1 (Pak1) with highly downregulated levels of phosphorylation at Ser-223 (cerebellum) and Ser-174 (cortex). Phosphorylation of Ser-223 is required for Pak1 activation and is performed by casein kinase (Csnk2a1), a known interactor of ataxin-3 [52, 55]. In general, Pak1 is implicated in neurodegenerative disorders, such as Alzheimer disease (AD), Huntington disease (HD), and Parkinson disease [56, 57]. Previously, Pak1 was shown to promote polyQ aggregation by enhancing its toxicity like in cellular models of HD, and this process was rescued by Pak1 knockdown [58]. Conversely, cell death was observed when the activity of Pak1 was downregulated in the 6-OHDA rat model of Parkinson disease [56]. In addition, it was demonstrated that oxidative stress reduced the active, phosphorylated form of Pak1 in dopaminergic neurons, which directly led to a reduction of anti-apoptotic Bcl2 protein levels via the ubiquitin/proteasome pathway. Moreover, an upstream phosphatase of Pak1 modulating its activity is Pp2b-A (Ppp3ca), which is upregulated in the cortex of Ki91 mouse. In addition, a core regulator of phosphatases and also PP2A (Ppp2r1a) [59], phospho Arpp19/Ensa (S62/67) is downregulated in the cerebellum.

Further analysis of dysregulated substrates in the kinases network (Fig. 7) underlies MAPT and MAP2 interconnected with the highest number of kinases dysregulated as phosphoproteins or total proteins. Those proteins are important for proper formation and stability of microtubule complexes [94]. Interestingly, only normal but not mutant ataxin-3 was shown to interact with microtubules [60, 61]. Coherently, we identified a number of other dysregulated proteins and phosphoproteins localized to cytoskeleton or dysregulated kinases with functions related to cytoskeleton such as Pak1, Mapk, Brsk1, and Brsk2 (axon guidance and neurite outgrowth) [62–65]; Src (cytoskeleton remodeling) [66]; and Gsk3b (tau phosphorylation, ataxin-3 is a substrate) [50, 67].

We have clustered the dysregulated proteins and phosphoproteins into three groups reflecting the cellular processes and mechanisms in which the proteins are involved. Group 1 comprises basic cellular processes such as translation and its possible premature termination, disturbed assembly of the ribosome, ubiquitination but also dysregulation of proteins that are characteristic for nucleus and take part in nuclear regulation such as nucleosomes forming, chromatin remodeling, splicing, DNA damage, and repair. Most likely, many of those initial processes result from cellular stress related to the excessive abundance of mutant ataxin-3 in the nucleus, which we demonstrate in young Ki91 animals. The transfer of mutated ataxin-3 into the nucleus could also be related to altered levels of Trim28 (log₂ FC 0.94 in the cerebellum, log₂ FC 1.59 in the cerebral cortex), which was shown to drive the nuclear accumulation of two distinct proteins: α -Syn and Tau implicated in Parkinson disease and Alzheimer disease, respectively [68]. Notably, 26% of dysregulated phosphoproteins in the cerebellum and 22% in the cerebral cortex were predicted to localize in the nucleus, having a role in cell cycle, DNA damage, and splicing.

DNA damage was already demonstrated in SCA3, which was linked to inactivation of polynucleotide kinase 3'-phosphatase (Pnkp) by ataxin-3, an important enzyme for repair of DNA damage [69, 70]. In our experiments, we detected upregulated damage-specific DNA binding protein 1 (Ddb1) in the cerebellar tissue of Ki91 mouse model (log₂ FC 1.65). The Ddb1 together with Chk1 is an ataxin-3 interactor; however, mutant ataxin-3 does not impair the interaction with Chk1 [53].

A molecule which may also be involved in the regulation of the level of other proteins is Pabpc1 which is highly upregulated in the cerebral cortex (log₂ FC 2.02). Its major function is its role in the regulation of translation initiation and mRNA stability and is part of “stress granules” [71, 72].

The second group of dysregulated proteins is related to altered turnover of cytoskeleton which influences neuronal cellular structures and organelles. It was shown that expression of expanded polyQ proteins (ataxin-1, ataxin-3, and huntingtin) substantially affects the dynamics of microtubule cytoskeleton, by nucleation of new microtubules and

rebuilding microtubule rods in neurons of a *Drosophila* model [73]. The cytoskeleton dysregulation potentially disturbs cell division, regulation of growth, structure, and guidance of neuronal projections and gap junctional communication. However, a particularly important resulting process detected among the dysregulated proteins seems to be the transport along microtubules and axons. Moreover, it was demonstrated that aggregates of the mutated form of ataxin-3 form inclusions inside the axon, which might perturb axonal transport [7]. The aberrant transport process may lead to disturbed synaptic transmission and energy metabolism and ultimately cause cell dysfunction and cellular death, and proteins involved in those processes were clustered in group 3.

An important part of SCA3 pathogenesis comprises impairments of the mitochondria, which include altered localization of ataxin-3 inside the mitochondria, enhanced interaction of ataxin-3 82Q with mitochondrial proteins (Sdhb and Ndufa4 which are also dysregulated in our analysis), and mitochondrial DNA damage documented in SCA3 models [51, 61, 74–76]. In line with those aberrations, in young Ki91 animals, we observed a number of dysregulated mitochondrial proteins belonging to group III such as Mt-co1 and mt-Co3 (cortex) and Uqcrh (cerebellum). Strikingly, in the cerebellum, proteins related to the mitochondria are all upregulated, whereas in the cerebral cortex, GO terms and pathways related only to upregulated proteins are mainly associated with mitochondrial electron transport chain and metabolism. Interestingly, it was shown that mitochondrial precursor accumulation may cause cellular stress influencing translation machinery [77]. Remarkably, there are no GO terms or pathways for dysregulated phosphoproteins referring to the mitochondria, which suggest that phosphorylation is not the mechanism responsible for altered levels of mitochondrial proteins.

In summary, we propose that the key proteins responsible for early pathogenic changes are various kinases interacting with mutant ataxin-3 and proteins dysregulated at the level of total or phosphorylation levels also demonstrating high log₂ FC in Ki91 mouse which are Pak1, Arpp19/Ensa, Darpp-32, Sirt2, Acin1, Ddb1, Ppp5c, Hdac2, Thrap3, Trim28, Hnrnph2, Rbbp4, Bclaf1, Nedd8, Pabpc1, and several ribosomal proteins and elongation and splicing factors.

Conclusions

In the current study, we demonstrate that early transcriptional changes influenced by mutant ataxin-3 do not occur in presymptomatic Ki91 SCA3/MJD mouse model; however, we identify prominent dysregulation of protein levels and phosphorylation. Based on the identified proteins and phosphoproteins, we dissected a set of most early events including impaired phosphorylation of proteins indicating the influence of mutant ataxin-3 on many kinases, proteins involved in DNA damage, and

mechanisms playing a role in translation initiation. Moreover, GO term and pathway analysis indicates that dysregulated proteins may further impair cellular pathways and processes such as autophagy, energy metabolism, and transport of molecules and vesicles along axons. Subsequently, this may lead to severe effects such as defective projections and synaptic transmission eventually leading to neuronal dysfunction, subsequent demyelination, and neurodegeneration. For each of the identified pathways, we propose key molecules which are affected by the change of levels in the cerebellum and cortex. Altogether, we conclude that early triggers of the disease act on the level of pathways and processes engaging proteins rather than the transcription stage, whereas late transcriptomic changes most likely result from degeneration of particular populations of cells in the brain such as GABAergic neurons and oligodendrocyte precursors. The relatively high number of dysregulated proteins and phosphoproteins in Ki91 SCA3/MJD mice indicates that there are important modifiers of disease and biomarkers or even target molecules for therapies among those proteins. The most prominent new candidate molecules are kinases, such as Pak1, which have a vast influence on distinct cellular processes. Therefore, a particularly promising area for further studies on disease mechanism and potential therapies in SCA3 is the proteome and phosphoproteome.

Methods

Animals

Maintaining and breeding were performed at standard conditions with an 18-/6-h light/dark cycle and water and food provided ad libitum. The animals were marked using numerical ear tags (National Band & Tag Company, Newport, USA). The animals were sacrificed according to AVMA Guidelines for the Euthanasia of Animals by placing them in the programmable CO₂ chamber (Rothacher Medical, Heitenried, Switzerland). The stress level of the animals was minimized throughout all the procedures and animal handling. The animal experimentation and handling were approved and monitored by the Local Ethical Commission for Animal Experiments in Poznan. The Ki91 SCA3/MJD mouse model was bred on C57BL/6 mouse genetic background for 10 generations and the animals were further maintained on the C57BL/6 genetic background. The homozygous (mut/mut) transgenic animals both from Ki91 knock-in mouse were generated by breeding heterozygous (mut/wt) animals. Homozygous Ki91 animals contained between 98 and 132 CAG repeats on a single mutant ataxin-3 allele. For RNAseq, Ki91 animals contained 100–110 CAG repeats. For total proteomics, Ki91 mice contained 98–106 CAG and Ki91 mice for phosphoproteomics contained 98–123 CAGs in mutant Atxn3 gene. For behavioral studies, Ki91 mice

contained 103–132 CAGs. The total number of 80 animals of various ages was used for collecting brain tissues and 36 animals at the age of 2 months were used for the behavioral experiments. The cortex and the cerebellum for proteomic and transcriptomic analysis were always collected from brain tissue of a typical experimental group consisting of four mutant mice versus four nontransgenic or C57BL/6 mice. For qPCR validation of RNAseq analysis, 2- and 4-month-old samples from the FVB mouse strain have been used as a second control since the FVB strain demonstrates the same SNP profile (MGI in chromosome 12)(e.g., Atxn3 and Serpina3n locus) as the 129sv genetic background originating from stem cells to which the Ki91 transgene was introduced. Supplementary Table 1 summarizes the number of animals by strain, genotype, age, experiment type, and tissue.

Behavioral Studies

Assessment of motor function was performed as previously described [14]. Tests included accelerating rotarod (4–40 rpm in 9.5 min), elevated beam walk (diameter of rods—35, 28, 21, 17, and 9 mm), and parallel rod floor test in which the number of foot slips and locomotor activity in the experimental cage were analyzed and measured during 10 min. Each test consisted of one training day (T) and three consecutive days of measurement. In addition, we also performed scoring tests designed for evaluation of ataxia phenotype in mouse models [78]. All mice were weighed during each testing session. Graphing and statistics were performed on PrismVR software (San Diego, CA, USA), using ANOVA with Bonferroni post hoc test.

RNAseq Analysis

NGS QC Toolkit (v 2.2.3) [79] was used to generate quality metrics for assessment of fastq input files. We used the statistics generated by the NGS QC Toolkit and prepared charts (Supplementary Fig. 6) which show the average quality score per base positions for each library. Fastq files were then aligned to the GRCh38.91 reference genome using STAR software (v 2.5.3a) [80] with parameters suggested by the QoRTs software (v 1.3.0) [81]. The parameters are used by default for estimation of genes and exon hit counts. The alignment statistics are demonstrated on charts in Supplementary Fig. 6A where the percentage of unique and multiply aligned reads are shown. The data were analyzed using three different experimental approaches which included the alignment/quantification of transcripts by Star/Deseq and HISAT/StringTie/Ballgown [82, 83]. In brief, the differential gene expression was calculated using DESeq2 software (v 1.14.1) [84]. To countercheck the results, the second software pipeline, namely HISAT2 (v 2.0.5) → StringTie (v 1.3.1c) → Ballgown (v 2.6.0) [82, 83, 85] was used. The results from

the HISAT2 pipeline were consistent with the primary analysis and are not shown in the results section. Additionally, JunctionSeq analysis has been applied in the identification of altered splicing variants [86].

Quantitative Real-Time PCR

Reverse transcription was performed with 500 ng of RNA using Maxima H Minus Reverse Transcriptase according to the manufacturer's protocol using random hexamers. qPCR was performed according to MIQE Guidelines where relative gene expression and splicing events were estimated using the $\Delta\Delta Ct$ method with ActinB, Pgk1, and Tfrc as control [87]. qPCR reaction was carried out on the BioRad CFX96 thermocycler using 5x HOT FIREPol EvaGreen qPCR Mix Plus (Solis Biodyne, Tartu, Estonia) with the following parameters: 95 °C 15 min and 45 cycles of (95 °C 15 min, 60 °C 1 min) using primers synthesized at IBB, PAS (oligo.pl). Statistical analysis between two groups of samples was performed using two-sample *t* test with *p* < 0.05 considered as significant.

Western Blot Analysis

Cerebellum and cortex samples were harvested from six young 2-month-old homozygous Ki91 and six age-matched C57BL mice. Tissues were homogenized in a buffer containing 60 mM TRIS-base, 2% SDS, 10% sucrose, and 2 mM PMSF using a Bioprep-6 homogenizer (Allsheng, China), followed by bath sonication for 3 min repeated three times while cooling the tube on ice in between the sonication. The protein concentration was estimated using a Pierce BCA protein assay kit (Thermo Scientific, Rockford, IL, USA) according to the manufacturer's instructions. For each analysis, 25 µg of total protein or 45 µg of total protein for analysis of phosphorylated proteins was diluted in a loading buffer containing 2-mercaptoethanol and boiled for 5 min. The proteins were separated by SDS-polyacrylamide gel electrophoresis (5% stacking/12 or 10% resolving gel), transferred to nitrocellulose, and stained with Ponceau S solution. The blots were blocked with 5% nonfat milk in PBS/0.05% Tween 20 (analysis of total proteins) or 5% BSA (GE Healthcare, South Logan, UT, USA) in PBS/0.05% Tween 20 (analysis of total phosphoproteins) for 1 h at RT and, subsequently, incubated for 24 h at 4 °C with the following primary antibodies: mouse anti-PABP1 (1:1000; Cell Signaling, Danvers, MA, USA), rabbit anti-MBP (1:1000; Cell Signaling, Danvers, MA, USA), rabbit anti-DDB-1 (1:1000; Cell Signaling, Danvers, MA, USA), rabbit anti-Phospho-DARPP32 (Ser97) (1:1000; Cell Signaling, Danvers, MA, USA), rabbit anti-Phospho-Tau (Ser416) (1:1000; Cell Signaling, Danvers, MA, USA), mouse

anti-Beta III Tubulin (1:1000; Darmstadt, Germany, Merck), mouse anti-NEFH (1:2000; DSHB Hybridoma Product RT97; deposited to the DSHB by Wood, J. [88]), and mouse anti- α -ACTIN (1:1000; DSHB Hybridoma Product JLA20; deposited to the DSHB by Lin, J.J.-C. [89]). The blots were probed with the respective HRP-conjugated secondary antibody (anti-rabbit or anti-mouse, 1:2000; Jackson ImmunoResearch, Suffolk, UK). The immunoreaction was detected using the ECL substrate (ThermoFisher Scientific, Waltham, MA, USA).

Protein Extraction Digestion and Enrichment for Proteomics

Mouse brain tissues were lysed in buffer containing 1 M triethylammonium bicarbonate (TEAB), 0.1% SDS, and 1 mM sodium orthovanadate (NaVO₃) in 2-ml tubes with stainless steel beads (Retch, Germany) followed by automatic homogenization using a Mixer Mill MM400 (Retch, Germany). Subsequently, the material was subjected to a threefold cycle of freezing and thawing followed by bath sonication for 3-min repeated three times while cooling the tube on ice in between the sonication. Protein concentration in the clear lysate was estimated using Pierce BCA protein assay kit (Thermo Scientific, Rockford, IL, USA) according to the manufacturer's instructions. Ten-microgram aliquots of proteins were diluted with 15 µl of 50 mM NH₄HCO₃ and reduced with 5.6 mM DTT for 5 min at 95 °C. Samples were then alkylated with 5 mM iodoacetamide for 20 min in the dark at RT. Subsequently, the proteins were digested with 0.2 µg of sequencing-grade trypsin (Promega) overnight at 37 °C. For labeled free quantitative proteomics, 10 µg of digested protein per sample was used for analyses on LC/MS. A similarly prepared set of samples was used for phosphoproteomics. For each sample, 300 µg of digested protein was used for phosphopeptide enrichment. Phosphorylated peptides were enriched using two different kits, one exploiting titanium dioxide (TiO₂) spin tips and the other high-capacity Fe-NTA spin column (Thermo Scientific, Rockford, IL, USA). Elution fractions containing phosphopeptides were further desalting on a C18 column (J.T. Baker, Center Valley, PA) prior to mass spectrometry quantitative measurements. To perform a global analysis of phosphoproteomic changes, we have collected another set of cerebellum and cortex samples. The final analysis was performed on eight cerebella of four young 2-month-old homozygous Ki91 and four age-matched C57BL mice and six cerebral cortices of three young 2-month-old homozygous Ki91 and three age-matched C57BL mice. Collected tissues were further subjected to protein isolation, trypsin fragmentation, and phospho-enrichment procedure (see "Methods" section).

Mass Spectrometry Analysis of the Proteome

The analysis was performed with the use of Dionex UltiMate 3000 RSLC nanoLC system connected to Q Exactive Orbitrap mass spectrometer (Thermo Fisher Scientific). Peptides derived from in-solution digestion were separated on a reverse phase Acclaim PepMap RSLC nanoViper C18 column ($75\text{ }\mu\text{m} \times 25\text{ cm}$, $2\text{ }\mu\text{m}$ granulation) using acetonitrile gradient (from 4 to 60%, in 0.1% formic acid) at $30\text{ }^{\circ}\text{C}$ and a flow rate of 300 nL/min (for 230 min). The spectrometer was operated in data-dependent MS/MS mode (tandem mass spectrometry) with survey scans acquired at a resolution of 70,000 at m/z 200 in MS mode and 17,500 at m/z 200 in MS2 mode. Spectra were recorded in the scanning range of 300–2000 m/z in the positive ion mode. Higher energy collisional dissociation (HCD) ion fragmentation was performed with normalized collision energies set to 25. Protein identification was performed using the Swiss-Prot mouse database with a precision tolerance 10 ppm for peptide masses and 0.08 Da for fragment ion masses. All raw data obtained for each dataset were imported into MaxQuant 1.5.3.30 version for protein identification and quantification. Protein was considered as positively identified if at least two peptides per protein were found by Andromeda search engine, and a peptide score reached the significance threshold FDR = 0.01.

Obtained data were exported to Perseus software ver. 1.5.3.2 (part of MaxQuant package). Numeric data were transformed to a logarithmic scale, and each sample was annotated with its group affiliation. Proteins only identified by site, reverse database hits, and contaminants were removed from the results. Next, data were filtered based on valid values for proteins. Proteins which contained valid values in 75% of samples in at least one group (the inclusion threshold: 3 or 4 values for control and 3 or 4 values for Ki91 mice) were included as valid hits. In addition, for supplementary analysis, we have selected proteins which produced valid values only in control or only in Ki91 SCA3/MJD mouse group (4 values inclusion). Prior to statistical analysis, normalization of data was performed by subtracting median from each value in a row. A two-sample *t* test was performed on analyzed sample data with *p* value < 0.05 being considered significant, and differentiating proteins were normalized using the Z-score algorithm for hierarchical clustering of data.

Bioinformatic Analysis of Proteomic Data

The power of the analyses was increased by using two separate set of tools, namely Consensus Path Database (version 32) (CPDB) [90] and Cytoscape version (version 3.6.0) containing the ClueGO plugin (academic version 2.3.5) [91, 92]. CPDB consolidates information from a considerably higher number of databases compared to ClueGO; however, the advantage of ClueGO is its ability to merge the same or similar

information about pathways or GO terms which forms general categories. The analysis paradigm included the discovery of affected pathways, molecular function of dysregulated proteins, biological processes affected by the dysregulated proteins, and prediction of subcellular localization of dysregulated proteins. For each analysis, names of genes corresponding to the names of dysregulated proteins or phosphoproteins were used.

Proteins were grouped using the Consensus Path Database according to the pathways (pathway enrichment *p* value cutoff < 0.01, minimum overlap with input list = 10% of total number of dysregulated proteins), GO term analyses by molecular function, biological process, and cellular component (GO term B, MF level 5, CC levels 4 and 5, *p* value cutoff < 0.0001).

The second analysis in CPDB was performed with lists of top dysregulated proteins ($\log_2 \text{FC} \leq -1.0$ for downregulated protein levels or $\log_2 \text{FC} \geq 1.0$ for upregulated protein levels) for pathway enrichment and GO terms with the same *p* value and minimum overlap with input list restrictions.

Subsequently, using ClueGO and Cytoscape, we have performed GO term annotation analysis and pathway enrichment (*p* value cutoff < 0.05, GO tree interval = 3–5, kappa score = 0.5). In ClueGO, the number of GO terms was restricted by the number of dysregulated proteins per GO term in proportional relation to the total number of dysregulated proteins in a dataset (51–100 dysregulated proteins—*inclusion of GO terms containing a minimum of 3 proteins from the input list, 101–150—minimum of 4 proteins, 301–350—minimum of 8 proteins*). The analysis in ClueGO was based on “biological process,” “molecular function,” and KEGG, Reactome, and WikiPathways [93–94]. The compatibility of results obtained with the Consensus Path Database and ClueGO was confirmed by identification of common GO terms with similar *p* values using both tools.

In a separate analysis, we performed identification of cell types in the brain which are affected by pathogenesis using the BrainMap tool of *Allen Brain Atlas* [22] for the cerebral cortex and the DropViz tool [21] for the cerebellum. This was accomplished by grouping of dysregulated proteins according to cell type in the brain in which they are expressed. Significantly dysregulated (*p* < 0.05) proteins identified from label-free proteomic and phosphoproteomic LCMS experiments were included together into two tissue groups, based on origin from the cerebellum and cortex. Relative expression is presented in BrainMap as counts per million in \log_{10} scale and in DropViz as the amount of transcripts per 100,000 in the cluster. Moreover, for the phosphoproteomic data, we have predicted kinases which phosphorylate dysregulated phosphoproteins using CPDB and PHOSIDA (using known motifs) [95]. For the analysis with PHOSIDA sequences of peptides with altered phosphorylation level, the FASTA format was used.

Neural Cultures from SCA3 Patients iPSC

The culture and differentiation of iPSC from SCA3 patients were performed as previously described [24]. Picked neural rosettes were cultured in suspension for 2 days in DMEM/F12, 2 mM l-glutamine, 1.6 g l⁻¹ glucose, 0.1 mg ml⁻¹ penicillin/streptomycin, and N2 supplement (1:100; Invitrogen), then dissociated with trypsin, plated onto poly-l-ornithine/laminin-coated plates, and propagated in N2 medium supplemented with B27 (1 µl ml⁻¹, Invitrogen), 10 ng ml⁻¹ FGF2, and 10 ng ml⁻¹ EGF (both from R&D Systems). Neuronal differentiation was induced by removing the growth factors FGF2 and EGF from the media and culturing the cells in Neurobasal medium supplemented with B27 (1:50, Invitrogen) and DMEM/F12 supplemented with N2 (1:100) mixed at a 1:1 ratio; 300 ng ml⁻¹ cAMP was added to the differentiation media. After 6 weeks, differentiation cells were harvested in TRIzol.

Immunohistochemistry

The animals were deeply anesthetized and transcardially perfused using saline followed by 4% PFA. The brains were removed, postfixed in 4% PFA for 48 h, and cryopreserved with graded sucrose (10–20–30%) over 72 h. The 20-µm parasagittal mouse brain sections were cut using a cryostat at -20 °C and collected on SuperFrost Plus slides (Thermo Scientific). The sections were processed immediately. The HIER procedure was applied by incubation of the sections in citrate buffer (pH 9.0) for 30 min at 60 °C. The sections were blocked via incubation in 4% normal goat serum in TBS for 1 h. For immunofluorescence staining, the sections were incubated overnight at 4 °C with the primary mouse anti-ataxin-3 antibody 1H9 (1:200) [] and, subsequently, with the anti-mouse antibody labeled by AlexaFluor488 (1:400; Jackson ImmunoResearch, Suffolk, UK). The sections were end-stained with Hoechst 33342 (Sigma) nuclear stain at 1:1000 and embedded in Fluoroshield (Sigma) mounting medium. Fluorescent confocal images were acquired using fixed excitation and detection parameters using the TCS SP5 II (Leica Microsystems, Poland).

Statistics

The data regarding behavioral experiments performed within 4 days (rotarod, elevated beam walk, parallel rod floor test) were subjected to a two-way ANOVA, followed by Bonferroni posttests. Scoring test and body weight were evaluated with unpaired Student's *t* test. The two-group comparisons of the gene expression data by qPCR were conducted using the unpaired Student's *t* test. *p* values less than 0.05 were considered significant with the exception of qPCR using C57BL/6 and FVB controls, where *p* values less than 0.01 were considered statistically significant. Identification of proteins on raw proteomic data was performed by Andromeda

search engine in Mascot using the following inclusion criteria: 1. At least two different peptides per protein were identified per sample, and a total peptide score reached the significance threshold FDR = 0.01. Identified proteins matching the inclusion criteria were subjected to further statistical analysis with two-sample *t* test, and dysregulation of protein level reaching *p* value < 0.05 was considered as significant. One asterisk indicates *p* value ≤ 0.05, two asterisks indicate *p* value ≤ 0.01, and three asterisks indicate *p* value ≤ 0.001.

Acknowledgments We thank Professor Ryszard Kierzek (IBCh, PAS, Poland) for kindly providing access to the BioRad CFX96 thermocycler. We thank Professor Yvon Trottier for kindly providing the anti-Ataxin-3 1H9 antibody. Imaging was performed using the facilities in the Laboratory of Subcellular Structures Analysis (IBCh, PAS, Poland). Proteomic mass spectrometry analyses were performed in the Laboratory of Mass Spectrometry and the library synthesis was performed in the Laboratory of Genomics (European Centre for Bioinformatics and Genomics; ECBiG; IBCH, PAS, Poznań, Poland). We thank Prof. Gabriela Bindea, from the Laboratory of Integrative Cancer Immunology INSERM UMRS1138, Cordeliers Research Center, Paris, France, for kindly providing an academic license key for ClueGO plugin for Cytoscape. We thank Joanna Nowak for her help in maintaining the animals. The mouse anti-NEFH (RT97) developed by Wood, J. and mouse anti-α-ACTIN (JLA20) developed by Lin, J.J.-C. were obtained from the Developmental Studies Hybridoma Bank (DSHB), created by the NICHD of the NIH and maintained at The University of Iowa, Department of Biology, Iowa City, IA 52242.

Authors' Contribution MacF conceived, designed, supervised all experiments, and analyzed the data. KW and LM performed all proteomic experiments. KW performed the main analysis of proteomic data; PP performed all transcriptomic qPCR experiments; RP, MR, LH, and MK, performed all works associated with NGS experiments; MacF, MarF, and PW performed the analyses of NGS data. OB and JJ provided and performed the culture and differentiation of SCA3 iPSC. MacF performed the collection of animal tissues. KW performed live animal behavioral experiments. MarF critically revised the article. MacF and KW wrote the paper. MacF was responsible for research concept and obtaining funding.

Funding This work was supported by grant from the National Science Centre (grant number 2013/10/E/NZ4/00621) and the Polish Ministry of Science and Higher Education under the KNOW Poznań RNA Centre 01/KNOW2/2014 and the German Ministry for Education and Research (BMBF; 01EK1603A-Neuro2D3).

Compliance with Ethical Standards

Competing Interests The authors declare that they have no competing interests.

Abbreviations SCA3, spinocerebellar ataxia type 3; MJD, Machado–Joseph disease; polyQ, polyglutamine; iPSC, induced pluripotent stem cell; MS, mass spectrometry; FC, fold change

Open Access This article is distributed under the terms of the Creative Commons Attribution 4.0 International License (<http://creativecommons.org/licenses/by/4.0/>), which permits unrestricted use, distribution, and reproduction in any medium, provided you give appropriate credit to the original author(s) and the source, provide a link to the Creative Commons license, and indicate if changes were made.

References

- Kawaguchi Y, Okamoto T, Taniwaki M, Aizawa M, Inoue M, Katayama S, Kawakami H, Nakamura S et al (1994) CAG expansions in a novel gene for Machado-Joseph disease at chromosome 14q32.1. *Nat Genet* 8:221–228.
- Riess O, Rüb U, Pastore A, Bauer P, Schöls L (2008) SCA3: neurological features, pathogenesis and animal models. *Cerebellum* 7: 125–137. <https://doi.org/10.1007/s12311-008-0013-4>
- Winborn BJ, Travis SM, Todi SV, Scaglione KM, Xu P, Williams AJ, Cohen RE, Peng J et al (2008) The deubiquitinating enzyme ataxin-3, a polyglutamine disease protein, edits lys63 linkages in mixed linkage ubiquitin chains. *J Biol Chem* 283:26436–26443.
- Todi SV, Scaglione KM, Blount JR, Basrur V, Conlon KP, Pastore A, Elenitoba-Johnson K, Paulson HL (2010) Activity and cellular functions of the deubiquitinating enzyme and polyglutamine disease protein ataxin-3 are regulated by ubiquitination at lysine 117. *J Biol Chem* 285:39303–39313. <https://doi.org/10.1074/jbc.M110.181610>
- Weishäupl D, Schneider J, Peixoto Pinheiro B, Ruess C, Dold SM, von Zwyerdt F, Gloeckner CJ, Schmidt J et al (2019) Physiological and pathophysiological characteristics of ataxin-3 isoforms. *J Biol Chem* 294:644–661. <https://doi.org/10.1074/jbc.RA118.005801>
- Matos CA, de Almeida LP, Nóbrega C (2019) Machado-Joseph disease/spinocerebellar ataxia type 3: lessons from disease pathogenesis and clues into therapy. *J Neurochem* 148:8–28. <https://doi.org/10.1111/jnc.14541>
- Seidel K, den Dunnen WFA, Schultz C, Paulson H, Frank S, de Vos RA, Brunt ER, Deller T et al (2010) Axonal inclusions in spinocerebellar ataxia type 3. *Acta Neuropathol* 120:449–460. <https://doi.org/10.1007/s00401-010-0717-7>
- Sowa AS, Martin E, Martins IM, Schmidt J, Depping R, Weber JJ, Rother F, Hartmann E et al (2018) Karyopherin α-3 is a key protein in the pathogenesis of spinocerebellar ataxia type 3 controlling the nuclear localization of ataxin-3. *Proc Natl Acad Sci U S A* 115: E2624–E2633. <https://doi.org/10.1073/pnas.1716071115>
- Araujo J, Breuer P, Dieringer S, Krauss S, Dorn S, Zimmermann K, Pfeifer A, Klockgether T et al (2011) FOXO4-dependent upregulation of superoxide dismutase-2 in response to oxidative stress is impaired in spinocerebellar ataxia type 3. *Hum Mol Genet* 20: 2928–2941. <https://doi.org/10.1093/hmg/ddr197>
- Hübener J, Weber JJ, Richter C et al (2013) Calpain-mediated ataxin-3 cleavage in the molecular pathogenesis of spinocerebellar ataxia type 3 (SCA3). *Hum Mol Genet* 22:508–518. <https://doi.org/10.1093/hmg/ddt449>
- Nascimento-Ferreira I, Santos-Ferreira T, Sousa-Ferreira L, Auregan G, Onofre I, Alves S, Dufour N, Colomer Gould VF et al (2011) Overexpression of the autophagic beclin-1 protein clears mutant ataxin-3 and alleviates Machado-Joseph disease. *Brain J Neurol* 134:1400–1415. <https://doi.org/10.1093/brain/awr047>
- Nóbrega C, Simões AT, Duarte-Neves J et al (2018) Molecular mechanisms and cellular pathways implicated in Machado-Joseph disease pathogenesis. *Adv Exp Med Biol* 1049:349–367. https://doi.org/10.1007/978-3-319-71779-1_18
- Switonski P, Szlachcic W, Gabka A et al (2012) Mouse models of polyglutamine diseases in therapeutic approaches: review and data table. Part II. *Mol Neurobiol* 46:430–466. <https://doi.org/10.1007/s12035-012-8316-3>
- Switonski PM, Szlachcic WJ, Krzyzosiak WJ, Figiel M (2015) A new humanized ataxin-3 knock-in mouse model combines the genetic features, pathogenesis of neurons and glia and late disease onset of SCA3/MJD. *Neurobiol Dis* 73:174–188. <https://doi.org/10.1016/j.nbd.2014.09.020>
- Figiel M, Szlachcic W, Switonski P et al (2012) Mouse models of polyglutamine diseases: review and data table. Part I. *Mol Neurobiol* 46:393–429. <https://doi.org/10.1007/s12035-012-8315-4>
- Watkins-Chow DE, Pavan WJ (2008) Genomic copy number and expression variation within the C57BL/6J inbred mouse strain. *Genome Res* 18:60–66. <https://doi.org/10.1101/gr.6927808>
- Leite C de MBA, Schieferdecker MEM, Frehner C et al (2018) Body composition in spinocerebellar ataxia type 3 and 10 patients: comparative study with control group. *Nutr Neurosci* 0:1–6. <https://doi.org/10.1080/1028415X.2018.1469282>
- Sauté JAM, da Silva ACF, Souza GN, Russo AD, Donis KC, Vedolin L, Saraiva-Pereira ML, Portela LVC et al (2012) Body mass index is inversely correlated with the expanded CAG repeat length in SCA3/MJD patients. *Cerebellum* 11:771–774. <https://doi.org/10.1007/s12311-011-0326-6>
- Yang J-S, Chen P-P, Lin M-T, Qian MZ, Lin HX, Chen XP, Shang XJ, Wang DN et al (2018) Association between body mass index and disease severity in Chinese spinocerebellar ataxia type 3 patients. *Cerebellum* 17:494–498. <https://doi.org/10.1007/s12311-018-0929-2>
- Diallo A, Jacobi H, Schmitz-Hübsch T, Cook A, Labrum R, Durr A, Brice A, Charles P et al (2017) Body mass index decline is related to spinocerebellar ataxia disease progression. *Mov Disord Clin Pract* 4:689–697. <https://doi.org/10.1002/mdc3.12522>
- Saunders A, Macosko EZ, Wysoker A, Goldman M, Krienen FM, de Rivera H, Bien E, Baum M et al (2018) Molecular diversity and specializations among the cells of the adult mouse brain. *Cell* 174: 1015–1030.e16. <https://doi.org/10.1016/j.cell.2018.07.028>
- Tasic B, Yao Z, Graybuck LT, Smith KA, Nguyen TN, Bertagnolli D, Goldy J, Garren E et al (2018) Shared and distinct transcriptomic cell types across neocortical areas. *Nature* 563:72–78. <https://doi.org/10.1038/s41586-018-0654-5>
- Koch P, Breuer P, Peitz M, Jungverdorben J, Kesavan J, Poppe D, Doerr J, Ladewig J et al (2011) Excitation-induced ataxin-3 aggregation in neurons from patients with Machado-Joseph disease. *Nature* 480:543–546. <https://doi.org/10.1038/nature10671>
- Koch P, Opitz T, Steinbeck JA, Ladewig J, Brustle O (2009) A rosette-type, self-renewing human ES cell-derived neural stem cell with potential for in vitro instruction and synaptic integration. *Proc Natl Acad Sci U S A* 106:3225–3230. <https://doi.org/10.1073/pnas.0808387106>
- Bateman A, Martin MJ, O'Donovan C et al (2017) UniProt: the universal protein knowledgebase. *Nucleic Acids Res* 45:D158–D169. <https://doi.org/10.1093/nar/gkw1099>
- Kini HK, Silverman IM, Ji X, Gregory BD, Liehaber SA (2016) Cytoplasmic poly(A) binding protein-1 binds to genomically encoded sequences within mammalian mRNAs. *RNA* 22:61–74. <https://doi.org/10.1261/rna.053447.115>
- Hu Z, Holzschuh J, Driever W (2015) Loss of DDB1 leads to transcriptional p53 pathway activation in proliferating cells, cell cycle deregulation, and apoptosis in zebrafish embryos. *PLoS One* 10:e0134299. <https://doi.org/10.1371/journal.pone.0134299>
- Boggs JM (2006) Myelin basic protein: a multifunctional protein. *Cell Mol Life Sci* 63:1945–1961. <https://doi.org/10.1007/s00018-006-6094-7>
- Kapitein LC, Hoogenraad CC (2015) Building the neuronal microtubule cytoskeleton. *Neuron* 87:492–506. <https://doi.org/10.1016/j.neuron.2015.05.046>
- Yuan A, Rao MV, Veeranna null, Nixon RA (2017) Neurofilaments and neurofilament proteins in health and disease. *Cold Spring Harb Perspect Biol* 9:. <https://doi.org/10.1101/cshperspect.a018309>
- Boeing S, Williamson L, Encheva V, Gori I, Saunders RE, Instrell R, Aygün O, Rodriguez-Martinez M, Weems JC, Kelly GP, Conaway JW, Conaway RC, Stewart A, Howell M, Snijders AP,

- Svejstrup JQ (2016) Multiomic Analysis of the UV-Induced DNA Damage Response. *Cell Reports* 15 (7):1597–1610
32. Zhang H, Head PE, Yu DS (2016) SIRT2 orchestrates the DNA damage response. *Cell Cycle* 15 (16):2089–2090
33. Vohhodina J, Barros EM, AL S, Liberante FG, Manti L, Bankhead P, Cosgrove N, Madden AF, Harkin PD, Savage KI (2017) The RNA processing factors THRAP3 and BCLAF1 promote the DNA damage response through selective mRNA splicing and nuclear export. *Nucleic Acids Research* 45 (22):12816–12833
34. Lomonosova E, Chinnadurai G (2008) BH3-only proteins in apoptosis and beyond: an overview. *Oncogene* 27 Suppl 1:S2–19. <https://doi.org/10.1038/onc.2009.39>
35. Wang T-Y, Jao C-W, Soong B-W, Wu HM, Shyu KK, Wang PS, Wu YT (2015) Change in the cortical complexity of spinocerebellar ataxia type 3 appears earlier than clinical symptoms. *PLoS One* 10: e0118828. <https://doi.org/10.1371/journal.pone.0118828>
36. Lu M-K, Chen J-C, Chen C-M, Duann JR, Ziemann U, Tsai CH (2017) Impaired cerebellum to primary motor cortex associative plasticity in Parkinson's disease and spinocerebellar ataxia type 3. *Front Neurol* 8:445. <https://doi.org/10.3389/fneur.2017.00445>
37. Farrar MA, Vucic S, Nicholson G, Kiernan MC (2016) Motor cortical dysfunction develops in spinocerebellar ataxia type 3. *Clin Neurophysiol* 127:3418–3424. <https://doi.org/10.1016/j.clinph.2016.09.005>
38. de Rezende TJR, D'Abreu A, Guimarães RP et al (2015) Cerebral cortex involvement in Machado-Joseph disease. *Eur J Neurol* 22: 277–283, e23–24. <https://doi.org/10.1111/ene.12559>
39. Schmidt J, Mayer AK, Bakula D, Freude J, Weber JJ, Weiss A, Riess O, Schmidt T (2018) Vulnerability of frontal brain neurons for the toxicity of expanded ataxin-3. *Hum Mol Genet* 28:1463–1473. <https://doi.org/10.1093/hmg/ddy437>
40. Chou A-H, Chen Y-L, Hu S-H, Chang YM, Wang HL (2014) Polyglutamine-expanded ataxin-3 impairs long-term depression in Purkinje neurons of SCA3 transgenic mouse by inhibiting HAT and impairing histone acetylation. *Brain Res* 1583:220–229. <https://doi.org/10.1016/j.brainres.2014.08.019>
41. Evert BO, Araujo J, Vieira-Saecker AM, de Vos RAI, Harendza S, Klockgether T, Wüllner U (2006) Ataxin-3 represses transcription via chromatin binding, interaction with histone deacetylase 3, and histone deacetylation. *J Neurosci* 26:11474–11486. <https://doi.org/10.1523/JNEUROSCI.2053-06.2006>
42. Evert BO, Vogt IR, Vieira-Saecker AM, Ozimek L, de Vos RAI, Brunt ERP, Klockgether T, Wüllner U (2003) Gene expression profiling in ataxin-3 expressing cell lines reveals distinct effects of normal and mutant ataxin-3. *J Neuropathol Exp Neurol* 62:1006–1018
43. Estebanez L, Hoffmann D, Voigt BC, Poulet JFA (2017) Parvalbumin-expressing GABAergic neurons in primary motor cortex signal reaching. *Cell Rep* 20:308–318. <https://doi.org/10.1016/j.celrep.2017.06.044>
44. Yu MC, Cho E, Luo CB, Li WWY, Shen WZ, Yew DT (1996) Immunohistochemical studies of GABA and parvalbumin in the developing human cerebellum. *Neuroscience* 70:267–276
45. Kazachkova N, Raposo M, Ramos A, Montiel R, Lima M (2017) Promoter variant alters expression of the autophagic BECN1 gene: implications for clinical manifestations of Machado-Joseph disease. *Cerebellum* 16:957–963. <https://doi.org/10.1007/s12311-017-0875-4>
46. Ramani B, Panwar B, Moore LR, Wang B, Huang R, Guan Y, Paulson HL (2017) Comparison of spinocerebellar ataxia type 3 mouse models identifies early gain-of-function, cell-autonomous transcriptional changes in oligodendrocytes. *Hum Mol Genet* 26: 3362–3374. <https://doi.org/10.1093/hmg/ddx224>
47. Raposo M, Bettencourt C, Ramos A, Kazachkova N, Vasconcelos J, Kay T, Bruges-Armas J, Lima M (2017) Promoter variation and expression levels of inflammatory genes IL1A, IL1B, IL6 and TNF in blood of spinocerebellar ataxia type 3 (SCA3) patients. *NeuroMolecular Med* 19:41–45. <https://doi.org/10.1007/s12017-016-8416-8>
48. Toonen LJA, Overzier M, Evers MM, Leon LG, van der Zeeuw SAJ, Mei H, Kielbasa SM, Goeman JJ et al (2018) Transcriptional profiling and biomarker identification reveal tissue specific effects of expanded ataxin-3 in a spinocerebellar ataxia type 3 mouse model. *Mol Neurodegener* 13:31. <https://doi.org/10.1186/s13024-018-0261-9>
49. Gibson EM, Purger D, Mount CW, Goldstein AK, Lin GL, Wood LS, Inema I, Miller SE et al (2014) Neuronal activity promotes oligodendrogenesis and adaptive myelination in the mammalian brain. *Science* 344:1252304. <https://doi.org/10.1126/science.1252304>
50. Fei E, Jia N, Zhang T, Ma X, Wang H, Liu C, Zhang W, Ding L et al (2007) Phosphorylation of ataxin-3 by glycogen synthase kinase 3beta at serine 256 regulates the aggregation of ataxin-3. *Biochem Biophys Res Commun* 357:487–492. <https://doi.org/10.1016/j.bbrc.2007.03.160>
51. Kristensen LV, Oppermann FS, Rauen MJ, Fog K, Schmidt T, Schmidt J, Harmuth T, Hartmann-Petersen R et al (2018) Mass spectrometry analyses of normal and polyglutamine expanded ataxin-3 reveal novel interaction partners involved in mitochondrial function. *Neurochem Int* 112:5–17. <https://doi.org/10.1016/j.neuint.2017.10.013>
52. Tao R-S, Fei E-K, Ying Z, Wang HF, Wang GH (2008) Casein kinase 2 interacts with and phosphorylates ataxin-3. *Neurosci Bull* 24:271–277. <https://doi.org/10.1007/s12264-008-0605-5>
53. Tu Y, Liu H, Zhu X, Shen H, Ma X, Wang F, Huang M, Gong J et al (2017) Ataxin-3 promotes genome integrity by stabilizing Chk1. *Nucleic Acids Res* 45:4532–4549. <https://doi.org/10.1093/nar/gkx095>
54. Vinayagam A, Stelzl U, Foulle R, Plassmann S, Zenkner M, Timm J, Assmus HE, Andrade-Navarro MA et al (2011) A directed protein interaction network for investigating intracellular signal transduction. *Sci Signal* 4:rs8. <https://doi.org/10.1126/scisignal.2001699>
55. Kim Y-B, Shin YJ, Roy A, Kim J-H (2015) The role of the Pleckstrin homology domain-containing protein CKIP-1 in activation of p21-activated kinase 1 (PAK1). *J Biol Chem* 290:21076–21085. <https://doi.org/10.1074/jbc.M115.675124>
56. Kim H, Oh J-Y, Choi S-L, Nam YJ, Jo A, Kwon A, Shin EY, Kim EG et al (2016) Down-regulation of p21-activated serine/threonine kinase 1 is involved in loss of mesencephalic dopamine neurons. *Mol Brain* 9:45. <https://doi.org/10.1186/s13041-016-0230-6>
57. Ma Q-L, Yang F, Frautschy SA, Cole GM (2012) PAK in Alzheimer disease, Huntington disease and X-linked mental retardation. *Cell Logist* 2:117–125. <https://doi.org/10.4161/cl.21602>
58. Luo S, Mizuta H, Rubinstein DC (2008) p21-activated kinase 1 promotes soluble mutant huntingtin self-interaction and enhances toxicity. *Hum Mol Genet* 17:895–905. <https://doi.org/10.1093/hmg/ddm362>
59. Wlodarchak N, Xing Y (2016) PP2A as a master regulator of the cell cycle. *Crit Rev Biochem Mol Biol* 51:162–184. <https://doi.org/10.3109/10409238.2016.1143913>
60. Mazzucchelli S, De Palma A, Riva M et al (2009) Proteomic and biochemical analyses unveil tight interaction of ataxin-3 with tubulin. *Int J Biochem Cell Biol* 41:2485–2492. <https://doi.org/10.1016/j.biocel.2009.08.003>
61. Pozzi C, Valtorta M, Tedeschi G, Galbusera E, Pastori V, Bigi A, Nonnis S, Grassi E et al (2008) Study of subcellular localization and proteolysis of ataxin-3. *Neurobiol Dis* 30:190–200. <https://doi.org/10.1016/j.nbd.2008.01.011>
62. Ding Y, Li Y, Lu L, Zhang R, Zeng L, Wang L, Zhang X (2015) Inhibition of Nischarin expression promotes neurite outgrowth through regulation of PAK activity. *PLoS One* 10:e0144948. <https://doi.org/10.1371/journal.pone.0144948>

63. Poplawski GHD, Tranziska A-K, Leshchyn's'ka I et al (2012) L1CAM increases MAP2 expression via the MAPK pathway to promote neurite outgrowth. *Mol Cell Neurosci* 50:169–178. <https://doi.org/10.1016/j.mcn.2012.03.010>
64. Sample V, Ramamurthy S, Gorshkov K, Ronnett GV, Zhang J (2015) Polarized activities of AMPK and BRSK in primary hippocampal neurons. *Mol Biol Cell* 26:1935–1946. <https://doi.org/10.1091/mbc.E14-02-0764>
65. Toriyama M, Kozawa S, Sakumura Y, Inagaki N (2013) Conversion of a signal into forces for axon outgrowth through Pak1-mediated shootin1 phosphorylation. *Curr Biol* 23:529–534. <https://doi.org/10.1016/j.cub.2013.02.017>
66. Winograd-Katz SE, Brunner MC, Mirlas N, Geiger B (2011) Analysis of the signaling pathways regulating Src-dependent remodeling of the actin cytoskeleton. *Eur J Cell Biol* 90:143–156. <https://doi.org/10.1016/j.ejcb.2010.07.006>
67. Rankin CA, Sun Q, Gamblin TC (2008) Pre-assembled tau filaments phosphorylated by GSK-3b form large tangle-like structures. *Neurobiol Dis* 31:368–377. <https://doi.org/10.1016/j.nbd.2008.05.011>
68. Rousseaux MW, de Haro M, Lasagna-Reeves CA, et al (2016) TRIM28 regulates the nuclear accumulation and toxicity of both alpha-synuclein and tau. *eLife* 5:. <https://doi.org/10.7554/eLife.19809>
69. Chatterjee A, Saha S, Chakraborty A, Silva-Fernandes A, Mandal SM, Neves-Carvalho A, Liu Y, Pandita RK et al (2015) The role of the mammalian DNA end-processing enzyme polynucleotide kinase 3'-phosphatase in spinocerebellar ataxia type 3 pathogenesis. *PLoS Genet* 11:e1004749. <https://doi.org/10.1371/journal.pgen.1004749>
70. Gao R, Liu Y, Silva-Fernandes A, Fang X, Paulucci-Holthausen A, Chatterjee A, Zhang HL, Matsuura T et al (2015) Inactivation of PNKP by mutant ATXN3 triggers apoptosis by activating the DNA damage-response pathway in SCA3. *PLoS Genet* 11:e1004834. <https://doi.org/10.1371/journal.pgen.1004834>
71. Peixeiro I, Inácio Á, Barbosa C et al (2012) Interaction of PABPC1 with the translation initiation complex is critical to the NMD resistance of AUG-proximal nonsense mutations. *Nucleic Acids Res* 40: 1160–1173. <https://doi.org/10.1093/nar/gkr820>
72. Nawaz MS, Vik ES, Bergeis N, Fladeby C, Bjørås M, Dalhus B, Alseth I (2016) Regulation of human endonuclease V activity and relocalization to cytoplasmic stress granules. *J Biol Chem* 291: 21786–21801. <https://doi.org/10.1074/jbc.M116.730911>
73. Chen L, Stone MC, Tao J, Rolls MM (2012) Axon injury and stress trigger a microtubule-based neuroprotective pathway. *Proc Natl Acad Sci U S A* 109:11842–11847. <https://doi.org/10.1073/pnas.112111809>
74. Chou A-H, Yeh T-H, Kuo Y-L, Kao YC, Jou MJ, Hsu CY, Tsai SR, Kakizuka A et al (2006) Polyglutamine-expanded ataxin-3 activates mitochondrial apoptotic pathway by upregulating Bax and down-regulating Bcl-xL. *Neurobiol Dis* 21:333–345. <https://doi.org/10.1016/j.nbd.2005.07.011>
75. Hsu J-Y, Jhang Y-L, Cheng P-H, Chang YF, Mao SH, Yang HI, Lin CW, Chen CM et al (2017) The truncated C-terminal fragment of mutant ATXN3 disrupts mitochondria dynamics in spinocerebellar ataxia type 3 models. *Front Mol Neurosci* 10:196. <https://doi.org/10.3389/fnmol.2017.00196>
76. Yu Y-C, Kuo C-L, Cheng W-L, Liu CS, Hsieh M (2009) Decreased antioxidant enzyme activity and increased mitochondrial DNA damage in cellular models of Machado-Joseph disease. *J Neurosci Res* 87:1884–1891. <https://doi.org/10.1002/jnr.22011>
77. Wang X, Chen XJ (2015) A cytosolic network suppressing mitochondria-mediated proteostatic stress and cell death. *Nature* 524:481–484. <https://doi.org/10.1038/nature14859>
78. Guyenet SJ, Furrer SA, Damian VM, Baughan TD, la Spada AR, Garden GA (2010) A simple composite phenotype scoring system for evaluating mouse models of cerebellar ataxia. *J Vis Exp* 1787:e1787. <https://doi.org/10.3791/1787>
79. Patel RK, Jain M (2012) NGS QC toolkit: a toolkit for quality control of next generation sequencing data. *PLoS One* 7:e30619. <https://doi.org/10.1371/journal.pone.0030619>
80. Dobin A, Davis CA, Schlesinger F, Drenkow J, Zaleski C, Jha S, Batut P, Chaisson M et al (2013) STAR: ultrafast universal RNA-seq aligner. *Bioinforma* 29:15–21. <https://doi.org/10.1093/bioinformatics/bts635>
81. Hartley SW, Mullikin JC (2015) QoRTs: a comprehensive toolset for quality control and data processing of RNA-Seq experiments. *BMC Bioinformatics* 16:224. <https://doi.org/10.1186/s12859-015-0670-5>
82. Kim D, Langmead B, Salzberg SL (2015) HISAT: a fast spliced aligner with low memory requirements. *Nat Methods* 12:357–360. <https://doi.org/10.1038/nmeth.3317>
83. Pertea M, Kim D, Pertea GM, Leek JT, Salzberg SL (2016) Transcript-level expression analysis of RNA-seq experiments with HISAT, StringTie and Ballgown. *Nat Protoc* 11:1650–1667. <https://doi.org/10.1038/nprot.2016.095>
84. Love MI, Huber W, Anders S (2014) Moderated estimation of fold change and dispersion for RNA-seq data with DESeq2. *Genome Biol* 15(550):550. <https://doi.org/10.1186/s13059-014-0550-8>
85. Pertea M, Pertea GM, Antonescu CM, Chang TC, Mendell JT, Salzberg SL (2015) StringTie enables improved reconstruction of a transcriptome from RNA-seq reads. *Nat Biotechnol* 33:290–295. <https://doi.org/10.1038/nbt.3122>
86. Hartley SW, Mullikin JC (2016) Detection and visualization of differential splicing in RNA-Seq data with JunctionSeq. *Nucleic Acids Res* 44:e127. <https://doi.org/10.1093/nar/gkw501>
87. Bustin SA, Benes V, Garson JA, Hellemans J, Huggett J, Kubista M, Mueller R, Nolan T et al (2009) The MIQE guidelines: minimum information for publication of quantitative real-time PCR experiments. *Clin Chem* 55:611–622. <https://doi.org/10.1373/clinchem.2008.112797>
88. Trottier Y, Cancel G, An-Gourfinkel I, Lutz Y, Weber C, Brice A, Hirsch E, Mandel JL (1998) Heterogeneous intracellular localization and expression of ataxin-3. *Neurobiol Dis* 5:335–347. <https://doi.org/10.1006/nbdi.1998.0208>
89. Kanehisa M, Furumichi M, Tanabe M, Sato Y, Morishima K (2017) KEGG: new perspectives on genomes, pathways, diseases and drugs. *Nucleic Acids Res* 45:D353–D361. <https://doi.org/10.1093/nar/gkw1092>
90. Herwig R, Hardt C, Lienhard M, Kamburov A (2016) Analyzing and interpreting genome data at the network level with ConsensusPathDB. *Nat Protoc* 11:1889–1907. <https://doi.org/10.1038/nprot.2016.117>
91. Bindea G, Galon J, Mlecnik B (2013) CluePedia Cytoscape plugin: pathway insights using integrated experimental and in silico data. *Bioinforma* 29:661–663. <https://doi.org/10.1093/bioinformatics/btt019>
92. Bindea G, Mlecnik B, Hackl H, Charoentong P, Tosolini M, Kirilovsky A, Fridman WH, Pagès F et al (2009) ClueGO: a Cytoscape plug-in to decipher functionally grouped gene ontology and pathway annotation networks. *Bioinforma* 25:1091–1093. <https://doi.org/10.1093/bioinformatics/btp101>
93. Fabregat A, Jupe S, Matthews L, Sidiropoulos K, Gillespie M, Garapati P, Haw R, Jassal B et al (2018) The Reactome pathway knowledgebase. *Nucleic Acids Res* 46:D649–D655. <https://doi.org/10.1093/nar/gkx1132>
94. Slenter DN, Kutmon M, Hanspers K, Riutta A, Windsor J, Nunes N, Mélius J, Cirillo E et al (2018) WikiPathways: a multifaceted pathway database bridging metabolomics to other omics research. *Nucleic Acids Res* 46:D661–D667. <https://doi.org/10.1093/nar/gkx1064>

95. Gnad F, Ren S, Cox J, Olsen JV, Macek B, Oroshi M, Mann M (2007) PHOSIDA (phosphorylation site database): management, structural and evolutionary investigation, and prediction of phosphosites. *Genome Biol* 8:R250. <https://doi.org/10.1186/gb-2007-8-11-r250>
96. J. J. Lin, (1981) Monoclonal antibodies against myofibrillar components of rat skeletal muscle decorate the intermediate filaments of cultured cells. *Proceedings of the National Academy of Sciences* 78 (4):2335–2339
97. Tapia-Rojas C, Cabezas-Opazo F, Deaton CA, Vergara EH, Johnson GVW, Quintanilla RA (2019) It's all about tau. *Progress in Neurobiology* 175:54–76
98. Wood JN, Anderton BH (1981) Monoclonal antibodies to mammalian neurofilaments. *Bioscience Reports* 1 (3):263–268

Publisher's Note Springer Nature remains neutral with regard to jurisdictional claims in published maps and institutional affiliations.



Broad Influence of Mutant Ataxin-3 on the Proteome of the Adult Brain, Young Neurons, and Axons Reveals Central Molecular Processes and Biomarkers in SCA3/MJD Using Knock-In Mouse Model

Kalina Wiatr¹, Łukasz Marczak¹, Jean-Baptiste Pérot², Emmanuel Brouillet²,
Julien Flament² and Maciej Figiel^{1*}

¹ Institute of Bioorganic Chemistry, Polish Academy of Sciences, Poznań, Poland, ² Université Paris-Saclay, Centre National de la Recherche Scientifique, Commissariat à l'Energie Atomique, Direction de la Recherche Fondamentale, Institut de Biologie François Jacob, Molecular Imaging Research Center, Neurodegenerative Diseases Laboratory, Fontenay-aux-Roses, France

OPEN ACCESS

Edited by:

Matthew L. MacDonald,
University of Pittsburgh, United States

Reviewed by:

Clevio Nobrega,
University of Algarve, Portugal
Utpal Das,
University of California, San Diego,
United States

*Correspondence:

Maciej Figiel
mfigiel@ibch.poznan.pl

Received: 25 January 2021

Accepted: 01 April 2021

Published: xx April 2021

Citation:

Wiatr K, Marczak Ł, Pérot J-B, Brouillet E, Flament J and Figiel M (2021) Broad Influence of Mutant Ataxin-3 on the Proteome of the Adult Brain, Young Neurons, and Axons Reveals Central Molecular Processes and Biomarkers in SCA3/MJD Using Knock-In Mouse Model. *Front. Mol. Neurosci.* 14:658339. doi: 10.3389/fnmol.2021.658339

Spinocerebellar ataxia type 3 (SCA3/MJD) is caused by CAG expansion mutation resulting in a long polyQ domain in mutant ataxin-3. The mutant protein is a special type of protease, deubiquitinase, which may indicate its prominent impact on the regulation of cellular proteins levels and activity. Yet, the global model picture of SCA3 disease progression on the protein level, molecular pathways in the brain, and neurons, is largely unknown. Here, we investigated the molecular SCA3 mechanism using an interdisciplinary research paradigm combining behavioral and molecular aspects of SCA3 in the knock-in ki91 model. We used the behavior, brain magnetic resonance imaging (MRI) and brain tissue examination to correlate the disease stages with brain proteomics, precise axonal proteomics, neuronal energy recordings, and labeling of vesicles. We have demonstrated that altered metabolic and mitochondrial proteins in the brain and the lack of weight gain in Ki91 SCA3/MJD mice is reflected by the failure of energy metabolism recorded in neonatal SCA3 cerebellar neurons. We have determined that further, during disease progression, proteins responsible for metabolism, cytoskeletal architecture, vesicular, and axonal transport are disturbed, revealing axons as one of the essential cell compartments in SCA3 pathogenesis. Therefore we focus on SCA3 pathogenesis in axonal and somatodendritic compartments revealing highly increased axonal localization of protein synthesis machinery, including ribosomes, translation factors, and RNA binding proteins, while the level of proteins responsible for cellular transport and mitochondria was decreased. We demonstrate the accumulation of axonal vesicles in neonatal SCA3 cerebellar neurons and increased phosphorylation of SMI-312 positive adult cerebellar axons, which indicate axonal dysfunction in SCA3. In summary, the SCA3 disease mechanism is based on the broad influence of mutant ataxin-3 on the neuronal proteome. Processes

central in our SCA3 model include disturbed localization of proteins between axonal and somatodendritic compartment, early neuronal energy deficit, altered neuronal cytoskeletal structure, an overabundance of various components of protein synthesis machinery in axons.

Keywords: spinocerebellar ataxia type 3 (SCA3), Machado-Joseph disease (MJD), ataxin-3, neurodegenerative, proteome, axon, vesicular transport, energy metabolism

INTRODUCTION

Spinocerebellar ataxia type 3 (SCA3), also known as Machado-Joseph disease (MJD), is a neurodegenerative, late-onset, genetic disorder caused by the expansion of CAG repeats in the coding region of the ATXN3 gene (>50 in patients) (McLoughlin et al., 2020). This mutation leads to an expanded polyglutamine (polyQ) tract in the ataxin-3 protein, causing a toxic gain of function (Orr and Zoghbi, 2007). SCA3 patients most typically display imbalance, motor incoordination, and neurodegeneration in the cerebellum, brainstem, spinal cord, and cerebral cortex (Bettencourt and Lima, 2011). Although the disease-causative mutation is known, the exact molecular and cellular mechanisms of SCA3 remain unclear. Several lines of evidence point to the disruption of axon organization and, therefore, connections between brain structures as one of the main traits in SCA3 pathogenesis (de Rezende et al., 2015; Farrar et al., 2016; Lu et al., 2017). Moreover, axonal impairment was observed in central nervous system (CNS) and peripheries in the form of white matter defects on magnetic resonance imaging (MRI) and peripheral axonal neuropathy in SCA3 patients (D'Abreu et al., 2009; Graves and Guiloff, 2011; Rezende et al., 2018). Axonal impairment may be related to the fact that mutant ataxin-3 aberrantly interacts with microtubules affecting cytoskeleton dynamics in neurons and forms inclusions in axons (Mazzucchelli et al., 2009; Seidel et al., 2010; Chen et al., 2012). Also, mitochondrial impairment is a component of axonal damage in neurodegeneration, and likely plays a role in SCA3 pathogenesis (Da Silva et al., 2019). We recently demonstrated that gross transcriptional changes are absent in the pre-symptomatic SCA3 brain of the Ki91 mouse model; however, dysregulations of proteins and phosphoproteins occurred in these animals, pointing at protein homeostasis as a more general and early trait in disease pathogenesis (Switonski et al., 2015; Wiatr et al., 2019).

The ataxin-3 protein is a particular type of protease, a deubiquitinase, and it has been previously demonstrated that the function in the mutant version of the protein is compromised (Neves-Carvalho et al., 2015), which should have a significant influence on the brain proteome. Therefore, the investigation

of proteins seems to be the strongest candidate to discover pathogenic mechanisms or identify the cluster of disease mechanisms. The number of known biomarkers and proteins reliably linked to SCA3 pathogenic processes is still relatively low. Surprisingly, the global model picture of SCA3 disease progression on the protein level, showing the most crucial proteins and pathways in the brain, and neurons, has not been generated and published previously. Therefore in the present work, we aimed to identify protein dysregulations and pathogenic processes in SCA3 on various levels, *in vitro*, and *in vivo*. We designed a research pipeline consisting of three complementary proteomic approaches, mouse behavior, and necessary functional validation assays to unveil with increased resolution the most critical processes influencing the SCA3 pathogenesis. The pipeline combines proteomics paralleled to behavioral milestones of SCA3 Ki91 and correlative proteomics for displaying the proteome linked to disease severity. In the third and the most focused approach, we used targeted proteomics of somatodendritic and axonal compartments from young SCA3 neurons. Our results indicate that the SCA3 disease mechanism is based on the broad influence of mutant ataxin-3 on the neuronal proteome affecting classes of proteins responsible for several central molecular processes. These include disturbed localization of proteins between axonal and somatodendritic compartment, early neuronal energy deficit, altered neuronal cytoskeletal structure, an overabundance of protein synthetic machinery in axons, and altered vesicular trafficking pointing at affected axonal maintenance.

RESULTS

The SCA3 in Ki91 Mice Gradually Progresses and Demonstrates Discrete Early and Late Phenotypes

We have previously demonstrated that by 2 months of age, Ki91 mice show no motor symptoms or other behavioral abnormalities, and we additionally defined the spectrum of Ki91 motor deficits using 14-month-old animals (Wiatr et al., 2019). Upon completing our longitudinal behavioral tests (4–18 months), we now demonstrate that the homozygous Ki91 model gradually develops disease symptoms resembling disease progression in SCA3 patients. Based on the large volume of longitudinal behavioral data (Figure 1), we have distinguished three stages of behavioral symptom development in Ki91 animals ($n = 36$). The first stage consists of progressive failure to gain body weight (4-month-old) followed by the

Abbreviations: ANOVA, analysis of variance; BP, biological process; CPDB, ConsensusPath Database; CC, cellular compartment; CNS, central nervous system; DIV, days *in vitro*; ECAR, extracellular acidification rate; FC, fold change; MJD, Machado-Joseph disease; MS, mass spectrometry; mo, month-old; MF, molecular function; mRFP, monomeric red fluorescent protein; MRI, magnetic resonance imaging; mRNP, messenger ribonucleoprotein; NF, neurofilament; OCR, oxygen consumption rate; OXPHOS, oxidative phosphorylation; polyQ, polyglutamine; PCA, principal component analysis; SCA3, Spinocerebellar ataxia type 3; TCA, tricarboxylic acid cycle; WT, wildtype.

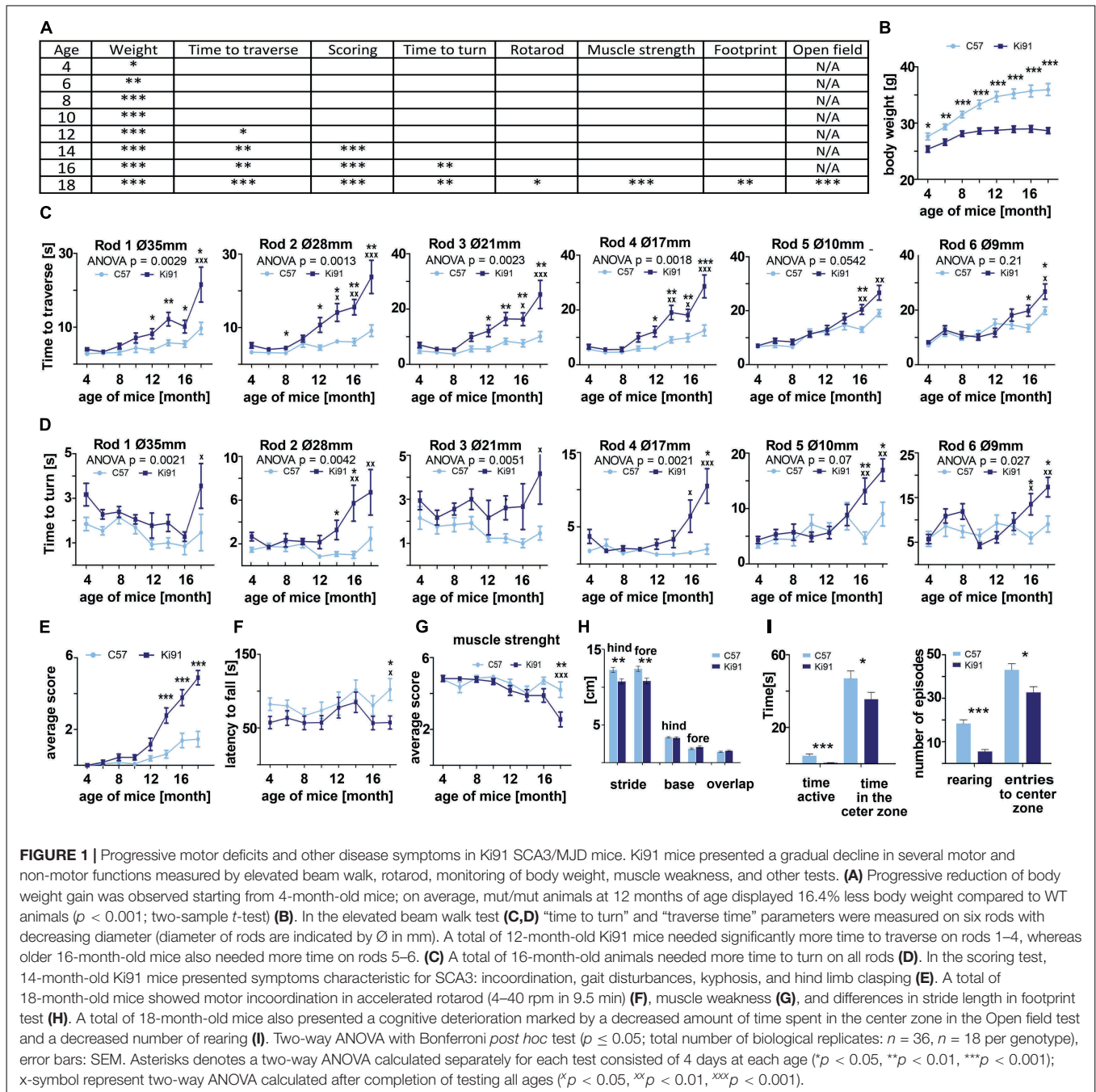


FIGURE 1 | Progressive motor deficits and other disease symptoms in Ki91 SCA3/MJD mice. Ki91 mice presented a gradual decline in several motor and non-motor functions measured by elevated beam walk, rotarod, monitoring of body weight, muscle weakness, and other tests. **(A)** Progressive reduction of body weight gain was observed starting from 4-month-old mice; on average, mut/mut animals at 12 months of age displayed 16.4% less body weight compared to WT animals ($p < 0.001$; two-sample t -test). **(B)** In the elevated beam walk test **(C,D)**, “time to turn” and “traverse time” parameters were measured on six rods with decreasing diameter (diameter of rods are indicated by Ø in mm). A total of 12-month-old Ki91 mice needed significantly more time to traverse on rods 1–4, whereas older 16-month-old mice also needed more time on rods 5–6. **(C)** A total of 16-month-old animals needed more time to turn on all rods **(D)**. In the scoring test, 14-month-old Ki91 mice presented symptoms characteristic for SCA3: incoordination, gait disturbances, kyphosis, and hind limb clasping **(E)**. A total of 18-month-old mice showed motor incoordination in accelerated rotarod (4–40 rpm in 9.5 min) **(F)**, muscle weakness **(G)**, and differences in stride length in footprint test **(H)**. A total of 18-month-old mice also presented a cognitive deterioration marked by a decreased amount of time spent in the center zone in the Open field test and a decreased number of rearing **(I)**. Two-way ANOVA with Bonferroni post hoc test ($p \leq 0.05$; total number of biological replicates: $n = 36$, $n = 18$ per genotype), error bars: SEM. Asterisks denotes a two-way ANOVA calculated separately for each test consisted of 4 days at each age (* $p < 0.05$, ** $p < 0.01$, *** $p < 0.001$); x-symbol represent two-way ANOVA calculated after completion of testing all ages (^ $p < 0.05$, xx $p < 0.01$, xxx $p < 0.001$).

early symptomatic stage (12-month-old), characterized by gait ataxia and motor incoordination. The final, symptomatic phase (18-month-old animals) is characterized by severe loss of balance and coordination, gait ataxia, dystonia, and muscle weakness (Figure 1A). Reduced rate of body weight gain was observed as the first symptom in 4-month-old Ki91 mice ($p < 0.05$; two-sample t -test), and the difference between Ki91 and wild-type (WT) littermates increased with age [$p < 0.001$; two-sample t -test, two-way analysis of variance (ANOVA), Bonferroni; Figure 1B]. At the age of 8 months, Ki91 mice stopped gaining weight, and their weight was stable across

further ages (Figure 1B) while the WT animals still regularly gained weight. First motor symptoms occurred in 12-month-old animals, which performed worse in the elevated beam walk (Figure 1C). Ki91 took more time to traverse rods (diameter: 35, 28, 21, and 17 mm) and committed more foot slips while performing the task ($p < 0.05$; two-way ANOVA, Bonferroni). As the disease progressed, 14-month-old Ki91 demonstrated overall deterioration of phenotype, including gait disturbances, loss of coordination, and balance, and several Ki91 animals demonstrated hindlimb clasping and kyphosis in the scoring test ($p < 0.0001$; one- and two-way ANOVA, Bonferroni)

(Figure 1E). Next, 16-month-old Ki91 mice needed more time to turn on a rod (diameter: 28, 17, 10, and 9 mm) in the elevated beam walk test ($p < 0.05$; two-way ANOVA, Bonferroni), showing loss of balance (Figure 1D). Besides, 18-month-old Ki91 mice demonstrated incoordination in the Rotarod ($p < 0.05$; two-way ANOVA, Bonferroni; Figure 1F), reduced muscle strength ($p < 0.001$; one- and two-way ANOVA, Bonferroni; Figure 1G), shorter stride, which indicated further gait disturbances in the footprint test ($p < 0.001$; two-sample *t*-test, ANOVA, Bonferroni; Figure 1H), and decreased activity and anxiety in the open field test ($p < 0.05$; two-sample *t*-test; Figure 1I). In this last test, Ki91 mice showed significantly less time spent moving ($p < 0.0001$; two-sample *t*-test), as well as decreased vertical activity (rearing) ($p < 0.0001$; two-sample *t*-test), a smaller number of the entries, and less time spent in the center zone ($p < 0.05$; two-sample *t*-test). Since mice showed differences in body weight, we ensured that no correlation existed between body weight and behavioral tests in each age to exclude the effect of the animals' weight on the results ($p < 0.05$, correlation test).

Ki91 SCA3/MJD Mice Demonstrate Multiple Brain Region Atrophy and the Presence of Atxn3 Inclusions Throughout the Brain

Magnetic resonance imaging was used on *ex vivo* brains of 18 months old animals ($n = 6$ per genotype) to measure brain volumes in Ki91 and WT mice (Figures 2A,B). As measured by MRI image segmentation, whole-brain volume showed significant global atrophy of the brain in Ki91 mice (-7% , $p < 0.001$; Figure 2A). When looking at regions volume, several structures seem particularly atrophied as parietal-temporal cortex (-11% , $p < 0.01$), entorhinal, piriform and motor cortices (-11% each, $p < 0.05$), corpus callosum (-7.5% , $p < 0.05$), striatum (-11% , $p < 0.05$), septum (-11% , $p < 0.01$), pons (-12% , $p < 0.01$), and hypothalamus (-8% , $p < 0.05$) (Figure 2B). There was no significant atrophy in the hippocampus, and cerebellar atrophy was not determined due to MRI coil performance at the end of the brain. Fractional Anisotropy (FA) was also investigated as a biomarker of the integrity of tissue organization. FA was significantly decreased in dentate gyrus (-17% , $p < 0.01$), and stratum granulosum (-19% , $p < 0.05$) (Figure 2C).

Next, we have performed brain sections from 18-month-old Ki91 and staining using the anti-ataxin-3 antibody (Figure 3). We found that all brain areas, including the cerebral cortex, striatum, midbrain, hippocampus, cerebellum, DCN, and pons, demonstrated intensive positive signals in the form of both inclusions and diffuse staining of cellular structures ($n = 4$; Figures 3A–E). In particular, intense anti-ataxin-3 staining was present in cell nuclei, and many cells demonstrated large inclusions (Figure 3A). Interestingly, a significant number of smaller and larger ataxin-3-positive inclusions were scattered along the neurites (particularly axons labeled by SMI-312 axonal marker) in the cerebellum (Figures 3C,E). Although we could not measure cerebellum atrophy by MRI, we determined that the inclusions are rich in the cerebellum, indicating an intense

pathogenic process. In the cerebellum, the large inclusions were predominantly present in the DCN area, white matter, and in some cells located in the granular layer (Figures 3B,D). Many of the atxn3 inclusions were ubiquitinated (Supplementary Figures 1A,B, 2). Considering widespread brain atrophy and the inclusions in all regions, we reasoned that the brain pathogenic SCA3 processes are multi-region and multi-thread. Therefore we selected the cerebellum and cerebral cortex to represent both classically reported SCA3 pathogenesis in the hindbrain and postulated SCA3 pathogenesis in more frontal parts of the brain.

Proteomics Parallel to Behavioral Milestones Implicates Disturbed Metabolism, Cytoskeleton, and Vesicular Trafficking in Ki91 SCA3/MJD Mice

Parallel to behavioral experiments and based on the occurrence of symptoms in behavioral tests, we have selected four mouse ages (4, 10, 12, and 14-month-old, $n = 4$ per genotype) to analyze proteomic changes in the cerebral cortex (entire region collected for analysis) and cerebellum. In detail, 4-month-old Ki91 animals displayed reduced body weight gain; a 10-months stage was just before the onset of motor symptoms, while 12 and 14-month-old mice showed a decline in motor functions (Figure 1); therefore, the protein dysregulation in those ages would be most relevant. The principal component analysis (PCA) mostly demonstrated distinct clustering of the Ki91 and WT datasets (Supplementary Figures 3A,B). Altogether, we identified 115, 126, 212, and 75 proteins that were significantly dysregulated ($p < 0.05$; two-sample *t*-test) in the cerebellum of 4-, 10-, 12-, and 14-month-old Ki91 mice, respectively (Supplementary Table 1 and Supplementary Figure 3C). In comparison, 178, 89, 170, and 279 proteins were significantly dysregulated ($p < 0.05$; two-sample *t*-test) in the cerebral cortex of 4-, 10-, 12-, and 14-month-old Ki91 animals, respectively (Supplementary Table 2 and Supplementary Figure 3C).

In order to reveal molecular pathways and cellular compartments (CCs), which might contribute to the SCA3 pathogenesis, we performed an analysis of dysregulated proteins using the ConsensusPath database (CPDB; pathways and GO CC for each age; level 4 and 5; $q < 0.01$). For simplicity, we have arbitrarily grouped pathways and CCs identified in CPDB into five categories for the cerebral cortex (Figure 4A) and cerebellum (Figure 4B) based on their biological relations and similarity. Lists of proteins with the highest log₂-fold changes (log₂-FC) belonging to five categories are presented for the cerebral cortex (Figure 4C) and cerebellum (Figure 4D).

The first category was related to vesicular transport and endocytosis. Cytoplasmic vesicles and extracellular exosomes were the localization for 24–32 and 33–51% of dysregulated proteins in every dataset from the cortex (Figure 4A) and similarly 21–24 and 45–51% in the cerebellum (Figure 4B). Moreover, vesicle-mediated transport and clathrin-mediated endocytosis are predicted to be disturbed in both the cerebral cortex (Vamp2, Cltb, and Rab10; Figure 4C) and cerebellum (Rab11b, Napa, Nsf, and Rab3d; Figure 4D).

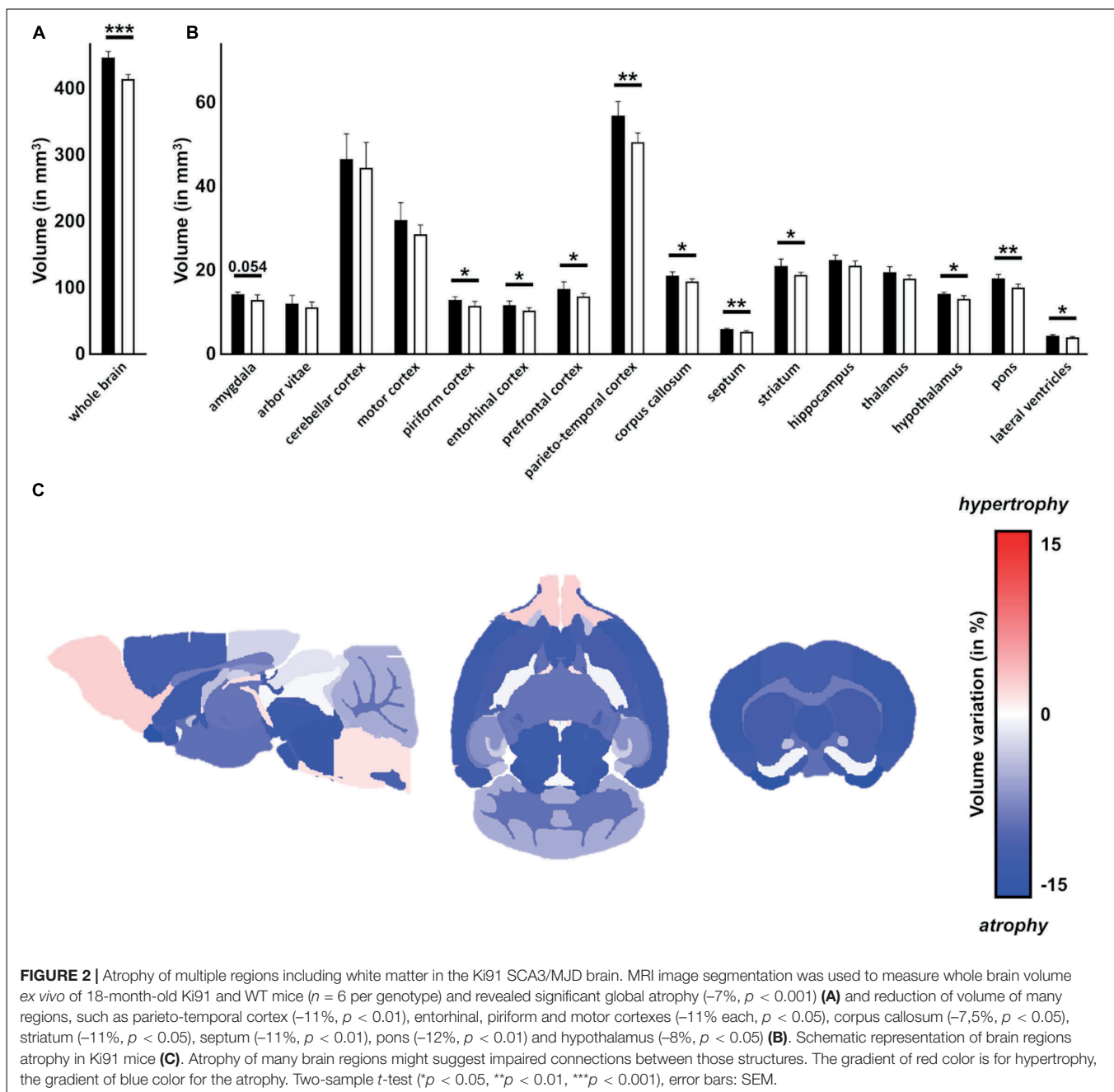


FIGURE 2 | Atrophy of multiple regions including white matter in the Ki91 SCA3/MJD brain. MRI image segmentation was used to measure whole brain volume ex vivo of 18-month-old Ki91 and WT mice ($n = 6$ per genotype) and revealed significant global atrophy (-7% , $p < 0.001$) **(A)** and reduction of volume of many regions, such as parieto-temporal cortex (-11% , $p < 0.01$), entorhinal, piriform and motor cortices (-11% each, $p < 0.05$), corpus callosum (-7.5% , $p < 0.05$), striatum (-11% , $p < 0.05$), septum (-11% , $p < 0.01$), pons (-12% , $p < 0.01$) and hypothalamus (-8% , $p < 0.05$) **(B)**. Schematic representation of brain regions atrophy in Ki91 mice **(C)**. Atrophy of many brain regions might suggest impaired connections between those structures. The gradient of red color is for hypertrophy, the gradient of blue color for the atrophy. Two-sample t -test (* $p < 0.05$, ** $p < 0.01$, *** $p < 0.001$), error bars: SEM.

The second category included dysregulated proteins involved in synaptic transmission. There was a relative increase in the number of altered proteins in older 12–14 month-old Ki91 mice in the cerebral cortex compared to younger ages (4–10-month-old). For instance, pathways such as “transmission across chemical synapses” contained $\sim 6\%$ of dysregulated proteins in 4–10-month-old vs. $\sim 10\%$ in 12–14% and “synaptic vesicle cycle” $\sim 3\%$ vs. 7% , respectively (Figure 4A). Proteins related to SNARE complex and synaptic vesicles such as Syn3, Syp, Sv2a, and Syt7 were dysregulated (Figure 4C). Interestingly, most of the proteins with a function in the synapse showed decreased levels in the cerebral cortex of older 12–14-month-old Ki91 mice

(Figure 4C). In the cerebellum, dysregulated proteins of synaptic vesicles or synapses were less frequent compared to the cortex (Figure 4B) and included Sv2a, Syt2, and Kcnab2 (Figure 4D). In both tested tissues, downregulation of Car2, Qdpr, and Glul, were detected in most of the tested ages (Figures 4C,D), which we also validated using vacuum dot-blot assay ($p < 0.05$; two-sample t -test; Supplementary Figure 4). Glul, Car2, and Qdpr play a role in the metabolism of amino acids and neurotransmitters, and Qdpr level is slightly and gradually dropping down across ages (Supplementary Tables 1, 2).

The third category was referring to altered proteins playing a role in regulating cytoskeletal structure and function.

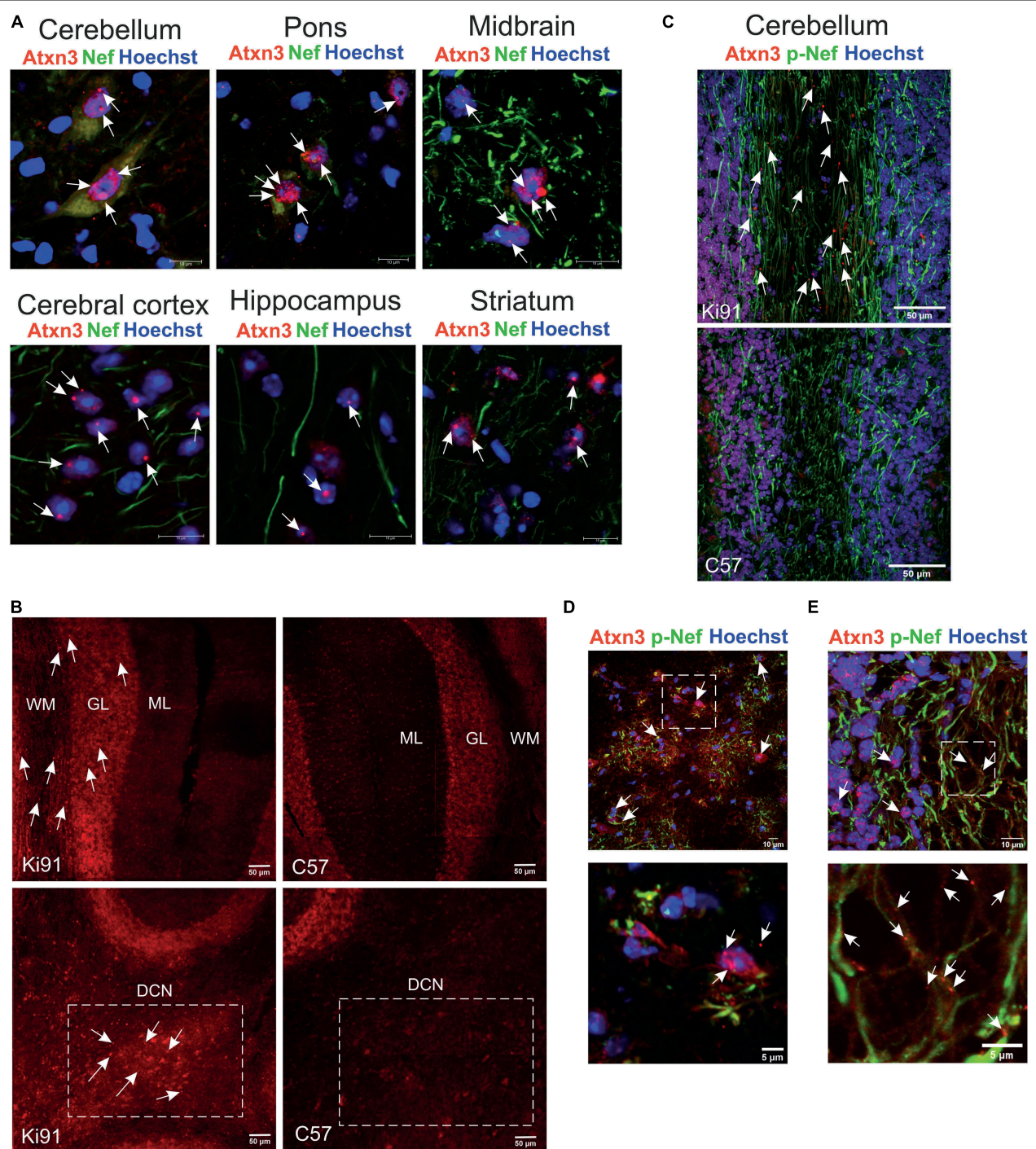
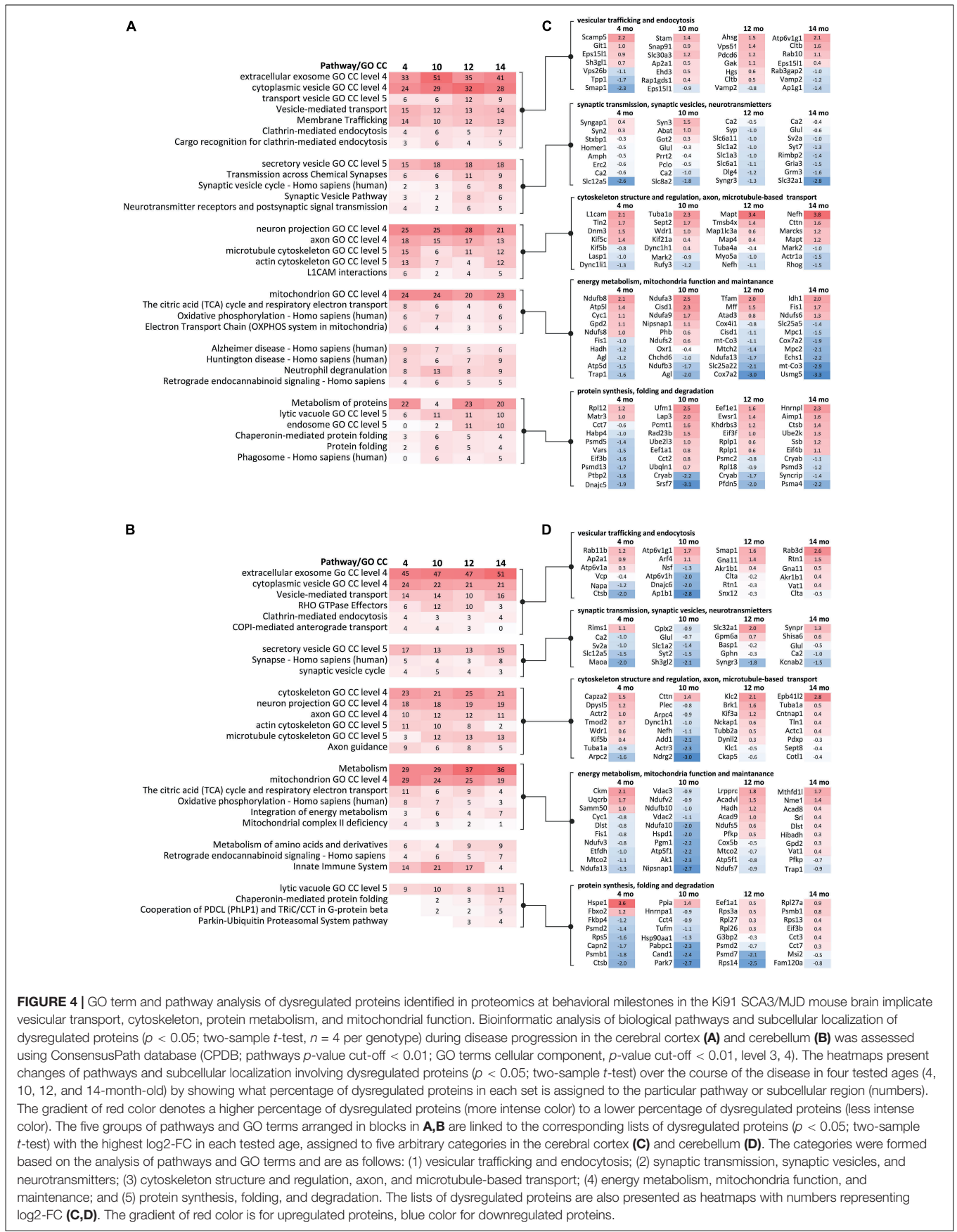


FIGURE 3 | The presence of multi-region intra-nuclear and intra-axonal inclusions in Ki91 SCA3/MJD brain. The ataxin-3 immunostaining of the 18-month-old Ki91 brain sections revealed a large number of cells within the cerebellum, midbrain, pons, cerebral cortex, hippocampus, and striatum with ataxin-3 (red; rabbit anti-ataxin-3 antibody) localizing mainly in the cell nucleus (blue; Hoechst 33342) (**A**). White arrows indicate large intra-nuclear inclusions; however, many smaller inclusions throughout the brain were present. A rich representation of Atxn3 aggregates (red; rabbit anti-ataxin-3 antibody) was present in DCN, granular layer (gl), and white matter (wm) of the Ki91 cerebellum (**B–D**). A significant number of small and large ataxin-3 inclusions were detected in the neurites (green; Smi-32, pan-neuronal or Smi-312, axon-specific antibody) of the Ki91 cerebellum (**C,E**). White box and arrows in **D** mark prominent Atxn3 aggregates in the DCN area (lower panel represents the magnification of selected region in the upper panel). White box and arrows in **E** mark the magnified area containing multiple intra-axonal inclusions of Atxn3 (lower panel). Scale bars: 50 µm (**B,C**); 10 µm (**A**); 5 µm on inserts (**D,E**). *N* = 4 biological replicates; at least 4 pictures per brain region of each kind were collected.



Dysregulated proteins localized to neuronal projections (axons and dendrites) constituted between 21 and 28% in the cortex and ~ 18% in the cerebellum (**Figures 4A,B**). Proteins assigned to cytoskeletal localization included actin (cortex: Actrla; cerebellum: Arpc2 and Actr3), microtubules (cortex: Tuba1a and Mapt) and neurofilaments (cortex and cerebellum: Nefh) (**Figures 4C,D**). Disturbances of the cytoskeleton structure may lead to cellular transport defects, and there were many proteins directly regulating anterograde and retrograde axonal transport. For instance, in the cerebral cortex, dysregulated proteins involved in anterograde microtubule-based transport were Kif5c, Kif5b, and Kif21a and retrograde transport: Dnm3, Dync1li1, Dync1h1, and microtubule-associated proteins: Map1lc3a and Mark2 (**Figure 4C**). In the cerebellum, proteins involved in the anterograde microtubule-based transport included Kif5b, Klc1, Klc2, and Kif3a, and in retrograde transport Dync1h1 and Dynll2 (**Figure 4D**).

The fourth category involved many dysregulated proteins related to energy metabolism and mitochondria maintenance (**Figures 4A–D**). Proteins predicted to localize in mitochondrion were between 20–24 and 19–29% in the cortex and cerebellum, respectively (**Figures 4A,B**). The top pathway involving dysregulated proteins in the Ki91 cerebellum was metabolism (**Figure 4B**). Moreover, the number of proteins dysregulated in the cerebellum and associated with metabolism increases with age (4–10-month-old: ~ 29%; 12–14-month-old: ~ 36%; **Figure 4B**). Proteins related to tricarboxylic acid cycle (TCA) and oxidative phosphorylation (OXPHOS) are dysregulated in the cerebral cortex (mitochondrial proteins Ndufb8 with; Ndufa3, Ndufs6, and mt-Co3; **Figure 4C**) and cerebellum (Ndufa13, Ndufa10, and Ndufs7; **Figure 4D**). There were also dysregulated proteins responsible for mitochondria fission (Fis1 and Mff) and mitochondrial chaperons (Hspd1 and Trap1) (**Figures 4C,D**). Also, several proteins with altered levels mostly related to metabolism were linked to Alzheimer's and Huntington disease in both the cerebellum and cerebral cortex (**Figures 4A,B**).

The fifth category included dysregulated proteins involved in protein metabolism. In the case of the cerebral cortex, there are 4–23% dysregulated proteins involved in the metabolism of proteins (**Figure 4A**). Noteworthy, the number of dysregulated proteins predicted to localize in lysosomes, endosomes, and phagosomes is higher in the cortex of older mouse (**Figures 4A,B**). Similarly, the number of altered proteins involved in protein folding and “Parkin-Ubiquitin Proteasomal System pathway” is increasing with age in the Ki91 cerebellum (**Figure 4B**). Dysregulated proteins in this category involve also various ribosomal subunits and translation factors (cortex: Rpl12 and Eif3b; cerebellum: Rpl27a), proteasome subunits (cortex: Psmd13 and Psma4; cerebellum: Psmb1 and Psmd7), and chaperons (cortex: Dnajc5 and Cryab; cerebellum: Hspe1 and Park7) (**Figures 4C,D**). Downregulation of Cryab, which was one of the most frequently identified proteins implicated in the pathology of neurodegenerative disease (Zhu and Reiser, 2018), was confirmed with vacuum dot blot assay ($p < 0.05$; two-sample *t*-test) in the cerebral cortex (10, 14, and 18-month-old; **Supplementary Figure 4A**) and cerebellum (18-month-old; **Supplementary Figure 4B**). Of note, most of the proteasome subunits and

chaperons demonstrated decreased levels in both tested tissues (**Figures 4C,D**).

Proteomics Correlative With SCA3 Behavioral Phenotype in 18-Month-Old Ki91 Mice Reveals Dysregulated Proteins Involved in Transport, Cytoskeleton, Synapse, and Mitochondria

Our correlative proteomic approach aimed to discover dysregulated proteins in the brain of animals that demonstrated consistent behavioral phenotype to establish a more exact relationship between the protein biomarkers and the degree of SCA3 disease severity (**Supplementary Figure 5**). Therefore, after the endpoint of behavioral studies (18 months), the animals were grouped by the intensity of phenotype, and three phenotype subgroups were established in the Ki91 cohort: severe, moderate, and mild ($n = 4$). The selection was based on score assessment on the 0–5 scale (Kruskal-Wallis test, $p < 0.05$) (**Supplementary Figure 6A**). The scores 0 or 1 represented the “mild phenotype” group, score 2 or 3 was the “moderate phenotype” group, and 4 or 5 was the “severe phenotype” group. The cerebellum and cerebral cortex were collected from each group, and the tissues were subjected to proteomics (**Supplementary Table 3** and **Supplementary Figures 5A,B**). The analysis of dysregulated proteins revealed that protein levels in the moderate group were mostly in between the level of the severe and mild group, demonstrating a gradual pattern of protein dysregulation in Ki91 mice (**Supplementary Figures 6B,C**). Therefore in further data processing, we focused on the protein levels in severe and mild phenotype.

We found that in the cerebellum of the Ki91 animals with the severe phenotype ($n = 4$), there were heat shock protein Dnaja1 and a nuclear importin Kpna4 upregulated compared to WT animals (WT; $n = 10$) (**Supplementary Figure 6B**). Another member of the importin family, Kpna3, was previously shown to control the nuclear localization of ataxin-3 (Sowa et al., 2018). There were also five upregulated proteins in the mild phenotype ($n = 4$) – Pvalb, Pak1, Kif5c, and neurofilaments (Nefl and Nefm). Pak1, a kinase implicated in vesicle-mediated transport and regulation of cytoskeleton dynamics, and Kif5c involved in microtubule-based transport, were also downregulated in severe phenotype (**Supplementary Figure 6B**). Moreover, in the severe group, there were also other downregulated proteins playing a pivotal role in transport along the microtubule (Klc1, Kif5c, Vat1, and Map4) and notably Purkinje cell protein 4 (Pcp4), which was not dysregulated in mild phenotype (**Supplementary Figure 6B**). Noteworthy, mitochondrial proteins were downregulated in both severe and mild phenotypes. Mitochondrial chaperone Timm9 showed lower levels in the “severe” group, while Ndufb5 and Fasn were downregulated in the “mild” group (**Supplementary Figure 6B**).

In the cerebellar cortex, the only upregulated protein was a subunit of mitochondrial ATP synthase, Atp5a1 (**Supplementary Figure 6C**). Proteins commonly downregulated in both severe and mild phenotype (**Supplementary Figure 6C**) included GluL, already identified in the proteomics performed

parallel to behavioral milestones and myelin protein Cnp, ubiquitinylating enzyme Ube2n, transcription factor Tcebf1, and Snx12 involved in intracellular trafficking. In the mild group only, there were downregulated proteins associated with synaptic vesicles and post-synaptic density (Akap5, Bsn, Pclo, and Gprin1; **Supplementary Figure 6C**). Whereas in a “severe” group, there were downregulated proteins related to intracellular transport and cytoskeleton (Snx12, Dlg3, Dnm2, Cap2, and Atcay), and mitochondrial protein Cox7a2 (**Supplementary Figure 6C**).

Altogether, we identified a set of proteins involved in intracellular and microtubule-based transport downregulated in the cerebellum and cerebral cortex of Ki91 mice displaying severe phenotype. Downregulated proteins in the “mild” phenotype were related to mitochondria in the cerebellum and synapse in the cerebral cortex. Proteins upregulated in the cerebellum were associated with cytoskeleton and neurofilaments in the “mild” group. Cellular processes and compartments associated with dysregulated proteins in “severe” phenotype were related to mitochondria, intracellular and microtubule-based transport, synaptic vesicles, and the cytoskeleton. Most of these processes and compartments were also identified in our approach parallel to behavioral milestones. An essential neuronal structure, which connected those terms, is the axon, which requires high energy production, highly efficient trafficking of cargoes toward its end, and is a location of synaptic vesicle release. Therefore, we further decided to go to the next level of neuronal complexity in our proteomic investigation and selectively explore proteins dysregulated in the SCA3 axons.

Targeted Axonal Proteomics Indicates the Abnormal Localization of Proteins Between Axons and Soma Such as Cytoskeletal, Vesicular Proteins, and Highly Increased Translation Machinery in Ki91 SCA3 Neurons

Our next aim was to define with high precision the specific processes which highly contribute to axonal dysfunction in SCA3 already at a very early level of neuronal maturation stage, where no neuronal damage takes place, and therefore no secondary post-symptomatic events occur. Therefore, we performed the analysis of enriched or decreased proteins in axons of the cerebellar (young postnatal; P5) and cortical neurons (embryonal; E18) growing in Boyden chambers ($n = 4$ per genotype; **Figure 5A**).

Both somatodendritic and axonal protein extracts were subjected to MS/MS proteomics, and the “raw levels” for each protein for both compartments were determined (**Supplementary Table 4**). To normalize the protein levels within fractions originating from neurons on the same filter, we calculated the protein level ratio between the axonal and somatodendritic compartments for each WT and Ki91 sample/filter (**Supplementary Table 4**). Such normalization

has proved very solid since the comparison of soma/axon ratios within the single genotype (WT or Ki91) demonstrated that the most significant difference was the abundance of nuclear proteins, such as histones, and nuclear enzymes characteristic for the somatodendritic compartment (ratio axon to soma < -3 ; **Supplementary Table 4**). Coherently, the PCA graph demonstrates a clear separation between axonal and somatodendritic samples (**Supplementary Figures 7C,D**).

Subsequently, we compared protein level ratios between WT and Ki91 SCA3/MJD neurons to calculate the fold change and estimate if the protein was enriched or depleted in axons ($p < 0.05$; two-sample *t*-test; **Supplementary Table 4**). In the cerebellar neurons, there were 34 proteins enriched (ratio axon/soma > 1 , $p < 0.05$; two-sample *t*-test; $n = 4$) and 41 proteins depleted (ratio axon/soma < 1 , $p < 0.05$; two-sample *t*-test; $n = 4$) in Ki91 vs. WT axons (**Figures 5B,C** and **Supplementary Tables 5, 6**). There were 27 and 20 such proteins in cortical neurons, respectively (**Figures 5D,E** and **Supplementary Tables 7, 8**). The analysis of proteins in both cerebellar and cortical Ki91 axons revealed a common functional characteristic. The majority of the axon-enriched proteins in SCA3 samples were related to the upregulation of protein production and degradation (**Figures 5B,D, 6A,B** and **Supplementary Tables 6, 8**). Strongly upregulated was the translation machinery, in particular the initiation step and nonsense-mediated decay together with the RNA binding proteins, including Cirbp (FC = 4.92; **Figure 5B**), which stabilizes mRNAs involved in cell survival during stress (Liao et al., 2017). Highly upregulated were the proteasome subunits and chaperones enriched in cerebellar Ki91 axons (Psmd14, Psma5, and Hspa8; **Supplementary Table 6**) and cortical Ki91 axons (Sel1l and Cct2; **Supplementary Table 8**), which altogether might be related to the neuronal response to cellular stress and misfolded proteins in SCA.

In contrast, proteins that were reduced in Ki91 axons comparing to WT were in the majority related to the actin cytoskeleton and vesicle-mediated transport, which may indicate the axonal structural dysfunction (**Figures 5C,E, 6A,B** and **Supplementary Tables 5, 7**). In Ki91 cerebellar axons, there were reduced levels of 13 proteins related to cytoskeleton, including 8 proteins regulating actin function (**Figures 5C, 6A** and **Supplementary Table 5**). The actin cytoskeleton is involved not only in maintaining the proper structure of the axon but also plays a pivotal role in the short-range transport, selection of cargoes targeted to the axon tip, formation of synapses, and scaffold for the mitochondria in the growth cone (Kevenaar and Hoogenraad, 2015). Along this line, we identified eight mitochondrial proteins with a lower ratio axon vs. soma in cerebellar SCA3 samples as compared to WT (**Figures 5C, 6A** and **Supplementary Table 5**). Altogether, this may indicate the disrupted delivery of mitochondria to the proper axon area due to the deregulated function of the actin cytoskeleton. Moreover, there are also proteins with a reduced level in cerebellar Ki91 axons directly related to intracellular trafficking (Actr1a, Ank2, Arf6, Nsf, and Rhob), synaptic/SNARE vesicles (Sv2b, Napa, and Vti1b), and COPI-mediated transport from ER to Golgi (Napa, Actr1a, Nsf,

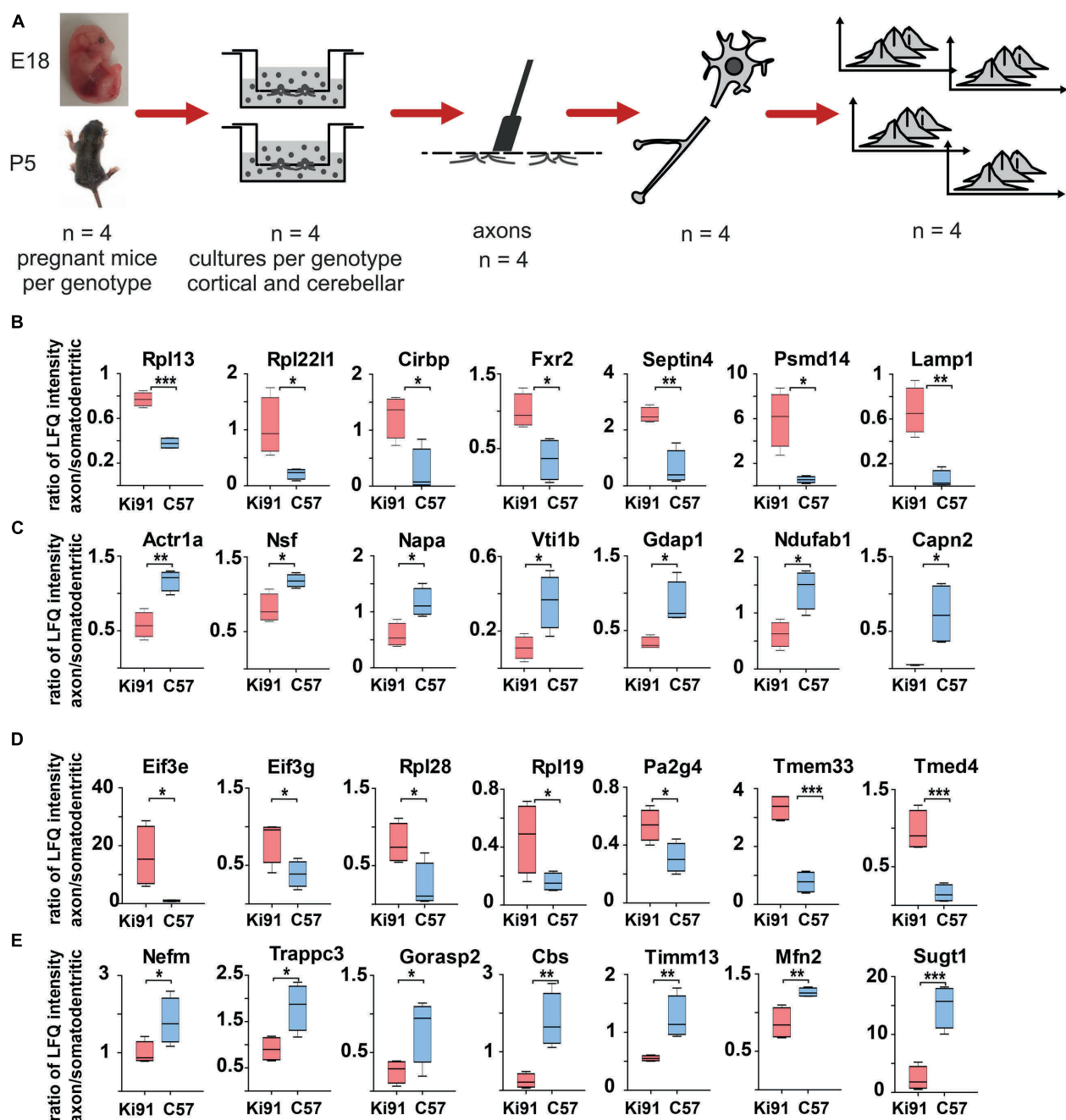
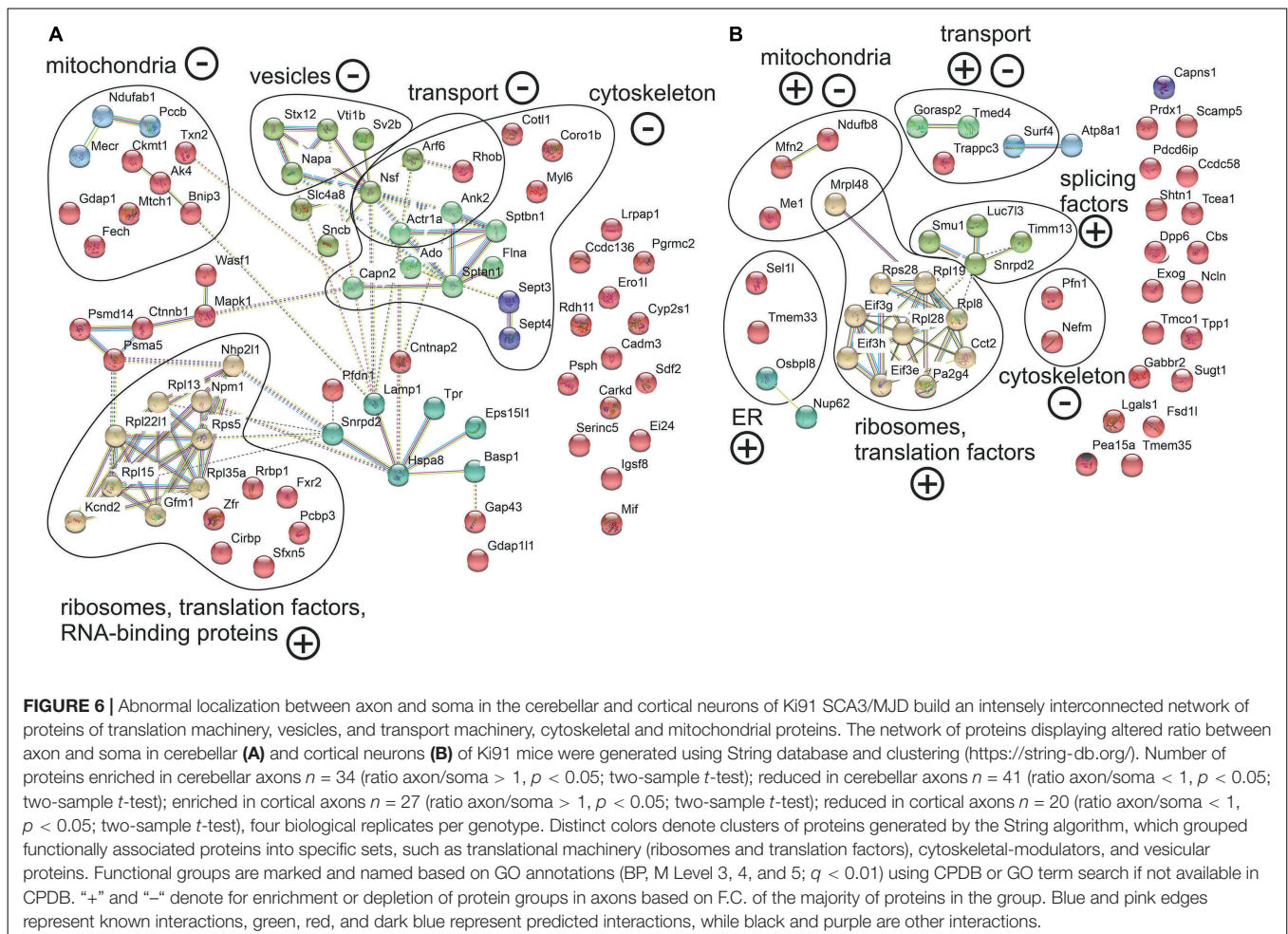


FIGURE 5 | Targeted axonal proteomics reveals sets of proteins enriched or depleted in the Ki91 SCA3/MJD cerebellar and cortical axons. Identification of proteins differentially localized in SCA3 neuronal compartments was performed by isolating two neuronal fractions (axonal and somatodendritic) from the same culture (Boyden chambers) obtained from E18 embryo (cortical) or P5 pups (cerebellar) – derived neurons. In brief, neurons were seeded on the inner side of the Boyden chamber inserts with a 1- μ m porous filter. After the period of neuronal differentiation and axonal growth through and toward the outer side of the insert membrane, both the inner side of the insert (somatodendritic) and the outer side (axonal) were scraped, and the fractions were collected for MS/MS analysis (**A**). Graphs present proteins with abnormal localization between axon and soma with the highest ratio between those compartments ($p < 0.05$; two-sample t-test) in the primary cerebellar (**B,C**) and cortical Ki91 neurons (**D,E**). In the P5-derived Ki91 cerebellar axons, there were enriched proteins related to ribosomes (Rpl13 and Rpl22l1), RNA-binding (Cirbp and Fxr2), and proteasome or lysosome (Psmd14 and Lamp1) (**B**). Proteins depleted in the Ki91 cerebellar axons involved important modulators of vesicular transport (Actr1a, Nsf, Napa, and Vti1b) (**C**). In the E18-derived Ki91 cortical axons, there were enriched translation factors (Eif3e and Eif3g), ribosome subunits (Rpl28 and Rpl19), RNA-binding (Pa2g4), and ER and Golgi (Tmed4 and Tmem33) (**D**). Proteins that were depleted in the Ki91 cortical axons included neurofilament (Nefm), related to intracellular trafficking (Trappc3 and Gorasp2), and mitochondria (Timm13 and Mfn2) (**E**). two-sample t-test (* $p < 0.05$, ** $p < 0.01$, *** $p < 0.001$), $n = 36$, $n = 4$ per phenotype, error bars: SEM.



Sptan1, Sptbn, and Ank2) (Figures 5C, 6A and Supplementary Table 5).

In cortical Ki91 axons, there were generally fewer proteins identified with lower ratio axons to the soma (Figure 5E and Supplementary Table 7). However, there were also proteins related to mitochondria, transport, and cytoskeleton, including neurofilament medium-chain (Nefm), playing an essential role in axonal function (Figures 5E, 6B and Supplementary Table 7).

Impairment of Mitochondrial Metabolic Potential in Ki91 SCA3/MJD Primary Cerebellar Neurons

Spinocerebellar ataxia type 3 patients show decreased BMI, and similarly, SCA3 Ki91 mice fail to gain weight. Moreover, our proteomic approaches identified mitochondria and energy metabolism failure in Ki91. The direct investigation of energy metabolism in presymptomatic young SCA3 neurons was not performed previously; therefore, it is unknown if the mitochondrial phenotype occurs early in SCA3 and if mitochondrial dysfunction is a primary contributor to the SCA3 pathology or only the secondary result of putative

mice and patient dysphagia. To address whether energy metabolism is disturbed in Ki91 neurons, we performed Cell Energy Phenotype Test with Seahorse XFp analyzer. The assay was performed on primary cerebellar neurons in days *in vitro* 3 (DIV3), 11, 18, and 21 ($n = 6$ per genotype and stage; Figures 7A–C). The oxygen consumption rate (OCR) and extracellular acidification rate (ECAR) were measured over time at baseline and stressed conditions (injection of oligomycin and FCCP mixture) (Supplementary Figure 8). Then, the metabolic potential of neurons was evaluated by calculating changes after stress conditions relative to baseline. The test demonstrated a significant increase in the ECAR metabolic potential in both Ki91 and WT neurons in every tested stage ($p < 0.0001$; two-sample t -test; Figures 7A,B). Likewise, an increase of the OCR metabolic potential was observed in WT neurons and Ki91 neurons, but only in DIV11 and 21 ($p < 0.05$; two-sample t -test; Figures 7A,B). Furthermore, under stressed conditions, the levels of ECAR were diminished in Ki91 neurons compared to WT in DIV3, 18, and 21 ($p < 0.001$; two-sample t -test; Figures 7A,C). Interestingly, both baseline and stressed OCR was increased in Ki91 neurons compared to WT in DIV 3 and 11 ($p < 0.0001$; two-sample t -test; DIV11 baseline $p = 0.13$; Figures 7A,C),

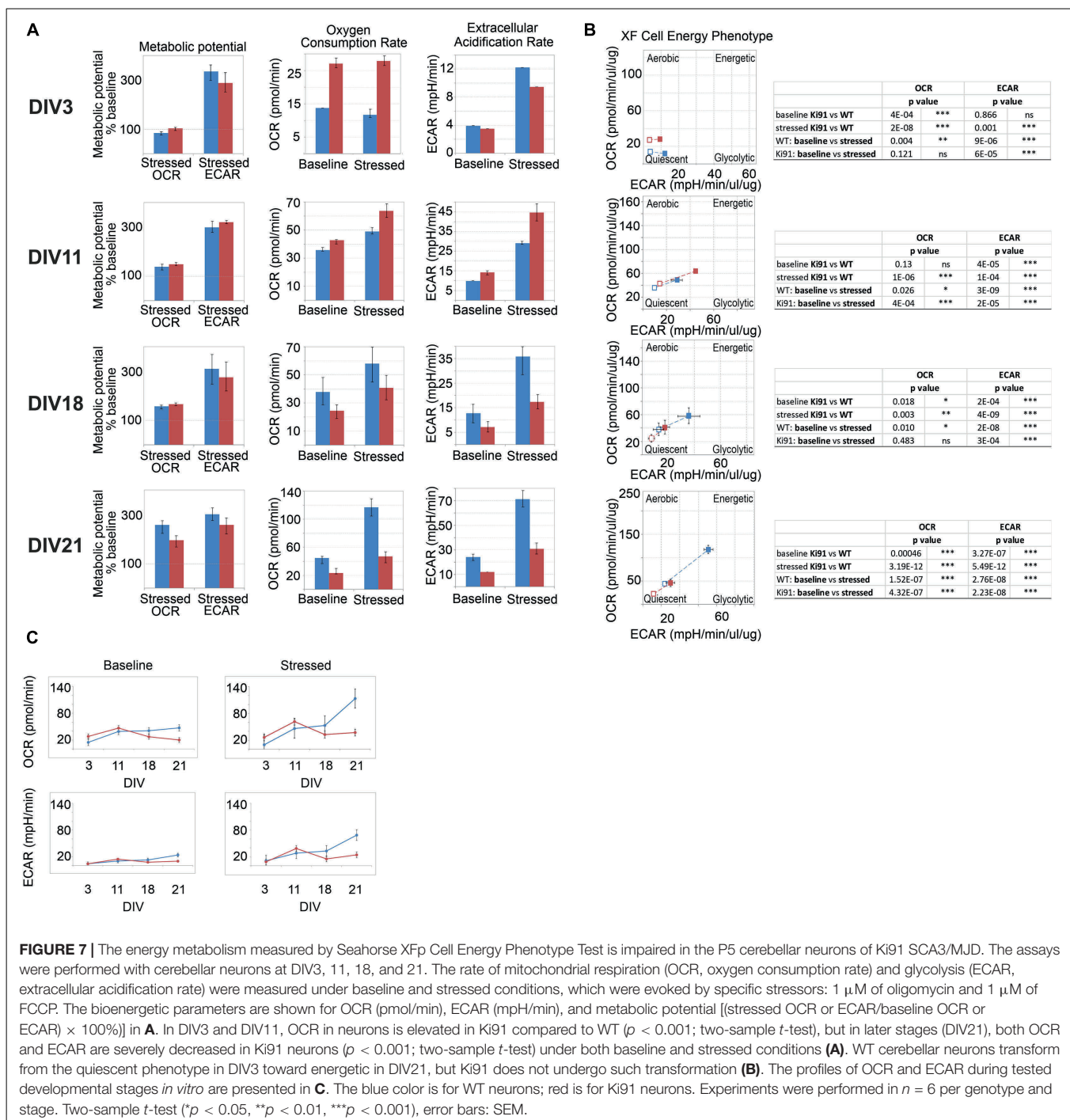


FIGURE 7 | The energy metabolism measured by Seahorse XF Cell Energy Phenotype Test is impaired in the P5 cerebellar neurons of Ki91 SCA3/MJD. The assays were performed with cerebellar neurons at DIV3, 11, 18, and 21. The rate of mitochondrial respiration (OCR, oxygen consumption rate) and glycolysis (ECAR, extracellular acidification rate) were measured under baseline and stressed conditions, which were evoked by specific stressors: 1 μ M of oligomycin and 1 μ M of FCCP. The bioenergetic parameters are shown for OCR (pmol/min), ECAR (mpH/min), and metabolic potential [(stressed OCR or ECAR/baseline OCR or ECAR) \times 100%] in **A**. In DIV3 and DIV11, OCR in neurons is elevated in Ki91 compared to WT ($p < 0.001$; two-sample t -test), but in later stages (DIV21), both OCR and ECAR are severely decreased in Ki91 neurons ($p < 0.001$; two-sample t -test) under both baseline and stressed conditions (**A**). WT cerebellar neurons transform from the quiescent phenotype in DIV3 toward energetic in DIV21, but Ki91 does not undergo such transformation (**B**). The profiles of OCR and ECAR during tested developmental stages *in vitro* are presented in **C**. The blue color is for WT neurons; red is for Ki91 neurons. Experiments were performed in $n = 6$ per genotype and stage. Two-sample t -test (* $p < 0.05$, ** $p < 0.01$, *** $p < 0.001$), error bars: SEM.

while in later stages, the trend was reversed and in DIV18 and 21 it was significantly decreased ($p < 0.01$; two-sample t -test; **Figures 7A,C**).

Overall, these data demonstrate that the potential for energy production is impaired in cerebellar Ki91 neurons. The glycolysis rate shows fluctuations in both baseline and stressed conditions. On the other hand, mitochondrial respiration shows a coherent pattern, which starts with an increase under both tested conditions, following by a decrease. The study

demonstrates that energy deficit occurs early in SCA3 neurons, and therefore it is not a secondary event resulting from previous neuronal damage.

Assessment of Vesicle State in Neurites of Ki91 SCA3/MJD Cerebellar Neurons

All proteomic approaches collectively demonstrated altered levels of proteins building cellular vesicles or regulating

intracellular vesicular trafficking. Therefore, our next goal was to assess a state of vesicles using the functional assay based on the labeling of neuronal vesicles using Rab7, a vesicular protein commonly occurring in late endosomes, lysosomes, and other types of vesicles that are undergoing active transport in axons and dendrites. Therefore we transfected monomeric red fluorescent protein (mRFP)-tagged Rab7 to SCA3 primary cerebellar neurons (neuron cultures isolated from three different sets of P5 pups, five independent transfections, with 5–10 neurons analyzed each time; **Figure 8A**).

We found that the average area of vesicles labeled with fluorescently tagged Rab7 was significantly (*t*-test, $p < 0.01$) increased by 40% in Ki91 as compared to WT neurons (**Figure 8B**). Distribution of vesicle size showed that Ki91 neurons had a lower number of small vesicles ($<0.25 \mu\text{m}^2$) and a higher number of large vesicles ($>0.5 \mu\text{m}^2$) (*t*-test, $p < 0.01$; **Figure 8C**). We did not detect any differences in the shape of vesicles. However, there was a significant increase in the number of vesicles normalized to the length of the measured axon (*t*-test, $p < 0.05$; **Figure 8D**). To assess whether Rab7-loaded vesicles accumulate in either the axon's proximal or distal region, we also calculated the number of vesicles in those regions, arbitrarily defined as 1/8 of the axon length starting either from the axon hillock or axon tip. There was a significant increase in the number of vesicles in the proximal region (*t*-test, $p < 0.01$) by 58% in Ki91 as compared to WT neurons and in the distal part (*t*-test, $p < 0.001$) by 110% (**Figure 8D**).

Ki91 SCA3/MJD Neurons Show Increased Phosphorylation of Axon-Specific Neurofilaments, Indicating the Stress of the Axonal Cytoskeleton

The proteomic approaches and, in particular, the axonal proteomics demonstrated that several classes of dysregulated proteins in SCA3 are located in the axonal compartment. We also found the ataxin-3-positive inclusions along axons in the cerebellum by co-staining with axon-specific marker smi-312 antibody (axon-specific p-Nef). The phosphorylation state of axonal neurofilaments reflects the health of the neuronal cytoskeleton. Therefore we further explored whether the structure and phosphorylation status of neurofilaments are disturbed in the SCA3 model. We assessed the phosphorylated and non-phosphorylated neurofilaments (axon-specific p-Nef and neuronal Nef; **Figure 9**) on immunostained sagittal brain slices from 12-month-old Ki91 and WT mice using. Increased phosphorylation of neurofilaments is often a sign of defective transport and maintenance also related to mitochondria. We found that both p-Nef levels (SMI-312 antibody) and non-phosphorylated Nef levels (SMI-32 antibody) were significantly increased in the cerebellum of SCA3 mice compared to WT animals (*t*-test, $p < 0.001$; $n = 3$ and five pictures per genotype; **Figures 9A–D**). In detail, we found increased levels of Nef in soma, dendrites, and axons of Purkinje cells (*t*-test, $p < 0.01$; **Figures 9A,C**). The increased level of axon-specific p-Nef was detected in axons of the molecular layer and axons of the granular

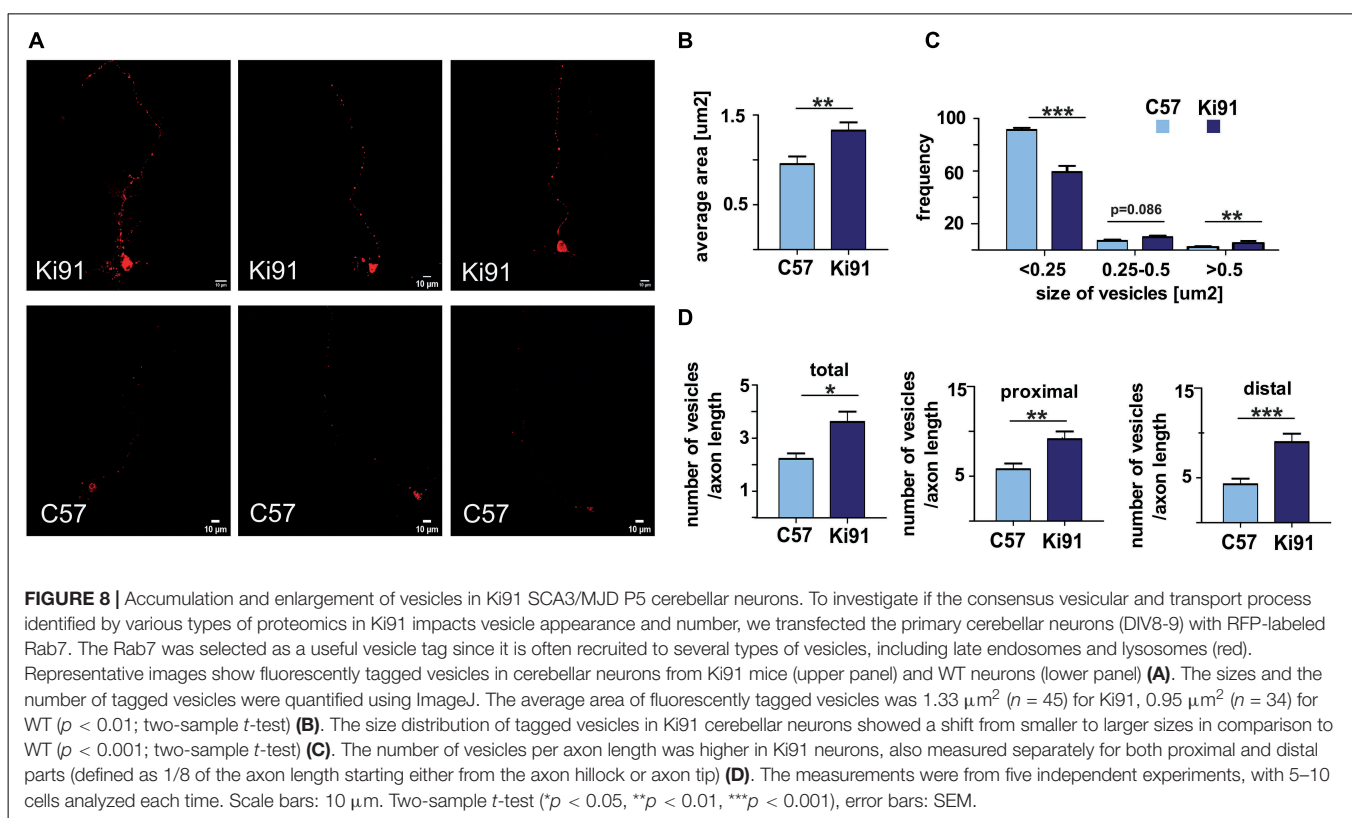
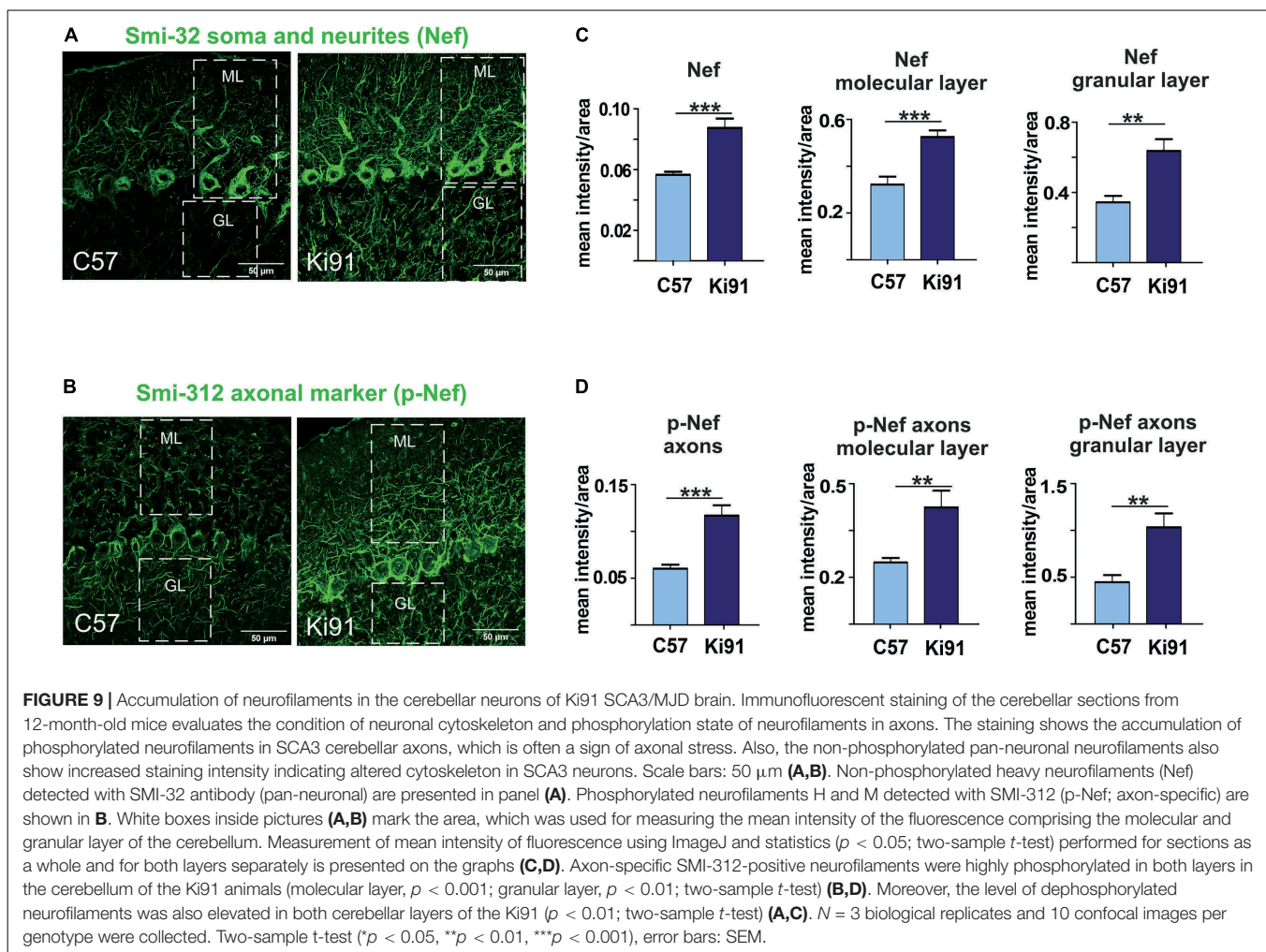


FIGURE 8 | Accumulation and enlargement of vesicles in Ki91 SCA3/MJD P5 cerebellar neurons. To investigate if the consensus vesicular and transport process identified by various types of proteomics in Ki91 impacts vesicle appearance and number, we transfected the primary cerebellar neurons (DIV8–9) with RFP-labeled Rab7. The Rab7 was selected as a useful vesicle tag since it is often recruited to several types of vesicles, including late endosomes and lysosomes (red). Representative images show fluorescently tagged vesicles in cerebellar neurons from Ki91 mice (upper panel) and WT neurons (lower panel) (**A**). The sizes and the number of tagged vesicles were quantified using ImageJ. The average area of fluorescently tagged vesicles was $1.33 \mu\text{m}^2$ ($n = 45$) for Ki91, $0.95 \mu\text{m}^2$ ($n = 34$) for WT ($p < 0.01$; two-sample *t*-test) (**B**). The size distribution of tagged vesicles in Ki91 cerebellar neurons showed a shift from smaller to larger sizes in comparison to WT ($p < 0.001$; two-sample *t*-test) (**C**). The number of vesicles per axon length was higher in Ki91 neurons, also measured separately for both proximal and distal parts (defined as 1/8 of the axon length starting either from the axon hillock or axon tip) (**D**). The measurements were from five independent experiments, with 5–10 cells analyzed each time. Scale bars: $10 \mu\text{m}$. Two-sample *t*-test (* $p < 0.05$, ** $p < 0.01$, *** $p < 0.001$), error bars: SEM.



layer and white matter (*t*-test, $p < 0.001$; **Figures 9B,D**). The altered phosphorylation of axons in the SCA3 Ki91 model may be related to disturbed protein and mitochondria localization and their transport in axons.

DISCUSSION

Very little is known about the proteome in the SCA3 brain, and it may be one of the reasons for the incomplete understanding of the disease mechanism and delay in finding a cure. Although there are transcriptomic alterations in symptomatic SCA3 animal models, knowledge about changes in levels of the proteins is still missing (Toonen et al., 2018; Zeng et al., 2018). Moreover, we previously demonstrated the lack of transcriptomic changes in the pre-symptomatic SCA3 mice (Wiatr et al., 2019). Here, we aimed to investigate the brain profile of altered proteins in the SCA3 knock-in model to unveil a consensus set of most critical molecular programs governing the disease and identify protein biomarkers. In detail, we aimed to investigate the proteome using three different approaches: at the *in vivo* level, at the CC level, and in relation to disease progression and

severity. Once the consensus set of altered candidate processes was established, we aimed to test if we can identify their physiological fingerprints by simple, functional assays, preferably using primary presymptomatic neurons.

We first performed a longitudinal behavioral study between 4 and 18 months of age of Ki91 (Switonski et al., 2015) to establish SCA3 behavioral and phenotypic milestones suitable for the investigation of brain proteome. The first milestone in symptomatic Ki91 mice was the reduced body weight gain identified in 4-month-old animals. Statistically significant gait ataxia at 12-month-old Ki91 was the second milestone, and the last milestone was the severe motor disturbances and progression of other symptoms in 18-month-old animals. Altogether, homozygous Ki91 represents a model of SCA3 progression and gradation of symptoms observed in SCA3 patients (Coutinho and Andrade, 1978; Jacobi et al., 2015; Pulido-Valdeolivas et al., 2016; Coarelli et al., 2018).

In the next step, we determined a range of affected brain areas by the MRI and detection of ataxin-3-positive inclusions using advanced, symptomatic Ki91 animals. The inclusions were present in almost all brain areas of both the posterior and frontal brain parts. The intra-nuclear inclusions dominated

in the cerebellum, mainly in the white matter, DCN, and in pons and midbrain; however, they were also present in the cerebral cortex, hippocampus, and striatum. Importantly, we have seen highly abundant ataxin-3-positive inclusions in SMI-312-positive cerebellar axons in white matter. The intra-axonal inclusions were also previously detected in nerves and various tracts in SCA3/MJD patients (Seidel et al., 2010). Also, the changes observed by brain MRI in Ki91 were not localized to one structure, but the atrophy was spreading on several brain regions, including frontal parts, cerebellum, and brainstem. Moreover, brain areas rich in axons such as the corpus callosum are atrophied in Ki91. Therefore, exploring our behavioral, neuropathologic, and MRI results led to selecting the consensus set of brain regions for further experiments. To identify molecular SCA3 pathogenesis by our three-way proteomic approach, we selected two representative brain regions: the cerebellum and cerebellar cortex. Both regions demonstrated a high number of inclusions; particularly, the cerebellum was affected more than other brain regions. Besides, the cerebral cortex demonstrated very pronounced atrophy on MRI. Even if it was not possible to determine cerebellar volume change on MRI (technical limitation of MRI setup), our previous works detected atrophy of Purkinje cells and occurrence of reactive gliosis by immunohistochemistry (Switonski et al., 2015). Also, the behavioral motor signs indicated the involvement of cerebellum atrophy. Such a selection of brain regions for further experiments involves both classically reported SCA3 pathogenesis in the hindbrain and postulated SCA3 pathogenesis in more frontal parts of the brain (Schmidt et al., 2019; Guo J. et al., 2020).

Our first proteomic approach corresponded to Ki91 behavioral milestones where we selected tissue from animals at the age of 4 months (lack of weight gain), 10 months (mice on the verge of behavioral phenotype), 12 months (motor decline statistically significant), and 14 months (an additional symptomatic age). The second proteomic approach, called “correlative,” was aimed to identify dysregulated proteins and processes in mouse subjects with carefully characterized and matching phenotype severity. The first two proteomic approaches offered insights into the disease pathogenesis at the level of tissue and disease stage; however, the perspective of cellular level and CCs were still missing in both approaches. Therefore we employed a third, targeted proteomics approach where we separately assessed proteins in somatodendritic and axonal compartments of primary neurons isolated from embryos or pups. An additional advantage of such primary neuronal SCA3 culture is the possibility of validation if processes discovered in two other approaches may occur early in the disease development.

The first pathogenic process, which was consensus among the proteomic approaches in our work, is the disturbed energy metabolism. We demonstrated many dysregulated proteins related to the mitochondrial compartment, which corresponds with the reduced body weight gain in Ki91. Notably, the BMI of SCA3 patients is significantly lower, and BMI decrease correlated with faster disease progression (Diallo et al., 2017; Yang et al., 2018). The energy metabolism was the most common pathway, and the proteins related

to metabolism were dysregulated already in 4-month-old presymptomatic Ki91 mice. For instance, many OXPHOS-related proteins, such as Nduf subunits, Aco2, and mt-Co proteins and several metabolic proteins such as Gpd2, Cs, Gpi, Pkm, Wdr1, Sdha, Ddx1, and Aldh1l1 demonstrated altered levels and were previously identified in AD, HD, and SCA1 (Sorolla et al., 2008; Sánchez et al., 2016; Lunnon et al., 2017). Similarly, the correlative approach also revealed downregulated mitochondrial proteins such as mitochondrial chaperone Timm9, Ndufb5, and Fasn in both “mild” and ‘severe’ phenotype, which suggest that disturbances of energy production is the primary pathology of SCA3. Several mitochondrial proteins were also depleted in axons compared to the somatodendritic compartment in SCA3 neurons, which may indicate the disrupted delivery of mitochondria to nerve terminals. The most frequently dysregulated protein, which we propose as one of a SCA3 biomarker candidate in both tested brain regions, is carbonic anhydrase 2 (Ca2). Ca2 is linked to a mechanism controlling an increased transport of lactate, which is an important energy source for neurons (Stridh et al., 2012; Karus et al., 2015).

Since many proteomic changes pointed out pathways related to energy metabolism, our first functional assay measured mitochondrial respiration and glycolysis rate in cultured cerebellar Ki91 neurons kept for DIV 3, 11, 18, and 21, which reflected the culture differentiating from young to more mature neurons. Commonly, the typical culture of such neurons and also our WT neurons represented a developing dependency on OXPHOS since mature neurons rely on OXPHOS to meet energy demands. In turn, SCA3 neurons demonstrated a lack of increase in OXPHOS dependency and even a slight drop in oxygen consumption during neuronal maturation. SCA3 neurons under stress reached their maximal OCR already as young as DIV 11 as compared to WT neurons, which reached the maximum at DIV 21. At DIV 3 and 11, SCA3 neuronal progenitors show higher overall oxygen consumption; therefore, at this early stage, the neurons may already be in deficiency of energy, or its production is aberrant. In the case of older SCA3 neurons with highly developed processes, a dramatic difference in energy metabolism compared to WT neurons can also be related to the failure of energy production in axons.

Overall, we demonstrated that the number of dysregulated proteins related to metabolism, lysosomes, endosomes, and protein folding increases with Ki91 age and is noticeably higher in older 10–14-month-old Ki91 mice, which represent the phase of the motor symptoms development. Moreover, the most advanced disease stage marked by highly reduced body weight, anxiety, and severe motor symptoms in 18-month-old animals is also characterized by the excessive size of Atxn3 inclusions and were observed both in the nuclei and axons, whereas in pre-symptomatic 2-month old SCA3 mice ataxin-3-positive aggregates were relatively smaller and detected only in cell nuclei (Wiatr et al., 2019).

Recent discoveries emphasize the role of degeneration of “wiring” between brain structures and axonal deficits as one of the main pathogenic events in neurodegenerative disorders (Sánchez-Valle et al., 2016; Ferrari Bardile et al., 2019; Casella et al., 2020). Also, in SCA3, the axonal defects and white matter

abnormalities are prominent disease symptoms (de Rezende et al., 2015; Farrar et al., 2016; Lu et al., 2017). Our proteomic approaches jointly demonstrated that the largest population of proteins with altered levels was involved in vesicular transport and endocytosis as a second consensus molecular process candidate in SCA3. Vesicular trafficking is crucial for axon maintenance, synaptic signaling, releasing, and recycling of neurotransmitters. Our proteomic data demonstrate highly downregulated levels of proteins related to vesicle transport or trans-synaptic signaling (Nrgn, Sh3gl1, Vamp2, Syngap1, Bsn, Syt7, Homer1, Rims1, Pclo, and Erc2; SNARE complex). Several vesicular Rab proteins were also dysregulated, such as Rab11b, Rab3d, and Rab10. Other Rab proteins were also dysregulated in SCA3/MJD patients (Sittler et al., 2018). Besides, there were dysregulated proteins related to protein metabolism localized to endosomes, exosomes, and lysosomes. Many of these proteins are involved in neurodegenerative diseases such as AD and HD (Skotte et al., 2018; Mendonça et al., 2019), and their loss brings significant neurological consequences (Yoo et al., 2001; Santos et al., 2017; Salpietro et al., 2019; Falck et al., 2020). Moreover, Qdpr (human homolog: DHPR) and Glul proteins responsible for neurotransmitters' metabolism are progressively downregulated throughout the SCA3 course in the Ki91 cerebellum and cortex. Both proteins are essential for proper CNS function (Breuer et al., 2019; Kurosaki et al., 2019; Zhou et al., 2019).

The 3rd consensus SCA3 candidate process was termed by us "the regulation of cytoskeletal structure and function" with dysregulated proteins localizing to neuronal processes. Coherently with vesicle trafficking, our proteomic results also revealed dysregulation of neurofilament proteins (NFs), such as heavy chain NF-H in both the cerebral cortex and cerebellum. Disturbed energy metabolism in neurons is often related to defects in the cellular cytoskeleton and phosphorylation state of NF-H, in particular, resulting in aberrant axonal transport of mitochondria (Jung et al., 2000; Shea and Chan, 2008). Furthermore, proteomic data contained dysregulated proteins pivotal for microtubular cytoskeleton stability and axon organization. Dysregulated proteins were also involved in anterograde and retrograde microtubule-based transport (Kif5c, Kif5b, Kif21a, Klc1, Klc2, and Kif3a; Dnm3, Dyncl1l1, Dyncl1h1, and Dynll2), in particular in "severe" phenotype, which may suggest that disruption of axonal transport contributes to increased severity of SCA3 symptoms. Among the microtubular proteins, Tau (Gao et al., 2018) was elevated in the cerebral cortex of symptomatic Ki91 mice, RhoG (Zinn et al., 2019), and dysregulated group of proteins that are also enriched in oligodendrocytes such as Cryab protein stabilizing cytoskeleton and previously proposed as a component of therapeutic strategy (Ghosh et al., 2007; Houck and Clark, 2010; Cox and Ecroyd, 2017; Zhu and Reiser, 2018). Dysregulation of Cryab, RhoG, Mbp, and Marcks indicates that oligodendrocytic processes and myelination contribute to axon dysfunction in SCA3 (Ishikawa et al., 2002; Guimarães et al., 2013; Zhang et al., 2017; Rezende et al., 2018). In addition, we previously identified altered levels of mRNA related to oligodendrocyte differentiation and function in older SCA3 mice (Wiatr et al., 2019). Interestingly, several oligodendrocytic marker proteins dysregulated in our proteomic

studies, such as Plp, Qdpr, Mbp, and Mog were predicted to localize in extracellular vesicles (EVs). EVs are often released by oligodendrocytes and deliver trophic support for axons but may also transfer pathogenic triggers (Krämer-Albers et al., 2007; Porro et al., 2019).

The investigation of two candidate consensus processes related to vesicle transport and neuronal cytoskeleton required a targeted proteomic approach focused on axons. The proteins that were deficient in SCA3 axons were associated with vesicles, axonal transport, and mitochondria. Depleted proteins suggesting altered transport along the axon in Ki91 included proteins interacting or forming dynein complex, required for mitochondria and endosome/lysosome and synaptic vesicles transport along the axons, such as Actrl1a and Ank2 (Holleran et al., 1996; Moughamian et al., 2013; Lorenzo et al., 2014). Besides, there were also essential cytoskeletal proteins involved in regulating axonal transport and actin dynamics, Arf6 and its interactor RhoB, targeted by Arf6 to endosomes (Eva et al., 2017; Zaoui et al., 2019). Components of SNAREs responsible for vesicular trafficking were also depleted in SCA3 axons, such as Napa (a.k.a. α -SNAP), Vti1b, and Nsf. Lower levels of Napa, Nsf, and Actrl1a were also identified by the "parallel" proteomic approach in the cerebellum of Ki91 mice. Of note, Nsf is the ATPase indispensable for membrane fusion and for regenerating active SNAREs. Nsf depletion results in the arrest of membrane trafficking and, consequently, neuronal damage and death (Stenbeck, 1998; Emperador-Melero et al., 2018; Yuan et al., 2018). In particular, disturbed axonal transport may affect delivery and proper localization of mitochondria since we detected several essential mitochondrial proteins with diminished levels in Ki91 axons.

In addition to defective energy metabolism, all of our proteomic approaches identified the vesicular processes and cytoskeletal structure and regulation processes in the SCA3 Ki91 brain. In addition to vesicular and cytoskeletal localization, most dysregulated proteins identified in proteomics were predicted to localize in axons. Therefore we designed two simple assays to detect functional fingerprints of vesicular and cytoskeletal phenotypes in neurons. We decided to load the neuronal vesicles with fluorescent Rab7 protein as the universal, external marker often occurring in a variety of vesicle species. We were able to detect the accumulation of vesicles in cell bodies and in the processes of SCA3 neurons. Moreover, the vesicles were enlarged in SCA3 neuronal processes. The second assay was based on immunostaining detection of axonal cytoskeleton phosphorylation to assess a putative pathogenic process related to the axonal cytoskeleton. We used the SMI-312 antibody, an axon-specific marker (phosphorylated NFs), and detected highly increased phosphorylation in the 12-month-old Ki91 cerebellum compared to WT cerebellum. Non-phosphorylated NFs (SMI-32; pan-neuronal staining) were also increased in the SCA3 Ki91 cerebellum. Accumulation and aggregation of phosphorylated neurofilaments in axons is a biomarker indicating axonal damage, which may disturb the transport of vesicles and mitochondria. Moreover, in neurodegenerative disorders and SCA3, the NFs could serve as a biomarker (Li et al., 2019).

Lastly, axonal proteomics in Ki91 has also demonstrated highly enriched protein translation machinery represented by ribosomal proteins, various RNA-binding proteins, and translation initiation factors (**Supplementary Tables 5, 7**). Protein synthetic machinery is intensively transported to the axons in response to cellular stress (Baleriola and Hengst, 2015). We detected the signs of cellular stress by identifying elevated Tpp1 and Tmem33 proteins, which play a role in unfolded protein response (UPR) (Sakabe et al., 2015; Mukherjee et al., 2019). Along this line, protein chaperons and proteasome subunits (Cct2 and Pmsd14) were highly enriched in SCA3 Ki91 axons. Moreover, ribosomal and RNA-binding proteins are also compounds of RNP granules (mRNPs, messenger ribonucleoproteins) or stress granules, both holding mRNAs translationally repressed (Sossin and DesGroseillers, 2006; El Fatimy et al., 2016). One of the crucial components of the granules is Fxr2 (Chyung et al., 2018), which is highly enriched in Ki91 cerebellar axons. Interestingly, vesicular platforms in axons were recently identified as carriers of translation machinery, mRNPs, and structure responsible for axonal mitochondria maintenance (Cioni et al., 2019). Furthermore, it was also demonstrated that protein inclusions specifically impair the transport of endosomes and autophagosomes (Volpicelli-Daley et al., 2014; Guo W. et al., 2020). Also, locally active translation machinery and local energy production are long known phenomena in axons since it provides critical substrates even to the most distal part of the neuronal terminals. However, in the case of accumulation of the polyQ proteins, such an organization of protein synthesis in long processes may accelerate neuronal dysfunction. In such a case, upregulated translation machinery may be a “vicious cycle” for the accumulation of polyQ proteins in axons, gradually aggravating the disease and leading to profound neuronal dysfunction.

CONCLUSION

Spinocerebellar ataxia type 3 molecular disease mechanism is insufficiently explored. Ataxin-3 is ubiquitin protease, but very little is known about the broader influence of mutant protein on other proteins in the SCA3 brain. The missing knowledge about the proteome may be one of the reasons for the incomplete understanding of the disease mechanism and lack of cure. Therefore, we present the first global model picture of SCA3 disease progression based on the alterations in protein levels in the brain and embryonic SCA3 axons, combined with an *in vivo* behavioral study and neuropathology. We propose the most relevant pathogenic processes in SCA3 involving disturbed energy metabolism, impairment of the vesicular system, cell and axon structure, and altered protein homeostasis. We demonstrate that the consensus processes identified in the SCA3 Ki91 brains show their functional signs in the primary pre-symptomatic neurons, and therefore may be the first steps of pathogenesis. Our data have demonstrated for the first time that one of the essential pathogenic aspects of SCA3 is the faulty localization of proteins between axons and soma. Further signs of affected SCA3 axons are vesicle accumulation and increased

neurofilament phosphorylation. The important novel finding is the highly increased axonal localization of proteins involved in the translation machinery in SCA3. It is possible that local mutant protein production in axons may accelerate neuronal dysfunction; therefore, upregulated translation machinery in axons may aggravate the disease. Moreover, we identified a variety of molecular signatures related to mitochondria in the SCA3/MJD Ki91 model, and we show that the earliest global process which occurs already in the neonatal neurons is the OXPHOS and glycolysis deficits. For the first time, we demonstrate that the young developing SCA3 neurons fail to undergo the transition from glycolytic to OXPHOS phenotype typical for normal neurons. Summarizing, we revealed that the SCA3 disease mechanism is related to the broad influence of mutant ataxin-3 on the brain, neuronal and axonal proteome, and disruption of the proper localization of axonal and somatodendritic proteins and organelles such as vesicles, translation machinery, and mitochondria (**Figure 10**).

MATERIALS AND METHODS

Animals

Maintaining and breeding were performed at standard conditions with an 18/6-h light/dark cycle and water and food *ad libitum*. No differences in food or water intake between Ki91 and WT mice were observed. The animals were marked using numerical ear tags (National Band & Tag Company, Newport, RI, United States). The stress level of the animals was minimized throughout all procedures and animal handling. The animal experimentation and handling were approved and monitored by the Local Ethical Commission for Animal Experiments in Poznan. The animals were sacrificed according to AVMA Guidelines for the Euthanasia of Animals by placing them in the programmable CO₂ chamber (Rothacher Medical, Heitenried, Switzerland). Homozygous SCA3 Ki91 animals contained between 103 and 132 CAG repeats on a single mutant ataxin3 allele. SCA3 Ki91 mice (C57BL/6 background) and age-matched WT littermates bred in-house were used for behavioral tests (*n* = 36) and collecting brain tissues for proteomic analysis (*n* = 32, and *n* = 21, after behavioral tests), validation of proteomics (*n* = 32), MRI (*n* = 12) and immunostaining (*n* = 8, after behavioral tests and *n* = 6 from a separate cohort of 12-month-old animals). The cerebellum and cerebral cortex for proteomic analysis were collected from 4, 10, 12, 14, and 18 month-old animals, which corresponded to the timepoints of behavioral testing. An experimental group consisted of four mutant mice vs. four WT littermates (proteomics: 4, 10, 12, and 14-month-old and immunostaining), and 11 mutant mice vs. 10 WT littermates (proteomics: 18-month-old).

Behavioral Studies

Mice were trained and tested for motor deficits, starting from 4-month-old animals, and consequently every 2 months, until the age of 18-month-old in a cohort of 18 mutant mice vs. 18 WT littermates. Tests included accelerating rotarod (4–40 rpm in 9.5 min), elevated beam walk (diameter of rods: 35, 28, 21,

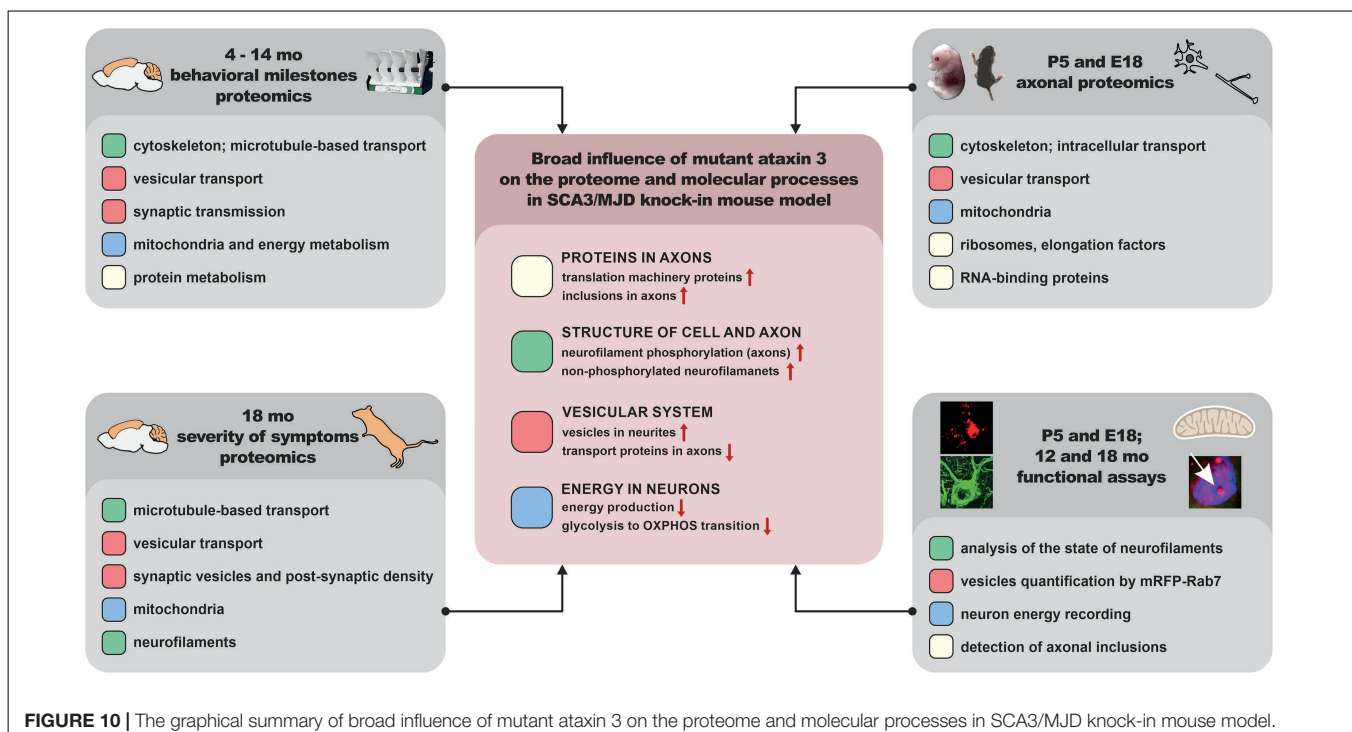


FIGURE 10 | The graphical summary of broad influence of mutant ataxin 3 on the proteome and molecular processes in SCA3/MJD knock-in mouse model.

17, and 9 mm) as previously described (Switonski et al., 2015), and additionally in 18-month-old animals open field test in which locomotor activity and zone preferences in the experimental cage (50 cm^2) were analyzed and measured during 10 min. Each test consisted of 1 training day (T) and 3 consecutive days of measurement. We also performed scoring tests designed for evaluation of the ataxia phenotype in mouse models (Guyenet et al., 2010), wire test for evaluating muscle strength, and footprint for gait ataxia. For gait analysis, the forelimbs of the mice were stained with black and hindlimbs with red non-toxic paint. Mice were placed on a sheet of paper inside a tunnel ($80 \times 10\text{ cm}$). Only the middle part of a series of steps was measured for the distance between two steps (stride length), for- and hindlimb base, and overlapping between for- and hindlimb. All mice were weighed during each testing session. Graphing and statistics were performed on PrismVR software (San Diego, CA, United States), using ANOVA with Bonferroni *post hoc* test.

Magnetic Resonance Imaging and Image Analysis

After PFA perfusion of the mice, brains ($n = 6$ per genotype) were removed and stained by a one-week soaking in Gadolinium solution (Dotarem, Guerbet, France) in PBS at 2.5 mM. This protocol enhances the signal- and contrast-to-noise ratios on MR images of fixed brains (Dhenain et al., 2006). *Ex vivo* MRI experiments were performed on a horizontal 11.7 T Bruker scanner (Bruker, Ettlingen, Germany). A quadrature cryoprobe (Bruker, Ettlingen, Germany) was used for radiofrequency transmission and reception. Diffusion Tensor Imaging (DTI) data were acquired using Echo Planar Imaging sequence (Resolution = $100 \times 100 \times 200\text{ }\mu\text{m}^3$, TR = 3,000 ms,

TE = 28 ms, 60 directions). To preserve their integrity and avoid deformations, brains were kept inside skulls for *ex vivo* MRI experiments. Anatomical images were co-registered in the same space to create a study template. Transformations to match the study template to an atlas composed of a high-resolution template and a map of region's labels adapted from the Allen mouse brain Atlas (Lein et al., 2007) were calculated. Finally, transformations to match the study template and labels to each anatomic image were calculated. The automated segmentation pipeline was performed using an in-house python library (SammBa-MRI¹).

Protein Sample Preparation

Protein extraction was performed as previously described (Wiatr et al., 2019). Mouse brain tissues were homogenized with a Mixer Mill MM400 (Retch, Haan, Germany), followed by a threefold cycle of freezing and thawing and bath sonication ($3 \times 3\text{-min}$). Protein concentration was estimated using Quant kit (GE Healthcare, Chicago, IL, United States). Ten-microgram aliquots of proteins were diluted with 15 μl of 50 mM NH4HCO3 and reduced with 5.6 mM DTT for 5 min at 95°C. Samples were then alkylated with 5 mM iodoacetamide for 20 min in the dark at RT. Subsequently, the proteins were digested with 0.2 μg of sequencing-grade trypsin (Promega, Madison, WI, United States) overnight at 37°C.

Liquid Chromatography Coupled to Tandem Mass Spectrometry

The analysis of the proteome was performed with the use of Dionex UltiMate 3000 RSLC nanoLC system connected to

¹<https://github.com/sammaba-mri/sammaba-mri>

the Q Exactive Orbitrap mass spectrometer (Thermo Fisher Scientific, Waltham, MA, United States). Peptides derived from in-solution digestion were separated on a reverse-phase Acclaim PepMap RSLC nanoViper C18 column ($75\text{ }\mu\text{m} \times 25\text{ cm}$, $2\text{ }\mu\text{m}$ granulation) using acetonitrile gradient (from 4 to 60%, in 0.1% formic acid) at 30°C and a flow rate of 300nL/min (for 230 min). The spectrometer was operated in data-dependent MS/MS mode with survey scans acquired at a resolution of 70,000 at m/z 200 in MS mode and 17,500 at m/z 200 in MS2 mode. Spectra were recorded in the scanning range of 300–2,000 m/z in the positive ion mode. Higher energy collisional dissociation (HCD) ion fragmentation was performed with normalized collision energies set to 25. Swiss-Prot mouse database was used for protein identification with a precision tolerance set to 10 ppm for peptide masses and 0.08 Da for fragment ion masses. Raw data obtained for each dataset were processed by MaxQuant 1.5.3.30 version for protein identification and quantification. Protein was considered as successfully identified if the Andromeda search engine found at least two peptides per protein, and a peptide score reached the significance threshold $\text{FDR} = 0.01$.

Obtained data were exported to Perseus software ver. 1.6.1.3 (part of MaxQuant package; Munich, Germany). Numeric data were transformed to a logarithmic scale, and each sample was annotated with its group affiliation. Proteins only identified by site, reverse database hits, and contaminants were removed from the results. Next, data were filtered based on valid values for proteins. Proteins that contained valid values in 75% of samples in at least one group were included as valid hits. Before statistical analysis, normalization of data was performed by subtracting the median from each value in a row. A two-sample *t*-test was performed on analyzed sample data with *p*-value < 0.05 was considered as significant, and differentiating proteins were normalized using the Z-score algorithm for the hierarchical clustering of data.

Bioinformatic Analysis of Proteomic Data

Proteins were grouped using the CPDB according to the pathways (pathway enrichment *p*-value cut-off < 0.01), GO term by molecular function (MF), biological process (BP), and cellular component (GO term B, MF level 5, CC level 4 and 5, *p*-value cut-off < 0.01). CPDB integrates data from 30 different resources, including such databases as Reactome, KEGG, and BioCarta (Kamburov et al., 2013). Next, common pathways and GO terms for four datasets separately in both tissues (4, 10, 12, and 14 months of age) containing the highest relative number of dysregulated proteins and *p*-values were selected. The relative number of dysregulated proteins was calculated as a number of dysregulated proteins involved in the pathway or GO term divided by the total number of dysregulated proteins in a given dataset (%). For each analysis, the names of genes corresponding to the names of dysregulated proteins were used. In the separate analysis, we performed identification of cell types in the brain, which are affected by pathogenesis with the use of the Dropviz tool (Saunders et al., 2018) for the cerebellum and cerebral cortex. Significantly dysregulated ($p < 0.05$) proteins identified from label-free proteomic and experiments were included together into two tissue groups based on origin from the cerebellum

and cortex. Relative expression is presented in Dropviz as the number of transcripts per 100,000 in the cluster. The analysis of proteins displaying altered ratio between axon and soma in cerebellar and cortical neurons of Ki91 mice was performed using the String database² and clustering tool (MCL clustering, inflation parameter = 6).

Vacuum Dot Immunoblot

Before use in the dot blot assay, each antibody was validated with western blot assay (WB). WB was performed as previously described (Wiatr et al., 2019). Cerebellum and cortex samples were harvested from 16 homozygous Ki91 animals and 16 WT littermates; $n = 4$ mice per tested age (4, 10, 14, and 18 months of age) and per each genotype. The protein concentration was estimated using a Pierce BCA protein assay kit (Thermo Fisher Scientific, Waltham, MA, United States). The nitrocellulose membrane and Whatman filters (all GE Healthcare, Chicago, IL, United States) were washed two times with Milli-Q H_2O and two times with Tris-Buffered Saline (TBS) by vacuum filtration. A total of $2.5\text{ }\mu\text{g}$ of each protein sample in $50\text{ }\mu\text{L}$ of PB lysis buffer with PMSF cocktail inhibitor (Sigma-Aldrich, St. Louis, MO, United States) was spotted on nitrocellulose membrane and washed two times with TBS by vacuum filtration, and then allowed to air-dry. The blots were stained with Ponceau S solution and blocked with 5% non-fat milk in PBS/0.05% Tween-20 for 1 h at RT and subsequently incubated at 4°C overnight with the following primary antibodies: rabbit anti-MBP (1:1,000; Cell Signaling, Danvers, MA, United States), mouse anti-CRYAB (1:1,000; Developmental Studies Hybridoma Bank, Iowa City, IA, United States), mouse anti-GLUL (1:1,000; BioLegend, San Diego, CA, United States), rabbit anti-CA2 (1:2,000; ProteinTech, Rosemont, IL, United States), rabbit anti-QDPR (1:2,000; ProteinTech, Rosemont, IL, United States). The blots were probed with the respective HRP-conjugated secondary antibody (anti-rabbit or anti-mouse, 1:2,000; Jackson Immuno Research, Suffolk, United Kingdom). The immunoreaction was detected using the ECL substrate (Thermo Fisher Scientific, Waltham, MA, United States).

Primary Neuron Culture and Transfection

Primary neuron cultures were derived from Ki91 and C57 mice according to AVMA Guidelines for the Euthanasia of Animals. Cortices were dissected from E18 mouse embryos and cerebella from P5 pups. Cortical neurons were dissociated by trypsin (Merck, Darmstadt, Germany) diluted $10\times$, and cerebellar neurons were dissociated by trypsin diluted $5\times$. Cells were washed two times in a disassociation medium consisting of HBSS (Thermo Fisher Scientific, Waltham, MA, United States), supplemented with 0.1% glucose, 1× penicillin-streptomycin (Thermo Fisher Scientific, Waltham, MA, United States), then two times in a plating medium consisting of Dulbecco's modified Eagle medium (DMEM), 1× CTS GlutaMAX-I supplement, 1× penicillin-streptomycin (all Thermo Fisher Scientific, Waltham, MA, United States). Clumps of tissue debris were allowed to settle to the bottom of a 15 ml tube, and the supernatant containing

²<https://string-db.org/>

dissociated cells was centrifuged for 3 min at 1,300 rpm. Cells were seeded onto coverslips, tissue culture inserts (Greiner Bio-One GmbH, Kremsmünster, Austria), or Seahorse XFp Cell Culture Miniplates (Agilent Technologies, Santa Clara, CA, United States) coated with poly-D-lysine (Thermo Fisher Scientific, Waltham, MA, United States). Neurons were maintained in conditioned Neurobasal medium (Thermo Fisher Scientific, Waltham, MA, United States) supplemented with 2% B27 supplement, 1× CTS GlutaMAX-I supplement, 1× penicillin-streptomycin (all Thermo Fisher Scientific, Waltham, MA, United States), 1× apo-transferrin (Sigma-Aldrich, St. Louis, MO, United States), and N2 (0.005 mg/ml insulin, 0.0161 mg/ml putrescine, 30 nM Na-Selenite, 51 nM T3, 20 nM progesterone) in a humidified incubator with 5% O₂ and 5% CO₂ in air at 37°C. The maintenance medium was replenished with half-feed changes every 2–3 days. For transfection, cells were seeded at a density of 2 × 10⁵ cells/well onto coverslips in 24-well culture plates. Neurons were transfected at DIV 3–4 with mRFP-Rab7 (Addgene plasmid # 14436³; dgene_14436) at a concentration of 0.8 µg DNA per well using Lipofectamine 2000 (Thermo Fisher Scientific, Waltham, MA, United States) followed by fixation (4% PFA, 15 min in RT) and confocal imaging at DIV 7–11 from three biological replicates and five independent transfections. An approximately 10–15% transfection efficiency was achieved.

Isolation of Axons

Dissociated neurons (cortical and cerebellar) were seeded at a density of 1 × 10⁶ cells/well onto tissue culture inserts containing porous membrane (1 µm pores; Greiner Bio-One GmbH, Kremsmünster, Austria) in a 6-well cell culture plates. The bottom compartment medium was supplemented with 15 ng/ml of BDNF (PeproTech, London, United Kingdom) so that it could act as a chemoattractant for axons growing through the insert membrane. Axonal fraction and the fraction containing neuronal body with dendrites were isolated by carefully detaching the cellular contents from the inner and outer insert membrane surface with a cell scraper in TAEB buffer (Merck, Darmstadt, Germany) four times, alternating the direction by 90° each time. Axons were collected after 11 days in culture because, after DIV14, dendrites, which grow at a slower rate, are also detected on the other side of the porous membrane. Before isolation of the axon part, the inner membrane surface was scrubbed with a cotton-tipped applicator, and the membranes were cut out from the insert. To examine whether the separation of axons from the somatodendritic part was correctly performed, we also immunostained culture filters isolated from the Boyden chamber before and after scraping off the cell bodies, with immunofluorescence assay (β-III-tubulin, 1:500; Burlington, MA, United States) and nuclear dye Hoechst (**Supplementary Figures 5A,B**). The presence of axons on the outer site of the membrane was examined, and the purity of the obtained axonal fraction was evaluated with nuclear and axonal markers (**Supplementary Table 3**). The axon isolation procedures were adapted from Unsain et al. (2014).

³<http://n2t.net/addgene:14436>

Seahorse XFp Cell Energy Phenotype Test

Seahorse XFp Cell Energy Phenotype assays (Seahorse, Agilent Technologies, Santa Clara, CA, United States) were performed according to the manufacturer's instructions on an XFp instrument. Dissociated cerebellar neurons were seeded at a density of 5,300 or 12,500 cells/well onto culture mini plates with the protocol described in the section "Primary neuron culture and transfection." The assays were performed at DIV3, 11, 18, and 21. On the day of assay, the XF assay medium was supplemented with 25 mM glucose, 0.5 mM pyruvate, and 2 mM glutamine, and the pH adjusted to 7.4. After assay performance, cells were lysed with PB1× buffer, and protein concentration was measured, and the obtained values were used for data normalization. Data analysis was performed using the Seahorse XFe Wave software and the Seahorse XF Cell Energy Phenotype Test Report Generator. The baseline OCR/ECAR ratio was higher than 4 only in DIV3, which means that the stressed ECAR parameter, in this case, may include both glycolysis and mitochondrial activity.

Immunofluorescence Staining

The animals were deeply anesthetized and transcardially perfused using saline, followed by 4% PFA. The brains were removed, post-fixed in 4% PFA for 48 h, and cryopreserved with graded sucrose (10–20–30%) over 72 h. The 20 or 30-µm parasagittal mouse brain sections were cut using a cryostat at –20°C and collected on SuperFrost Plus slides (Thermo Fisher Scientific, Waltham, MA, United States). The sections were processed immediately. The HIER procedure was applied by incubation of the sections in citrate buffer (pH 9.0) for 30 min at 60°C. The sections were blocked via incubation in 4% normal goat serum in TBS for 1 h. For immunofluorescent staining, the sections were incubated overnight at 4°C with the primary mouse anti-ataxin-3 antibody 1H9 (1:200; kindly provided by Yvon Trottier), rabbit anti-ataxin-3 (1:200; ProteinTech, Rosemont, IL, United States), rabbit anti-ubiquitin (1:500; Z0458, Dako, Jena, Germany), mouse SMI-32 against non-phosphorylated heavy and medium neurofilament subunits (1:1,000) and mouse SMI-312 against phosphorylated heavy and medium neurofilaments (1:1,000) (Biologics, San Diego, CA, United States), and subsequently with the anti-mouse or anti-rabbit antibody labeled by AlexaFluor488, Dylight594, or AlexaFluor647 (1:400; Jackson ImmunoResearch; Suffolk, United Kingdom). The sections were end-stained with Hoechst 33342 (Sigma) nuclear stain at 1:1,000 and embedded in Fluoroshield (Sigma) mounting medium.

Image Acquisition and Quantification

Confocal images were acquired using two microscope systems. The first system was Opera LX (PerkinElmer) using 40× water objective, 200 ms exposure time, and 50–70% laser power. For each picture, 25–50 confocal sections were collected, from which 10 sections were dissected for further analysis. The second system was TCS SP5 II (Leica Microsystems; Poland), using oil immersion 63× objective with a sequential acquisition setting. For fluorescent quantification, images were acquired using the

same settings at a resolution of 1024×1024 pixels and 100 Hz. Confocal sections (8–10) were acquired to a total Z-stack thickness of $0.13\text{ }\mu\text{m}$. For each condition, we performed three independent cultures; and five independent transfections from which 46 pictures of Ki91 and 33 pictures of WT were collected and analyzed. For analyzing the state of mRFP-Rab7+ vesicles in fixed neurons, we selected axons, which were distinguished from dendrites based on known morphological characteristics: greater length and sparse branching (Banker and Cowan, 1979). For immunostaining of mouse brains, we used four slices, and randomly acquired from each slice, ≥ 5 fields were. Offline analysis of the image Z-stack was performed using the open-source image-processing package Fiji/ImageJ. Morphometric measurements were performed using Fiji/ImageJ. Measured data were imported into Excel software for analysis. The thresholds in all images were set to similar levels. Data were obtained from at least three independent experiments, and the number of cells or imaging sections used for quantification is indicated in the figures. All statistical analyses were performed using the Student's *t*-test and are presented as mean \pm SEM.

Statistical Analysis

The data regarding behavioral experiments were subjected to a two-way ANOVA, followed by Bonferroni post-tests. *p*-values of less than 0.05 were considered significant. Identification of proteins on raw proteomic data was performed by the Andromeda search engine in Mascot using the following inclusion criteria: at least two different peptides per protein were identified per sample, and a total peptide score reached the significance threshold FDR = 0.01. Identified proteins matching the inclusion criteria were subjected to further statistical analysis with a two-sample *t*-test, and dysregulation of protein level reaching *p*-value < 0.05 was considered as significant. Kruskal-Wallis test was used to perform a score assessment in the 0–5 scale of mild, moderate, and severe phenotype in 18-month-old animals (*p*-value < 0.05).

DATA AVAILABILITY STATEMENT

The datasets presented in this study can be found in online repositories. The names of the repository/repositories and accession number(s) can be found below: PRIDE, PXD024945.

ETHICS STATEMENT

The animal study was reviewed and approved by the Local Ethical Committee for Animal Experiments in Poznań.

AUTHOR CONTRIBUTIONS

MF was responsible for the research concept and obtaining funding, conceived, designed, and supervised all experiments, and analyzed the data. KW and ŁM performed all proteomic experiments. KW analyzed the data, designed and performed

all experiments except of MRI. EB, J-BP, and JF performed the MRI experiment and analyzed the data. MF and KW wrote the manuscript. All authors contributed to the article and approved the submitted version.

FUNDING

This work was supported by the grant from the National Science Centre (grant number 2013/10/E/NZ4/00621), the European Research Projects On Rare Diseases (JTC 2017) grant from the National Centre for Research and Development (grant numbers: ERA-NET-E-RARE-3/III/TreatPolyQ/08/2018 and ERA-NET-E-RARE-3/III/SCA-CYP/09/2018), and a grant of Polish Ministry of Science and Higher Education for young scientists GM_KW_ICHB.

ACKNOWLEDGMENTS

Proteomic mass spectrometry analyses were performed in the Laboratory of Mass Spectrometry (European Centre for Bioinformatics and Genomics; ECBiG; IBCh, PAS, Poznań, Poland). Confocal imaging was performed using the facilities in the Laboratory of Subcellular Structures Analysis and Laboratory of Molecular Assays (IBCh, PAS, Poland). Primary neuron cultures were maintained in the Cell and Tissue Culture Laboratory (IBCh, PAS, Poland). We thank Adam Plewinski for his help in maintaining the colonies of mice. We also thank Joanna Mieloch for help in maintaining the animals. We also thank Magdalena Surdyka and Łukasz Przybył for collecting tissues, which were sent for MRI. We also thank Yvon Trottier for kindly providing anti-ataxin-3 1H9 antibody and Ari Helenius for supplying mRFP-Rab7 plasmid via Addgene (#14437). We also thank Chengbiao Wu and Ruinan Shen for help with the analysis of Rab-7 transfection in Fiji. We also thank Krzysztof Sobczak for kindly providing a vacuum dot-blot apparatus.

SUPPLEMENTARY MATERIAL

The Supplementary Material for this article can be found online at: <https://www.frontiersin.org/articles/10.3389/fnmol.2021.658339/full#supplementary-material>

Supplementary Table 1 | MS/MS proteomic data for each tested age (4, 10, 12, and 14-month-old) in the parallel approach in the cerebellum.

Supplementary Table 2 | MS/MS proteomic data for each tested age (4, 10, 12, and 14-month-old) in the parallel approach in the cerebral cortex.

Supplementary Table 3 | MS/MS proteomic data for 18-month-old Ki91 cerebellum and cortex in the correlative approach.

Supplementary Table 4 | MS/MS proteomic data for the of protein levels in somatodendritic and axon compartment in cerebellar and cortical samples.

Supplementary Table 5 | Proteins depleted in Ki91 cerebellar axons.

Supplementary Table 6 | Proteins enriched in Ki91 cerebellar axons.

Supplementary Table 7 | Proteins depleted in Ki91 cortical axons.

Supplementary Table 8 | Proteins enriched in Ki91 cortical axons.

REFERENCES

- Baleriola, J., and Hengst, U. (2015). Targeting axonal protein synthesis in neuroregeneration and degeneration. *Neurotherapeutics* 12, 57–65. doi: 10.1007/s13311-014-0308-8
- Banker, G. A., and Cowan, W. M. (1979). Further observations on hippocampal neurons in dispersed cell culture. *J. Comp. Neurol.* 187, 469–493. doi: 10.1002/cne.901870302
- Bettencourt, C., and Lima, M. (2011). Machado-Joseph disease: from first descriptions to new perspectives. *Orphanet J. Rare Dis.* 6:35. doi: 10.1186/1750-1172-6-35
- Breuer, M., Guglielmi, L., Zielonka, M., Hemberger, V., Kölker, S., Okun, J. G., et al. (2019). QDPR homologues in *Danio rerio* regulate melanin synthesis, early gliogenesis, and glutamine homeostasis. *PLoS One* 14:e0215162. doi: 10.1371/journal.pone.0215162
- Casella, C., Lipp, I., Rosser, A., Jones, D. K., and Metzler-Baddeley, C. (2020). A critical review of white matter changes in Huntington's disease. *Mov. Disord. Off. J. Mov. Disord. Soc.* 35, 1302–1311. doi: 10.1002/mds.28109
- Chen, L., Stone, M. C., Tao, J., and Rolls, M. M. (2012). Axon injury and stress trigger a microtubule-based neuroprotective pathway. *Proc. Natl. Acad. Sci. U.S.A.* 109, 11842–11847. doi: 10.1073/pnas.1121180109
- Chyung, E., LeBlanc, H. F., Fallon, J. R., and Akins, M. R. (2018). Fragile X granules are a family of axonal ribonucleoprotein particles with circuit-dependent protein composition and mRNA cargos. *J. Comp. Neurol.* 526, 96–108. doi: 10.1002/cne.24321
- Cioni, J.-M., Lin, J. Q., Holtermann, A. V., Koppers, M., Jakobs, M. A. H., Azizi, A., et al. (2019). Late endosomes act as mRNA translation platforms and sustain mitochondria in axons. *Cell* 176, 56.e15–72.e15. doi: 10.1016/j.cell.2018.11.030
- Coarelli, G., Brice, A., and Durr, A. (2018). Recent advances in understanding dominant spinocerebellar ataxias from clinical and genetic points of view. *F1000Research* 7:F1000FacultyRev-1781. doi: 10.12688/f1000research.15788.1
- Coutinho, P., and Andrade, C. (1978). Autosomal dominant system degeneration in Portuguese families of the Azores Islands. A new genetic disorder involving cerebellar, pyramidal, extrapyramidal and spinal cord motor functions. *Neurology* 28, 703–709.
- Cox, D., and Ecroyd, H. (2017). The small heat shock proteins α B-crystallin (HSPB5) and Hsp27 (HSPB1) inhibit the intracellular aggregation of α -synuclein. *Cell Stress Chaperones* 22, 589–600. doi: 10.1007/s12192-017-0785-x
- Da Silva, J. D., Teixeira-Castro, A., and Maciel, P. (2019). From pathogenesis to novel therapeutics for spinocerebellar ataxia type 3: evading potholes on the way to translation. *Neurotherapeutics* 16, 1009–1031. doi: 10.1007/s13311-019-00798-1
- D'Abreu, A., França, M., Appenzeller, S., Lopes-Cendes, I., and Cendes, F. (2009). Axonal dysfunction in the deep white matter in Machado-Joseph disease. *J. Neuroimaging Off. J. Am. Soc. Neuroimaging* 19, 9–12. doi: 10.1111/j.1552-6569.2008.00260.x
- de Rezende, T. J. R., D'Abreu, A., Guimarães, R. P., Lopes, T. M., Lopes-Cendes, I., Cendes, F., et al. (2015). Cerebral cortex involvement in Machado-Joseph disease. *Eur. J. Neurol.* 22, e23–e24. doi: 10.1111/ene.12559
- Dhenain, M., Delatour, B., Walczak, C., and Volk, A. (2006). Passive staining: a novel ex vivo MRI protocol to detect amyloid deposits in mouse models of Alzheimer's disease. *Magn. Reson. Med.* 55, 687–693. doi: 10.1002/mrm.20810
- Diallo, A., Jacobi, H., Schmitz-Hübsch, T., Cook, A., Labrum, R., Durr, A., et al. (2017). Body mass index decline is related to spinocerebellar ataxia disease progression. *Mov. Disord. Clin. Pract.* 4, 689–697. doi: 10.1002/mdc3.12522
- El Fatimi, R., Davidovic, L., Tremblay, S., Jaglin, X., Dury, A., Robert, C., et al. (2016). Tracking the fragile X mental retardation protein in a highly ordered neuronal ribonucleoparticles population: a link between stalled polyribosomes and RNA granules. *PLoS Genet.* 12:e1006192. doi: 10.1371/journal.pgen.1006192
- Emperador-Melero, J., Huson, V., van Weering, J., Bollmann, C., Fischer, von Mollard, G., et al. (2018). Vti1a/b regulate synaptic vesicle and dense core vesicle secretion via protein sorting at the Golgi. *Nat. Commun.* 9:3421. doi: 10.1038/s41467-018-05699-z
- Eva, R., Koseki, H., Kanamarlapudi, V., and Fawcett, J. W. (2017). EFA6 regulates selective polarised transport and axon regeneration from the axon initial segment. *J. Cell Sci.* 130, 3663–3675. doi: 10.1242/jcs.207423
- Falck, J., Bruns, C., Hoffmann-Conaway, S., Straub, I., Plautz, E. J., Orlando, M., et al. (2020). Loss of piccolo function in rats induces cerebellar network dysfunction and pontocerebellar hypoplasia Type 3-like phenotypes. *J. Neurosci. Off. J. Soc. Neurosci.* 40, 2943–2959. doi: 10.1523/JNEUROSCI.2316-19.2020
- Farrar, M. A., Vucic, S., Nicholson, G., and Kiernan, M. C. (2016). Motor cortical dysfunction develops in spinocerebellar ataxia type 3. *Clin. Neurophysiol. Off. J. Int. Fed. Clin. Neurophysiol.* 127, 3418–3424. doi: 10.1016/j.clinph.2016.09.005
- Ferrari Bardile, C., Garcia-Miralles, M., Caron, N. S., Rayan, N. A., Langley, S. R., Harmston, N., et al. (2019). Intrinsic mutant HTT-mediated defects in oligodendroglia cause myelination deficits and behavioral abnormalities in Huntington disease. *Proc. Natl. Acad. Sci. U.S.A.* 116, 9622–9627. doi: 10.1073/pnas.1818042116
- Gao, Y.-L., Wang, N., Sun, F.-R., Cao, X.-P., Zhang, W., and Yu, J.-T. (2018). Tau in neurodegenerative disease. *Ann. Transl. Med.* 6:175. doi: 10.21037/atm.2018.04.23
- Ghosh, J. G., Houck, S. A., and Clark, J. I. (2007). Interactive sequences in the stress protein and molecular chaperone human alphaB crystallin recognize and modulate the assembly of filaments. *Int. J. Biochem. Cell Biol.* 39, 1804–1815. doi: 10.1016/j.biocel.2007.04.027
- Graves, T. D., and Guiloff, R. J. (2011). SCA3 presenting as an isolated axonal polyneuropathy. *Arch. Neurol.* 68, 653–655. doi: 10.1001/archneurol.2011.86
- Guimarães, R. P., D'Abreu, A., Yasuda, C. L., França, M. C., Silva, B. H. B., Cappabianco, F. A. M., et al. (2013). A multimodal evaluation of microstructural white matter damage in spinocerebellar ataxia type 3. *Mov. Disord. Off. J. Mov. Disord. Soc.* 28, 1125–1132. doi: 10.1002/mds.25451
- Guo, J., Chen, H., Biswal, B. B., Guo, X., Zhang, H., Dai, L., et al. (2020). Gray matter atrophy patterns within the cerebellum-neostriatum-cortical network in SCA3. *Neurology* 95, e3036–e3044. doi: 10.1212/WNL.0000000000010986
- Guo, W., Stoklund Dittlau, K., and Van Den Bosch, L. (2020). Axonal transport defects and neurodegeneration: molecular mechanisms and therapeutic implications. *Semin. Cell Dev. Biol.* 99, 133–150. doi: 10.1016/j.semcdb.2019.07.010
- Guyenet, S. J., Furrer, S. A., Damian, V. M., Baughan, T. D., Spada, A. R. L., and Garden, G. A. (2010). A simple composite phenotype scoring system for evaluating mouse models of cerebellar ataxia. *JoVE J. Vis. Exp.* 39:e1787. doi: 10.3791/1787
- Holleran, E. A., Tokito, M. K., Karki, S., and Holzbaur, E. L. (1996). Centractin (ARP1) associates with spectrin revealing a potential mechanism to link dynactin to intracellular organelles. *J. Cell Biol.* 135, 1815–1829. doi: 10.1083/jcb.135.6.1815
- Houck, S. A., and Clark, J. I. (2010). Dynamic subunit exchange and the regulation of microtubule assembly by the stress response protein human alphaB crystallin. *PLoS One* 5:e11795. doi: 10.1371/journal.pone.0011795
- Ishikawa, Y., Katoh, H., Nakamura, K., Mori, K., and Negishi, M. (2002). Developmental changes in expression of small GTPase RhoG mRNA in the rat brain. *Brain Res. Mol. Brain Res.* 106, 145–150. doi: 10.1016/s0169-328x(02)00413-8
- Jacobi, H., du Montcel, S. T., Bauer, P., Giunti, P., Cook, A., Labrum, R., et al. (2015). Long-term disease progression in spinocerebellar ataxia types 1, 2, 3, and 6: a longitudinal cohort study. *Lancet Neurol.* 14, 1101–1108. doi: 10.1016/S1474-4422(15)00202-1
- Jung, C., Yabe, J. T., Lee, S., and Shea, T. B. (2000). Hypophosphorylated neurofilament subunits undergo axonal transport more rapidly than more extensively phosphorylated subunits in situ. *Cell Motil. Cytoskeleton* 47, 120–129. doi: 10.1002/1097-0169(200010)47:2<120::AID-CM3<3.0.CO;2-6
- Kamburov, A., Stelzl, U., Lehrach, H., and Herwig, R. (2013). The ConsensusPathDB interaction database: 2013 update. *Nucleic Acids Res.* 41, D793–D800. doi: 10.1093/nar/gks1055
- Karus, C., Ziemens, D., and Rose, C. R. (2015). Lactate rescues neuronal sodium homeostasis during impaired energy metabolism. *Channels Austin Tex* 9, 200–208. doi: 10.1080/19336950.2015.1050163
- Kevenaar, J. T., and Hoogenraad, C. C. (2015). The axonal cytoskeleton: from organization to function. *Front. Mol. Neurosci.* 8:44. doi: 10.3389/fnmol.2015.00044
- Krämer-Albers, E.-M., Bretz, N., Tenzer, S., Winterstein, C., Möbius, W., Berger, H., et al. (2007). Oligodendrocytes secrete exosomes containing major myelin

- and stress-protective proteins: Trophic support for axons? *Proteomics Clin. Appl.* 1, 1446–1461. doi: 10.1002/prca.200700522
- Kurosaki, H., Yamaguchi, K., Man-Yoshi, K., Muramatsu, S.-I., Hara, S., and Ichinose, H. (2019). Administration of tetrahydrobiopterin restored the decline of dopamine in the striatum induced by an acute action of MPTP. *Neurochem. Int.* 125, 16–24. doi: 10.1016/j.neuint.2019.02.005
- Lein, E. S., Hawrylycz, M. J., Ao, N., Ayres, M., Bensinger, A., Bernard, A., et al. (2007). Genome-wide atlas of gene expression in the adult mouse brain. *Nature* 445, 168–176. doi: 10.1038/nature05453
- Li, Q.-F., Dong, Y., Yang, L., Xie, J.-J., Ma, Y., Du, Y.-C., et al. (2019). Neurofilament light chain is a promising serum biomarker in spinocerebellar ataxia type 3. *Mol. Neurodegener.* 14:39. doi: 10.1186/s13024-019-0338-0
- Liao, Y., Tong, L., Tang, L., and Wu, S. (2017). The role of cold-inducible RNA binding protein in cell stress response. *Int. J. Cancer* 141, 2164–2173. doi: 10.1002/ijc.30833
- Lorenzo, D. N., Badea, A., Davis, J., Hostettler, J., He, J., Zhong, G., et al. (2014). A PIK3C3-ankyrin-B-dynactin pathway promotes axonal growth and multiorganelle transport. *J. Cell Biol.* 207, 735–752. doi: 10.1083/jcb.201407063
- Lu, M.-K., Chen, J.-C., Chen, C.-M., Duann, J.-R., Ziemann, U., and Tsai, C.-H. (2017). Impaired cerebellum to primary motor cortex associative plasticity in Parkinson's disease and spinocerebellar ataxia type 3. *Front. Neurol.* 8:445. doi: 10.3389/fneur.2017.00445
- Lunnion, K., Keohane, A., Pidsley, R., Newhouse, S., Riddoch-Contreras, J., Thubron, E. B., et al. (2017). Mitochondrial genes are altered in blood early in Alzheimer's disease. *Neurobiol. Aging* 53, 36–47. doi: 10.1016/j.neurobiolaging.2016.12.029
- Mazzucchelli, S., De Palma, A., Riva, M., D'Urzo, A., Pozzi, C., Pastori, V., et al. (2009). Proteomic and biochemical analyses unveil tight interaction of ataxin-3 with tubulin. *Int. J. Biochem. Cell Biol.* 41, 2485–2492. doi: 10.1016/j.biocel.2009.08.003
- McLoughlin, H. S., Moore, L. R., and Paulson, H. L. (2020). Pathogenesis of SCA3 and implications for other polyglutamine diseases. *Neurobiol. Dis.* 134:104635. doi: 10.1016/j.nbd.2019.104635
- Mendonça, C. F., Kuras, M., Nogueira, F. C. S., Plá, I., Hortobágyi, T., Csiba, L., et al. (2019). Proteomic signatures of brain regions affected by tau pathology in early and late stages of Alzheimer's disease. *Neurobiol. Dis.* 130:104509. doi: 10.1016/j.nbd.2019.104509
- Moughamian, A. J., Osborn, G. E., Lazarus, J. E., Maday, S., and Holzbaur, E. L. F. (2013). Ordered recruitment of dynein to the microtubule plus-end is required for efficient initiation of retrograde axonal transport. *J. Neurosci. Off. J. Soc. Neurosci.* 33, 13190–13203. doi: 10.1523/JNEUROSCI.0935-13.2013
- Mukherjee, A. B., Appu, A. P., Sadhukhan, T., Casey, S., Mondal, A., Zhang, Z., et al. (2019). Emerging new roles of the lysosome and neuronal ceroid lipofuscinoses. *Mol. Neurodegener.* 14:4. doi: 10.1186/s13024-018-0300-6
- Neves-Carvalho, A., Logarinho, E., Freitas, A., Duarte-Silva, S., Costa, M., do, C., et al. (2015). Dominant negative effect of polyglutamine expansion perturbs normal function of ataxin-3 in neuronal cells. *Hum. Mol. Genet.* 24, 100–117. doi: 10.1093/hmg/ddu422
- Orr, H. T., and Zoghbi, H. Y. (2007). Trinucleotide repeat disorders. *Annu. Rev. Neurosci.* 30, 575–621. doi: 10.1146/annurev.neuro.29.051605.113042
- Porro, C., Panaro, M. A., Lofrumento, D. D., Hasalla, E., and Trotta, T. (2019). The multiple roles of exosomes in Parkinson's disease: an overview. *Immunopharmacol. Immunotoxicol.* 41, 469–476. doi: 10.1080/08923973.2019.1650371
- Pulido-Valdeolivas, I., Gómez-Andrés, D., Sanz-Gallego, I., Rausell, E., and Arpa, J. (2016). Patterns of motor signs in spinocerebellar ataxia type 3 at the start of follow-up in a reference unit. *Cerebellum Ataxias* 3:4. doi: 10.1186/s40673-016-0042-6
- Rezende, T. J. R., Paiva, J. L. R., de Martinez, A. R. M., Lopes-Cendes, I., Pedroso, J. L., Barsottini, O. G. P., et al. (2018). Structural signature of SCA3: from presymptomatic to late disease stages. *Ann. Neurol.* 84, 401–408. doi: 10.1002/ana.25297
- Sakabe, I., Hu, R., Jin, L., Clarke, R., and Kasid, U. N. (2015). TMEM33: a new stress-inducible endoplasmic reticulum transmembrane protein and modulator of the unfolded protein response signaling. *Breast Cancer Res. Treat.* 153, 285–297. doi: 10.1007/s10549-015-3536-7
- Salpietro, V., Malintan, N. T., Llano-Rivas, I., Spaeth, C. G., Efthymiou, S., Striano, P., et al. (2019). Mutations in the neuronal vesicular SNARE VAMP2 affect synaptic membrane fusion and impair human neurodevelopment. *Am. J. Hum. Genet.* 104, 721–730. doi: 10.1016/j.ajhg.2019.02.016
- Sánchez, I., Balagüé, E., and Matilla-Dueñas, A. (2016). Ataxin-1 regulates the cerebellar bioenergetics proteome through the GSK3β-mTOR pathway which is altered in Spinocerebellar ataxia type 1 (SCA1). *Hum. Mol. Genet.* 25, 4021–4040. doi: 10.1093/hmg/ddw242
- Sánchez-Valle, R., Monté, G. C., Sala-Llonch, R., Bosch, B., Fortea, J., Lladó, A., et al. (2016). White matter abnormalities track disease progression in PSEN1 autosomal dominant Alzheimer's disease. *J. Alzheimers Dis. JAD* 51, 827–835. doi: 10.3233/JAD-150899
- Santos, T. C., Wierda, K., Broeke, J. H., Toonen, R. F., and Verhage, M. (2017). Early golgi abnormalities and neurodegeneration upon loss of presynaptic proteins Munc18-1, Syntaxis-1, or SNAP-25. *J. Neurosci. Off. J. Soc. Neurosci.* 37, 4525–4539. doi: 10.1523/JNEUROSCI.3352-16.2017
- Saunders, A., Macosko, E. Z., Wysoker, A., Goldman, M., Krienen, F. M., Rivera, H., et al. (2018). Molecular diversity and specializations among the cells of the adult mouse brain. *Cell* 174, 1015.e16–1030.e16. doi: 10.1016/j.cell.2018.07.028
- Schmidt, J., Mayer, A. K., Bakula, D., Freude, J., Weber, J. J., Weiss, A., et al. (2019). Vulnerability of frontal brain neurons for the toxicity of expanded ataxin-3. *Hum. Mol. Genet.* 28, 1463–1473. doi: 10.1093/hmg/ddy437
- Seidel, K., den Dunnen, W. F. A., Schultz, C., Paulson, H., Frank, S., de Vos, R. A., et al. (2010). Axonal inclusions in spinocerebellar ataxia type 3. *Acta Neuropathol.* 120, 449–460. doi: 10.1007/s00401-010-0717-7
- Shea, T. B., and Chan, W. K.-H. (2008). Regulation of neurofilament dynamics by phosphorylation. *Eur. J. Neurosci.* 27, 1893–1901. doi: 10.1111/j.1460-9568.2008.01616.x
- Sittler, A., Muriel, M.-P., Marinello, M., Brice, A., den Dunnen, W., and Alves, S. (2018). Dereulation of autophagy in postmortem brains of Machado-Joseph disease patients. *Neuropathol. Off. J. Jpn. Soc. Neuropathol.* 38, 113–124. doi: 10.1111/neup.12433
- Skotte, N. H., Andersen, J. V., Santos, A., Aldana, B. I., Willert, C. W., Nørremolle, A., et al. (2018). Integrative characterization of the R6/2 mouse model of Huntington's disease reveals dysfunctional astrocyte metabolism. *Cell Rep.* 23, 2211–2224. doi: 10.1016/j.celrep.2018.04.052
- Sorolla, M. A., Reverter-Branchat, G., Tamarit, J., Ferrer, I., Ros, J., and Cabiscol, E. (2008). Proteomic and oxidative stress analysis in human brain samples of Huntington disease. *Free Radic. Biol. Med.* 45, 667–678. doi: 10.1016/j.freeradbiomed.2008.05.014
- Sossin, W. S., and DesGroseillers, L. (2006). Intracellular trafficking of RNA in neurons. *Traffic* 15, 1581–1589. doi: 10.1111/j.1600-0854.2006.00500.x
- Sowa, A. S., Martin, E., Martins, I. M., Schmidt, J., Depping, R., Weber, J. J., et al. (2018). Karyopherin α-3 is a key protein in the pathogenesis of spinocerebellar ataxia type 3 controlling the nuclear localization of ataxin-3. *Proc. Natl. Acad. Sci. U.S.A.* 115, E2624–E2633. doi: 10.1073/pnas.1716071115
- Stenbeck, G. (1998). Soluble NSF-attachment proteins. *Int. J. Biochem. Cell Biol.* 30, 573–577. doi: 10.1016/s1357-2725(97)00064-2
- Stridh, M. H., Alt, M. D., Wittmann, S., Heidtmann, H., Aggarwal, M., Riederer, B., et al. (2012). Lactate flux in astrocytes is enhanced by a non-catalytic action of carbonic anhydrase II. *J. Physiol.* 590, 2333–2351. doi: 10.1113/jphysiol.2011.220152
- Switonski, P. M., Szlachcic, W. J., Krzyzosiak, W. J., and Figiel, M. (2015). A new humanized ataxin-3 knock-in mouse model combines the genetic features, pathogenesis of neurons and glia and late disease onset of SCA3/MJD. *Neurobiol. Dis.* 73, 174–188. doi: 10.1016/j.nbd.2014.09.020
- Toonen, L. J. A., Overzier, M., Evers, M. M., Leon, L. G., van der Zeeuw, S. A. J., Mei, H., et al. (2018). Transcriptional profiling and biomarker identification reveal tissue specific effects of expanded ataxin-3 in a spinocerebellar ataxia type 3 mouse model. *Mol. Neurodegener.* 13:31. doi: 10.1186/s13024-018-0261-9
- Unsain, N., Heard, K. N., Higgins, J. M., and Barker, P. A. (2014). Production and isolation of axons from sensory neurons for biochemical analysis using porous filters. *J. Vis. Exp. Jove.* 89, 51795. doi: 10.3791/51795
- Volpicelli-Daley, L. A., Gamble, K. L., Schultheiss, C. E., Riddle, D. M., West, A. B., and Lee, V. M.-Y. (2014). Formation of α-synuclein Lewy neurite-like

- aggregates in axons impedes the transport of distinct endosomes. *Mol. Biol. Cell* 25, 4010–4023. doi: 10.1091/mbc.E14-02-0741
- Wiatr, K., Piasecki, P., Marczak, Ł., Wojciechowski, P., Kurkowiak, M., Płoski, R., et al. (2019). Altered levels of proteins and phosphoproteins, in the absence of early causative transcriptional changes, shape the molecular pathogenesis in the brain of young presymptomatic Ki91 SCA3/MJD Mouse. *Mol. Neurobiol.* 56, 8168–8202. doi: 10.1007/s12035-019-01643-4
- Yang, J.-S., Chen, P.-P., Lin, M.-T., Qian, M.-Z., Lin, H.-X., Chen, X.-P., et al. (2018). Association between body mass index and disease severity in chinese spinocerebellar ataxia type 3 patients. *Cerebellum Lond. Engl.* 17, 494–498. doi: 10.1007/s12311-018-0929-2
- Yoo, B. C., Cairns, N., Fountoulakis, M., and Lubec, G. (2001). Synaptosomal proteins, beta-soluble N-ethylmaleimide-sensitive factor attachment protein (beta-SNAP), gamma-SNAP and synaptotagmin I in brain of patients with Down syndrome and Alzheimer's disease. *Dement. Geriatr. Cogn. Disord.* 12, 219–225. doi: 10.1159/000051261
- Yuan, D., Liu, C., and Hu, B. (2018). Dysfunction of membrane trafficking leads to ischemia-reperfusion injury after transient cerebral ischemia. *Transl. Stroke Res.* 9, 215–222. doi: 10.1007/s12975-017-0572-0
- Zaoui, K., Rajadurai, C. V., Duhamel, S., and Park, M. (2019). Arf6 regulates RhoB subcellular localization to control cancer cell invasion. *J. Cell Biol.* 218, 3812–3826. doi: 10.1083/jcb.201806111
- Zeng, L., Zhang, D., McLoughlin, H. S., Zalon, A. J., Aravind, L., and Paulson, H. L. (2018). Loss of the Spinocerebellar Ataxia type 3 disease protein ATXN3 alters transcription of multiple signal transduction pathways. *PLoS One* 13:e0204438. doi: 10.1371/journal.pone.0204438
- Zhang, Z.-H., Ma, F.-F., Zhang, H., and Xu, X.-H. (2017). MARCKS is necessary for oligodendrocyte precursor cell maturation. *Neurochem. Res.* 42, 2933–2939. doi: 10.1007/s11064-017-2324-7
- Zhou, Y., Dhaher, R., Parent, M., Hu, Q.-X., Hassel, B., Yee, S.-P., et al. (2019). Selective deletion of glutamine synthetase in the mouse cerebral cortex induces glial dysfunction and vascular impairment that precede epilepsy and neurodegeneration. *Neurochem. Int.* 123, 22–33. doi: 10.1016/j.neuint.2018.07.009
- Zhu, Z., and Reiser, G. (2018). The small heat shock proteins, especially HspB4 and HspB5 are promising protectants in neurodegenerative diseases. *Neurochem. Int.* 115, 69–79. doi: 10.1016/j.neuint.2018.02.006
- Zinn, A., Goicochea, S. M., Kreider-Letterman, G., Maity, D., Awadia, S., Cedeno-Rosario, L., et al. (2019). The small GTPase RhoG regulates microtubule-mediated focal adhesion disassembly. *Sci. Rep.* 9:5163. doi: 10.1038/s41598-019-41558-7

Conflict of Interest: The authors declare that the research was conducted in the absence of any commercial or financial relationships that could be construed as a potential conflict of interest.

Copyright © 2021 Wiatr, Marczak, Pérot, Brouillet, Flament and Figiel. This is an open-access article distributed under the terms of the Creative Commons Attribution License (CC BY). The use, distribution or reproduction in other forums is permitted, provided the original author(s) and the copyright owner(s) are credited and that the original publication in this journal is cited, in accordance with accepted academic practice. No use, distribution or reproduction is permitted which does not comply with these terms.